

Basics of Power Systems Analysis

Carlo Alberto Nucci , Alberto Borghetti , Fabio Napolitano , Fabio Tossani 

This chapter provides the background required to understand the main aspects of power systems analysis and operation under steady-state and transient or dynamic conditions. It is intended for senior undergraduate or graduate students of electrical engineering as well as practitioners, so readers are assumed to have a solid background knowledge of electrical engineering.

The main technical issues associated with power systems analysis are addressed, focusing in particular on alternating current (AC) transmission lines, networks, load-flow and short-circuit calculations, stability analysis, frequency control, and electromagnetic transient appraisal. The chapter also references the most important and popular model frameworks and calculation/modeling tools that have been developed by researchers and engineers working within the electric power systems area in the last few decades. It is emphasized in this chapter that an understanding of the issues dealt with here is required to comprehend other chapters of this handbook devoted to distributed generation and smart grids, and this knowledge will also be needed to be able to operate upcoming power systems.

The chapter is divided into sections focusing on the following topics:

1. Power systems evolution, from the origins to the traditional structure
2. Transmission lines in steady state, transmitted active and reactive power
3. Power flow analysis (load-flow equations and resolution methods)
4. Short-circuit calculations for unbalanced faults (symmetrical components, fault equations, and sequence networks)
5. Stability (states of operation, classification, P-delta curves, rotor angle stability, equal area criterion, multi-machine stability and voltage stability)
6. Generators reserve and dynamics, frequency dependence of the load, control structure for frequency control

7. Traveling waves in a lossless line, reflection and transmission coefficients, multiple reflections in a line of finite length; electromagnetic transients (classification of transients, EMTP)
8. Power systems in the future (why we need a smart(er) grid, microgrids and energy communities)

Additional information and supplementary exercises for this chapter are available online.

| | | |
|------------|---|-----|
| 5.1 | Electric Power System Evolution | 274 |
| 5.1.1 | The Dawn of Electric Power Systems..... | 274 |
| 5.1.2 | From the War of the Currents to the Twenty-First Century | 275 |
| 5.2 | Mission and Traditional Structure | 276 |
| 5.3 | Transmission Line Equations in the Steady State | 279 |
| 5.3.1 | The Telegrapher's Equations | 279 |
| 5.3.2 | The Line as a Two-Port Network..... | 283 |
| 5.3.3 | Transmitted Active and Reactive Power Expressions | 284 |
| 5.4 | Load Flow | 285 |
| 5.4.1 | From the Real Network to the Admittance Matrix..... | 285 |
| 5.4.2 | The Equations | 290 |
| 5.4.3 | Capability Curves | 292 |
| 5.4.4 | Solution Methods..... | 293 |
| 5.4.5 | Approximations for Calculating the Load Flow..... | 295 |
| 5.4.6 | Concluding Remarks..... | 298 |
| 5.5 | Unsymmetrical Fault Analysis | 300 |
| 5.5.1 | Types of Faults in Electric Power Systems | 300 |
| 5.5.2 | Protection Measures Against Faults..... | 301 |
| 5.5.3 | Unbalanced Faults: Short-Circuit Calculation | 301 |
| 5.5.4 | Direct, Inverse, and Homopolar Sequence Impedances..... | 307 |
| 5.5.5 | Fault at Any Point in the Network | 309 |
| 5.5.6 | Three-Phase Short Circuit at a Synchronous Generator's Terminals | 311 |
| 5.6 | Stability | 319 |
| 5.6.1 | Transient Phenomena | 319 |

| | | | | | |
|-------|--|-----|-------------------------|---|-----|
| 5.6.2 | Definition of Stability | 320 | 5.8.2 | Reflection and Transmission Coefficients | 348 |
| 5.6.3 | States of Operation | 320 | 5.8.3 | Multiple Reflections in a Line of Finite Length | 352 |
| 5.6.4 | Classification of Power System Stability | 320 | 5.9 | Electric Power Systems of the Future: Smart Grids | 360 |
| 5.6.5 | P - δ Curves of Synchronous Machines..... | 321 | 5.9.1 | Evolution of Power Systems Towards Increased Deployment of Renewable Energy Resources | 360 |
| 5.6.6 | Rotor Angle Stability | 327 | 5.9.2 | Power System Structure: Why We Need Smart(er) Grids | 361 |
| 5.6.7 | Voltage Stability | 333 | 5.9.3 | The Definition of a Smart Grid..... | 362 |
| 5.7 | Power System Control | 336 | 5.9.4 | Growth in the Utilization of ICT in Power Systems..... | 362 |
| 5.7.1 | Generation Reserve | 336 | 5.9.5 | Microgrids | 363 |
| 5.7.2 | Dynamics of the Generators | 337 | 5.9.6 | Energy Communities | 363 |
| 5.7.3 | Frequency Dependence of the Load | 338 | References | | 364 |
| 5.7.4 | Dynamic Response of an Uncontrolled Power System | 338 | | | |
| 5.7.5 | Control Structure for Frequency Control | 339 | | | |
| 5.8 | Propagation of Electromagnetic Transients Along Transmission Lines | 345 | | | |
| 5.8.1 | Traveling Waves in a Lossless Line..... | 345 | | | |

In this chapter, we present a succinct summary of the fundamentals of power systems analysis and operation under steady-state, dynamic, and transient conditions. We consider the main technical issues that are relevant to the transmission of electric energy, focusing mainly on AC transmission lines and networks and addressing load-flow and short-circuit calculations, stability, frequency control, voltage control, and electromagnetic transient appraisal. However, it should be noted that there are a number of excellent books that cover these subjects in a far more comprehensive manner than possible in this chapter (e.g., [5.1–32]).

In the context of this handbook, an understanding of the subjects covered by this chapter is useful for comprehending Chap. 15 on distributed generation and smart grids, and thus how modern power systems work, given that renewables are increasingly being con-

nected to networks through power electronic converters. It should, however, be noted that HVDC (high-voltage direct current) and DC (direct current) applications, modeling, analysis, and operation are deliberately overlooked in this chapter, as these topics are covered in Chap. 12.

This chapter is intended for use by senior undergraduate or graduate electrical engineering students and practitioners who are familiar with the theory of electrical circuits and of electrical machines. We therefore assume that the reader has a solid background knowledge of electrical engineering, along with an understanding of the per unit method.

After some sections or paragraphs, there are web-links to files that contain illustrative examples, exercises, or even animations, which are generally accompanied by the input file of the relevant program codes.

5.1 Electric Power System Evolution

5.1.1 The Dawn of Electric Power Systems

In its simplest form, an electric power system consists of an electric power generator, a distribution system consisting of one or more distribution lines connecting the generator to users, and some protection/maneuver devices (see Fig. 5.1). Nowadays, this simple configuration is used for off-grid power systems or microgrids operating under islanded conditions, but it is also the configuration that was employed for the first power systems built at the end of the nineteenth century to provide lighting in New York City [5.33].

The history of electric power systems is commonly considered to have begun in the year 1882, when a power station on Pearl Street in New York was inau-

gurated by Thomas Alva Edison (Fig. 5.2). This plant, which generated DC power using 175 HP high-speed steam engines, was designed to supply electrical energy to 400 lamps belonging to 82 customers in the business district of Wall Street.

The construction of the first power station was hugely important: although Volta had invented the first primary cell a century earlier, and more efficient primary cells had been constructed since then (such as the one devised by George Leclanché in 1865), these modest electrochemical power sources were not able to provide the amount of energy needed to power a whole district.

Immediately after the discovery of electromagnetic induction by Faraday in 1831, a variety of generators

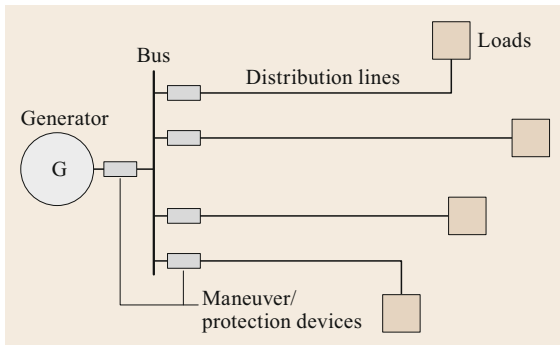


Fig. 5.1 The simplest configuration of an electric power system

were proposed. In 1869, not only was the first DC dynamo revealed in Vienna by Gramme and Pacinotti, but its working principle was also discovered to be reversible, resulting in the creation of the motor.

Furthermore, following the invention of the arc lamp by Foucault in 1841, it was subsequently improved by others until a satisfactory design was devised by Jablochkov in 1876. While the resulting lamp was suitable for generating the large luminous intensities required for public lighting (indeed, it was used along the Avenue de l'Opéra in Paris from 1879 to 1881), it was too bright for private use. Edison's lamp, consisting of a filament housed in a glass vacuum bulb, was far more appropriate for this purpose.

Thus, in summary, two types of light sources and two types of power sources (direct current and alternating current) were available in 1882, but the transformer was yet to be invented.

Table 5.1 summarizes the advances discussed above as well as subsequent developments that are discussed in the next section.

5.1.2 From the War of the Currents to the Twenty-First Century

There is no general consensus concerning the year in which the transformer was invented, although it seems fair to ascribe its invention to the Hungarian engineers Zipernowski, Blàthi, and Dèri in 1984. However, there is little doubt that the introduction of transformers was the factor that ultimately caused AC power systems to become more convenient and therefore popular than DC power systems, even though Edison was a passionate supporter of the use of DC (which is as convenient as AC for powering filament lamps, and more convenient than AC for powering arc lamps).

We now consider some of the main steps that shaped the evolution of power systems towards those that are used today. In 1889, René Thury developed the first commercial HVDC transmission system in Europe. This system used hydroturbines on the Gorzente River to supply Genoa in Italy. The generators were connected in series to attain the high transmission voltages needed. When loads were added to the system, more generators were added to maintain the voltage at the load. The first long-distance transmission of DC electricity in the US occurred in 1889 at Willamette Falls Station in Oregon. A flood destroyed this station in 1890, but it was quickly rebuilt, and the Falls Electric Company replaced the DC generators with experimental AC generators from Westinghouse in the same year. In 1896, the construction of the first AC generation and transmission system was completed at Niagara Falls using Westinghouse equipment. Nikola Tesla's work, such as his invention of the induction motor in 1888, helped to make AC power systems increasingly attractive. But the event that marked the success of alternating current was a few years before 1896: The Frankfurt ex-

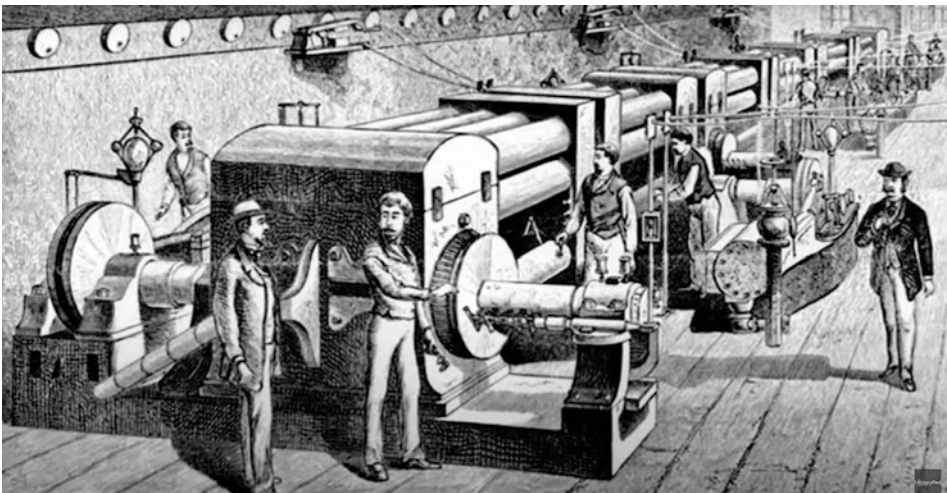


Fig. 5.2 Thomas Edison's power station on Pearl Street (adapted from [5.34])

Table 5.1 Key scientific advances and events (including dates and relevant scientists) that facilitated the development of power systems engineering

| Primary cells | Generators |
|----------------------------------|--|
| 1800 – Volta (pile) | 1831 – Faraday (electromagnetic (EM) induction) |
| 1830 – Grove (Zn-Pt) | 1832 – Pixii (rudimentary alternator) |
| 1841 – Bunsen (Zn-C) | 1856 – Siemens & Alliance |
| 1877 – Leclanché (Zn-Mn) | 1860 – Pacinotti (dynamo) |
| 1881 – Thiebaut and Gassner | 1869 – Gramme (dynamo) |
| Light sources (lamps) | Transformers, AC, and three-phase |
| 1841 – Foucault (first arc lamp) | 1884 – Zipernowski, Blàthi, and Dèri (transformer) |
| 1876 – Jablochkov (arc lamp) | 1888 – Ferraris (AC rotating field) |
| 1878 – Edison (1879 Menlo Park) | 1888 – Tesla (induction motor) |
| | 1889 – Blàthi (induction meter) |
| | 1891 – Dobrowolski (three-phase systems) |

hibition in August 1891: three-phase transmission line (42 Hz) at 25 000 V, which started from the hydroelectric plant built for a cement factory in Lauffen, on the Neckar river and with a distance of 175 km reached Frankfurt. Promoted by industrialists such as George Westinghouse, the major advantages of AC electric utility services soon became obvious, so DC systems declined in popularity towards the end of the nineteenth century. The advent of the transformer, three-phase circuits, and the induction motor all helped to drive the adoption of AC electric systems as the global standard [5.35].

There are objective advantages of operating electric power systems using AC rather than DC. First, only AC systems can make use of transformers, which allow the same power to be transported at higher voltages and lower current amplitudes—thus minimizing power losses and voltage drops along power lines—and different voltage levels to be used for generation, transmission, distribution, and utilization. With AC, it is possible to implement three-phase networks, allowing smooth, nonpulsating power flows and easy interruption of current in high-voltage equipment. Also, induction motors—which are inexpensive, rugged, and can serve most of the needs of industrial and residential users—can be employed with AC power systems. Further, the advent of steam turbines (which work best at high speeds) made AC generators highly advantageous, as

the commutators of DC motors and generators impose limitations on the voltage, size, and especially the speed of those machines.

Inventors such as Galileo Ferraris, Nicola Tesla, William Stanley, Michael von Dolivo-Dobrowolsky, Elihu Thomson, Lucien Gaulard, John Gibbs, and others working in Europe and North America all contributed to advances in AC technology. Much has been written about the so-called *War of the Currents* in the late 1880s, but it was more of a media fight; it was not a significant factor in the subsequent dominance of AC power systems [5.35]. The final decision on the type of system to be applied in a particular scenario has always been made based largely on technical aspects, and AC systems offered more advantages than DC systems given the system requirements and the technology available at that time. It should be noted, however, that although AC power systems have dominated around the world since the late nineteenth century, some DC distribution systems are still used in electric traction systems (trolley bus, railways, or subways). Also, some cities continued to use DC well into the twentieth century: Helsinki had a DC network until the late 1940s, Stockholm lost its dwindling DC network as late as the 1970s, London had some DC loads until 1981, and certain locations in Boston still used 110 V DC in the 1960s. The last DC circuit—a vestige of the nineteenth-century DC system of New York City—was shut down in 2007 [5.35].

5.2 Mission and Traditional Structure

The traditional mission of a power system is to provide electricity at the rated frequency and the rated voltage to customers. While the frequency is the same in all parts of the system, the rated voltage can differ depending on the part of the network of interest. The rated voltages of alternators located at power stations typically

range between 15 and 25 kV. Such voltages need to be substantially increased to 66–1000 kV or more by the step-up transformers that connect power stations to high-voltage (HV) and extra-high voltage (EHV) transmission networks (which are relatively well meshed) if the power is to be transmitted with minimal line losses

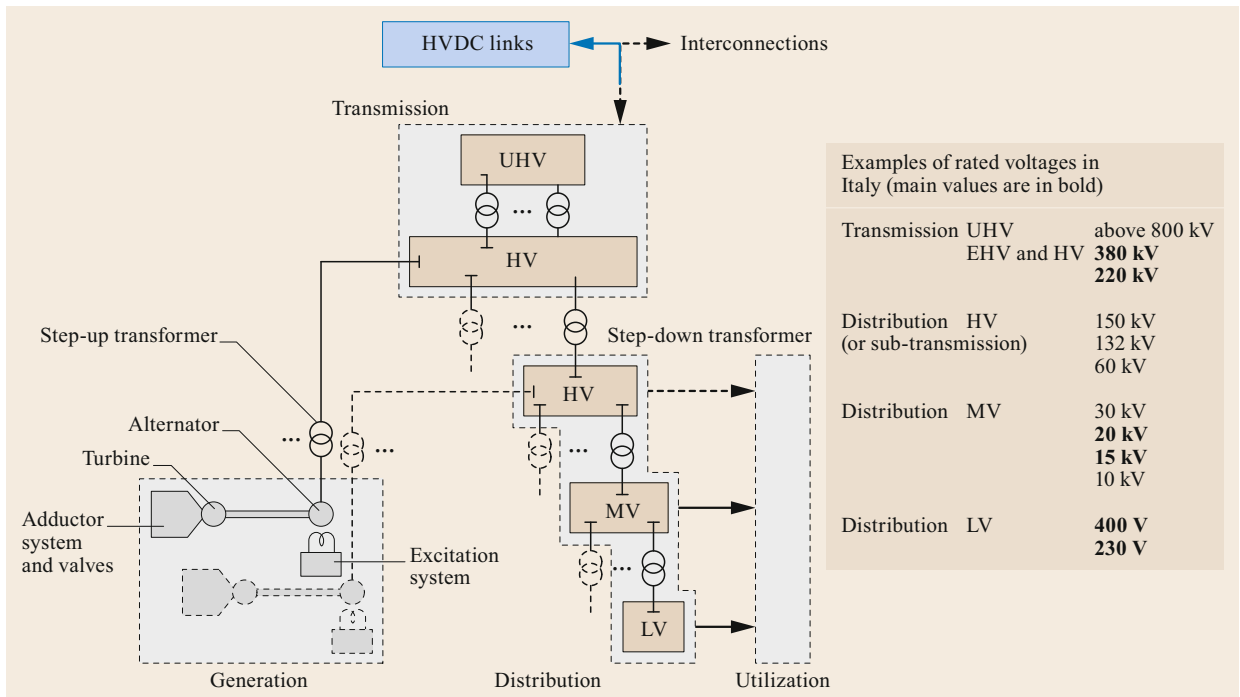


Fig. 5.3 Basic elements of an electric power system in its traditional form (EHV, HV, MV, and LV refer to extra-high, high, medium, and low voltage, respectively; adapted from [5.9])

and voltage drops. A single generic HV or EHV line of the transmission network carries hundreds or even thousands of megawatts, possibly in both directions, depending on its operating conditions. Very large power systems (e.g., those of neighboring countries) are generally interlinked through their transmission networks. In some cases, HVDC links are employed to interconnect systems that are not synchronized with each other, to transmit power over very long distances, and for long underground/submarine links. The high-voltage part of the network is then connected to the *high-voltage distribution network*, which is frequently referred to as the *subtransmission network*, to carry power towards a load area. The geographical extent of the subtransmission network depends on the user density in the load area (the power typically ranges from a few megawatts to tens of megawatts for each HV distribution line). Electric power is then carried to each user via *medium-voltage (MV) distribution networks*, where each line can carry around a megawatt of power, and by *low-voltage (LV) distribution networks*. Such a structure is depicted in Fig. 5.3, which also shows possible interconnections with other networks.

We now consider the power system scenario in Italy, which is representative of the situation in quite a few

other countries. The aim of the power system in Italy is to meet the demand for electricity 24 h a day, 365 days a year. This demand arises from:

- 700 HV users (20%)
- 100 000 MV users (35%)
- 35 000 000 LV users (20% domestic, 25% others).

Up to the end of the twentieth century, this aim was accomplished using a number of thermal power plants equipped with steam turbines driven by traditional fuels (coal, oil, gas, etc.) or with gas turbines and/or hydroelectric plants (with a reservoir or basin, or the fluent-water type). Over the last couple of decades, however, the increasing popularity of so-called *distributed generation*, which often utilizes renewable energy sources, has led to some significant changes to the traditional power system structure. In Italy, as well as in many other countries, a considerable amount of power has been connected to the distribution network (LV and MV). To realize large power values (e.g., larger than 10 MW), renewable energy sources (RESs) must be connected directly to the HV network, which is in turn interconnected to the synchronous grid of continental Europe. This structure is depicted in Fig. 5.4; note the presence of *microgrids*—small networks of electricity

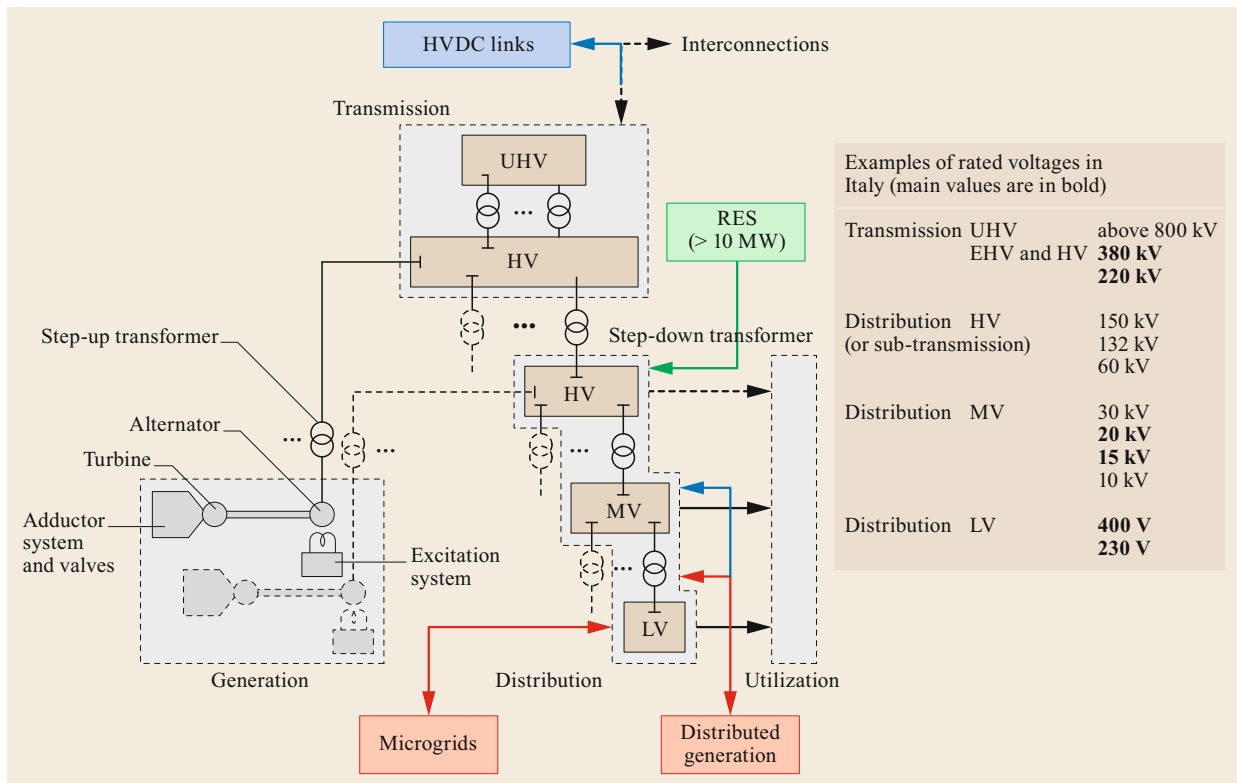


Fig. 5.4 Basic elements of a modern electric power system; note the inclusion of distributed generation, which is connected to the MV and LV distribution networks, as well as the presence of microgrids and a massive amount of renewable energy sources (RES) that is connected to the HV network (adapted from [5.9])

users with a local source—that are usually attached to the centralized national grid but are also able to function independently. The relatively complex operation of modern networks such as this will be briefly addressed in Sect. 5.9.

In Italy, there are over 560 000 power plants (including thermal, hydro, and RES plants), one transmission system operator – Terna (<https://www.terna.it>), which is part of the European Network of Transmission System Operators for Electricity, ENTSO-E –, and 150 entities that are involved in distribution.

If an electric power system is to accomplish its mission, a number of classical issues must be addressed:

- Planning
- Unit commitment and economic dispatch (according to market constraints)
- Power flow
- Fault analysis and protection system design
- Frequency control and voltage control
- Stability
- Insulation coordination and protection against the effects of lightning and overvoltages
- Power quality.

Due to its introductory nature, this chapter will ignore all aspects relating to the planning of power systems and those concerning the generation of power (i.e., traditional power station or RES generating plant design, operation and control, unit commitment, and economic dispatch). Nor are power system relays, insulation coordination, protection against overvoltages, and power quality covered here; most of these topics are dealt with in other chapters of this handbook.

In what follows, we shall focus on the fundamentals of transmission line theory in both the steady-state and transient regimes, on power flow and fault analysis, on stability assessment, and on frequency (and voltage) control, in order to impart the technical background required to understand and develop modern power systems as well as upcoming power systems (the topic covered in the last section of the chapter).

5.3 Transmission Line Equations in the Steady State

5.3.1 The Telegrapher's Equations

Let us consider a symmetrical, balanced, three-phase line in a sinusoidal steady state. By making these assumptions, we can refer to the positive-sequence single-phase equivalent model of the line. The relevant distributed parameter circuit is represented in Fig. 5.5. The infinitesimal element dx is located a distance x from the origin of the line. Therefore, the reference frame is oriented in the positive direction from the start of the line—where we can imagine a power source to be located (indicated by the subscript p)—to the end of the line, where the power arrives (indicated by the subscript a).

In Fig. 5.5, r and l are the resistance and inductance of the line per unit length, while c and g are the capacitance and conductance per unit length.

We define the primary parameters of the line as follows:

- *Longitudinal impedance* per unit length

$$\bar{z} = r + j\omega l \quad [\Omega \text{ m}^{-1}] \quad (5.1)$$

- *Transverse admittance* per unit length

$$\bar{y} = g + j\omega c \quad [\text{S m}^{-1}]. \quad (5.2)$$

Derivation and Integration of the Equations

Utilizing Steinmetz's symbolic notation and setting $e(x, j\omega) = \bar{E}_x$ and $i(x, j\omega) = \bar{I}_x$, the line equations can be derived by applying Kirchhoff's voltage law to the positive-oriented loop in Fig. 5.5, thus obtaining (5.3) below, and Kirchhoff's current law to the bus, thus obtaining (5.4). In these equations, higher-order infinitesimals are neglected.

$$\frac{d\bar{E}_x}{dx} + \bar{z}\bar{I}_x = 0 \quad (5.3)$$

$$\frac{d\bar{I}_x}{dx} + \bar{y}\bar{E}_x = 0. \quad (5.4)$$

Differentiating (5.3) and (5.4) with respect to x yields the differential equations

$$\frac{d^2\bar{E}_x}{dx^2} + \bar{z}\frac{d\bar{I}_x}{dx} = 0 \quad (5.5)$$

$$\frac{d^2\bar{I}_x}{dx^2} + \bar{y}\frac{d\bar{E}_x}{dx} = 0. \quad (5.6)$$

Upon combining (5.5) with (5.4) and (5.6) with (5.3), we obtain

$$\frac{d^2\bar{E}_x}{dx^2} - \bar{z}\bar{y}\bar{E}_x = 0 \quad (5.7)$$

$$\frac{d^2\bar{I}_x}{dx^2} - \bar{z}\bar{y}\bar{I}_x = 0. \quad (5.8)$$

We define the following secondary parameters of the line:

- *Propagation constant*

$$\bar{\gamma} = \sqrt{\bar{z}\bar{y}} = \alpha + j\beta = \sqrt{(r + j\omega l)(g + j\omega c)} \quad [\text{m}^{-1}] \quad (5.9)$$

- *Characteristic impedance*

$$\bar{Z}_0 = \sqrt{\frac{\bar{z}}{\bar{y}}} = \sqrt{\frac{r + j\omega l}{g + j\omega c}} \quad [\Omega]. \quad (5.10)$$

The real and imaginary parts of the characteristic impedance are the *attenuation constant* α and the *phase or distortion constant* β , which are given by the expres-

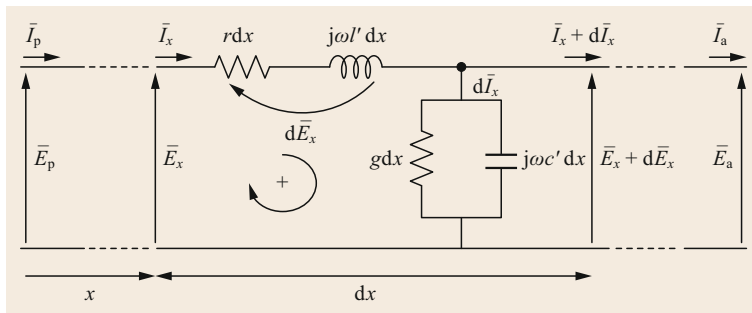


Fig. 5.5 Single-phase representation of a three-phase line in a symmetrical, balanced, sinusoidal steady state

sions

$$\alpha = \sqrt{\frac{1}{2} \left[\sqrt{(r^2 + \omega^2 l^2)(g^2 + \omega^2 c^2)} + rg - \omega^2 lc \right]} \quad (5.11)$$

$$\beta = \sqrt{\frac{1}{2} \left[\sqrt{(r^2 + \omega^2 l^2)(g^2 + \omega^2 c^2)} - rg + \omega^2 lc \right]} \quad (5.12)$$

It is worth noting that $\alpha = 0$ and $\beta = \omega \sqrt{lc}$ for a lossless line.

Under steady-state conditions and at a frequency of 50 Hz, typical values for the phase constant are as follows:

- Overhead line: $\beta = 1 \times 10^{-6} \text{ rad m}^{-1}$
- Cable line: $\beta = (3-5) \times 10^{-6} \text{ rad m}^{-1}$.

When there are losses, typical values for the attenuation constant are as follows:

- Overhead line: $\alpha = (0.05-0.5) \times 10^{-6} \text{ m}^{-1}$
- Cable line: $\alpha = (0.2-2) \times 10^{-6} \text{ m}^{-1}$.

If the primary line parameters are constant, the general integrals of (5.7) and (5.8) are

$$\bar{E}_x = \bar{K}_1 e^{\bar{\gamma}x} + \bar{K}_2 e^{-\bar{\gamma}x} \quad (5.13)$$

$$\bar{I}_x = \frac{1}{\bar{Z}_0} (-\bar{K}_1 e^{\bar{\gamma}x} + \bar{K}_2 e^{-\bar{\gamma}x}). \quad (5.14)$$

Alternatively, using hyperbolic functions, the solutions to (5.7) and (5.8) can be expressed as

$$\bar{E}_x = (\bar{C}_1 \cosh \bar{\gamma}x + \bar{C}_2 \sinh \bar{\gamma}x) \quad (5.15)$$

$$\bar{I}_x = \frac{1}{\bar{Z}_0} (-\bar{C}_1 \sinh \bar{\gamma}x - \bar{C}_2 \cosh \bar{\gamma}x). \quad (5.16)$$

The constants in (5.13)–(5.16) can be determined by setting appropriate boundary conditions; for instance, by fixing the conditions at the left termination of the line ($\bar{E}_x|_{x=0} = \bar{E}_p$ and $\bar{I}_x|_{x=0} = \bar{I}_p$).

If we impose these conditions and introduce (5.13) and (5.14), we obtain the system

$$\bar{E}_p = \bar{K}_1 + \bar{K}_2 \quad (5.17)$$

$$\bar{I}_p = \frac{1}{\bar{Z}_0} (-\bar{K}_1 + \bar{K}_2), \quad (5.18)$$

which yield

$$\bar{E}_x = \frac{1}{2} (\bar{E}_p - \bar{Z}_0 \bar{I}_p) e^{\bar{\gamma}x} + \frac{1}{2} (\bar{E}_p + \bar{Z}_0 \bar{I}_p) e^{-\bar{\gamma}x} \quad (5.19)$$

$$\bar{I}_x = \frac{1}{2} \left(\bar{I}_p - \frac{\bar{E}_p}{\bar{Z}_0} \right) e^{\bar{\gamma}x} + \frac{1}{2} \left(\bar{I}_p + \frac{\bar{E}_p}{\bar{Z}_0} \right) e^{-\bar{\gamma}x}. \quad (5.20)$$

On the other hand, if we use (5.15) and (5.16), we obtain

$$\bar{E}_p = \bar{C}_1 \quad (5.21)$$

$$\bar{I}_p = \frac{1}{\bar{Z}_0} (-\bar{C}_2), \quad (5.22)$$

which give

$$\bar{E}_x = \bar{E}_p \cosh \bar{\gamma}x - \bar{Z}_0 \bar{I}_p \sinh \bar{\gamma}x \quad (5.23)$$

$$\bar{I}_x = \bar{I}_p \cosh \bar{\gamma}x - \frac{\bar{E}_p}{\bar{Z}_0} \sinh \bar{\gamma}x. \quad (5.24)$$

It is worth noting that (5.19) and (5.20) are equivalent to (5.23) and (5.24), respectively.

Choosing a reference frame oriented in the opposite direction (i.e., with x increasing from the right terminal of the line to the left), the solutions to the line equations can be expressed by introducing a change of variable of the type $\tilde{x} = -x$ into (5.19) and (5.20). Moreover, the boundary conditions for the left-hand side of the line ($x = 0$) become $\bar{E}_x|_{x=0} = \bar{E}_a$ and $\bar{I}_x|_{x=0} = \bar{I}_a$, leading to the equations

$$\bar{E}_x = \frac{1}{2} (\bar{E}_a + \bar{Z}_0 \bar{I}_a) e^{\bar{\gamma}x} + \frac{1}{2} (\bar{E}_a - \bar{Z}_0 \bar{I}_a) e^{-\bar{\gamma}x} \quad (5.25)$$

$$\bar{I}_x = \frac{1}{2} \left(\bar{I}_a + \frac{\bar{E}_a}{\bar{Z}_0} \right) e^{\bar{\gamma}x} + \frac{1}{2} \left(\bar{I}_a - \frac{\bar{E}_a}{\bar{Z}_0} \right) e^{-\bar{\gamma}x}. \quad (5.26)$$

Using hyperbolic functions, the expressions become

$$\bar{E}_x = \bar{E}_a \cosh \bar{\gamma}x + \bar{Z}_0 \bar{I}_a \sinh \bar{\gamma}x \quad (5.27)$$

$$\bar{I}_x = \bar{I}_a \cosh \bar{\gamma}x + \frac{\bar{E}_a}{\bar{Z}_0} \sinh \bar{\gamma}x. \quad (5.28)$$

Direct and Inverse Waves

Let us consider the solutions to the line equations (5.25) and (5.26), where the positive x direction is oriented from the load to the generator (from right to the left). These equations show that either the voltage distribution or the current distribution can be considered the

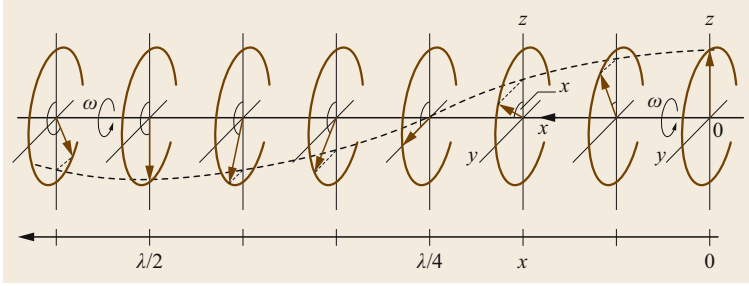


Fig. 5.6 Voltage distribution along an infinitely long lossless line in the steady state and at 50 Hz (adapted from [5.36])

result of two components. The first component, proportional to $e^{\bar{\gamma}x}$, is called the *direct wave*, which increases in the positive x direction. The second component, proportional to $e^{-\bar{\gamma}x}$, is called the *inverse wave* and decreases in the positive x direction. Similar considerations are valid for (5.27) and (5.28), where the positive x direction is oriented from the generator to the load.

With reference to (5.25), we set

$$\bar{E}_d = \frac{\bar{E}_a + \bar{Z}_0 \bar{I}_a}{2} \quad (5.29)$$

$$\bar{E}_r = \frac{\bar{E}_a - \bar{Z}_0 \bar{I}_a}{2}, \quad (5.30)$$

where the symbols have obvious meanings. The voltage at a generic point x along the line can then be expressed as

$$\bar{E}_x = \bar{E}_d e^{\bar{\gamma}x} + \bar{E}_r e^{-\bar{\gamma}x}. \quad (5.31)$$

The superposition of the direct and inverse waves determines the line operation and consequently the voltage and current distributions along the whole line.

Intuitively, all of these considerations for the voltage can also be applied to the current, which leads us to

$$\bar{I}_x = \frac{\bar{E}_d}{\bar{Z}_0} e^{\bar{\gamma}x} - \frac{\bar{E}_r}{\bar{Z}_0} e^{-\bar{\gamma}x}. \quad (5.32)$$

Finally, it should be noted that the inverse wave (i.e., the second terms of (5.19) and (5.20) or (5.25) and (5.26)) is equal to zero in the case of an infinitely long line.

Propagation Wavelength and Propagation Speed

Let us consider the voltage distribution along a lossless line of infinite length under steady-state conditions and a frequency of 50 Hz. The propagation wavelength is defined as the distance λ such that

$$\lambda\beta = 2\pi \Rightarrow \lambda = \frac{2\pi}{\beta} \quad [\text{m}], \quad (5.33)$$

i.e., such that two measured voltage phasors separated by a distance of λ are in phase (i.e., the distance between two consecutive maxima in Fig. 5.6).

In the additional material for this chapter, there is an animation that demonstrates the voltage and current propagation (sinusoidal waveforms at the utility frequency) for a matched line and for a line terminated at a resistance that differs from the characteristic impedance.

The wave propagation speed as a function of the frequency f is

$$v = \lambda f = \frac{2\pi f}{\beta} = \frac{\omega}{\beta} \quad [\text{m s}^{-1}]. \quad (5.34)$$

For a lossless overhead line, the propagation speed is

$$v_a = \frac{\omega}{\beta} = \frac{1}{\sqrt{LC}} = \frac{1}{\sqrt{\mu_0 \epsilon_0}} = 3 \times 10^8 \quad [\text{m s}^{-1}]. \quad (5.35)$$

Therefore, the propagation speed is equal to the speed of light in vacuum and is not dependent on the line geometry. If losses cannot be ignored, the speed will be slightly lower.

The wavelength is inversely proportional to the frequency, so

$$\text{At 50 Hz: } \lambda_a = \frac{v}{f} = \frac{3 \times 10^8}{50} = 6 \times 10^6 \text{ m}$$

$$\text{At 60 Hz: } \lambda_a = \frac{v}{f} = \frac{3 \times 10^8}{60} = 5 \times 10^6 \text{ m}.$$

If losses are considered, these values will be slightly lower.

For a lossless cable line with a relative permittivity $\epsilon_r = 3.5$, the propagation speed and wavelength are calculated as

$$v_c = \frac{1}{\sqrt{3.5\mu_0\epsilon_0}} = 1.6 \times 10^8 \quad [\text{m s}^{-1}] \quad (5.36)$$

$$\lambda_c = \frac{v_c}{f} = \frac{1.6 \times 10^8}{50} = 3.2 \times 10^6 \quad [\text{m}]. \quad (5.37)$$

Let us consider a voltage wave with a generic profile for a generic angular frequency ω . If the Heaviside condition $r/g = l/c$ is respected, then $\alpha = \sqrt{rg}$ and $\beta = \omega\sqrt{lc}$, therefore $v = 1/\sqrt{lc}$, which means that both α and v are independent of ω ; the transmitted voltage waveform along the line is not distorted, only attenuated. Although this fact is not relevant for power transmission lines at the utility frequency, it is important for telecommunication lines.

Line Terminated with its Characteristic Impedance

Let us now consider a line with a load equal to the characteristic impedance \bar{Z}_0 , such that

$$\bar{Z}_2 = \frac{\bar{E}_a}{\bar{I}_a} = \bar{Z}_0. \tag{5.38}$$

In this case, we obtain the important relationships

$$\begin{cases} \bar{E}_x = \bar{E}_a e^{\bar{y}x} \\ \bar{I}_x = \bar{I}_a e^{\bar{y}x} \\ \frac{\bar{E}_x}{\bar{I}_x} = \frac{\bar{E}_a}{\bar{I}_a} = \bar{Z}_0. \end{cases} \tag{5.39}$$

The propagation of voltage and current waves along a line that terminates on its characteristic impedance is equivalent to the case in which the line is infinitely long, since the ratio of the voltage to the current is the same at every point along the line. As a consequence, voltage and current waves that are directed to the load are not affected by any reflection.

For a lossless line, the characteristic impedance is a real quantity, and its value is expressed as

$$\bar{Z}_0 = \sqrt{\frac{l}{c}}. \tag{5.40}$$

In this particular case, the characteristic impedance is called the *surge impedance*.

Figures 5.7 and 5.8 show the value of the surge impedance in some practical cases.

Natural Power

The complex power at the termination in the case where the line terminates on its characteristic impedance is given by

$$\begin{aligned} \bar{S}_{0a} &= P_{0a} + jQ_{0a} = 3\bar{E}_a\bar{I}_a^* = 3\bar{E}_a\frac{\bar{E}_a^*}{\bar{Z}_a} \\ &= \frac{V_a^2}{Z_0(\cos\psi - j\sin\psi)} = \frac{V_a^2}{Z_0}(\cos\psi + j\sin\psi). \end{aligned} \tag{5.41}$$

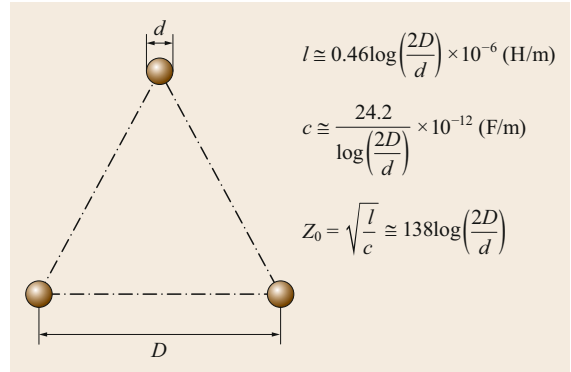


Fig. 5.7 Formulas for the positive sequence line parameters of lossless overhead transmission lines

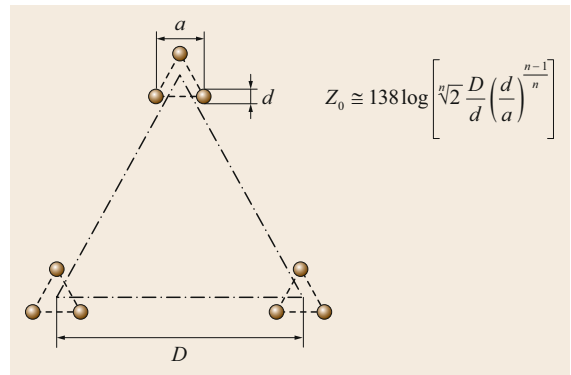


Fig. 5.8 Formulas for the positive sequence line parameters of lossless overhead transmission lines with bundle conductors

For a lossless line, we obtain

$$P_0 = \frac{V_a^2}{Z_0}, \tag{5.42}$$

which is called the *natural power*.

Under these conditions, the line transmits active power to the load without absorbing reactive power (the power factor is equal to 1), i.e.,

$$Z_0^2 = \frac{E_x^2}{I_x^2} = \frac{\omega dx}{\omega c dx}. \tag{5.43}$$

For each infinitesimal element of the line, we can observe that

$$\omega dx I_x^2 = \omega c dx E_x^2. \tag{5.44}$$

This equation gives perfect compensation between the electromagnetic energy and the electrostatic energy of the line (i.e., the line is compensated regarding the reactive power). Therefore, the voltage magnitude is

Table 5.2 Typical surge impedance and characteristic power values for overhead lines

| Voltage (kV) | Overhead line | |
|--------------|---------------|------------|
| | Z_0 (P) | P_0 (MW) |
| 20 | 400 | 1 |
| 50 | 400 | 6 |
| 132 | 400 | 44 |
| 220 | 390 | 124 |
| 380 | 260 | 560 |
| 700 | 240 | 2000 |
| 1000 | 240 | ≈ 4000 |

constant along the line. This represents ideal operating conditions for an overhead line (not for a cable line, as surge impedances are one order of magnitude lower in that case, so current values would be too high). Table 5.2 shows typical values of the surge impedance and characteristic power for overhead lines.

5.3.2 The Line as a Two-Port Network

A single conductor line in steady state can be represented as two port passive network as shown in Fig. 5.9, therefore voltage and currents at one port can be expressed as

$$\begin{aligned} \bar{E}_p &= \bar{A}\bar{E}_a + \bar{B}\bar{I}_a \\ \bar{I}_p &= \bar{C}\bar{E}_a + \bar{D}\bar{I}_a. \end{aligned} \tag{5.45}$$

The system considered has two degrees of freedom, which are characterized by two independent relationships between four quantities (voltages and currents) that identify the electric states of the two pairs of terminals.

Using hyperbolic functions, the constants \bar{A} , \bar{B} , \bar{C} , and \bar{D} can be expressed as

$$\begin{cases} \bar{A} = \bar{D} = \cosh \bar{\gamma}L \\ \bar{B} = \bar{Z}_0 \sinh \bar{\gamma}L \\ \bar{C} = \frac{1}{\bar{Z}_0} \sinh \bar{\gamma}L. \end{cases} \tag{5.46}$$

The constants \bar{A} , \bar{B} , \bar{C} , and \bar{D} are called *chain matrix parameters*. It is easy to verify that the two-port network is symmetric ($\bar{A} = \bar{D}$) and reciprocal ($\bar{A}\bar{D} - \bar{B}\bar{C} = 1$).

The chain matrix parameters have the following characteristics:

- Constant \bar{A} : the ratio between the input and output voltages of the open line or between the input and output currents of the short-circuited line. This constant is a pure number and can be expressed via

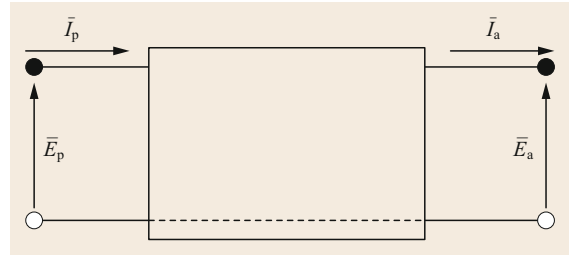


Fig. 5.9 Two-port network representation of a transmission line

the Cartesian coordinates $a_1 + ja_2$ ($a_1 < 1; a_2 \ll 1$) or the polar coordinates $Ae^{j\alpha_A}$.

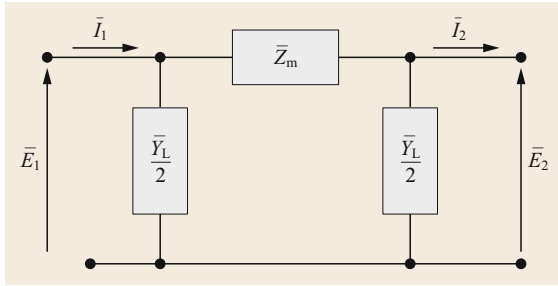
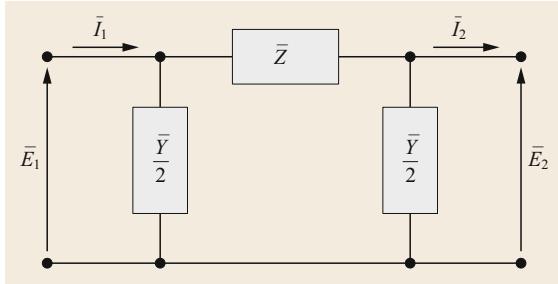
- Constant \bar{B} : the ratio of the input voltage to the output current of the short-circuited line. This ratio has the dimensions of an impedance and can be expressed via the Cartesian coordinates $b_1 + jb_2$ ($b_1 \approx rL = R; b_2 \approx xL = X$) or the polar coordinates $Be^{j\beta_B}$ ($\bar{B} \approx \bar{Z}$, the total longitudinal impedance of the line).
- Constant \bar{C} : the ratio between the input current and the output voltage of the open line. It has the dimensions of an admittance and can be expressed via the Cartesian coordinates $c_1 + jc_2$ (c_1 is really small and usually negative when the line is really long, and $c_2 \approx B$ is the susceptance of admittance Y) or the polar coordinates $Ce^{j\gamma_C}$ ($\bar{C} \approx \bar{Y}$, the total transverse admittance of the line). A passive reciprocal two-port network can always be represented by three impedances or admittances that are connected to form a Π circuit, as represented in Fig. 5.10, or a T circuit. The equations relevant to the equivalent π circuit of a generic line are

$$\begin{aligned} \bar{Y}_L &= \bar{Y} \frac{\tanh(\bar{\gamma}L/2)}{\bar{\gamma}L/2} \\ \bar{Z}_m &= \bar{Z} \frac{\sinh \bar{\gamma}L}{\bar{\gamma}L}. \end{aligned} \tag{5.47}$$

For lines with typical lengths (i.e., $50 \text{ km} < L < 200 \text{ km}$) in the steady state, we can assume that $\sinh \bar{\gamma}L \approx \bar{\gamma}L$ and $\tanh(\bar{\gamma}L/2) \approx \bar{\gamma}L/2$, which in turn yield

$$\begin{aligned} \bar{Y}_a &= \bar{Y}_b = \bar{Y} \\ \bar{Z}_m &= \bar{Z}. \end{aligned} \tag{5.48}$$

In this case the calculation of the parameters of the equivalent circuit is simplified, as shown in Fig. 5.11.

Fig. 5.10 Equivalent Π circuit of a transmission lineFig. 5.11 Equivalent Π circuit of a short transmission line

5.3.3 Transmitted Active and Reactive Power Expressions

Let us consider the equations

$$\begin{aligned}\bar{E}_p &= \bar{A}\bar{E}_a + \bar{B}\bar{I}_a \\ \bar{I}_p &= \bar{C}\bar{E}_a + \bar{D}\bar{I}_a\end{aligned}\quad (5.49)$$

which are relevant to the phasor diagram of Fig. 5.12. This phasor diagram is known as a Perrine–Baum diagram.

When the line is open, we can see that $E_p < E_a$ (known as the Ferranti effect).

The voltage drop along the line varies with the load; e.g.,

$$\begin{aligned}P_a + jQ_a(R) &\rightarrow \text{voltage drop} = 21\% \\ P_a(R') &\rightarrow \text{voltage drop} = 6\%.\end{aligned}$$

In order to compensate for the voltage drop by keeping the absorbed active power P_a constant, it is necessary to ensure that the end of phasor E_p coincides with R'' . In this configuration, the load has to be capacitive. We should therefore generate the reactive power $Q = RR''$ at the end of the line. The fraction RR' is absorbed by the load, while the fraction $R'R''$ is necessary to compensate for the reactive power absorbed by the line.

Some Remarks on the Transmitted Active and Reactive Power

The absolute value of the complex power at the end of the line is (superscript * for phasors denotes their conjugate)

$$\bar{S}_a = P_a + jQ_a = 3\bar{E}_a\bar{I}_a^* \quad (5.50)$$

Observing that

$$\begin{aligned}\bar{E}_p &= \bar{A}\bar{E}_a + \bar{B}\bar{I}_a \Rightarrow \bar{I}_a = \frac{\bar{E}_p - \bar{A}\bar{E}_a}{\bar{B}} \\ \Rightarrow \bar{S}_a &= 3\bar{E}_a \left(\frac{\bar{E}_p - \bar{A}\bar{E}_a}{\bar{B}^*} \right),\end{aligned}\quad (5.51)$$

assuming that \bar{E}_a is real, and introducing θ as the phase difference between \bar{E}_p and \bar{E}_a , we obtain

$$\begin{aligned}\bar{S}_a &= P_a + jQ_a = 3 \frac{\bar{E}_a \bar{E}_p^*}{\bar{B}^*} - 3 \frac{\bar{E}_a \bar{E}_a \bar{A}^*}{\bar{B}^*} \\ &= 3 \frac{E_a E_p}{B} \frac{e^{-j\theta}}{e^{-j\beta_B}} - 3 \frac{E_a^2 A}{B} \frac{e^{-j\alpha_A}}{e^{-j\beta_B}} \\ &= 3 \frac{E_a E_p}{B} e^{j(\beta_B - \theta)} - 3 E_a^2 \frac{A}{B} e^{j(\beta_B - \alpha_A)} \\ &= \frac{3E_a E_p}{B} \cos(\beta_B - \theta) - 3E_a^2 \frac{A}{B} \cos(\beta_B - \alpha_A) \\ &\quad + j \left[\frac{3E_a E_p}{B} \sin(\beta_B - \theta) - 3E_a^2 \frac{A}{B} \sin(\beta_B - \alpha_A) \right].\end{aligned}\quad (5.52)$$

Therefore,

$$P_a = \frac{3E_a E_p}{B} \cos(\beta_B - \theta) - 3E_a^2 \frac{A}{B} \cos(\beta_B - \alpha_A) \quad (5.53)$$

$$Q_a = \frac{3E_a E_p}{B} \sin(\beta_B - \theta) - 3E_a^2 \frac{A}{B} \sin(\beta_B - \alpha_A) \quad (5.54)$$

$$P_p = -\frac{3E_a E_p}{B} \cos(\beta_B + \theta) + 3E_p^2 \frac{A}{B} \cos(\beta_B - \alpha_A) \quad (5.55)$$

$$Q_p = -\frac{3E_a E_p}{B} \sin(\beta_B + \theta) + 3E_p^2 \frac{A}{B} \sin(\beta_B - \alpha_A). \quad (5.56)$$

If the line is lossless and transverse capacities are neglected ($\alpha_A = 0$, $A = 1$, $\beta_B = \pi/2$, and $B = X$), the expressions assume the simplified forms

$$P_p = P_a = \frac{3E_p E_a}{X} \sin \theta \quad (5.57)$$

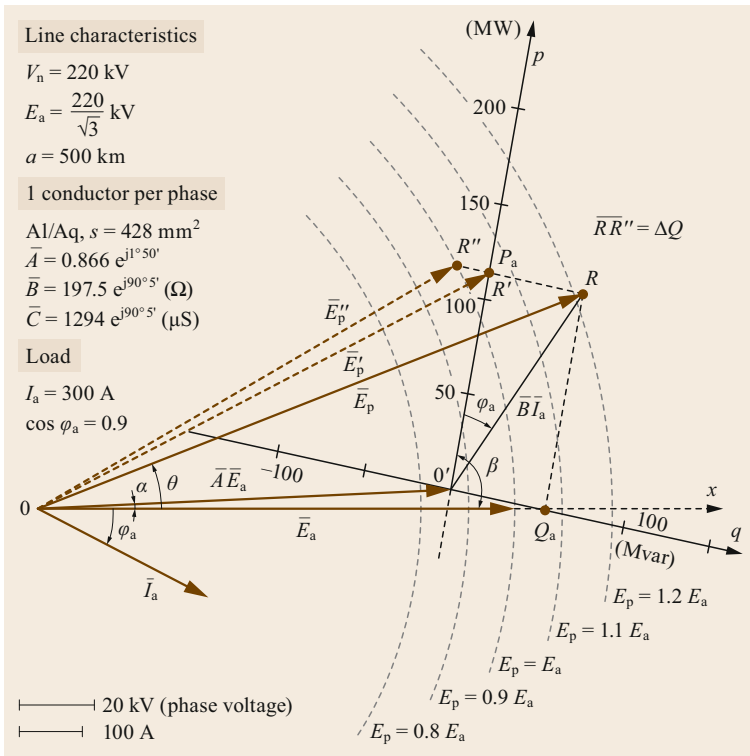


Fig. 5.12 Perrine–Baum diagram (adapted from [5.3])

$$P_p = P_a = \frac{3E_p E_a}{X} \sin \theta \tag{5.58}$$

$$Q_a = \frac{3E_a}{X} (E_p \cos \theta - E_a) \tag{5.59}$$

$$Q_p = \frac{3E_p}{X} (E_p - E_a \cos \theta), \tag{5.60}$$

which leads us to conclude that:

- The active power flow P is proportional to the sine of the phase shift θ (i.e., the difference between the voltage phases of the line terminals).
- The reactive power flow Q is proportional to the difference between the magnitudes of the voltages at the line terminals, and the sign of Q also depends on that difference. Note that the function $\cos \theta$ does not vary much for small values of the argument (typically, $\theta = 10\text{--}25^\circ$).

5.4 Load Flow

5.4.1 From the Real Network to the Admittance Matrix

A classical transmission network essentially comprises:

- *Buses*, which may be divided into *generation buses* (corresponding to the terminals of the alternators or, in general, the electric power sources), *reactive compensation buses* (corresponding to synchronous and static compensator terminals), *interconnection buses* (where many lines are connected to each other), and *load buses* (which supply the equivalent loads seen by the high-voltage network)
- *Capacitor banks*
- *Transformers*

- *Reactors*
- *Lines*; either overhead lines or cable lines that connect the various buses.

The study can be simplified by focusing only on the high-voltage part of the network and assuming that the parts at lower voltages, namely the distribution network, can be represented by their equivalent concentrated loads. Even so, the network is remarkably complex; for example, the Italian 380–220 kV network shown in Figs. 5.13 and 5.14 contains hundreds of buses, while the inclusion of the 132 kV network boosts this up to a thousand buses.

For the load flow study (also commonly denoted as power flow study) a number of assumptions are made.



Fig. 5.13 Italian 380 kV network on 31.12.2018 (<https://www.terna.it>)

The three-phase symmetric and balanced network is in its steady state; the parameters and the configuration of the system as well as the load power request are considered to be constant. We also assume all the electric components are linear. All voltages, power flows, and impedances will be represented by their per-unit values. The active power injected by the generators at the buses is known.

Based on these assumptions, the load flow problem consists of determining the real and reactive power flowing in various components of the network (lines and transformers) under steady-state conditions. As the structure of the system and the values of the admittances of the network are known, the real and reactive power flow on each branch as well as the reactive power output of the generators can be determined analytically once the bus voltages are known. For this reason, the goal of a load-flow study is to determine voltage phase and magnitude values for each bus of a power system.

There are several reasons we need load-flow studies:

(a) To determine—on a daily basis, or more precisely every quarter of an hour—the network operating

conditions that best satisfy the required load under secure conditions and with the minimum operational cost

- (b) To plan the expansion of a power system (either *long- or medium-term planning*, in which plans are made for 5–15 years into the future, or *short-term planning*, in which the plans are made for 1–3 years ahead)
- (c) To monitor and control the network in *real time*.

Nodal Analysis of the Network

Nodal analysis of the network involves determining the voltages at the various nodes (buses) of the network in terms of the branch currents. It is important to bear in mind that each component of the network can be replaced by its n -port representation, as shown in Fig. 5.15.

Using the assumptions mentioned above, let us consider a generic bus of a network containing $n + 1$ buses, including g generation buses and u load buses, as shown in Fig. 5.16. Conductor $n + 1$ is the reference bus or *neutral*. Note that buses that are neither generation nor load buses (interconnection buses) can be seen as either

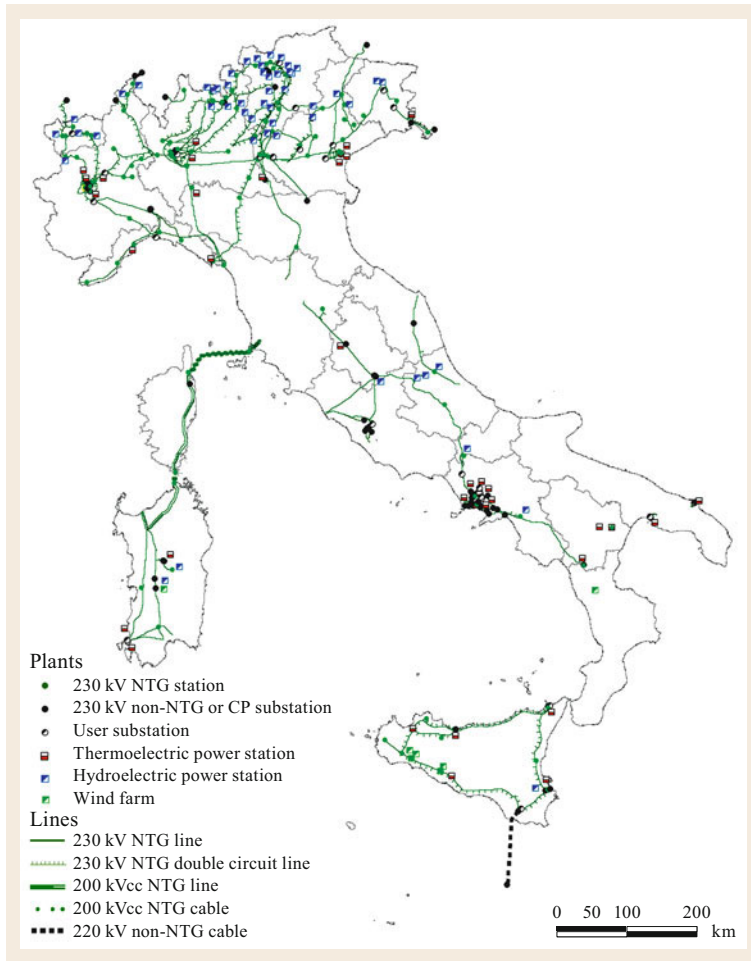


Fig. 5.14 Italian 230 kV network on 31.12.2018 (<https://www.terna.it>)

generation or load buses with zero active and reactive power injected or absorbed, respectively. The total number of buses in the network, $n + 1$, is not necessarily equal to $g + u + 1$, as we need to have at least one bus that is not a generation or load bus. The network consists of m branches, each of which is characterized by a single linear admittance.

For the generic bus, or node i , we shall make use of the following notation:

- E_i is the bus voltage
- I_i is the nodal current (i.e., the current supplied by the generator or absorbed by the load connected to the bus)
- I_{ij} is the current flowing in the branch that connects node i to node j
- y_{ij} is the admittance between nodes i and j
- y_{i0} is the sum of all the admittances between the i th node and the neutral.

For the currents flowing in the branches connected to node i , we get

$$\begin{cases} \bar{I}_{i0} = \bar{y}_{i0} \bar{E}_i \\ \bar{I}_{i1} = \bar{y}_{i1} (\bar{E}_i - \bar{E}_1) \\ \vdots \\ \bar{I}_{in} = \bar{y}_{in} (\bar{E}_i - \bar{E}_n), \end{cases} \quad (5.61)$$

and by using the Kirchoff law, we obtain

$$\begin{aligned} \bar{I}_i &= \bar{y}_{i0} \bar{E}_i + \bar{y}_{i1} (\bar{E}_i - \bar{E}_1) + \cdots + \bar{y}_{in} (\bar{E}_i - \bar{E}_n) \\ &= (\bar{y}_{i0} + \bar{y}_{i1} + \cdots + \bar{y}_{in}) \bar{E}_i - \bar{y}_{i1} \bar{E}_1 - \cdots - \bar{y}_{in} \bar{E}_n \\ &= (\bar{y}_{i0} + \bar{y}_{i1} + \cdots + \bar{y}_{in}) \bar{E}_i - \sum_{\substack{h=1 \\ h \neq i}}^n \bar{y}_{ih} \bar{E}_h. \end{aligned} \quad (5.62)$$

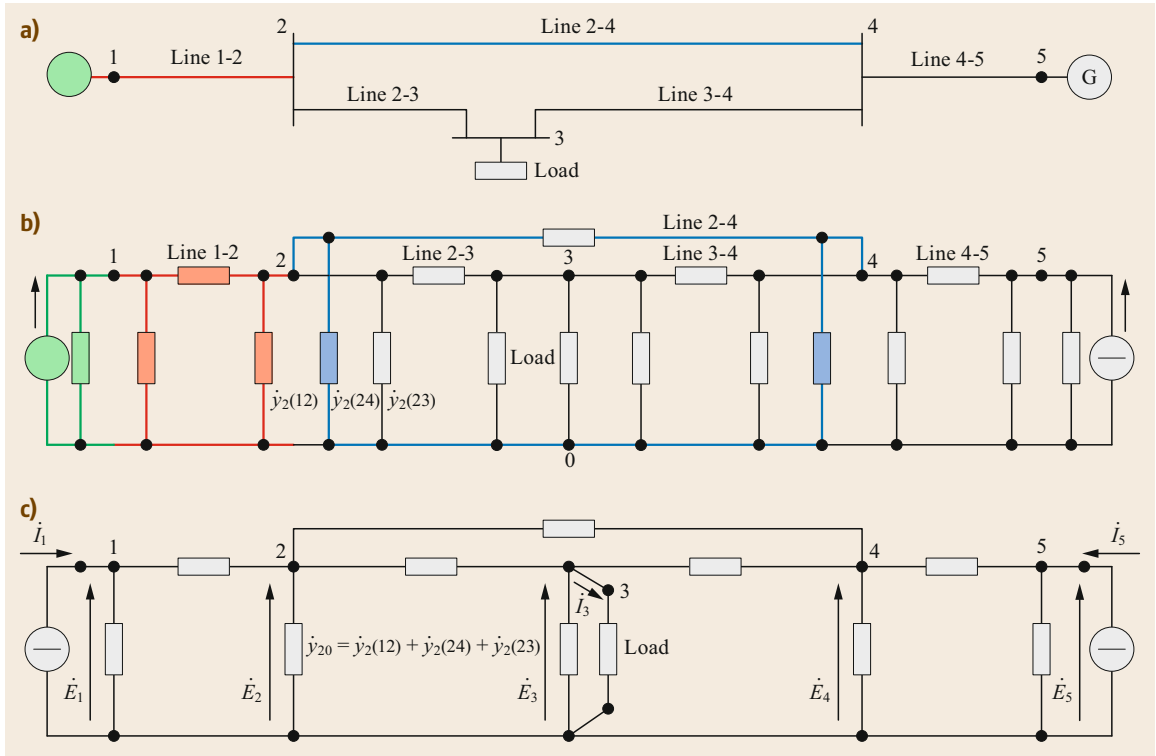


Fig. 5.15 (a) One-line diagram of a three-bus power network (buses 3, 4, and 5) with two generators (connected at buses 1 and 5) that supply one equivalent load impedance (connected at bus 3). (b) Relevant circuit representation where each generator is represented by its Norton equivalent one-port circuit and each line is represented by its two-port p equivalent circuit, and (c) simplified version of this circuit in which line admittances connected to the same bus have been added to each other. Voltage, current, and admittance symbols with dots are complex quantities (adapted from [5.2])

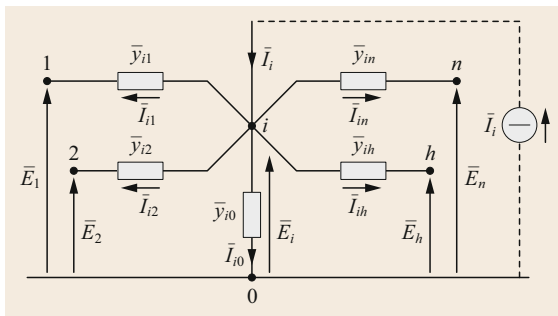


Fig. 5.16 Network presentation used for nodal analysis

Setting

$$\begin{aligned} \bar{Y}_{ii} &= \bar{y}_{i0} + \bar{y}_{i1} + \dots + \bar{y}_{in} = \sum_{h=0}^n \bar{y}_{ih} \\ \bar{Y}_{i1} &= -\bar{y}_{i1} \\ &\vdots \\ \bar{Y}_{in} &= -\bar{y}_{in}, \end{aligned} \tag{5.63}$$

we get

$$\begin{aligned} \bar{I}_i &= \bar{Y}_{i1}\bar{E}_1 + \bar{Y}_{i2}\bar{E}_2 + \dots + \bar{Y}_{ii}\bar{E}_i + \dots + \bar{Y}_{in}\bar{E}_n \\ &= \sum_{h=1}^n \bar{Y}_{ih}\bar{E}_h \end{aligned} \tag{5.64}$$

and, analogously for the other buses,

$$\begin{cases} \bar{I}_1 = \bar{Y}_{11}\bar{E}_1 + \dots + \bar{Y}_{1h}\bar{E}_h + \dots + \bar{Y}_{1n}\bar{E}_n \\ \vdots \\ \bar{I}_h = \bar{Y}_{h1}\bar{E}_1 + \dots + \bar{Y}_{hh}\bar{E}_h + \dots + \bar{Y}_{hn}\bar{E}_n \\ \vdots \\ \bar{I}_n = \bar{Y}_{n1}\bar{E}_1 + \dots + \bar{Y}_{nh}\bar{E}_h + \dots + \bar{Y}_{nn}\bar{E}_n. \end{cases} \tag{5.65}$$

These equations can be conveniently written in matrix form as

$$\begin{bmatrix} \bar{I}_1 \\ \vdots \\ \bar{I}_h \\ \vdots \\ \bar{I}_n \end{bmatrix} = \begin{bmatrix} \bar{Y}_{11} & \dots & \bar{Y}_{1h} & \dots & \bar{Y}_{1n} \\ \vdots & \vdots & \vdots & \vdots & \vdots \\ \bar{Y}_{h1} & \dots & \bar{Y}_{hh} & \dots & \bar{Y}_{hn} \\ \vdots & \vdots & \vdots & \vdots & \vdots \\ \bar{Y}_{n1} & \dots & \bar{Y}_{nh} & \dots & \bar{Y}_{nn} \end{bmatrix} \cdot \begin{bmatrix} \bar{E}_1 \\ \vdots \\ \bar{E}_h \\ \vdots \\ \bar{E}_n \end{bmatrix}. \quad (5.66)$$

Using a compact notation, we get

$$[\mathbf{I}] = [\mathbf{Y}] [\mathbf{E}], \quad (5.67)$$

where $\bar{\mathbf{Y}}$ is the *admittance matrix* of the network.

The elements of $\bar{\mathbf{Y}}$ satisfy a number of conditions (see also (5.63)), as follows.

The off-diagonal elements \bar{Y}_{ij} are called *mutual admittances* of the buses, and each equals the negative of the sum of all admittances connected directly between the buses i and j , i.e.,

$$\bar{Y}_{ij} = -\bar{y}_{ij} = \bar{I}_i \Big|_{\substack{\bar{E}_j=1 \\ \bar{E}_h=0 \forall h \neq j}}. \quad (5.68)$$

The diagonal elements \bar{Y}_{ii} are called *self-admittances* of the buses, and each equals the sum of all the admittances connected to the buses identified by double subscripts, i.e.,

$$\bar{Y}_{ii} = \bar{y}_{i0} + \sum \bar{y}_{ij} = \bar{I}_i \Big|_{\substack{\bar{E}_i=1 \\ \bar{E}_j=0 \forall j \neq i}}. \quad (5.69)$$

The calculation of the admittance matrix is demonstrated as an exercise in the supplementary material for this chapter.

Admittance Matrix Update

The previous equations provide the relationship between the bus impedance and the admittance matrix. However, it is possible for the topology of the power system to change due to the connection or disconnection of a line, a transformer, etc. Below, we show that it is not necessary to redetermine the admittance matrix from scratch in this case. Before doing so, however, we examine the three basic changes that can occur to an n -bus network:

1. *The addition of bus $n+1$, which is connected to the generic bus k with an admittance $\bar{y}_{n+1,k}$.*

The updated matrix order is now $n+1$.

Bus k is the only bus adjacent to the new bus. Therefore, the only change in the matrix is the k th self-admittance.

By denoting the parameters of the updated matrix with a prime symbol, we get

$$\begin{aligned} \bar{Y}'_{k,k} &= \bar{Y}_{k,k} + \bar{y}_{n+1,k} \\ \bar{Y}'_{n+1,n+1} &= \bar{y}_{n+1,k} \\ \bar{Y}'_{n+1,k} &= \bar{Y}'_{k,n+1} = -\bar{y}_{n+1,k}. \end{aligned} \quad (5.70)$$

All the other elements of the $(n+1)$ th row and column of matrix $[\bar{\mathbf{Y}}']$ are equal to zero.

2. *The addition of an admittance $\bar{y}^*_{k,0}$ from an existing bus k to the reference bus.*

In this case, the matrix order does not change. The only term that must be updated is the self-admittance of bus k , i.e.,

$$\bar{Y}'_{k,k} = \bar{Y}_{k,k} + \bar{y}^*_{k,0}. \quad (5.71)$$

3. *The addition of an admittance $\bar{y}^*_{k,i}$ between two generic buses k and i .*

Again, the matrix order does not change; the only terms that need to be updated are the self-admittances of buses k and i and their relative mutual admittances such that

$$\begin{aligned} \bar{Y}'_{k,k} &= \bar{Y}_{k,k} + \bar{y}^*_{k,i} \\ \bar{Y}'_{i,i} &= \bar{Y}_{i,i} + \bar{y}^*_{k,i} \\ \bar{Y}'_{k,i} &= \bar{Y}'_{i,k} = \bar{Y}_{i,k} - \bar{y}^*_{k,i}. \end{aligned} \quad (5.72)$$

When appropriately combined and repeated, the three basic operations described above allow the admittance matrix to be updated for any physical modification of the network configuration.

Let us now consider a few typical cases:

- A line (represented by its π -equivalent two-port circuit) is added between two existing buses k and i . In this case, operation (2) is applied twice and operation (3) once.
- A new line (represented by its π -equivalent two-port circuit) is added that connects an existing bus k in the network with a new bus $(n+1)$. Here, operation (1) is applied once and operation (2) twice.
- A line between two buses is disconnected. Removing a branch is equivalent to adding admittances with opposite values to the admittances that are already present in the network. Hence, this case is analogous to the first one, but with opposite admittance values.

5.4.2 The Equations

In an n -bus system, the n voltages and the n complex currents are related by n equations with complex variables and coefficients. These relationships comprise the *internal or network constraints*. The $2n$ complex voltages and currents are equivalent to $4n$ real variables. On the other hand, the n equations with complex variables and coefficients are equivalent to $2n$ linear equations with real variables and coefficients that can be obtained by separating the real and imaginary parts (or magnitudes and arguments). Thus, among the $4n$ real variables, $2n$ can be set arbitrarily, and the remaining $2n$ can be calculated by solving the system of network equations.

When the solution to the system of equations has been evaluated and the bus voltages and currents have been determined, the active and reactive power absorbed and injected in the buses along with the power and current flows along the lines and the active and reactive power losses can be determined relatively simply. If the operating conditions of the network can be effectively represented by imposing only RMS values and phases of bus voltages and currents as external constraints, it follows from the above discussion that the power flows can be calculated by solving a system of linear equations.

In practice, the operating conditions imposed on the networks—the *external constraints*—are expressed by setting other quantities. This implies that the system of equations to be solved becomes nonlinear, as will be clarified shortly.

In particular:

- For *load buses*, the quantities that are generally set are the active and reactive power required at the buses: P_i^* and Q_i^* . It is worth noting that the use of constant admittances to represent loads is not generally appropriate. Consider, for instance, asynchronous motors, which absorb active power almost independently of the voltage (for voltage variations of $\pm 10\%$), thus conflicting with the quadratic law that applies to impedances. Moreover, the dependence on the voltage is expressed by the general relations

$$P = P_0 \left(\frac{V}{V_0} \right)^{\alpha_p} \quad (5.73)$$

$$Q = Q_0 \left(\frac{V}{V_0} \right)^{\alpha_q}, \quad (5.74)$$

where the values of the exponentials depend on the nature of the load (they vary between 0 and 2).

- For *generation buses*, it is convenient to set the generated active power P_i^* and the RMS value of the voltage at their terminals E_i^* . The power P_i^* is assumed to be equal to the power that each generation unit must provide in accordance with the optimal repartition plan of the total grid demand among all production plants (namely the result of the *dispatching problem*, which will be briefly summarized at the end of this section). Setting the voltage E_i^* instead of the reactive power Q_i^* is convenient for various reasons. First, fixing the voltage value (at a value between E_n and $1.1E_n$, depending on the distance between the generation bus and the loads) leads to rapid convergence of the numerical procedure that is used to solve the nonlinear system of equations. Second, the reactive power of each generator can be varied by acting on the excitation system. Clearly, it will then be necessary to check that the upper and lower limits on Q imposed by the capability curves of each generator are not exceeded, and—more generally—that the maximum active and reactive power loadings can be supplied without exceeding the heating limits of each generator.

It is important to realize that it is not possible to fix the active power at an arbitrary value for each and every generation and load bus simultaneously. This would be equivalent to arbitrarily fixing the power losses of the network, which actually depend on the solution we are seeking. It is therefore possible to fix a maximum of $(n-1)$ active power values. It is useful to fix the magnitude and the phase of the voltage for the n th bus, which is commonly termed the *slack bus*. The real power at this bus will be equal and opposite to the sum of all real load powers, all of the network losses, and all the real powers of the other generators. The slack bus is commonly considered to be a generation bus with a high capability for real power generation, and it is also the phase-reference bus ($\arg(\bar{E}) = 0$).

Table 5.3 summarizes the types of buses that we have defined so far.

Because the operating conditions of the grids (external constraints) are expressed mainly by setting power

Table 5.3 Types of buses used in a power network, and relevant electric quantities to be imposed and determined

| Type of bus | Fixed quantities ($2n$) | | Quantities to be determined ($2n$) | |
|------------------|------------------------------|-----------------|---|-------------|
| Generation buses | P_G | E_G | Q_G | $\arg(E_G)$ |
| Load buses | P_L | Q_L | E_L | $\arg(E_L)$ |
| Slack bus | E_n | $\arg(E_n) = 0$ | P_n | Q_n |

values rather than currents, we can conclude from the above considerations that the equation system to be solved becomes nonlinear, as further clarified below.

Cartesian Coordinates

The following notation will be used for the equations in Cartesian coordinates

$$\begin{aligned}\bar{E}_i &= E'_i + jE''_i && \text{voltage at bus } i \\ \bar{E}_h &= E'_h + jE''_h && \text{voltage at bus } h \\ \bar{Y}_{ih} &= G_{ih} + jB_{ih} && \text{element } ih \text{ of admittance matrix } [\bar{\mathbf{Y}}],\end{aligned}\quad (5.75)$$

where the meanings of the symbols are obvious.

The complex power injected or absorbed at each bus is

$$\bar{S}_i = P_i + jQ_i = \bar{E}_i \bar{I}_i. \quad (5.76)$$

Given that

$$\bar{I}_i = \sum_{h=1}^n \bar{Y}_{ih} \bar{E}_h \Rightarrow \bar{I}_i = \sum_{h=1}^n \underline{Y}_{ih} \underline{E}_h, \quad (5.77)$$

(5.76) becomes

$$\begin{aligned}\bar{S}_i &= \bar{E}_i \sum_{h=1}^n \underline{Y}_{ih} \underline{E}_h \\ &= (E'_i + jE''_i) \sum_{h=1}^n (G_{ih} - jB_{ih})(E'_h - jE''_h).\end{aligned}\quad (5.78)$$

The active and reactive powers of the i th node will therefore be expressed as

$$\begin{cases} P_i = E'_i \sum_{h=1}^n (G_{ih} E'_h - B_{ih} E''_h) \\ \quad + E''_i \sum_{h=1}^n (B_{ih} E'_h + G_{ih} E''_h) \\ Q_i = -E'_i \sum_{h=1}^n (B_{ih} E'_h + G_{ih} E''_h) \\ \quad + E''_i \sum_{h=1}^n (G_{ih} E'_h - B_{ih} E''_h). \end{cases} \quad (5.79)$$

Recall that g and u are used to indicate the number of generator nodes and users (loads), respectively. Since we also need to account for one slack bus, it follows that $g + u = n - 1$.

In Cartesian coordinates, the entire system of equations takes the form

$$\begin{cases} E''_i = 0 \\ i = n \text{ for slack bus only} \\ E_i^{*2} = E_i'^2 + E_i''^2 \\ i = 1, 2, \dots, g + i = n \text{ for } g \text{ generation buses} \\ \quad + \text{slack bus} \\ P_i^* = E'_i \sum_{h=1}^n (G_{ih} E'_h - B_{ih} E''_h) \\ \quad + E''_i \sum_{h=1}^n (B_{ih} E'_h + G_{ih} E''_h) \\ i = 1, 2, \dots, g + u \text{ for generation buses} \\ \quad + u \text{ load buses} \\ Q_i^* = -E'_i \sum_{h=1}^n (B_{ih} E'_h + G_{ih} E''_h) \\ \quad + E''_i \sum_{h=1}^n (G_{ih} E'_h - B_{ih} E''_h) \\ i = g + 1, \dots, g + u \text{ for load buses,} \end{cases} \quad (5.80)$$

where an asterisk indicates a quantity that is set (i.e., imposed by the transmission system operator). Thus, we eventually obtain $1 + (g + 1) + (g + u) + u = 2(g + u + 1) = 2n$ equations.

Polar Coordinates

The following notation will be used for the equations in polar coordinates, where φ_i and θ_i are the arguments of the current and the voltage of the i th bus, respectively, and γ_{ih} is the argument of the admittance \bar{Y}_{ih} :

- $\bar{E}_i = E_i e^{j\theta_i}$ is the voltage of the i th bus
- $\bar{I}_i = I_i e^{j\varphi_i}$ is the current of the i th bus
- $\bar{Y}_{ih} = Y_{ih} e^{j\gamma_{ih}}$ is element ih of the admittance matrix.

The complex power injected or absorbed at each bus is

$$\bar{S}_i = P_i + jQ_i = \bar{E}_i \bar{I}_i. \quad (5.81)$$

Thus, using (5.67) for the current, we get

$$\begin{aligned}\bar{S}_i &= \bar{E}_i \sum_{h=1}^n \underline{Y}_{ih} \underline{E}_h = \sum_{h=1}^n \bar{E}_i \underline{Y}_{ih} \underline{E}_h \\ &= \sum_{h=1}^n E_i E_h Y_{ih} e^{j(\theta_i - \theta_h - \gamma_{ih})}.\end{aligned}\quad (5.82)$$

The real and reactive power at the i th bus are therefore

$$\begin{cases} P_i = \sum_{h=1}^n E_i E_h Y_{ih} \cos(\theta_i - \theta_h - \gamma_{ih}) \\ Q_i = \sum_{h=1}^n E_i E_h Y_{ih} \sin(\theta_i - \theta_h - \gamma_{ih}) \end{cases} \quad (5.83)$$

The entire system of equations in polar coordinates takes the form

$$\begin{cases} 0 = \theta_i \\ i = n \text{ for the slack bus only} \\ E_i^* = E_i \\ i = 1, 2, \dots, g \text{ and } i = n \\ \text{for the slack bus and the generation buses} \\ P_i^* = E_i \sum_{h=1}^n E_h Y_{ih} \cos(\theta_{ih} - \gamma_{ih}) \\ i = 1, 2, \dots, g + u \text{ for load and generation buses} \\ Q_i^* = E_i \sum_{h=1}^n E_h Y_{ih} \sin(\theta_{ih} - \gamma_{ih}) \\ i = g + 1, \dots, g + u \text{ for } u \text{ load buses,} \end{cases} \quad (5.84)$$

where, as before, an asterisk indicates a quantity that is set (imposed by the transmission system operator). Also, we again ultimately obtain $1 + (g + 1) + (g + u) + u = 2n$ equations, of which $g + 2$ are identities.

Power Flow

The power flowing from bus i to bus h is given by

$$\bar{S}_{ih} = P_{ih} + jQ_{ih} = \bar{E}_i (\underline{E}_i - \underline{E}_h) y_{ih} + E_i^2 y_{i(ih)} \quad (5.85)$$

In polar coordinates,

$$\begin{aligned} \bar{S}_{ih} &= \bar{E}_i (\underline{E}_i - \underline{E}_h) y_{ih} + E_i^2 y_{i(ih)} \\ &= E_i e^{j\theta_i} (E_i e^{-j\theta_i} - E_h e^{-j\theta_h}) y_{ih} e^{-j\gamma_{ih}} + E_i^2 y_{i(ih)} e^{-j\gamma_i} \\ &= E_i^2 y_{ih} e^{-j\gamma_{ih}} - E_i E_h y_{ih} e^{j(\theta_i - \theta_h - \gamma_{ih})} + E_i^2 y_{i(ih)} e^{-j\gamma_i}, \end{aligned} \quad (5.86)$$

where γ_i is the argument of the admittance $y_{i(ih)}$.

In Cartesian coordinates,

$$\begin{aligned} P_{ih} &= (g_{ih} + g_{i(ih)}) (E_i'^2 + E_h''^2) - g_{ih} (E_i' E_h' + E_i'' E_h'') \\ &\quad + b_{ih} (E_i' E_h'' - E_h' E_i'') \\ Q_{ih} &= -(b_{ih} + b_{i(ih)}) (E_i'^2 + E_h''^2) + g_{ih} (E_i' E_h'' - E_i'' E_h') \\ &\quad + b_{ih} (E_i' E_h' + E_i'' E_h''). \end{aligned} \quad (5.87)$$

Expressing the voltages in polar coordinates and the admittances in Cartesian coordinates, we obtain the useful relationship

$$P_{ih} = E_i^2 (g_{ih} + g_{i(ih)}) - E_i E_h (g_{ih} \cos \theta_{ih} + b_{ih} \sin \theta_{ih}) \quad (5.88)$$

$$Q_{ih} = -E_i^2 (b_{ih} + b_{i(ih)}) - E_i E_h (g_{ih} \sin \theta_{ih} - b_{ih} \cos \theta_{ih}). \quad (5.89)$$

5.4.3 Capability Curves

In this section, we briefly review the concept of generator capability curves. The generator must be able to meet the active and reactive power demands within the limits of appropriate generator operation under both steady-state and transient conditions. Let us consider a round-rotor synchronous generator with a linear magnetic circuit. We can define the following operational limits, which are known as *capability limits* (see also Fig. 5.18):

- The *armature current limit*. The maximum allowable heating of the stator windings sets the maximum value of the phase current I_n for the machine. This is equivalent to setting the maximum apparent power of the generator.
- The *field current limit*. The maximum allowable heating of the rotor excitation windings sets the maximum field current I_F of the machine. This is equivalent to setting the maximum no-load emf E_{0M} for the machine. Note that E_{0M} is larger than E_{0n} .
- The *stability limit*. During underexcitation, the power angle must not exceed a certain value in order to maintain steady-state stability $\delta < \delta_{\max}$, therefore, the supplied active power should not exceed a certain threshold. A particular safety margin, e.g., 10% of the rated active power P_n power should be maintained for stability reasons.
- The *end region*. During underexcitation, the current leads the voltage by almost 90° and leakage flux is directed along the direct axis—a condition which can produce some local heating in the end regions of some machines.
- The *prime mover limit*. Limits on the mechanical input power from the prime mover impose constraints on the active power generated. The maximum and minimum active power generated (P_{\max} and P_{\min} , respectively) are determined directly from the characteristics of the prime mover. This is shown in Fig. 5.17.

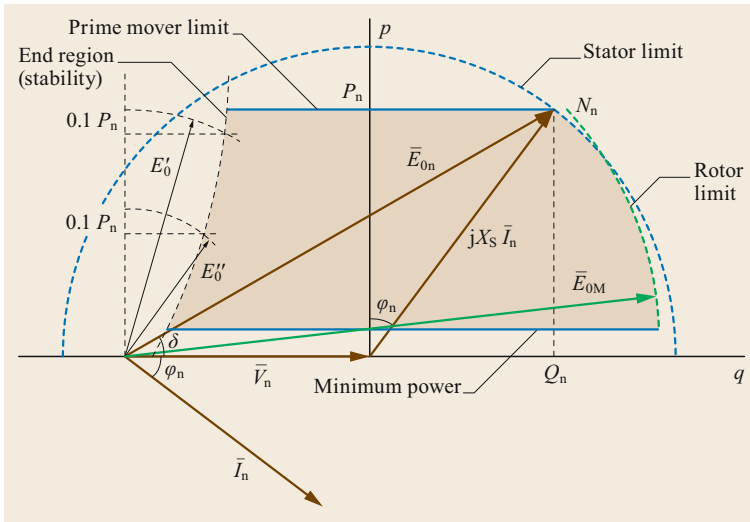


Fig. 5.17 Capability curve showing the mechanical, rotor, and stator limits

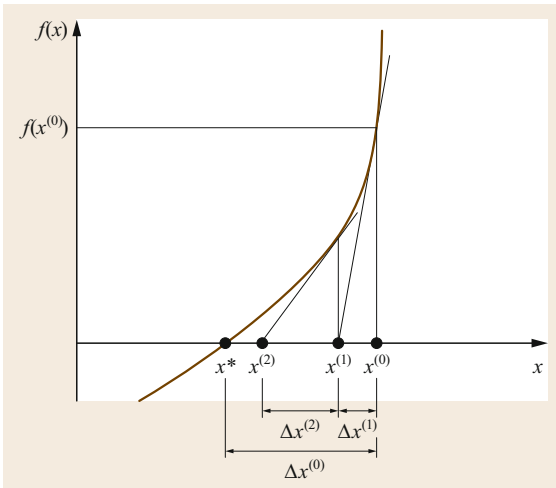


Fig. 5.18 Graphical interpretation of Newton–Raphson’s method

5.4.4 Solution Methods

Newton–Raphson’s Method

Let us first briefly recall the basis for Newton–Raphson’s method for solving nonlinear equations and systems of nonlinear equations. Given a generic function $f(x)$ that is derivable and nonlinear, we want to determine the value x^* of the unknown x such that $f(x)$ assumes a fixed value y^* ; in other words,

$$f(x^*) = y^* . \tag{5.90}$$

Since $x^{(0)}$ is close to x^* , we can define

$$\Delta x^{(0)} = x^* - x^{(0)} . \tag{5.91}$$

We now consider the Taylor expansion of $f(x)$ in the neighborhood of $x^{(0)}$,

$$\begin{aligned} f(x^*) &= f(x^{(0)} + \Delta x^{(0)}) \\ &= f(x^{(0)}) + \left(\frac{df}{dx}\right)^{(0)} \Delta x^{(0)} \\ &\quad + \left(\frac{d^2f}{dx^2}\right)^{(0)} \frac{(\Delta x^{(0)})^2}{2!} + \dots \end{aligned} \tag{5.92}$$

Provided that $x^{(0)}$ is close enough to x^* , we can linearize and write

$$f(x^*) \cong f(x^{(0)}) + \left(\frac{df}{dx}\right)^{(0)} \Delta x^{(0)} . \tag{5.93}$$

Equation (5.90) can be rewritten as

$$f(x^{(0)}) + \left(\frac{df}{dx}\right)^{(0)} \Delta x^{(0)} = y^* . \tag{5.94}$$

Using (5.94), we can infer a value of Δx that will generally differ from that expressed by (5.91) because of the above approximation (the truncation of the Taylor expansion after the first term). We shall therefore denote this value $\Delta x^{(1)}$, where

$$\Delta x^{(1)} = \frac{y^* - f(x^{(0)})}{\left(\frac{df}{dx}\right)^{(0)}} = \frac{\Delta y^{(0)}}{\left(\frac{df}{dx}\right)^{(0)}} \tag{5.95}$$

and

$$\Delta y^{(0)} = y^* - f(x^{(0)}) . \tag{5.96}$$

If we now add the value of $\Delta x^{(1)}$ to the value of the initial guess $x^{(0)}$, we get a new value of x that is closer to the initial solution. We shall call this new value $x^{(1)}$, and

$$x^{(1)} = x^{(0)} + \Delta x^{(1)} = \begin{cases} x^{(0)} + \frac{\Delta y^{(0)}}{\left(\frac{df}{dx}\right)^{(0)}} & \text{if } y^* \neq 0 \\ x^{(0)} - \frac{f(x^{(0)})}{\left(\frac{df}{dx}\right)^{(0)}} & \text{if } y^* = 0. \end{cases} \quad (5.97)$$

Generalizing, the $(v + 1)$ th iteration yields

$$x^{(v+1)} = x^{(v)} + \Delta x^{(v+1)} = \begin{cases} x^{(v)} + \frac{\Delta y^{(v)}}{\left(\frac{df}{dx}\right)^{(v)}} & \text{if } y^* \neq 0 \\ x^{(v)} - \frac{f(x^{(v)})}{\left(\frac{df}{dx}\right)^{(v)}} & \text{if } y^* = 0, \end{cases} \quad (5.98)$$

where

$$\begin{aligned} \Delta x^{(v+1)} &= x^{(v+1)} - x^{(v)} \\ \Delta y^{(v)} &= y^* - f(x^{(v)}), \end{aligned}$$

so we obtain

$$\left(\frac{df}{dx}\right)^{(v)} \Delta x^{(v+1)} = \begin{cases} \Delta y^{(v)} & \text{if } y^* \neq 0 \\ -f(x^{(v)}) & \text{if } y^* = 0, \end{cases} \quad (5.99)$$

which is Newton–Raphson’s iterative formula. A graphical interpretation of this method is given in Fig. 5.18.

The iterative process performed in Newton–Raphson’s method stops when either

$$\Delta x^{(v+1)} < \varepsilon \quad (5.100)$$

or

$$\begin{cases} \Delta y^{(v+1)} < \varepsilon & \text{if } y^* \neq 0 \\ f(x^{(v+1)}) < \varepsilon & \text{if } y^* = 0, \end{cases} \quad (5.101)$$

where ε is defined as the *tolerance* and $f(x^{(v+1)})$ or $\Delta y^{(v+1)}$ is the *residual*.

If the function exhibits smooth behavior around $x^{(0)}$ (i.e., its derivative does not change sign or vary too much), convergence can be attained after a reasonable (i.e., not excessive) number of iterations, even without recalculating the derivative at each iteration.

When there are n equations with n unknowns, the system

$$\begin{cases} f_1(x_1, x_2, \dots, x_n) = y_1^* \\ f_2(x_1, x_2, \dots, x_n) = y_2^* \\ \vdots \\ f_n(x_1, x_2, \dots, x_n) = y_n^* \end{cases} \quad (5.102)$$

is considered. Using a procedure similar to that followed for a single-variable function, the $(v + 1)$ th iteration yields

$$\begin{bmatrix} \frac{\partial f_1}{\partial x_1} & \frac{\partial f_1}{\partial x_2} & \dots & \frac{\partial f_1}{\partial x_n} \\ \frac{\partial f_2}{\partial x_1} & \frac{\partial f_2}{\partial x_2} & \dots & \frac{\partial f_2}{\partial x_n} \\ \vdots & \vdots & \ddots & \vdots \\ \frac{\partial f_n}{\partial x_1} & \frac{\partial f_n}{\partial x_2} & \dots & \frac{\partial f_n}{\partial x_n} \end{bmatrix}^{(v)} \times \begin{bmatrix} \Delta x_1 \\ \Delta x_2 \\ \vdots \\ \Delta x_n \end{bmatrix}^{(v+1)} = \begin{bmatrix} \Delta y_1 \\ \Delta y_2 \\ \vdots \\ \Delta y_n \end{bmatrix}^{(v)}, \quad (5.103)$$

which can be written in compact form as

$$[\mathbf{J}]^{(v)} \times [\Delta \mathbf{x}]^{(v+1)} = [\Delta \mathbf{y}]^{(v)}, \quad (5.104)$$

where

$$[\mathbf{J}]^{(v)} = \begin{bmatrix} \frac{\partial f_1}{\partial x_1} & \frac{\partial f_1}{\partial x_2} & \dots & \frac{\partial f_1}{\partial x_n} \\ \frac{\partial f_2}{\partial x_1} & \frac{\partial f_2}{\partial x_2} & \dots & \frac{\partial f_2}{\partial x_n} \\ \vdots & \vdots & \ddots & \vdots \\ \frac{\partial f_n}{\partial x_1} & \frac{\partial f_n}{\partial x_2} & \dots & \frac{\partial f_n}{\partial x_n} \end{bmatrix}^{(v)} \quad (5.105)$$

$$\Delta x_i^{(v+1)} = x_i^{(v+1)} - x_i^{(v)} \quad (5.106)$$

and

$$\Delta y_i^{(v)} = y_i^* - f_i(x_1^{(v)}, x_2^{(v)}, \dots, x_n^{(v)}). \quad (5.107)$$

The solution is given by

$$\begin{bmatrix} x_1 \\ x_2 \\ \vdots \\ x_n \end{bmatrix}^{(v+1)} = \begin{bmatrix} x_1 \\ x_2 \\ \vdots \\ x_n \end{bmatrix}^{(v)} + \begin{bmatrix} \Delta x_1 \\ \Delta x_2 \\ \vdots \\ \Delta x_n \end{bmatrix}^{(v+1)}, \quad (5.108)$$

where

$$\begin{bmatrix} \Delta x_1 \\ \Delta x_2 \\ \vdots \\ \Delta x_n \end{bmatrix}^{(v+1)} = \left(\begin{bmatrix} \frac{\partial f_1}{\partial x_1} & \frac{\partial f_1}{\partial x_2} & \dots & \frac{\partial f_1}{\partial x_n} \\ \frac{\partial f_2}{\partial x_1} & \frac{\partial f_2}{\partial x_2} & \dots & \frac{\partial f_2}{\partial x_n} \\ \vdots & \vdots & \ddots & \vdots \\ \frac{\partial f_n}{\partial x_1} & \frac{\partial f_n}{\partial x_2} & \dots & \frac{\partial f_n}{\partial x_n} \end{bmatrix}^{(v)} \right)^{-1} \times \begin{bmatrix} \Delta y_1 \\ \Delta y_2 \\ \vdots \\ \Delta y_n \end{bmatrix}^{(v)}. \quad (5.109)$$

In compact form,

$$[\mathbf{x}]^{(v+1)} = [\mathbf{x}]^{(v)} + [\Delta \mathbf{x}]^{(v+1)} \quad (5.110)$$

$$[\Delta \mathbf{x}]^{(v+1)} = ([\mathbf{J}]^{(v)})^{-1} \times [\Delta \mathbf{y}]^{(v)}. \quad (5.111)$$

To solve the system represented by (5.102), we make an initial guess of $(x_1^{(0)}, x_2^{(0)}, \dots, x_n^{(0)})$ and then calculate $\Delta y_i^{(0)} = y_i^* - f_i(x_1^{(0)}, x_2^{(0)}, \dots, x_n^{(0)})$. It is reasonable to assume that $\Delta y_i^{(1)}$ will not satisfy the condition $\Delta y_i^{(1)} < \varepsilon_i$ at the first iteration, so we need to calculate the elements of the Jacobian using $(x_1^{(0)}, x_2^{(0)}, \dots, x_n^{(0)})$ in order to obtain all terms $\Delta x_i^{(1)}$, which are then used to derive the values of $x_i(1)$. This process is repeated until the $(n+1)$ th iteration, when condition $\Delta y_i^{(n+1)} \leq \varepsilon_i$ or condition $\Delta x_i^{(n+1)} \leq \varepsilon_i$ is satisfied.

Let us now apply this method to the load-flow problem [5.37–39].

For the u load buses, we have

$$\begin{bmatrix} \frac{\partial P}{\partial E} & \frac{\partial P}{\partial \vartheta} \\ \frac{\partial Q}{\partial E} & \frac{\partial Q}{\partial \vartheta} \end{bmatrix}^{(v)} \times \begin{bmatrix} \Delta E \\ \Delta \vartheta \end{bmatrix}^{(v+1)} = \begin{bmatrix} \Delta P \\ \Delta Q \end{bmatrix}^{(v)}. \quad (5.112)$$

For the g generation buses, we have

$$\begin{bmatrix} \frac{\partial P}{\partial E} & \frac{\partial P}{\partial \vartheta} \end{bmatrix}^{(v)} \times \begin{bmatrix} \Delta E \\ \Delta \vartheta \end{bmatrix}^{(v+1)} = [\Delta \mathbf{P}]^{(v)}. \quad (5.113)$$

Note that we have a total of g equations rather than the $2g$ equations that would be obtained with the Cartesian formulation. This is because the remaining g ones, which correspond to the amplitudes of the voltages of the generator buses, are known quantities.

The overall compact formulation of the problem is

$$\begin{bmatrix} J_{PE} & J_{P\vartheta} \\ J_{QE} & J_{Q\vartheta} \end{bmatrix}^{(v)} \times \begin{bmatrix} \Delta E \\ \Delta \vartheta \end{bmatrix}^{(v+1)} = \begin{bmatrix} \Delta P \\ \Delta Q \end{bmatrix}^{(v)}, \quad (5.114)$$

in which the elements of the Jacobian are expressed as

$$\begin{cases} \frac{\partial P_i}{\partial E_i} = Y_{ih} E_i \cos(\vartheta_i - \vartheta_h - \gamma_{ih}) \\ \frac{\partial P_i}{\partial E_i} = 2Y_{ii} E_i \cos \gamma_{ii} + \sum_{h=1, h \neq i}^n Y_{ih} E_h \cos(\vartheta_i - \vartheta_h - \gamma_{ih}) \\ \frac{\partial P_i}{\partial \vartheta_h} = Y_{ih} E_i E_h \sin(\vartheta_i - \vartheta_h - \gamma_{ih}) \\ \frac{\partial P_i}{\partial \vartheta_i} = -E_i \sum_{h=1, h \neq i}^n Y_{ih} E_h \sin(\vartheta_i - \vartheta_h - \gamma_{ih}) \end{cases} \quad (5.115)$$

and

$$\begin{cases} \frac{\partial Q_i}{\partial E_h} = Y_{ih} E_i \sin(\vartheta_i - \vartheta_h - \gamma_{ih}) \\ \frac{\partial Q_i}{\partial E_i} = -2Y_{ii} E_i \sin \gamma_{ii} + \sum_{h=1, h \neq i}^n Y_{ih} E_h \sin(\vartheta_i - \vartheta_h - \gamma_{ih}) \\ \frac{\partial Q_i}{\partial \vartheta_h} = -Y_{ih} E_i E_h \cos(\vartheta_i - \vartheta_h - \gamma_{ih}) \\ \frac{\partial Q_i}{\partial \vartheta_i} = E_i \sum_{h=1, h \neq i}^n Y_{ih} E_h \cos(\vartheta_i - \vartheta_h - \gamma_{ih}) \end{cases} \quad (5.116)$$

A load-flow calculation that uses the Newton–Raphson method and is performed with the EMTP-RV (electromagnetic transient program) code is included in the supplementary material for this chapter.

5.4.5 Approximations for Calculating the Load Flow

Carpentier's Approximation

Before we dive any further into this section, it is important to note that the word *approximation* is not used in this section to describe the nature of the results (which are always approximate given that we utilize iterative solution methods), but to refer to the nature of the equations used to compute the load flow.

The first approximation that we introduce is Carpentier's approximation [5.40], which makes the assumption that the active powers injected in the nodes depend only on the phases of the voltages, whereas the reactive powers depend only on the magnitudes of the voltages. This allows us to decouple system (5.114). In other words, the elements of the submatrix $[\partial P / \partial \vartheta]$ are normally much larger than those of the submatrix $[\partial P / \partial E]$, and the elements of $[\partial Q / \partial E]$ are much larger than those of $[\partial Q / \partial \vartheta]$.

The new system of equations becomes

$$\begin{aligned} & \begin{bmatrix} \frac{\partial P}{\partial E} & \frac{\partial P}{\partial \vartheta} \\ \frac{\partial Q}{\partial E} & \frac{\partial Q}{\partial \vartheta} \end{bmatrix}^{(v)} \times \begin{bmatrix} \Delta E \\ \Delta \vartheta \end{bmatrix}^{(v+1)} = \begin{bmatrix} \Delta P \\ \Delta Q \end{bmatrix}^{(v)} \\ \Rightarrow & \begin{bmatrix} 0 & \frac{\partial P}{\partial \vartheta} \\ \frac{\partial Q}{\partial E} & 0 \end{bmatrix}^{(v)} \times \begin{bmatrix} \Delta E \\ \Delta \vartheta \end{bmatrix}^{(v+1)} = \begin{bmatrix} \Delta P \\ \Delta Q \end{bmatrix}^{(v)}, \end{aligned} \quad (5.117)$$

which corresponds to the two subsystems

$$\begin{bmatrix} \frac{\partial P}{\partial \vartheta} \end{bmatrix}^{(v)} \times [\Delta \vartheta]^{(v+1)} = [\Delta \mathbf{P}]^{(v)} \quad (5.118)$$

$$\begin{bmatrix} \frac{\partial Q}{\partial E} \end{bmatrix}^{(v)} \times [\Delta E]^{(v+1)} = [\Delta \mathbf{Q}]^{(v)}. \quad (5.119)$$

What we have achieved here is known as *active and reactive power decoupling*.

It is useful to recall that, for a very short line (i.e., a line in which transversal admittance can be neglected), the expressions for the active and reactive power in absolute values (i.e., not in pu) at the terminations are

$$P_1 = P_2 = \frac{3E_1 E_2}{X} \sin \vartheta \quad (5.120)$$

$$Q_1 = \frac{3E_1}{X} (E_1 - E_2 \cos \vartheta) \quad (5.121)$$

$$Q_2 = \frac{3E_2}{X} (E_1 \cos \vartheta - E_2). \quad (5.122)$$

In general, especially when the line is short and not overloaded, ϑ is a small angle. As a first approximation,

we can therefore state that the active power depends on the phase shift between the two voltages, while the reactive power depends on the voltage magnitudes.

The statements made above regarding a very short line are normally also valid for longer lines, and generally extend to the grids. Recall the equations for power transmission along a generic transmission line,

$$\begin{cases} P_{ih} = E_i^2(g_{ih} + g_{i(ih)}) - E_i E_h [g_{ih} \cos(\vartheta_i - \vartheta_h) \\ \quad + b_{ih} \sin(\vartheta_i - \vartheta_h)] \\ Q_{ih} = -E_i^2(b_{ih} + b_{i(ih)}) - E_i E_h [g_{ih} \sin(\vartheta_i - \vartheta_h) \\ \quad - b_{ih} \cos(\vartheta_i - \vartheta_h)]. \end{cases} \quad (5.123)$$

Differentiating with respect to the magnitudes and phases of the voltages, we obtain the real power derivatives

$$\begin{cases} \frac{\partial P_{ih}}{\partial E_i} = 2E_i(g_{ih} + g_{i(ih)}) \\ \quad - E_h [g_{ih} \cos(\vartheta_i - \vartheta_h) + b_{ih} \sin(\vartheta_i - \vartheta_h)] \\ \frac{\partial P_{ih}}{\partial E_h} = -E_i [g_{ih} \sin(\vartheta_i - \vartheta_h) + b_{ih} \cos(\vartheta_i - \vartheta_h)] \end{cases} \quad (5.124)$$

$$\begin{cases} \frac{\partial P_{ih}}{\partial \vartheta_i} = E_i E_h [g_{ih} \sin(\vartheta_i - \vartheta_h) - b_{ih} \cos(\vartheta_i - \vartheta_h)] \\ \frac{\partial P_{ih}}{\partial \vartheta_h} = -\frac{\partial P_{ih}}{\partial \vartheta_i} \end{cases} \quad (5.125)$$

and the reactive power derivatives

$$\begin{cases} \frac{\partial Q_{ih}}{\partial E_i} = -2E_i(b_{ih} + b_{i(ih)}) \\ \quad - E_h [g_{ih} \sin(\vartheta_i - \vartheta_h) - b_{ih} \cos(\vartheta_i - \vartheta_h)] \\ \frac{\partial Q_{ih}}{\partial E_h} = -E_i [g_{ih} \sin(\vartheta_i - \vartheta_h) - b_{ih} \cos(\vartheta_i - \vartheta_h)] \end{cases} \quad (5.126)$$

$$\begin{cases} \frac{\partial Q_{ih}}{\partial \vartheta_i} = -E_i E_h [g_{ih} \cos(\vartheta_i - \vartheta_h) + b_{ih} \sin(\vartheta_i - \vartheta_h)] \\ \frac{\partial Q_{ih}}{\partial \vartheta_h} = -\frac{\partial Q_{ih}}{\partial \vartheta_i} \end{cases} \quad (5.127)$$

The conductance g_{ij} and the angle $\vartheta_{ih} = \vartheta_i - \vartheta_h$ are generally small. As a consequence, we can state that

$$\frac{\partial P_{ih}}{\partial E_i} \ll \frac{\partial P_{ih}}{\partial \vartheta_i}, \quad \frac{\partial Q_{ih}}{\partial \vartheta_i} \ll \frac{\partial Q_{ih}}{\partial E_i}. \quad (5.128)$$

As a result, small variations in the voltage magnitudes do not appreciably affect the active power transmission and, analogously, small phase variations do not substantially alter the reactive power flow. It follows that the active power transmission mainly depends on the voltage phase shifts, while the reactive power flow is mainly influenced by the difference in the voltage magnitudes at the line terminations.

Stott's Approximation

This approximation is also known as fast decoupled load flow [5.41, 42]. As discussed earlier, the power injection at bus i can be written as

$$\bar{S}_i = \bar{E}_i \sum_{h=1}^n \underline{Y}_{ih} \bar{E}_h = \sum_{h=1}^n \bar{E}_i \underline{Y}_{ih} \bar{E}_h. \quad (5.129)$$

We know that

$$\begin{cases} \bar{E}_i = E_i e^{j\vartheta_i} = E_i (\cos \vartheta_i + j \sin \vartheta_i) \\ \bar{E}_h = E_h e^{-j\vartheta_h} = E_h [\cos(-\vartheta_h) + j \sin(-\vartheta_h)] \\ \underline{Y}_{ih} = G_{ih} - jB_{ih}, \end{cases} \quad (5.130)$$

so we can substitute (5.130) into (5.129), which yields

$$\begin{aligned} \bar{S}_i &= E_i \sum_{h=1}^n E_h (G_{ih} - jB_{ih}) [\cos(\vartheta_i - \vartheta_h) + j \sin(\vartheta_i - \vartheta_h)] \\ &= E_i \sum_{h=1}^n E_h (G_{ih} - jB_{ih}) [\cos \vartheta_{ih} + j \sin \vartheta_{ih}]. \end{aligned} \quad (5.131)$$

Using (5.131), it is possible to obtain the expressions for P and Q presented in the previous section, i.e.,

$$\begin{cases} P_i = E_i \sum_{h=1}^n E_h (G_{ih} \cos \vartheta_{ih} + B_{ih} \sin \vartheta_{ih}) \\ Q_i = E_i \sum_{h=1}^n E_h (G_{ih} \sin \vartheta_{ih} - B_{ih} \cos \vartheta_{ih}). \end{cases} \quad (5.132)$$

Extracting the term relevant to node i from the summation, we have

$$\begin{cases} P_i = G_{ii} E_i^2 + E_i \sum_{h \neq i}^n E_h (G_{ih} \cos \vartheta_{ih} + B_{ih} \sin \vartheta_{ih}) \\ Q_i = -B_{ii} E_i^2 + E_i \sum_{h \neq i}^n E_h (G_{ih} \sin \vartheta_{ih} - B_{ih} \cos \vartheta_{ih}). \end{cases} \quad (5.133)$$

Differentiating the active power with respect to ϑ_i and the reactive power with respect to E_i leads to

$$\begin{aligned} \frac{\partial P_i}{\partial \vartheta_i} &= -E_i \sum_{\substack{h=1 \\ h \neq i}}^n E_h (G_{ih} \sin \vartheta_{ih} - B_{ih} \cos \vartheta_{ih}) \\ &= -B_{ii} E_i^2 - Q_i \\ \frac{\partial Q_i}{\partial E_i} &= -2B_{ii} E_i + \sum_{\substack{h=1 \\ h \neq i}}^n E_h (G_{ih} \sin \vartheta_{ih} - B_{ih} \cos \vartheta_{ih}) \\ &= -2B_{ii} E_i + \frac{Q_i + B_{ii} E_i^2}{E_i} = \frac{Q_i}{E_i} - B_{ii} E_i. \end{aligned} \quad (5.134)$$

We can make the following assumptions (known as Stott's assumptions) based on (5.134) [5.41]:

- $B_{ih} \cos \vartheta_{ih} \cong B_{ih}$, given that the displacements ϑ_{ih} at the ends of a single link are small (i.e., $Q_i \ll B_{ii}E_i^2$)
- $G_{ih} \sin \vartheta_{ih} \ll B_{ih}$ as both the conductances and ϑ_{ih} are small
- $Q_i \ll B_{ii}E_i^2$, which is explained below.

Let us consider a generation node connected to the high-voltage grid by means of the corresponding elevator transformer, which has a reactance x of 0.1 pu (referred to its own rated power A_n). Taking E_i to be equal to 1 pu, we obtain $B_{ii}E_i^2 = 10$ pu. It is reasonable to assume that the reactive power produced or absorbed by a generator under normal operating conditions is 0.6–0.7 pu; furthermore, as the rated power of the elevator transformer is approximately equal to that of the generator, we can conclude that the assumption is acceptable ($B_{ii}E_i^2 = 10 \gg Q_i \cong 0.7$).

Similar statements can be made for the load nodes. It can be observed that the longitudinal reactance of a line (in pu of the characteristic power) is about 0.1 pu for a 100 km overhead line. The reactive power absorbed by the loads is usually very small compared to the active one ($\cos \varphi \cong 0.8$ – 0.9), and two lines converge in every load bus on average.

In view of the discussion above, introducing Stott's assumptions into (5.134) leads us to

$$\begin{cases} \frac{\partial P_i}{\partial \vartheta_h} = -E_i E_h B_{ih} \\ \frac{\partial P_i}{\partial \vartheta_i} = -E_i^2 B_{ii} \end{cases} \quad h \neq i \Rightarrow \frac{\partial P_i}{\partial \vartheta_h} = -E_i E_h B_{ih} \quad \forall h \quad (5.135)$$

$$\begin{cases} \frac{\partial Q_i}{\partial E_h} = -E_i B_{ih} \\ \frac{\partial Q_i}{\partial E_i} = -E_i B_{ii} \end{cases} \quad h \neq i \Rightarrow \frac{\partial Q_i}{\partial E_h} = -E_i B_{ih} \quad \forall h. \quad (5.136)$$

Like Carpentier's method, Stott's method is based on the approximation that the active power and reactive power are related to the voltage angles and magnitudes, respectively, i.e., it is also based on active/reactive decoupling. If we consider the load-flow equations obtained using Carpentier's approximation,

$$\begin{cases} \Delta P_i^{(v)} = \sum_{h=1}^n \frac{\partial P_i^{(v)}}{\partial \vartheta_h} \Delta \vartheta_h^{(v+1)} \\ \Delta Q_i^{(v)} = \sum_{h=1}^n \frac{\partial Q_i^{(v)}}{\partial E_h} \Delta E_h^{(v+1)}, \end{cases} \quad (5.137)$$

replacing the partial derivatives with expressions (5.135) and (5.136) yields

$$\begin{cases} \frac{\Delta P_i^{(v)}}{E_i} = \sum_{h=1}^n -B_{ih} E_h^{(v)} \Delta \vartheta_h^{(v+1)} \\ \frac{\Delta Q_i^{(v)}}{E_i} = \sum_{h=1}^n -B_{ih} \Delta E_h^{(v+1)}. \end{cases} \quad (5.138)$$

The great advantage of Stott's method is that the partial derivatives of the Jacobian matrix are replaced with simple susceptances, so there is no need to update the Jacobian at each iteration.

DC Approximation

The load-flow solution methods shown so far have been *AC methods* in the sense that the unknowns to be determined are the voltages (magnitude and phase) that affect the distributions of active and reactive power in the various branches of the network.

Considerable time is needed to perform these methods when dealing with large networks. On the other hand, in some situations it is sufficient to estimate only the active power flows in the various lines, which leads to a marked reduction in computational time. Such situations include the initial planning stage of a transmission network, short-term operational planning (daily and weekly programs implemented *off-line*), and even the *on-line* control of a transmission system that checks for the consequences of a possible sudden loss of a critical component (such as a line or large generator) every few minutes.

The *direct current* load-flow solution method [5.42] is based on the following simplifications:

- The conductor resistances are generally negligible compared to the series reactances of the lines and transformers. The ratio between the reactance and the resistance is about 10 for a distribution line, but can reach 50 for large interconnecting lines. Therefore, losses are neglected in this method.
- The transversal admittances of power components are neglected. The line capacitances generate reactive power that does not significantly affect the active power flow.
- The transversal conductances are neglected.
- Based on similar considerations, the shunt reactances and bank of capacitors can also be neglected.

Let us now consider a branch of the network characterized by a longitudinal reactance x_{ih} . \bar{E}_i and \bar{E}_h are the voltages at the ends of the line, with a phase shift ϑ_{ih} between them.

The active power flow in the branch is

$$P_{ih} = \frac{3E_i E_h}{x_{ih}} \sin \vartheta_{ih}. \quad (5.139)$$

Let us also assume that the voltages are close to their nominal values, i.e.,

$$\bar{E}_i \cong \bar{E}_h. \quad (5.140)$$

Also, noting that the angle $\vartheta_{ih} = \vartheta_i - \vartheta_h$ is generally small, the pu expression of (5.139) becomes

$$p_{ih} = \frac{1}{x_{ih}} \vartheta_{ih}. \quad (5.141)$$

This relationship is analogous to Ohm's law in a DC circuit with a current p_{ih} flowing through a resistor of value x_{ih} , causing a voltage drop ϑ_{ih} across it.

As a consequence of this expression, the active power injection in the generic node i (in pu) is

$$p_i = \sum_{\substack{h=1 \\ h \neq i}}^n p_{ih} = \frac{\vartheta_{i1}}{x_{i1}} + \frac{\vartheta_{i2}}{x_{i2}} + \dots + \frac{\vartheta_{in}}{x_{in}}$$

$$\stackrel{\vartheta_{ih} = \vartheta_i - \vartheta_h}{\Rightarrow} \left(\frac{1}{x_{i1}} + \frac{1}{x_{i2}} + \dots + \frac{1}{x_{in}} \right) \vartheta_i - \sum_{\substack{h=1 \\ h \neq i}}^n \frac{1}{x_{ih}} \vartheta_h. \quad (5.142)$$

The terms in parentheses can be interpreted as self-admittances, while the terms in the summation can be considered transadmittances. Therefore, we define that

$$\sum_{\substack{h=1 \\ h \neq i}}^n \frac{1}{x_{ih}} = \frac{1}{X_{ii}} \quad ; \quad \frac{1}{x_{ih}} = \frac{1}{-X_{ih}}, \quad (5.143)$$

and the active power injection becomes

$$p_i = \sum_{h=1}^n \frac{1}{X_{ih}} \vartheta_h \Rightarrow p_i = \sum_{h=1}^n B_{ih} \vartheta_h. \quad (5.144)$$

Thus, the linear matrix equation

$$[\mathbf{p}] = [\mathbf{B}] \times [\boldsymbol{\vartheta}] \quad (5.145)$$

is obtained for the whole network, where $[\mathbf{B}]$ is the susceptance matrix of the entire transmission network in pu. The diagonal terms B_{ii} of this matrix are the sum of the susceptances of all the lines that converge at the i th node, and are positive since the susceptances are inductive. The other terms are all negative and satisfy the condition $B_{hk} = B_{kh} = -b_{hk} = -b_{kh}$.

An exercise to calculate the load flow of a simple three-bus network using the current approximation is included in the supplementary material.

5.4.6 Concluding Remarks

The methods examined so far do not consider any constraints. In real applications, however, there can be many types of constraints:

- The voltages in the various nodes must not be too different from the nominal ones

- In the generation nodes, the reactive power injection resulting from the calculation must be compatible with the capability curves of the generators
- When the slack bus—which is also a generation node—is assumed to be concentrated in one bus and not distributed, it must have an active and reactive power output compatible with the above production of the generators.

The limits are therefore of the type

$$\begin{cases} Q_{i,\min} \leq Q_i \leq Q_{i,\max} \\ i = 1, 2, \dots, g \end{cases} \quad (5.146)$$

$$\begin{cases} E_{i,\min} \leq E_i \leq E_{i,\max} \\ i = 1, 2, \dots, g + u \end{cases} \quad (5.147)$$

$$P_{n,\min} \leq P_n \leq P_{n,\max}. \quad (5.148)$$

Load-flow calculations with constrained variables must be performed to account for these issues ([5.43], from which the following discussion is adapted).

Now suppose that constraints (5.146) are violated; in other words, the computation yields reactive powers that exceed the limit in some generation buses and are lower than the limit in others. In order to obtain a load-flow solution that is technically feasible, it is necessary to change the voltages in the various buses. These buses, originally of (P, E) type, can therefore be converted into (P, Q) ones by fixing their reactive power production (i.e., $Q_i \cong Q_{i,\max}$ or $Q_i \cong Q_{i,\min}$), so the voltage magnitude E_i becomes unknown. Note that the effect of forcing a generator to decrease its reactive power production is that the reactive power generation of the other groups must increase, because the loads do not change.

If the violated constraints are of the type represented by (5.148) for the active power, it will be necessary to vary the power distribution among the other generators of the network. If, for instance, the upper limit is violated (i.e., if the active power to be produced in the slack bus is larger than the maximum allowed), it is necessary to increase the production of the other groups. This does not guarantee a priori that the constraints will be respected, as changing the active power production changes the phases of the voltages and therefore the currents in the branches. Consequently, the transmission losses change too. In other words, it will be necessary to verify that the new calculated active power respects constraints (5.148).

Modern computer software can automatically consider:

- The effects of generator speed control and shifting transformers, in order to determine their optimal set-ups
- The dependence of the loads on the voltage

- Primary and secondary frequency control and the frequency dependence of the loads
- Secondary voltage regulation.

These topics are discussed in the optimal load flow, more commonly known as optimal power flow, (OPF) chapters of several books [5.13, 43]. OPF is closely related to economic dispatch and unit commitment, and any attempt to realize OLF will need to take electricity market rules and constraints into consideration (see Chap. 18). We do not address these topics in this chapter, but we do delve into the essential elements of economic dispatching below.

Some Basic Elements of Economic Dispatching

For simplicity's sake, suppose that we have a system, as depicted in Fig. 5.19, consisting of:

- g thermal power stations
- one network
- u users.

In a vertically integrated system, we wish to determine the power that the generators (the power plants) must provide in order to meet the power requirements of the users at minimum cost. Any technical constraints on the groups are disregarded for simplicity.

The plot presented in Fig. 5.20 shows the hourly cost curve of a power plant: the efficiency is constant regardless of the power produced. The curved line, on the other hand, shows a more realistic trend for the hourly



Fig. 5.19 Single-bus power system

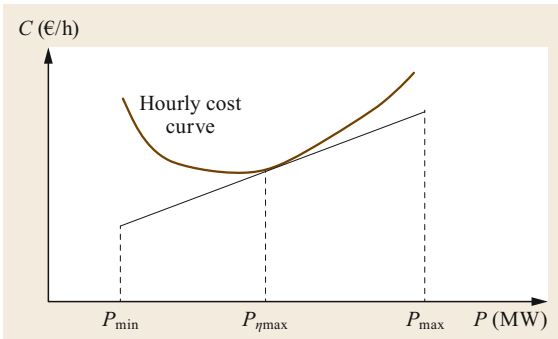


Fig. 5.20 Hourly cost curve for a thermal power plant as a function of the power produced

cost—there is a point on the curve at which the cost is minimized, and we would like to operate the plant at the power corresponding to this point.

Defining C as the overall cost, the function to be minimized is

$$C = C_1(P_1) + C_2(P_2) + \cdots + C_g(P_g). \quad (5.149)$$

In accordance with the constraint,

$$P_1 + P_2 + \cdots + P_g - (P_{U1} + P_{U2} + \cdots + P_{Uu}) - p = 0, \quad (5.150)$$

where p represents the losses of the system. It is worth noting that

$$p = p(P_1, P_2, \dots, P_g); \quad (5.151)$$

in other words, the losses are linked to the power produced, as expected.

To solve the problem, it is necessary to use the method of Lagrange multipliers. We define the Lagrangian as

$$\begin{aligned} L &= (\text{condition to be minimized}) - \lambda(\text{constraint}) \\ &= C(P_1, P_2, \dots, P_g) - \lambda \left(\sum_{i=1}^g P_i - \sum_{i=1}^u P_{Ui} - p \right). \end{aligned} \quad (5.152)$$

In order to solve it, we must calculate

$$\begin{cases} \frac{\partial L}{\partial P_i} = 0 \\ \frac{\partial L}{\partial \lambda} = 0 \end{cases} \Rightarrow P_1, P_2, \dots, P_g, \lambda, \quad (5.153)$$

which means that

$$\begin{cases} \frac{\partial C_1}{\partial P_1} - \lambda \left(1 - \frac{\partial p}{\partial P_1} \right) = 0 \\ \frac{\partial C_2}{\partial P_2} - \lambda \left(1 - \frac{\partial p}{\partial P_2} \right) = 0 \\ \vdots \\ \frac{\partial C_g}{\partial P_g} - \lambda \left(1 - \frac{\partial p}{\partial P_g} \right) = 0 \\ P_1 + P_2 + \cdots + P_g \\ = P_{U1} + P_{U2} + \cdots + P_{Uu} + p \end{cases} \Rightarrow P_1, P_2, \dots, P_g, \lambda. \quad (5.154)$$

If the system losses p are negligible, it follows that $p = 0$. This is equivalent to neglecting the power losses along the lines, i.e.,

$$\frac{\partial p}{\partial P_1}, \frac{\partial p}{\partial P_2}, \dots, \frac{\partial p}{\partial P_g}, p = 0. \quad (5.155)$$

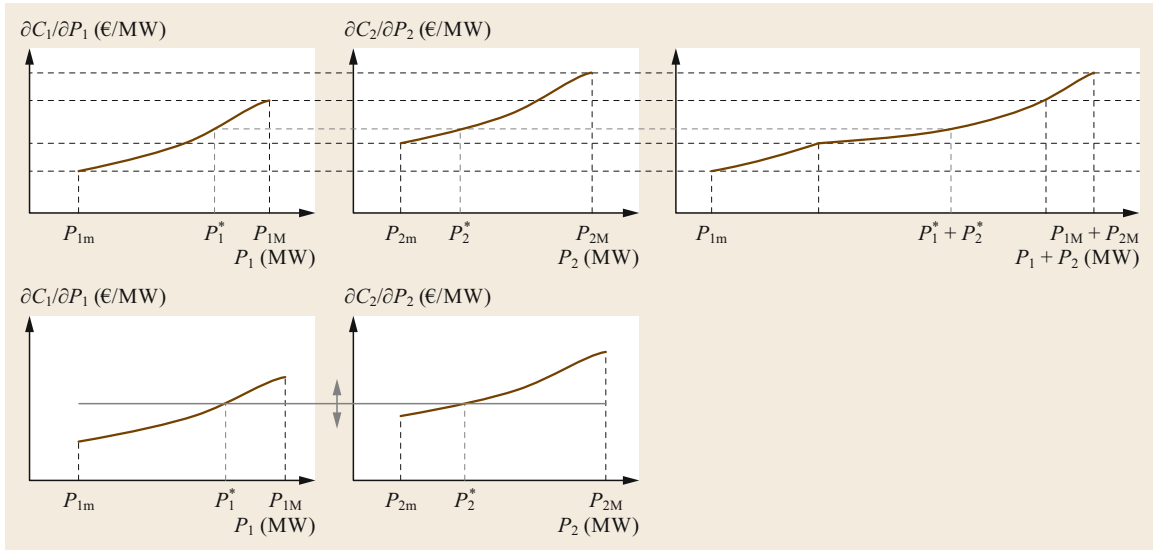


Fig. 5.21 Dispatched Power for two Power Stations 1 and 2 (adapted from [5.36])

In this case, the system is called a *single-bar system*, and the equations reduce to

$$\frac{\partial C_1}{\partial P_1} = \frac{\partial C_2}{\partial P_2} = \dots = \frac{\partial C_g}{\partial P_g} \quad (5.156)$$

Rewriting the partial derivatives as total derivatives yields

$$\frac{dC_1}{dP_1} = \frac{dC_2}{dP_2} = \dots = \frac{dC_g}{dP_g} = \lambda \quad (5.157)$$

Equality of marginal hourly costs is therefore the minimum condition sought.

The simplified assumptions of this section permit the problem to be solved in a simple way graphically using the known hourly cost curves for two power stations, as shown in Fig. 5.21. The incremental hourly cost is obtained by deriving the hourly costs with respect to the power variable. To determine the operating point, it is sufficient to draw a horizontal line that intercepts both curves such that the sum of the power on the first graph (P_1^*) and that on the second graph (P_2^*) equals the power required by the load.

5.5 Unsymmetrical Fault Analysis

A short circuit is the term given to the unintended flow of current along a low-impedance connection between two points at different potentials in an electric circuit (phase-to-phase or phase-to-ground) rather than along the intended path. The most common types of faults in power systems are single line-to-ground (or phase-to-ground), three-phase, line-to-line (or phase-to-phase), and double line-to-ground. Faults can occur for various reasons, such as insulation breakdown (due to overvoltage or aging) or direct contact with bare conductors.

5.5.1 Types of Faults in Electric Power Systems

The following fault phenomena can occur in electric power systems:

- (a) A sudden increase in conductor temperature θ due to the Joule effect, as calculated via

$$\Delta\theta = KI^2\Delta t \quad (5.158)$$

As the temperature θ increases, the extra heat alters the dielectric properties of the insulating materials. Heating also alters the mechanical properties of the conductor, and the disconnecter contacts deteriorate. For faults of this nature, it is clear that reducing the duration of the fault is of paramount importance.

- (b) Electrodynamical forces that are proportional to the square of the peak current amplitude, i.e.,

$$F = KI_p^2 \quad (5.159)$$

which deform or even disrupt conductors and insulation materials.

There are a range of relevant effects, including:

- Damage caused by an electric arc at the location of the fault is common, and often leads to fusion or erosion of the relevant parts (conductors, electrical machines, ferromagnetic plates), representing a fire risk.
- Voltage dips at the faulty bus and in the adjacent network portion, causing malfunctions, trips (of, e.g., synchronous motors and mercury-vapor lamps), disturbing users that are sensitive to voltage drops, and possibly leading to a loss of system stability.
- Dangerous step and touch voltages caused by the large short-circuit currents
- Electromotive force (EMF) induction in telecommunication circuits that are located parallel to power lines
- When present, homopolar sequence current circulation through cable sheaths, pipelines, or other underground structures leads to heating or electric arcs and metal fusion, pipeline punctures, and the potential for fire.

5.5.2 Protection Measures Against Faults

Although electric power systems are well designed, faults are relatively frequent phenomena in such systems, so relevant countermeasures must be taken, including:

- i. Installing circuit breakers and fuses with adequate short-circuit breaking capacities to withstand/open the short-circuit current
- ii. Ensuring that components are designed/selected to withstand thermal and electrodynamic stresses without incurring damage
- iii. Designing appropriate grounding systems that keep touch and step voltages within standard limits
- iv. Appropriate calibration/setting of protection relays. Note that setting these devices to open the maximum short-circuit current may result in the failure of the devices to open the lowest fault currents.

To realize the above measures, it is necessary to perform fault current calculations for the various types of possible faults at each network bus. Indeed, as already mentioned, ignoring the calculation of a modest fault current (corresponding to the minimum load operation of the network with different units out of service) during the calibration and validation of protection relays can be critical.

To determine the breaking capacity, it is convenient to calculate short circuits with null fault impedance ($Z_g = 0$). Since this type of fault is rare, for complete-

ness, we shall extend the discussion to the more general case of a nonzero Z_g .

In fault analysis, the network is generally unbalanced, as most short circuits have this characteristic (e.g., single-line to ground, line-to-line, double line-to-ground).

5.5.3 Unbalanced Faults: Short-Circuit Calculation

To simplify the analysis of fault currents in networks, we follow the approach given in [5.3] and make the following simplifications:

- Transmission lines are represented by their series reactance
- Transformers are represented by their short-circuit reactance
- Synchronous machines are modeled as a Thévenin equivalent network consisting of an ideal generator and the direct-axis transient (or subtransient) reactance
- Induction motors are ignored or treated as synchronous machines
- Other (nonspinning) loads are ignored
- The voltage level of the neutral conductor is common to all the voltage levels of the network (i.e., there are no voltage levels with an isolated neutral).

We shall denote the phase voltages and currents by $\bar{E}_a, \bar{E}_b, \bar{E}_c, \bar{I}_a, \bar{I}_b,$ and \bar{I}_c , respectively, and the direct (or positive), inverse (or negative), and homopolar (or zero) sequence symmetrical components of the voltages and currents by $\bar{E}_d, \bar{E}_i, \bar{E}_0, \bar{I}_d, \bar{I}_i,$ and \bar{I}_0 , respectively. Fortescue theory provides various phase voltage and current transformations,

$$\begin{cases} \bar{E}_d = \frac{1}{3}(\bar{E}_a + \alpha\bar{E}_b + \alpha^2\bar{E}_c) \\ \bar{E}_i = \frac{1}{3}(\bar{E}_a + \alpha^2\bar{E}_b + \alpha\bar{E}_c) \\ \bar{E}_0 = \frac{1}{3}(\bar{E}_a + \bar{E}_b + \bar{E}_c) \end{cases} \quad (5.160)$$

$$\begin{cases} \bar{I}_d = \frac{1}{3}(\bar{I}_a + \alpha\bar{I}_b + \alpha^2\bar{I}_c) \\ \bar{I}_i = \frac{1}{3}(\bar{I}_a + \alpha^2\bar{I}_b + \alpha\bar{I}_c) \\ \bar{I}_0 = \frac{1}{3}(\bar{I}_a + \bar{I}_b + \bar{I}_c) \end{cases} \quad (5.161)$$

$$\begin{cases} \bar{E}_a = \bar{E}_d + \bar{E}_i + \bar{E}_0 \\ \bar{E}_b = \alpha^2\bar{E}_d + \alpha\bar{E}_i + \bar{E}_0 \\ \bar{E}_c = \alpha\bar{E}_d + \alpha^2\bar{E}_i + \bar{E}_0 \end{cases} \quad (5.162)$$

$$\begin{cases} \bar{I}_a = \bar{I}_d + \bar{I}_i + \bar{I}_0 \\ \bar{I}_b = \alpha^2\bar{I}_d + \alpha\bar{I}_i + \bar{I}_0 \\ \bar{I}_c = \alpha\bar{I}_d + \alpha^2\bar{I}_i + \bar{I}_0, \end{cases} \quad (5.163)$$

where $\alpha = e^{j2\pi/3}$. Note that for simplicity α has not been overlined.

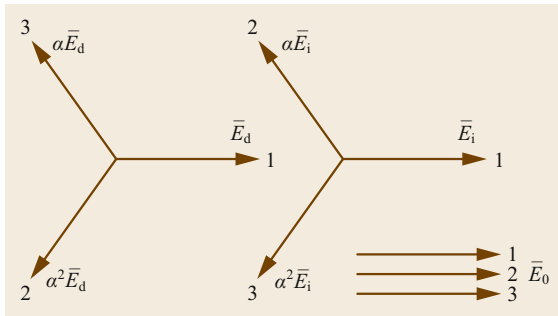


Fig. 5.22 Direct, inverse, and homopolar sequence components of the phase voltages. The amplitudes of E_d , E_i , and E_0 are not necessarily equal

A phasor diagram of the direct, inverse, and homopolar sequence components of the phase voltages is reported in Fig. 5.22.

Let us connect a system of nonsymmetrical (unbalanced) impedances to a point in the symmetrical three-phase network, as shown in Fig. 5.23.

After the relevant transient, the voltages \bar{E}'_a , \bar{E}'_b , and \bar{E}'_c and the currents \bar{I}'_a , \bar{I}'_b , and \bar{I}'_c are obtained (note that the relevant quantities are denoted by an apex). It is clear that these values depend on the impedances \bar{Z}_a , \bar{Z}_b , \bar{Z}_c , and \bar{Z}_n shown in Fig. 5.23, as well as the network parameters. In the postfault steady state, the system in Fig. 5.23 is equivalent to both of those presented in Fig. 5.24.

Note that if we connect the three voltage sources \bar{E}'_a , \bar{E}'_b , and \bar{E}'_c at the fault point (Fig. 5.24a), the three currents in the considered section will actually be equal to the three currents \bar{I}'_a , \bar{I}'_b , and \bar{I}'_c injected at the fault point by the three current sources shown in Fig. 5.24b.

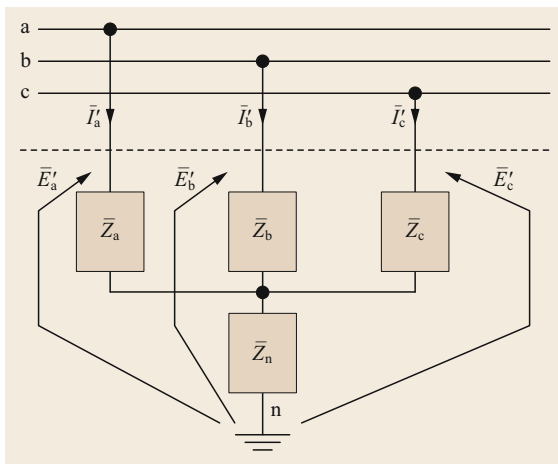


Fig. 5.23 Connection of unsymmetrical (unbalanced) impedances

Let us suppose that \bar{E}'_a , \bar{E}'_b , and \bar{E}'_c are known quantities. According to the superposition principle and the Fortescue theorem, each of the three voltage sources can be decomposed into three series generators (as shown in Fig. 5.24b), and further decomposed into three different circuits (as presented in Fig. 5.26).

The asymmetrical network of Fig. 5.25 has now been decomposed into three symmetrical three-phase ones (Fig. 5.26). In the first network, only the positive (direct) sequence set of sources \bar{E}'_d is present, in addition to those impressed by the generators of the network. The second network only has the negative (inverse) sequence source \bar{E}'_i , whereas the third only has the zero (homopolar) sequence source \bar{E}'_0 . It is worth noting that, because it is symmetrical, the starting network only has direct-sequence internal emfs.

The three networks of Fig. 5.26 are symmetrical (balanced), so they can be studied by means of three equivalent single-phase circuits, as shown in Fig. 5.27. Once all the quantities in the sequence networks have been determined, the starting network voltages and currents can be calculated using (5.162) and (5.163).

Note that the three sequence networks only differ from each other and the given network in the following ways:

- The set of three emfs that simulate the set of impedances \bar{Z}_a , \bar{Z}_b , \bar{Z}_c , and \bar{Z}_n differ for each of the three networks and differ from the emfs of the starting network
- In inverse and homopolar networks, there is no internal EMF (power system generators only provide direct emf).

In view of the above, we can now transform the three networks of Fig. 5.27 into their Thévenin equivalent networks, as represented in Fig. 5.28.

The parameters in these single-phase Thévenin equivalent networks are as follows: \bar{E} is the voltage present before nonsymmetrical impedance insertion (i.e., the prefault voltage) at the fault position; \bar{Z}_d , \bar{Z}_i , and \bar{Z}_0 are the equivalent sequence impedances of the network measured at the faulty bus. Voltage \bar{E} is known from the load-flow calculation. In the absence of further information, it can be assumed to be equal to the rated voltage E_n , or, conservatively, to the maximum permissible operating voltage, which is often $1.1E_n$. It is evident that this assumption leads to the largest short-circuit current values.

The six quantities \bar{E}'_d , \bar{E}'_i , \bar{E}'_0 , \bar{I}'_d , \bar{I}'_i , and \bar{I}'_0 can be determined once \bar{Z}_a , \bar{Z}_b , \bar{Z}_c , and \bar{Z}_n are known. Three vector equations are therefore needed (six scalars), in addition to the three expressed by the Thévenin circuits

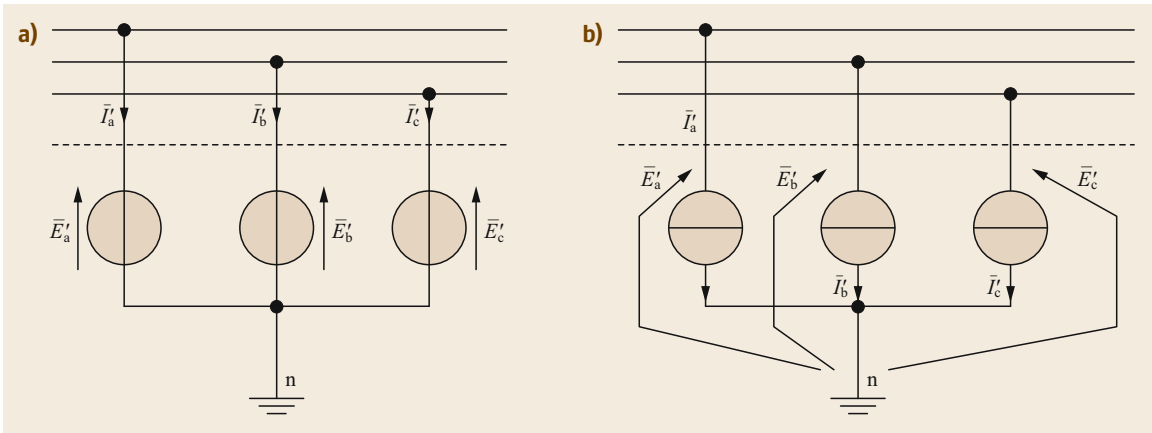


Fig. 5.24a,b Equivalent circuits of the system shown in Fig. 5.23 after the fault in terms of equivalent ideal voltage sources (a) and ideal current sources (b)

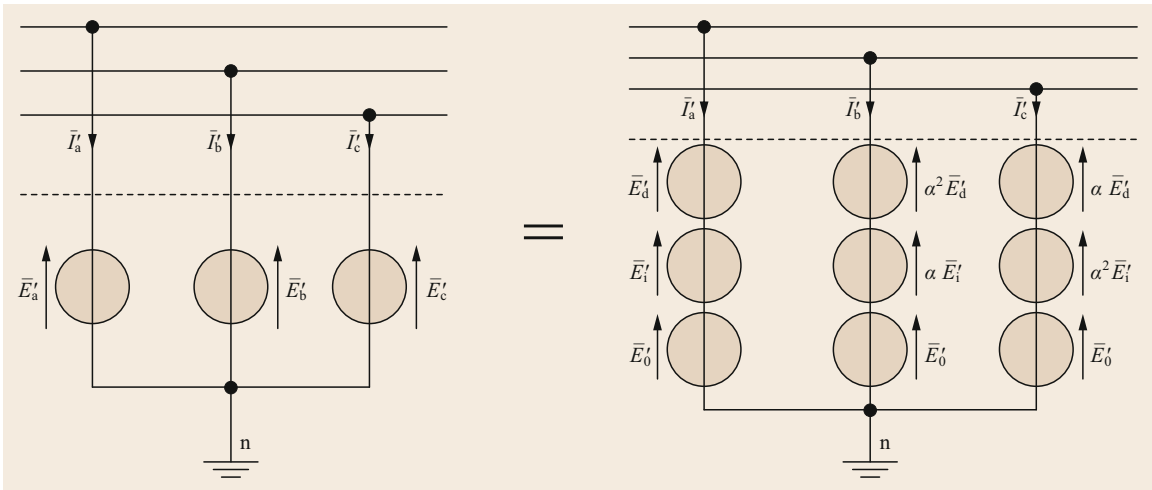


Fig. 5.25 Representation of the Fortescue transformation

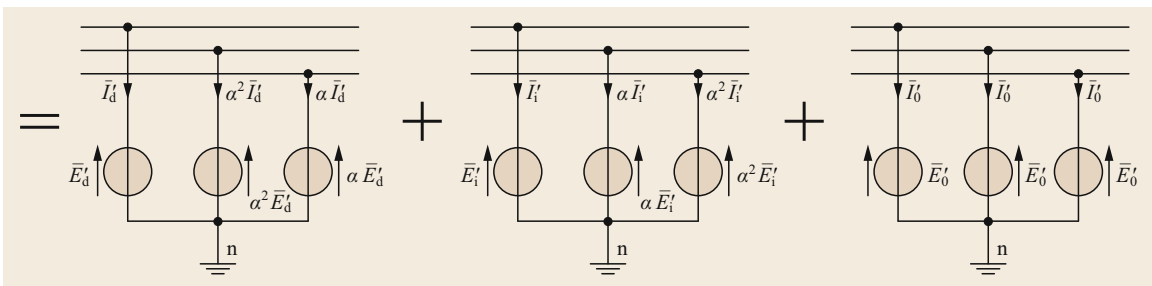


Fig. 5.26 Representation of the Fortescue transformation: superposition of the three different circuits

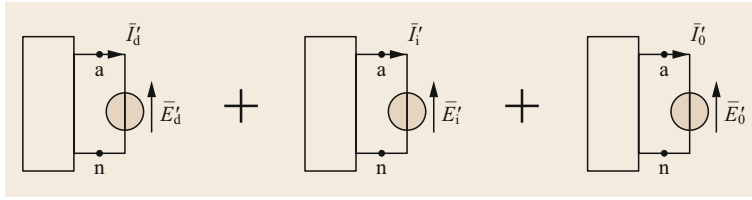


Fig. 5.27 Single-phase equivalent networks of the systems represented in Fig. 5.26

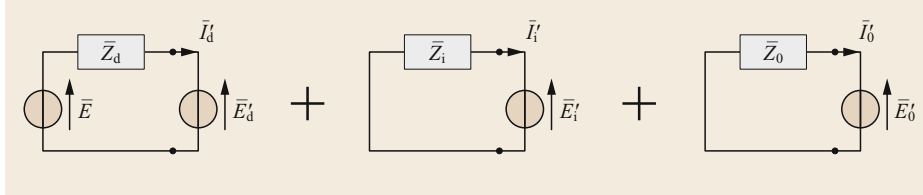


Fig. 5.28 Single-phase Thévenin equivalent networks

$(\bar{E} = \bar{Z}_d \bar{I}_d + \bar{E}_d; 0 = \bar{Z}_i \bar{I}_i + \bar{E}_i; 0 = \bar{Z}_0 \bar{I}_0 + \bar{E}_0)$, which depend on the particular nature of the fault.

Note that different emf systems are applied in the three networks: direct, inverse, and homopolar, respectively. Therefore, the reduction to single-phase circuits described above leads to different parameters for the equivalent circuits of the various elements of the network.

Three-Phase Fault

Let us consider the general case depicted in Fig. 5.29a. The system shown in Fig. 5.29a is obtained from Fig. 5.20 by setting $\bar{Z}_a = \bar{Z}_b = \bar{Z}_c = \bar{Z}_a$. Due to the symmetrical configuration of the system, \bar{E}'_n is equal to zero regardless of the value of \bar{Z}_n , so the circuits presented in Fig. 5.29a and b are equivalent.

In this symmetrical configuration, the only nonzero current is the positive-sequence one. In phase a, the cur-

rent is

$$\bar{I}'_a = \bar{I}'_d = \frac{\bar{E}'_d}{\bar{Z}} \quad (5.164)$$

The equivalent circuit for the three-phase fault is provided in Fig. 5.30, and consists of the positive-sequence Thévenin equivalent network for Fig. 5.25.

The fault current is therefore

$$\bar{I}'_a = \bar{I}'_d = \frac{\bar{E}}{\bar{Z}_d + \bar{Z}} \quad (5.165)$$

In the case of a bolted fault, this becomes

$$\bar{I}'_a = \bar{I}'_d = \frac{\bar{E}}{\bar{Z}_d} \quad (5.166)$$

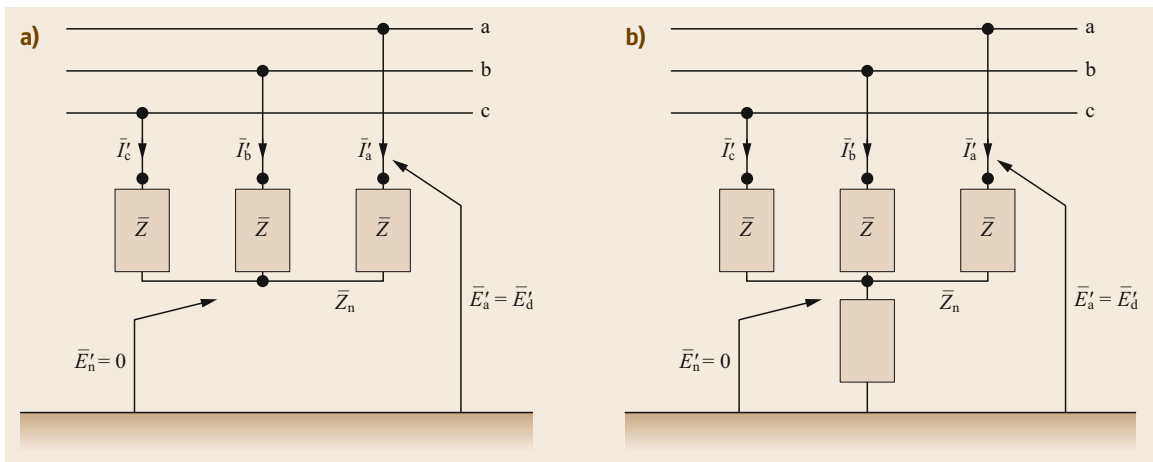


Fig. 5.29a,b Three-phase balanced fault

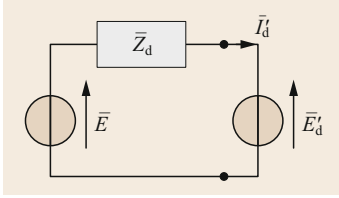


Fig. 5.30 Equivalent circuit at the positive sequence of a three-phase fault

$$\bar{E}'_d - \bar{E}'_i = 2\bar{Z}\bar{I}'_d, \text{ so}$$

$$\begin{cases} \bar{I}'_0 = 0 \\ \bar{I}'_1 = -\bar{I}'_d \\ \bar{E}'_d - \bar{E}'_i = -2\bar{Z}\bar{I}'_d \end{cases} \quad (5.168)$$

Line-to-Line Fault

Now consider the circuit presented in Fig. 5.31. In this case, $\bar{Z}_a = \infty, \bar{Z}_b = \bar{Z}_c = \bar{Z}, \bar{Z}_n = \infty$.

The system of equations

$$\begin{cases} \bar{I}'_a = 0 \\ \bar{I}'_b + \bar{I}'_c = 0 \\ \bar{E}'_b - \bar{Z}\bar{I}'_c = \bar{E}'_c - \bar{Z}\bar{I}'_b \end{cases} \quad (5.167)$$

are obtained from Fig. 5.31. Upon applying Fortescue's current transformations (5.161), we find that $\bar{I}'_d = -\bar{I}'_i$ and $\bar{I}'_0 = 0$. Then, utilizing the second and third equations of (5.162) and (5.163), respectively, we obtain

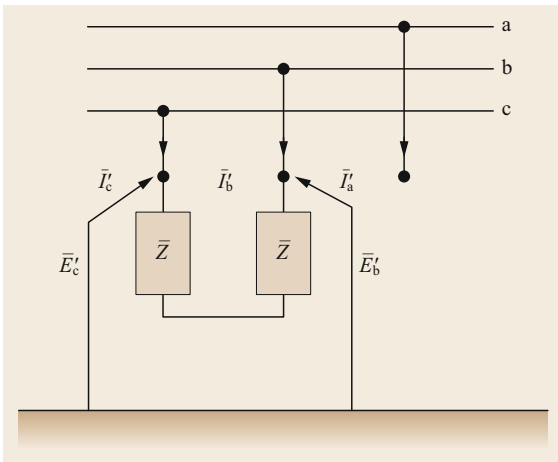


Fig. 5.31 Line-to-line fault

Using (5.168), it is possible to infer the equivalent circuit of the system, which is shown in Fig. 5.32. The zero sequence is not involved in the fault.

Employing the circuit shown in Fig. 5.32, we can derive the expressions

$$\begin{cases} \bar{E}'_0 = 0 \\ \bar{I}'_d = \frac{\bar{E}}{\bar{Z}_d + \bar{Z}_i + 2\bar{Z}} = -\bar{I}'_i \\ \bar{E}'_i = \frac{\bar{E}\bar{Z}_i}{\bar{Z}_d + \bar{Z}_i + 2\bar{Z}} \\ \bar{E}'_d = \frac{\bar{E}(\bar{Z}_i + 2\bar{Z})}{\bar{Z}_d + \bar{Z}_i + 2\bar{Z}} \end{cases} \quad (5.169)$$

Finally, by applying Fortescue's transformations, the line-to-line fault current is obtained as

$$\bar{I}'_b = \frac{-j\sqrt{3}\bar{E}}{\bar{Z}_d + \bar{Z}_i + 2\bar{Z}} \quad (5.170)$$

Double Line-to-Ground Fault

The circuit of interest here is that reported in Fig. 5.33, with $\bar{Z}_a = \infty, \bar{Z}_b = \bar{Z}_c = 0, \bar{Z}_n = \bar{Z}$.

From Fig. 5.33, we can infer that

$$\begin{cases} \bar{I}'_a = 0 \\ \bar{E}'_b = \bar{E}'_c \\ \bar{E}'_b = \bar{Z}(\bar{I}'_c + \bar{I}'_b) \end{cases} \quad (5.171)$$

If we employ the same procedure we adopted for the line-to-line fault, i.e., we apply Fortescue's transforma-

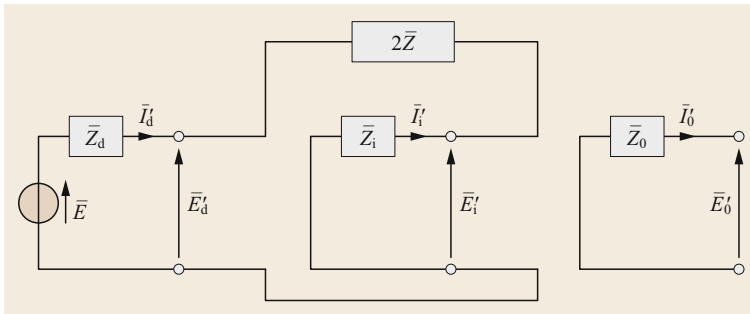


Fig. 5.32 Equivalent circuit of the line-to-line fault

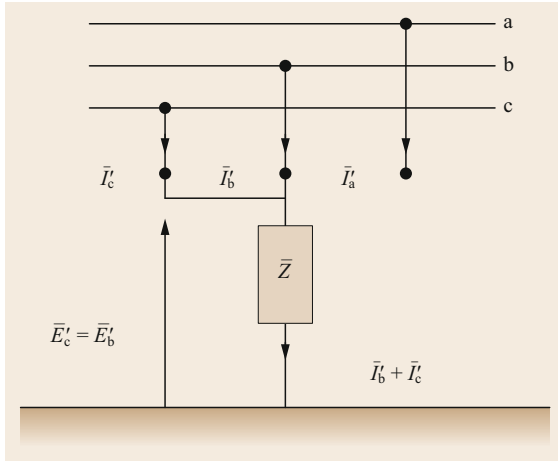


Fig. 5.33 Double line-to-ground fault

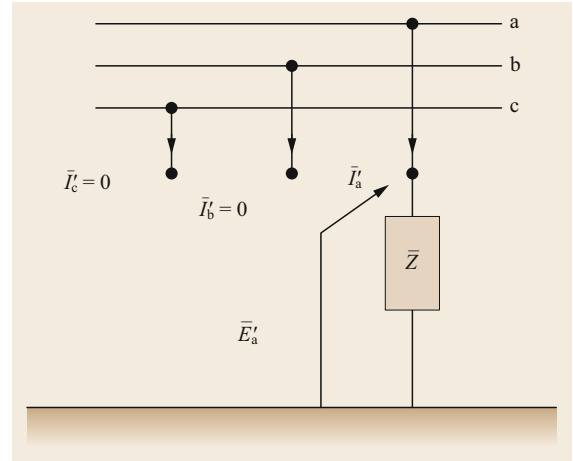


Fig. 5.35 Line-to-ground fault

tions to (5.171), we obtain the system

$$\begin{cases} \bar{I}'_d + \bar{I}'_i + \bar{I}'_0 = 0 \\ \bar{E}'_i = \bar{E}'_d \\ \bar{E}'_0 = \bar{E}'_d + 3\bar{Z}\bar{I}'_0 \end{cases} \quad (5.172)$$

Figure 5.34 presents the equivalent circuit resulting from (5.172); this equivalent circuit leads to the expressions

$$\begin{cases} \bar{I}'_d = \frac{\bar{E}}{\bar{Z}_d + [(\bar{Z}_0 + 3\bar{Z})\bar{Z}_i] / (\bar{Z}_i + \bar{Z}_0 + 3\bar{Z})} \\ \bar{I}'_i = -\bar{I}'_d \frac{\bar{Z}_0 + 3\bar{Z}}{\bar{Z}_i + \bar{Z}_0 + 3\bar{Z}} \\ \bar{E}'_d = \bar{E} - \bar{Z}_d \bar{I}'_d = \bar{E}'_i \\ \bar{E}'_0 = -\bar{Z}_0 \bar{I}'_0 \end{cases} \quad (5.173)$$

After some mathematical manipulation, we get

$$\bar{I}'_b = -j\sqrt{3}\bar{E} \frac{\bar{Z}_0 - \alpha\bar{Z}_i}{\bar{Z}_d\bar{Z}_i + \bar{Z}_d\bar{Z}_0 + \bar{Z}_i\bar{Z}_0} \quad (5.174)$$

for a bolted fault.

Line-to-Ground Fault

We now investigate the circuit depicted in Fig. 5.35, with $\bar{Z}_a = \bar{Z}$, $\bar{Z}_b = \bar{Z}_c = \infty$, $\bar{Z}_n = 0$.

Figure 5.35 leads to the expressions

$$\begin{cases} \bar{E}'_a = \bar{Z}\bar{I}'_a \\ \bar{I}'_b = 0 \\ \bar{I}'_c = 0 \end{cases} \quad (5.175)$$

Applying Fortescue's transformations to (5.175) yields

$$\begin{cases} \bar{I}'_d = \bar{I}'_i = \bar{I}'_0 \\ \bar{E}'_d + \bar{E}'_i + \bar{E}'_0 = 3\bar{Z}\bar{I}'_0 \end{cases} \quad (5.176)$$

The equivalent circuit resulting from system (5.176) is shown in Fig. 5.36. Note that the impedance $3\bar{Z}$ is in series with the direct, inverse, and homopolar circuit.

The expressions

$$\begin{cases} \bar{I}'_d = \bar{I}'_i = \bar{I}'_0 = \frac{\bar{E}}{\bar{Z}_d + \bar{Z}_i + \bar{Z}_0 + 3\bar{Z}} \\ \bar{E}'_d = \bar{E} - \bar{Z}_d \bar{I}'_d \\ \bar{E}'_i = -\bar{Z}_i \bar{I}'_i \\ \bar{E}'_0 = -\bar{Z}_0 \bar{I}'_0 \end{cases} \quad (5.177)$$

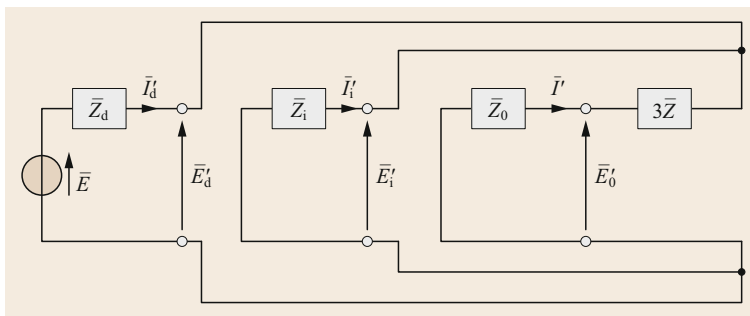


Fig. 5.34 Equivalent circuit of the double line-to-ground fault

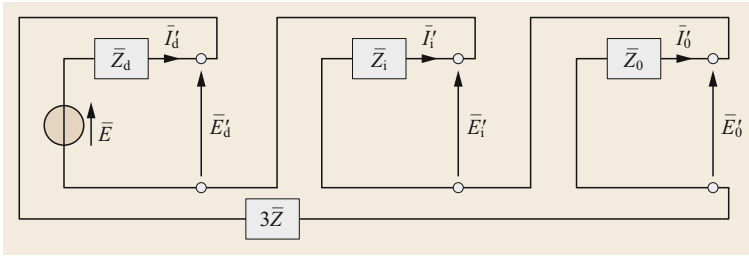


Fig. 5.36 Equivalent circuit of the line-to-ground fault

are readily obtained from the circuit shown in Fig. 5.36. Finally, the fault current for the line-to-ground fault is

$$\bar{I}'_a = \frac{3\bar{E}}{\bar{Z}_d + \bar{Z}_i + \bar{Z}_0 + 3\bar{Z}} \quad (5.178)$$

5.5.4 Direct, Inverse, and Homopolar Sequence Impedances

This section provides the main guidelines for determining the direct, inverse, and homopolar sequence impedances of the main power system elements. The following simplifying assumptions are made:

- Transversal parameters are negligible
- The equations are written using the per unit (pu) method.

The pu values of the component parameters (e.g., the reactance \dot{x} of a generator or transformer, etc.), which are provided by the manufacturer based on the rated voltage V_b and the rated apparent power of the equipment S_b , need to be converted to suitable base values of power, voltage V'_b , and apparent power S'_b for the various parts of the system according to

$$\dot{x}' = \dot{x} \left(\frac{V_b}{V'_b} \right)^2 \frac{S'_b}{S_b} \quad (5.179)$$

For *generators*, the equivalent circuits for direct, inverse, and homopolar sequences are shown in Fig. 5.37. Note that:

- To a good approximation, z_d can be represented by x''_d , the direct-axis subtransient reactance (which is

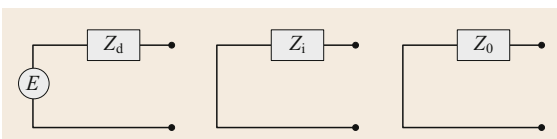


Fig. 5.37 Equivalent circuit of a generator: direct, inverse, and homopolar sequences

provided by the manufacturer and is typically in the range 0.1–0.3 pu).

- The inverse sequence $z_i \approx x''_d$ does not produce an effective armature reaction.
- z_0 is given by the manufacturer. Any impedance that is connected between the neutral point and the earth is multiplied by 3 and inserted into the equivalent circuit in series with Z_0 .

For *power transformers*, the inverse sequence is equal to the direct sequence and—as shown in Fig. 5.38—can be assumed to be equal to the short-circuit impedance in pu, i.e.,

$$z_{cc} = 0.01 v_{cc\%} \quad (5.180)$$

In the case of a three-winding transformer, the impedance of a particular winding can be calculated on the basis of the short-circuit test measurements

$$z_1 + z_2 = v_{cc,p-s\%} \times 0.01 \quad (5.181)$$

$$z_1 + z_3 = v_{cc,p-t\%} \times 0.01 \quad (5.182)$$

$$z_2 + z_3 = v_{cc,s-t\%} \times 0.01 \quad (5.183)$$

$$z_1 = 0.5(v_{cc,p-s\%} + v_{cc,p-t\%} - v_{cc,s-t\%}) \times 0.01 \quad (5.184)$$

$$z_2 = 0.5(v_{cc,p-s\%} + v_{cc,s-t\%} - v_{cc,p-t\%}) \times 0.01 \quad (5.185)$$

$$z_3 = 0.5(v_{cc,s-t\%} + v_{cc,p-t\%} - v_{cc,p-s\%}) \times 0.01 \quad (5.186)$$

where $v_{cc,p-s\%}$, $v_{cc,s-t\%}$, and $v_{cc,p-t\%}$ are the short-circuit impedances measured in three cases: when winding 1 is supplied, 2 is short-circuited, and 3 is open; when winding 2 is supplied, 3 is short-circuited, and 1 is open; and

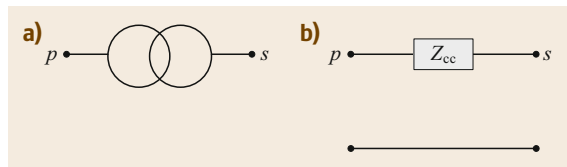


Fig. 5.38a,b Equivalent circuit of a transformer at the direct (a) and inverse sequences (b)

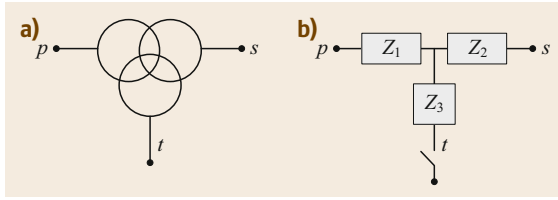


Fig. 5.39 Equivalent circuit of a three-winding transformer at the direct (a) and inverse sequences (b)

when 2 is supplied, 3 is short-circuited, and 1 is open, respectively. The equivalent circuit of a three-winding transformer at the direct and inverse sequences is represented in Fig. 5.39b.

Finally, Figs. 5.40 and 5.41 show the homopolar sequence impedances of the transformer and the three-winding transformer for different groups and connections of windings.

Any impedance connected between the neutral point and the earth is multiplied by 3 and introduced into the equivalent circuit in series to Z_0 (or, for the three-winding transformer, in series to Z_p or Z_s).

The equivalent circuits of a *transmission line* can be approximated as shown in Fig. 5.42. The positive and negative-sequence impedances Z_d and Z_i are equal. The

zero-sequence impedance Z_0 is typically 3 to 4 times larger than Z_d .

For three-phase and single-phase faults in a *generic network with given short-circuit power* (Fig. 5.43), the equivalent impedances are given by

$$z_d = \frac{E_{nom}}{I_{cc,3}} \tag{5.187}$$

$$z_d = z_i \tag{5.188}$$

$$z_0 = 3 \frac{E_{nom}}{I_{cc,1}} - 2z_d, \tag{5.189}$$

where $I_{cc,3}$ and $I_{cc,1}$ are the values for balanced and line-to-ground faults, respectively.

The short-circuit power for a three-phase fault is calculated via

$$P_{cc,3f} = E_{nom} I_{cc,3f}, \tag{5.190}$$

while the short-circuit power for a single-phase fault is obtained using

$$P_{cc,1f} = E_{nom} I_{cc,1f}. \tag{5.191}$$

An *infinite power bus* can be assumed to be equivalent to the bus of a network with infinite short-circuit cur-

| Case | Connections | Zero sequence circuit |
|------|-------------|-----------------------|
| a | | |
| b | | |
| c | | |
| d | | |
| e | | |

Fig. 5.40 Equivalent circuit of a transformer at the homopolar sequence (adapted from [5.6, 44])

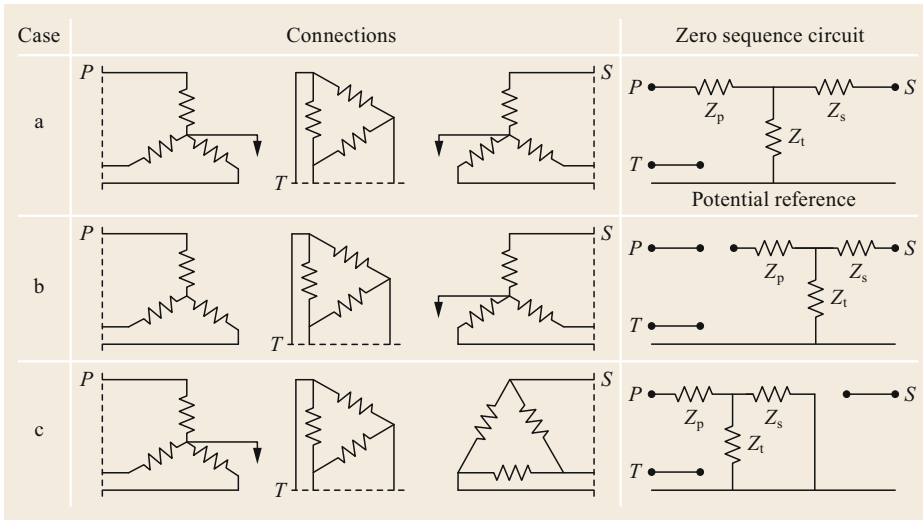


Fig. 5.41 Equivalent circuit of a three-phase transformer at the homopolar sequence (adapted from [5.6, 44])

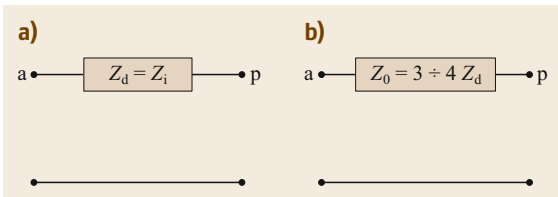


Fig. 5.42a,b Equivalent circuits of a transmission line: (a) positive sequence = negative sequence, (b) zero sequence

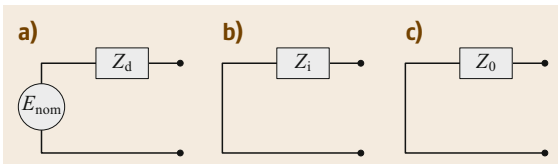


Fig. 5.43a-c Generic network with given short-circuit power: (a) positive sequence, (b) negative sequence, and (c) zero sequence

rent (for single-phase and three-phase faults). Also, we can assume that a bus without generators is equivalent to the bus of a network with null short-circuit current (for single-phase and three-phase faults). Loads, unless otherwise indicated, are neglected in the calculations.

5.5.5 Fault at Any Point in the Network

Consider the network depicted in Fig. 5.44. A symmetrical fault occurs at bus 3. We shall refer to the equivalent single-phase network, neglecting the presence of loads (no current is absorbed).

According to Thévenin's theorem, the linear part of the network can be replaced with an ideal indepen-

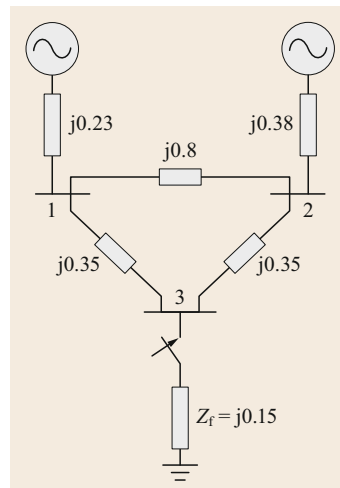


Fig. 5.44 The network considered; there is a fault at bus 3 (adapted from [5.12])

dent generator with an emf E (*no-load* emf) and an impedance Z_{th} (the equivalent impedance with all emfs short-circuited) in series, as shown in Fig. 5.45.

In the presence of loads, the voltage prior to the fault is given by the steady-state solution. Otherwise, it is approximated by the maximum permissible operating voltage of the transmission network, 1.1 pu.

By neglecting the loads and the transversal parameters of the network components, Z_{th} can be obtained by calculating the equivalent series and parallel impedances and by star-delta transformations (Z_{33} in Fig. 5.45, which is equal to $j0.34$, was obtained in this way).

The equivalent impedance Z_{th} can also be determined by inverting the nodal admittance matrix of the network to obtain the impedance matrix; Z_{th} is the element of the main diagonal of the impedance matrix that corresponds to the fault node.

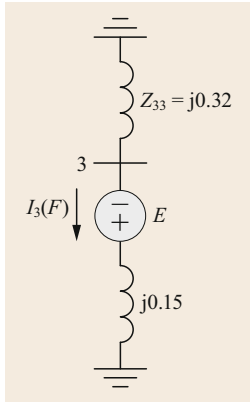


Fig. 5.45 The network following the application of Thévenin's theorem; there is a fault at bus 3 (adapted from [5.12])

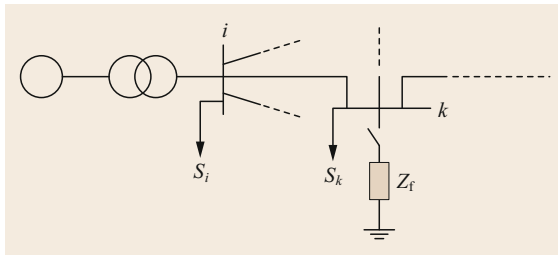


Fig. 5.46 Power system consisting of n buses; there is a fault at bus k (adapted from [5.12])

Let us consider the bus of a power system consisting of n buses, as shown in Fig. 5.46.

We now assume a symmetrical fault at bus k such that the fault impedance is Z_f .

The nodal voltages before the fault can be obtained by calculating the load flow, and are represented by the vector

$$\mathbf{E}(0) = \begin{bmatrix} E_1(0) \\ \vdots \\ E_k(0) \\ \vdots \\ E_n(0) \end{bmatrix}. \quad (5.192)$$

The voltage variations caused by the fault with impedance Z_f are equivalent to those caused by the voltage $E_k(0)$ when all the other generators are short-circuited.

The Thévenin equivalent circuit, as shown in Fig. 5.47, can be obtained by short-circuiting all of the generators and representing all of the loads and network components by their respective impedances.

Although we have ignored loads so far (since the steady-state currents are much lower than the short-circuit ones), the loads at the various buses can be accounted for by introducing a constant impedance. The

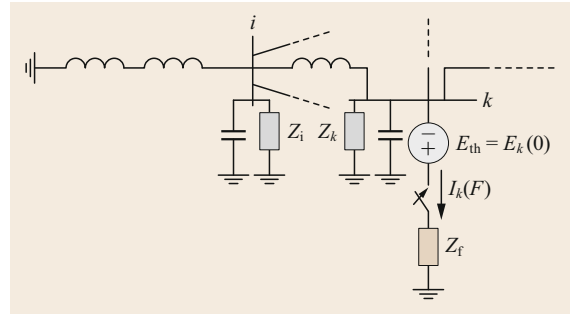


Fig. 5.47 Thévenin equivalent network of a power system consisting of n buses; there is a fault at bus k (adapted from [5.12])

value of this impedance can be obtained by

$$Z_{iL} = \frac{|E_i(0)|^2}{S_L}, \quad (5.193)$$

S_L being the power absorbed by the load before the fault. Let us denote the fault-induced nodal voltage variations by the vector

$$\Delta \mathbf{E} = \begin{bmatrix} \Delta E_1 \\ \vdots \\ \Delta E_k \\ \vdots \\ \Delta E_n \end{bmatrix}. \quad (5.194)$$

The nodal voltages during the fault are therefore given by the sum of the voltages before the fault and the variations due to the fault current, i.e.,

$$\begin{bmatrix} E_1(F) \\ \vdots \\ E_k(F) \\ \vdots \\ E_n(F) \end{bmatrix} = \begin{bmatrix} E_1(0) \\ \vdots \\ E_k(0) \\ \vdots \\ E_n(0) \end{bmatrix} + \begin{bmatrix} \Delta E_1 \\ \vdots \\ \Delta E_k \\ \vdots \\ \Delta E_n \end{bmatrix}. \quad (5.195)$$

In compact form,

$$\mathbf{E}(F) = \mathbf{E}(0) + \Delta \mathbf{E}. \quad (5.196)$$

The voltages at the nodes are related to the current by the expression

$$\mathbf{I} = \mathbf{Y} \cdot \mathbf{E}. \quad (5.197)$$

In the Thévenin circuit shown in Fig. 5.47, the incoming current at each node is zero except at node k , where it is

considered positive if injected (so we consider it to be negative).

Therefore, we get

$$\begin{bmatrix} 0 \\ \vdots \\ -I_k(F) \\ \vdots \\ 0 \end{bmatrix} = \begin{bmatrix} Y_{11} & \dots & Y_{1k} & \dots & Y_{1n} \\ \vdots & \vdots & \vdots & \vdots & \vdots \\ Y_{k1} & \dots & Y_{kk} & \dots & Y_{kn} \\ \vdots & \vdots & \vdots & \vdots & \vdots \\ Y_{n1} & \dots & Y_{nk} & \dots & Y_{nn} \end{bmatrix} \begin{bmatrix} \Delta E_1 \\ \vdots \\ \Delta E_k \\ \vdots \\ \Delta E_n \end{bmatrix}, \quad (5.198)$$

which can be rewritten in compact form as

$$\mathbf{I}(F) = \mathbf{Y} \cdot \Delta \mathbf{E}, \quad (5.199)$$

leading to

$$\Delta \mathbf{E} = \mathbf{Z} \cdot \mathbf{I}(F), \quad (5.200)$$

where

$$\mathbf{Z} = \mathbf{Y}^{-1}, \quad (5.201)$$

which is known as the impedance matrix.

Therefore, from (5.196),

$$\mathbf{E}(F) = \mathbf{E}(0) + \mathbf{Z} \cdot \mathbf{I}(F). \quad (5.202)$$

In matrix form,

$$\begin{bmatrix} E_1(F) \\ \vdots \\ E_k(F) \\ \vdots \\ E_n(F) \end{bmatrix} = \begin{bmatrix} E_1(0) \\ \vdots \\ E_k(0) \\ \vdots \\ E(0)_n \end{bmatrix} + \begin{bmatrix} Z_{11} & \dots & Z_{1k} & \dots & Z_{1n} \\ \vdots & \vdots & \vdots & \vdots & \vdots \\ Z_{k1} & \dots & Z_{kk} & \dots & Z_{kn} \\ \vdots & \vdots & \vdots & \vdots & \vdots \\ Z_{n1} & \dots & Z_{nk} & \dots & Z_{nn} \end{bmatrix} \begin{bmatrix} 0 \\ \vdots \\ -I_k(F) \\ \vdots \\ 0 \end{bmatrix}. \quad (5.203)$$

This leads to

$$E_k(F) = E_k(0) - Z_{kk} I_k(F). \quad (5.204)$$

We also know from Fig. 5.47 that

$$E_k(F) = Z_f I_k(F), \quad (5.205)$$

and that $E_k(F) = 0$ for a solid balanced fault (i.e., $Z_f = 0$). Therefore,

$$I_k(F) = \frac{E_k(0)}{Z_{kk} + Z_f}. \quad (5.206)$$

Hence, for a fault at bus k , we only need the element Z_{kk} , which is the Thévenin equivalent impedance of the network viewed from the fault location.

We also have that

$$E_k(F) = Z_f I_k(F). \quad (5.207)$$

Substituting the previous expression for I_k into this equation yields

$$E_i(F) = E_i(0) - \frac{Z_{ik}}{Z_{kk} + Z_f} E_k(0). \quad (5.208)$$

The knowledge of the nodal voltages during the fault allows the fault current to be calculated for all of the lines. The short-circuit current in the line that connects buses i and j (where the current is defined to be positive in the $i \rightarrow j$ direction) through impedance z_{ij} is given by

$$I_{ij}(F) = \frac{E_i(F) - E_j(F)}{z_{ij}}. \quad (5.209)$$

Note that the knowledge of the impedance matrix allows the fault current and the node voltage during the fault to be readily evaluated for every node of the network.

This method is simple and practical: all the calculations relevant to a specific fault are formulated with respect to the fault bus using the impedance matrix \mathbf{Z} which can be calculated by inverting \mathbf{Y} , although this inversion is computationally prohibitive for large power systems with many nodes. A more efficient method of determining \mathbf{Z} is to construct it by adding one element of the network at a time.

5.5.6 Three-Phase Short Circuit at a Synchronous Generator's Terminals

A synchronous machine operating as a generator can be studied by considering it as an active two-port network. It is also linear when the working conditions are far from saturation, as is usual during faults. The following considerations are made for a round rotor machine, but they can easily be extended to the case of a salient pole machine.

The equivalent two-port equation of the alternator is

$$\bar{E} - \bar{Z}_s \bar{I} = \bar{V}, \quad (5.210)$$

where:

- \bar{E} is the emf generated in the alternator by the excitation current I_f (the voltage measured at the machine's terminal under no-load conditions)
- \bar{V} is the voltage measured at the machine's terminal when the machine supplies current \bar{I}
- \bar{Z}_s is the internal impedance of the machine, commonly termed the synchronous impedance, which is the sum of two components: (i) the impedance of the stator's windings and (ii) the armature's reaction.

For a given value of the excitation current and a given current \bar{I} flowing in the stator's windings, the voltage \bar{V} at the machine's terminals is different from the no-load emf \bar{E} . The difference

$$\bar{Z}_s \bar{I} = \bar{E} - \bar{V} \quad (5.211)$$

is the voltage drop due to the current \bar{I} and its shift with respect to \bar{V} . This voltage drop is given by the two components mentioned above:

- The drop in the impedance of the stator's windings $(R_1 + jX_1)\bar{I}$, where R_1 and X_1 are the resistance of the stator's windings and the leakage reactance, respectively
- The armature's reaction, which is equal to $jX_r\bar{I}$ for a round rotor machine.

Therefore, it holds that

$$\bar{Z}_s = R_1 + j(X_1 + X_r) \quad (5.212)$$

The quantity

$$X_s = X_1 + X_r \quad (5.213)$$

is the synchronous reactance of the machine.

Let us assume that a synchronous generator is supplying an inductive load. In this case, we assume that I lags E and V by 90° (ignoring the circuit resistance): the flux produced by the stator (the armature flux) has the opposite polarity to the main flux Φ , thus reducing the main flux. Consequently, the total emf induced in the stator decreases. This phenomenon is called the demagnetizing effect and it is represented in Figs. 5.48 and 5.49.

Let us assume that the synchronous generator is supplying a capacitive load. In this case, we assume that I leads E and V by 90° (the excitation current is kept the same as in the previous case): the flux produced by the stator (armature flux) is in phase with the main flux Φ , thus increasing the main flux. Consequently, the total emf induced in the stator increases. This phenomenon is known as the magnetizing effect and it is represented in Figs. 5.50 and 5.51.

In order to simulate the alternator under transient conditions, we make use of the EMTP-RV model pre-

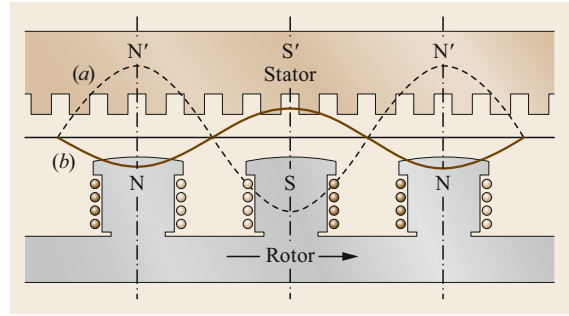


Fig. 5.48 Armature reaction: the current I lags the voltage by 90° . Waveform (a) shows the main flux Φ , while waveform (b) shows the armature flux (adapted from [5.1])

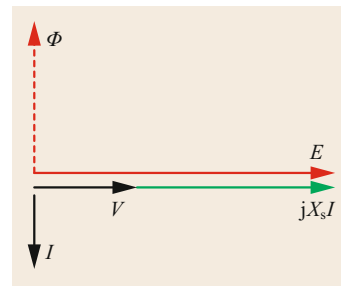


Fig. 5.49 Phasor diagram of the alternator for an inductive load

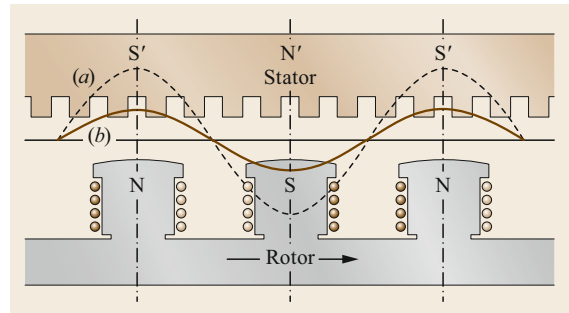


Fig. 5.50a,b Armature reaction: current I leads the voltage by 90° . Waveform (a) shows the main flux Φ , while waveform (b) shows the armature flux (adapted from [5.1])

sented in [5.8, 45]. Park's transformation is initially used with saturation neglected to obtain linear relations and apply superposition.

The magnetic circuits of the rotor windings are assumed to be symmetric with respect to the direct axis, which is the axis of the field created by the rotor. The quadrature axis lags the direct one by 90° .

A current in any winding produces a sinusoidal magnetic field in the air gap. This field can be decomposed along the direct and quadrature axes. The effects of harmonics in the field distribution are negligible for a correctly dimensioned machine. The effects of hysteresis are neglected. Eddy currents are negli-

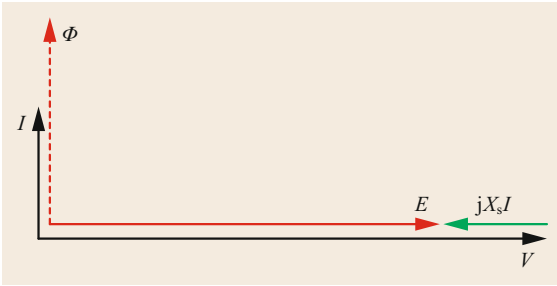


Fig. 5.51 Phasor diagram of the alternator for a capacitive load

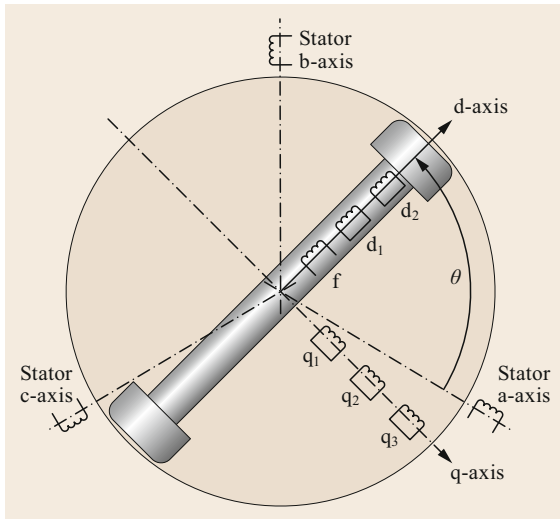


Fig. 5.52 Schematic representation of the machine showing the d-axis and q-axis (adapted from EMTP-RV help)

ble, except in the case of a solid rotor (cylindrical rotor) machine, where they can be represented by a q-axis winding.

The synchronous machine model consists of nine windings:

- Three for the stator (one for each phase); these are denoted by the indices a, b, and c, respectively.
- Six for the rotor. Along the axis of the rotor field (the direct axis), we have the excitation winding f and a maximum of two damper windings: d_1 and d_2 . There are also a maximum of three damper windings, denoted q_1 , q_2 , and q_3 , along the quadrature axis.

This machine is represented in Fig. 5.52.

Short-Circuit Currents with the Generator Initially at No Load

Let us consider a three-phase synchronous generator with the following parameters:

- Rated power: 1000 MVA
- Nominal frequency: 50 Hz
- Rated voltage (RMSLL (RMS line-to-line)): 20 kV
- Winding (armature) resistance: 0.002 pu
- Armature leakage reactance: 0.188 pu
- Direct-axis synchronous reactance: $x_d = 2$ pu
- Quadrature-axis synchronous reactance: $x_q = 2$ pu
- Direct-axis transient reactance: $x'_d = 0.4$ pu
- Quadrature-axis transient reactance: $x'_q = 0.4$ pu
- Direct-axis short-circuit transient constant: $T'_d = 1$ s
- Quadrature-axis short-circuit transient constant: $T'_q = 1$ s.

It is initially assumed that the d-axis and q-axis sub-transient reactances are negligible. As a consequence, if we refer to the equivalent model in Fig. 5.52, only the field winding is relevant along the d-axis, while only one damper is considered along the q-axis (winding q_1).

Let us assume that no-load steady-state conditions apply. A three-phase short circuit occurs at the machine's terminals at $t = 200$ ms. At $t_{\text{fault}} = 200$ ms, a three-phase bolted short circuit occurs at the machine's terminals. Figure 5.53 shows the currents in the three stator windings during the fault. The subtransient reactance is neglected. If the winding resistances are neglected, the stator current lags the voltage by 90° , as the machine's reactances are equivalent to a purely inductive load. Therefore, at the instant that the short circuit occurs, the current in phase a is at its natural zero crossing, so this current has no unidirectional component—only the symmetrical component. Initially, the current reaches a peak value of approximately 100 kA, before decreasing exponentially to reach its steady-state value. The current in phase b reaches its maximum and the current in phase c reaches its minimum at the instant that the short circuit occurs, meaning that those currents have unidirectional components, as shown in Fig. 5.53.

The envelope for the current in phase a is shown in Fig. 5.54, and is given by

$$y(t) = \sqrt{2} \left[\left(\frac{1}{x'_d} - \frac{1}{x_d} \right) e^{-\frac{t}{T'_d}} + \frac{1}{x_d} \right] I_{\text{base}}, \quad (5.214)$$

where

$$I_{\text{base}} = \frac{A_n}{\sqrt{3}V_n} = 28.9 \text{ kA}. \quad (5.215)$$

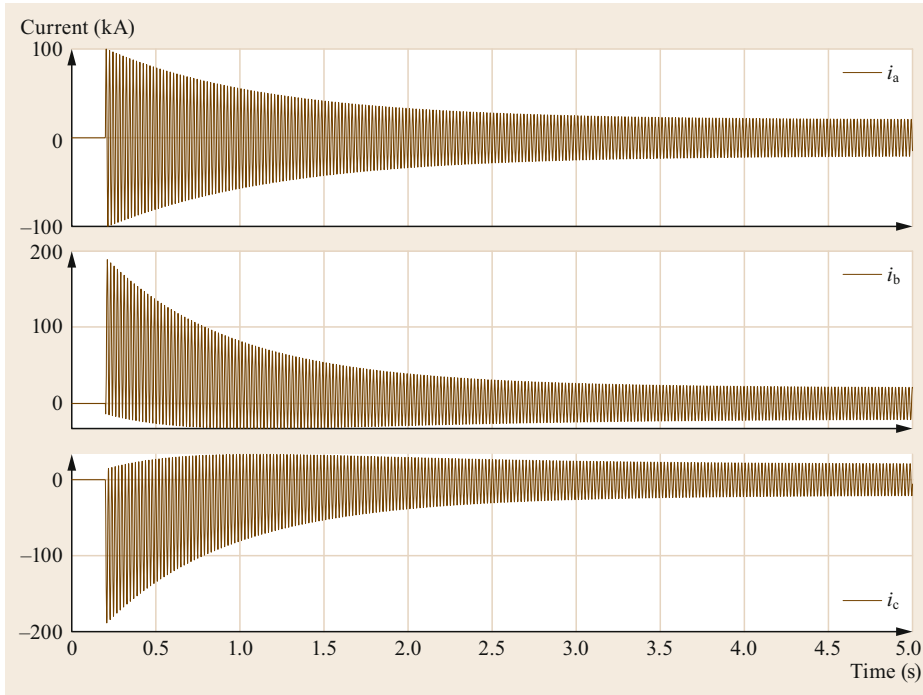


Fig. 5.53 Phase currents: three-phase fault at 200 ms (subtransient state neglected)

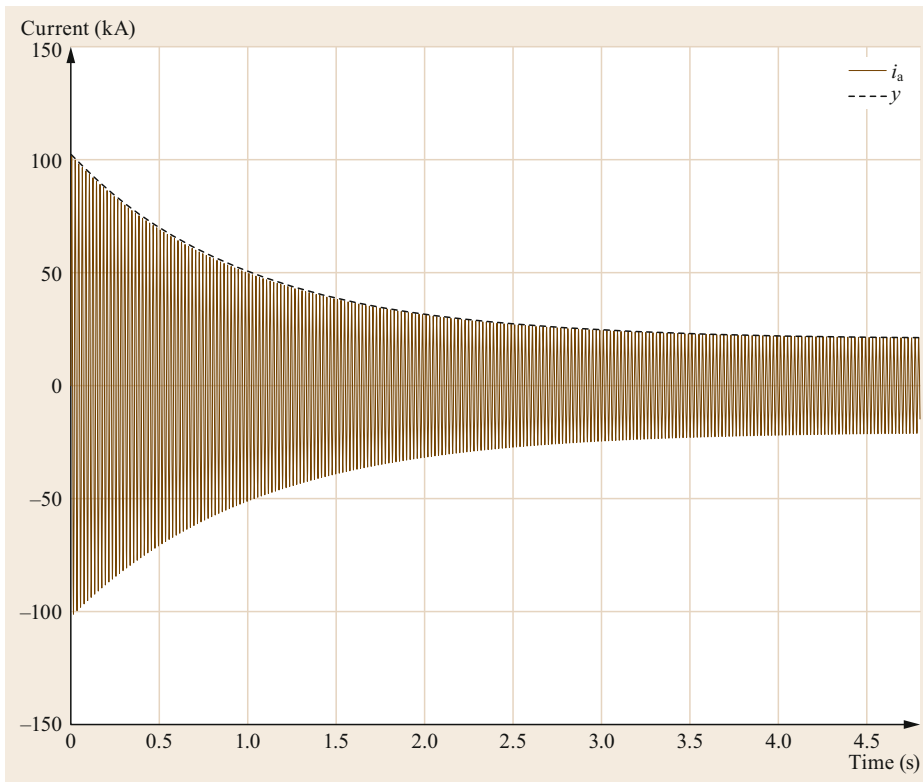


Fig. 5.54 The current and the current envelope in phase a (subtransient state neglected); 200 ms time shift

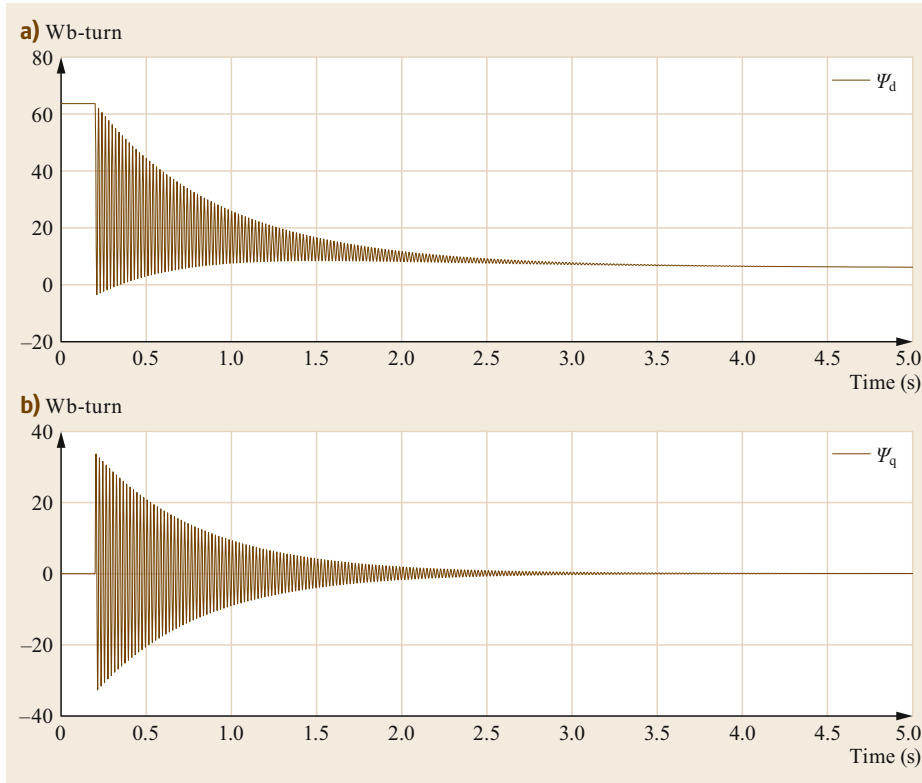


Fig. 5.55a,b Flux linkages along (a) the d-axis and (b) the q-axis (subtransient state neglected)

The envelope of the symmetrical component of the short circuit current $y(t)$, in pu, is initially equal to

$$y(t = t_{\text{fault}}) = \frac{1}{x'_d} \quad (5.216)$$

In the first few moments, the armature reaction is weakened by the rapid variation of the total flux linkage. At the beginning of the electromagnetic transient, therefore, the armature reactance is not equal to the synchronous reactance of the machine but to the transient one (ignoring the subtransient state).

The steady-state value of the symmetrical component (in pu) is given by

$$y(t \rightarrow \infty) = \frac{1}{x_d} \quad (5.217)$$

Upon substituting the values of the reactances into (5.214), it becomes apparent that the peak value of $y(t)$ for the configuration of interest is initially equal to 102 kA, and it reaches 20.4 kA in the steady state.

The flux linkages along the d-axis and the q-axis are shown in Fig. 5.55. Prior to short-circuit inception, the flux along the d-axis is at a constant value dictated by

the excitation winding current. During the transient, it decreases exponentially until it attains a low constant value in the steady state. This is due to the demagnetizing effect of the short-circuit current, in agreement with the phasor diagram of Fig. 5.49. Since the machine operates under no-load conditions before the fault, the total flux is equal to the d-axis flux, while the flux linkage along the q-axis is null. The sudden variation in the armature current leads to rapid variation of the q-axis flux, which quickly reaches its peak value before decreasing exponentially to zero again.

It is worth noting that, besides the exponential decay, the flux along each axis shows an oscillatory component. This component oscillates at a frequency of 50 Hz with respect to the d-q frame because it is induced by the unidirectional components of the currents in phases b and c. These components generate a magnetic field that is stationary with respect to the stator but appears to be a magnetic field rotating at 50 Hz in the d-q frame. This is confirmed by the detail shown in Fig. 5.56. The amplitude of the oscillatory component along the q-axis decays with the same time constant as the unidirectional component of the stator winding current. Similar considerations apply for the current flowing in the q-axis damper winding i_{q1} , as shown in

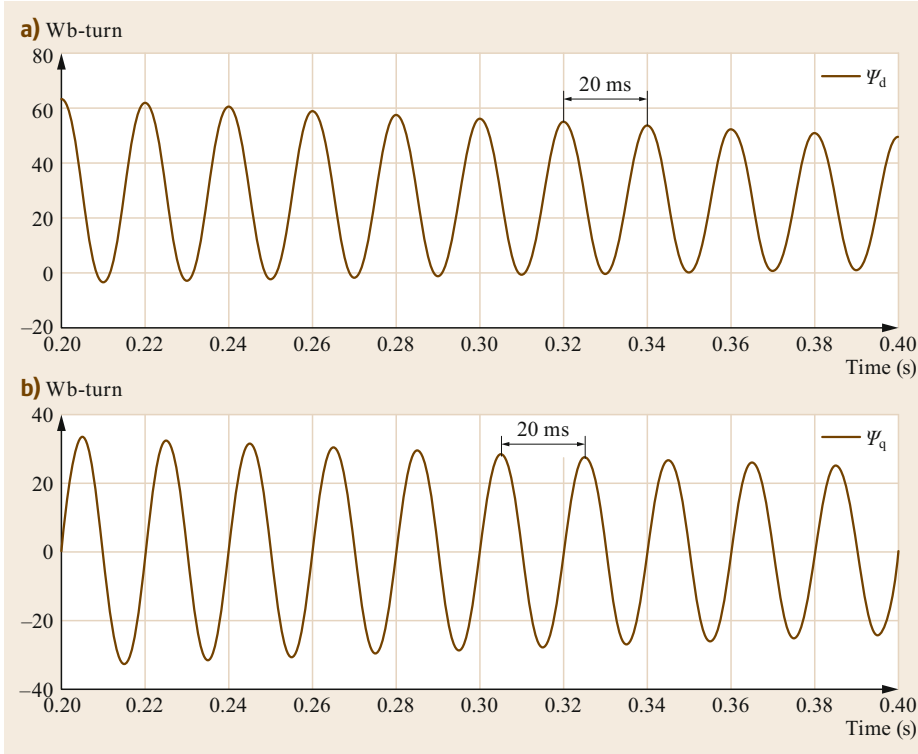


Fig. 5.56a,b Flux linkages along (a) the d-axis and (b) the q-axis shown in detail (the subtransient state is neglected)

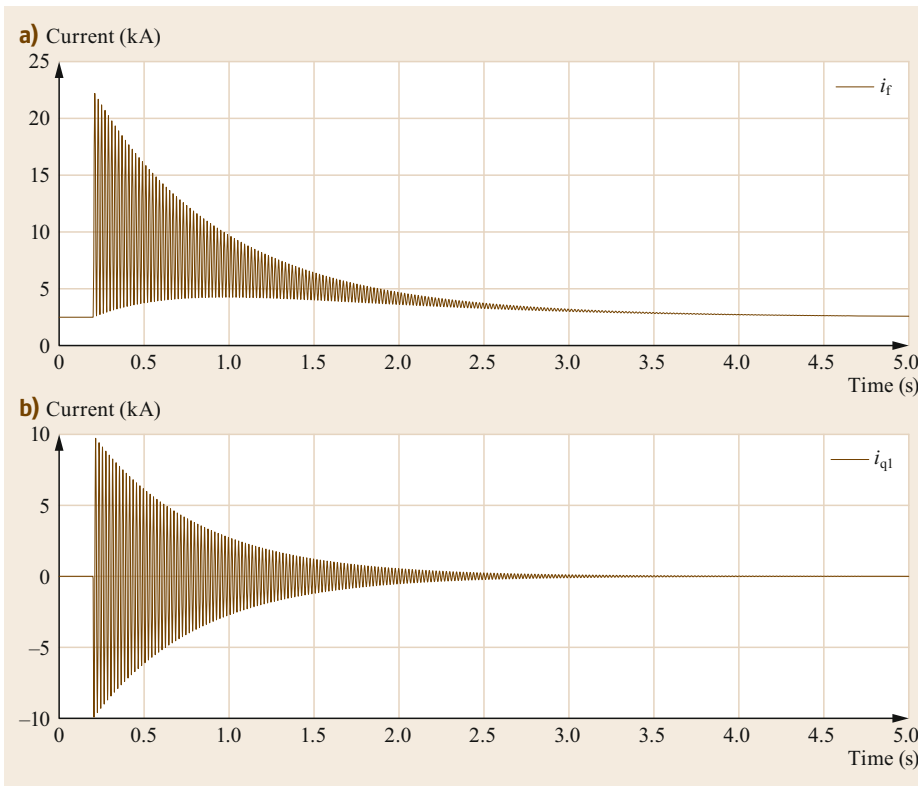


Fig. 5.57a,b Currents in the field winding (a) and the first q-axis damper winding (b)

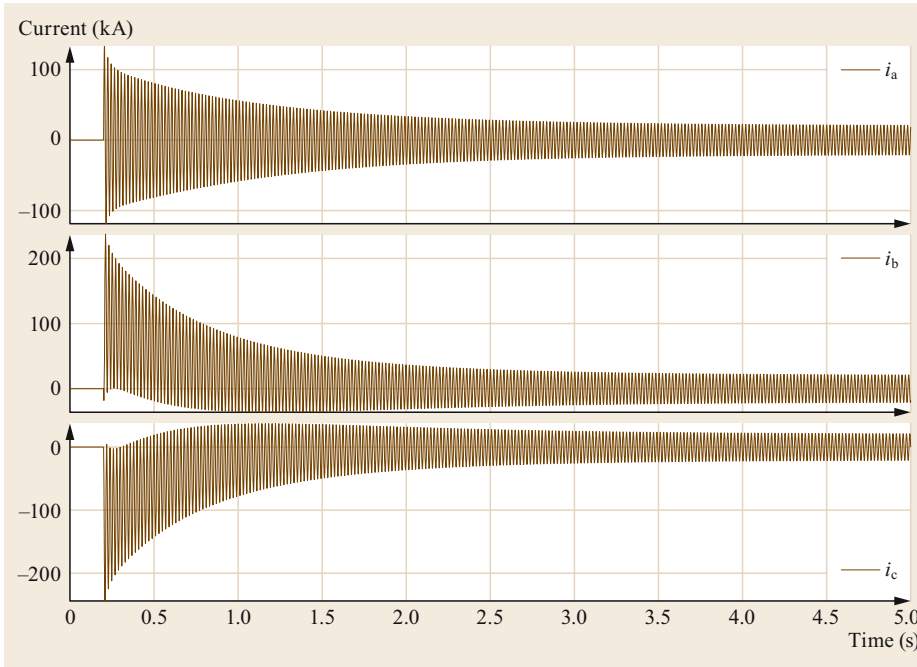


Fig. 5.58 Phase currents with the subtransient state considered

Fig. 5.57. According to the Faraday–Neumann–Lenz law, the magnetic field generated by the current flowing in the damper windings during the transient opposes the initial changing magnetic field. The current i_f that flows in the rotor field winding is also reported in Fig. 5.57. Before the fault, i_f is set to 2494 A. The sudden variation in the current in the stator windings induces an emf in the rotor field winding, which causes an increase of the currents in both the field and damper windings, as shown in Fig. 5.57. Just as for the damper windings, the magnetic field created by the current induced in the field winding opposes the initial changing magnetic field. Similar to the flux linkage and i_{q1} , the oscillatory component of i_f is generated by the unidirectional component of the stator winding current. In the steady state, as the flux linkage is constant with respect to the rotor frame of reference, the value of the rotor current i_f returns to its previous value, 2494 A.

Let us now consider the effects of the damper windings on the direct axis and a second damper on the q-axis. The d-axis and q-axis subtransient reactances are $x_d'' = x_q'' = 0.3$ pu, and the short-circuit subtransient constant is $T_d'' = 0.03$ s.

Figure 5.58 shows the currents in the three stator windings during the fault. The current waveforms in the three stator windings are similar to those in the previous case in which the subtransient state was neglected, but the initial current peaks are larger.

The envelope of the current in phase a is shown in Fig. 5.59 and is given by the expression

$$y_s(t) = \sqrt{2} \left[\left(\frac{1}{x_d''} - \frac{1}{x_d'} \right) e^{-\frac{t}{T_d''}} + \left(\frac{1}{x_d'} - \frac{1}{x_d} \right) e^{-\frac{t}{T_d}} + \frac{1}{x_d} \right] I_{\text{base}} . \quad (5.218)$$

The armature reaction during the subtransient state is lower than those in the transient and steady states. As a consequence, the initial value of the current is higher than that given by (5.214).

Short-Circuit Currents in the Loaded Generator

In this final comparison, we consider the case in which the generator is supplying a load before the fault occurs. Figure 5.60 shows the current in phase a when the machine is under no-load and on-load conditions. In the latter case, the current is not null before the fault. The peak value is similar to that calculated for the machine under no-load conditions, but the final steady-state current amplitude is slightly larger.

It is interesting to observe the variation in the flux linkage—particularly that along the q-axis (see Fig. 5.61)—during the transient. Unlike the case shown in Fig. 5.55, the flux is not null before fault inception, but the steady-state value after the fault is zero due to the demagnetizing effect of the short-circuit current.

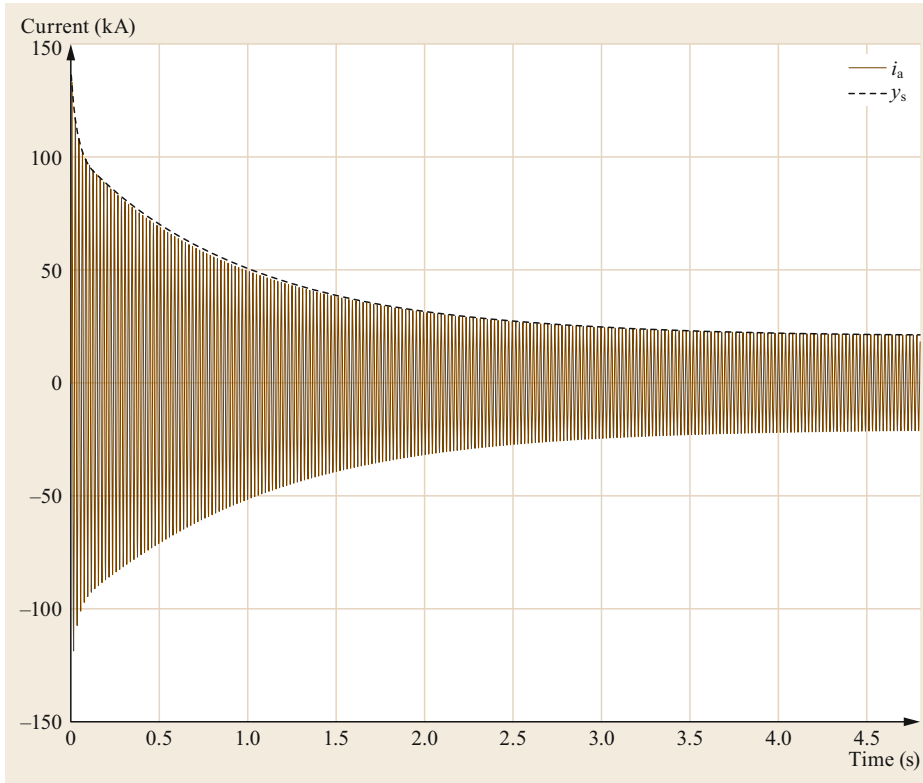


Fig. 5.59 The current and the current envelope in phase a with the subtransient state considered; 200 ms time shift

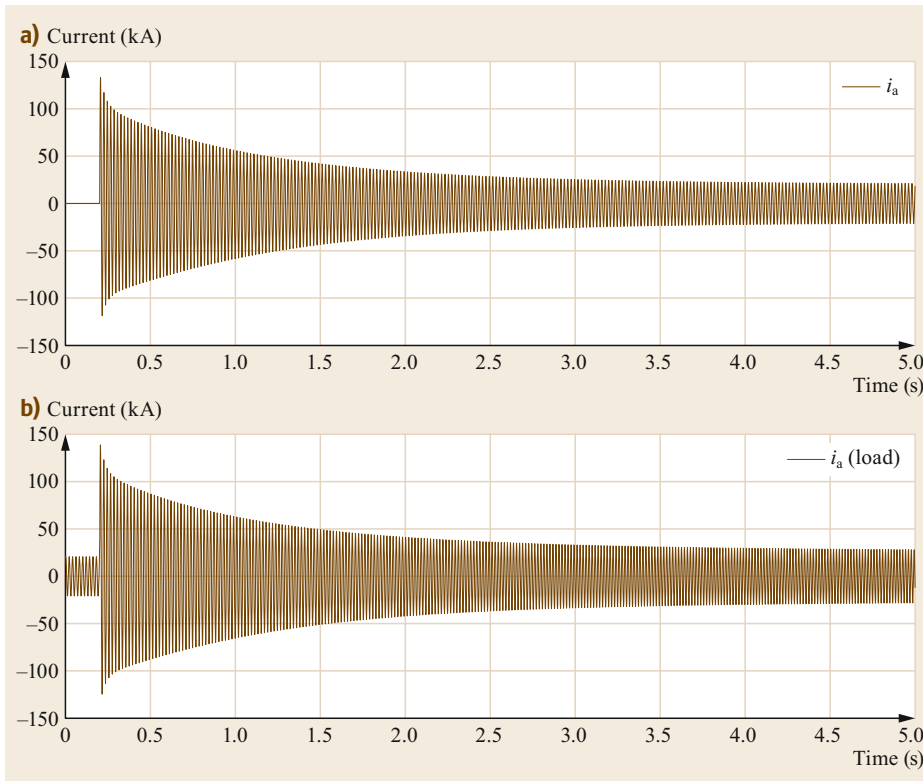


Fig. 5.60a,b Current in phase a under (a) no-load and (b) on-load conditions

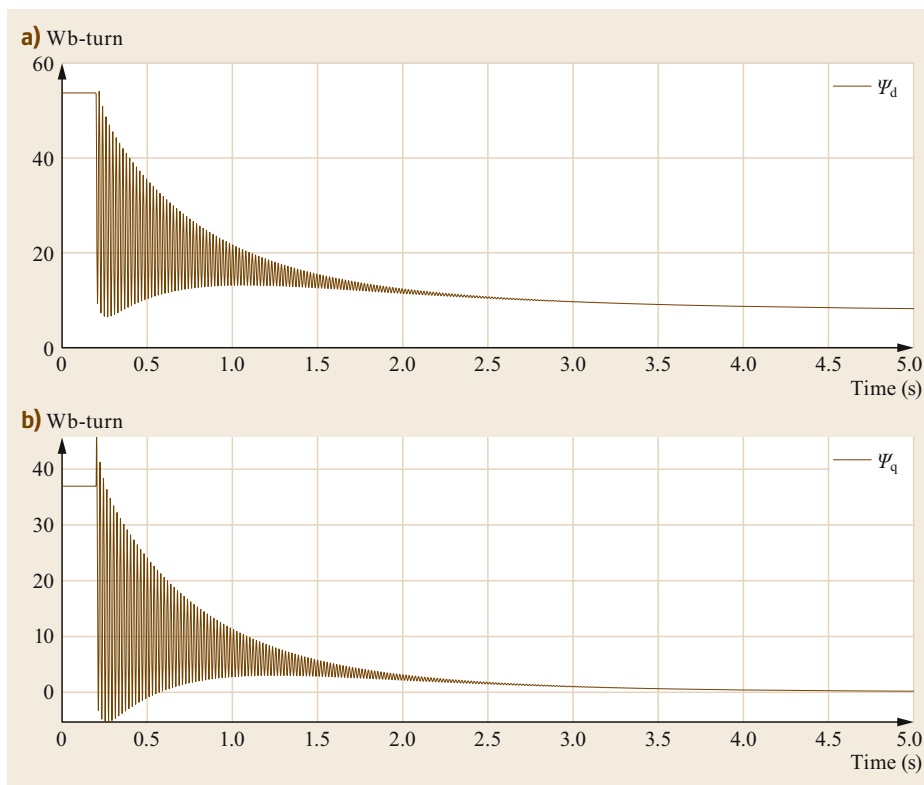


Fig. 5.61a,b Flux linkages along (a) the d-axis and (b) the q-axis under on-load conditions

5.6 Stability

A wide variety of dynamic phenomena occur in electric power systems. These phenomena are often called transients. Transients have various physical origins and timescales. Ignoring small variations in the operating conditions (which are always present), a transient corresponds to a significant perturbation of the steady state of a system. During the transient, several other perturbations may occur due to control and protective actions.

5.6.1 Transient Phenomena

Listed in order of the fastest to the slowest, transients in power systems are usually categorized into:

- Propagating electromagnetic transients that affect lines, transformers, and other connected components. These transients are caused by lightning or switching maneuvers, and have typical time horizons of between 10^{-7} and 10^{-3} s (corresponding to frequencies ranging from 10 MHz to kHz).
- Electromagnetic transients in rotating machine windings that are caused by disturbances, switch-

ing maneuvers, or interactions between machines (time horizon: 10^{-3} – 10^{-1} s; frequency: a few kHz to 10 Hz).

- Electromechanical transients, namely rotor swings in synchronous machines and motors. These originate in the same way as for the two types of transients defined above, as well as from voltage and frequency control (0.1–10 s; 10–0.1 Hz).
- Non-electrodynamic transients, including mechanical phenomena, thermodynamic phenomena, and their interactions with the control systems of power plants (10 – 10^4 s, 0.1 Hz–0.1 mHz).

Obviously, real events can be very complex and often involve dynamics associated with all four groups listed above. For example, when lightning strikes a power line, it produces traveling surges that propagate along the line. The overvoltage may cause a fault, which may cause transients in the synchronous machines, leading to interventions by relays. Also, protective operations can cause frequency transients that may require interventions from power-plant governors and control systems.

5.6.2 Definition of Stability

For given operating conditions, the power system stability is the ability of the system to regain the state of operating equilibrium after being subjected to a disturbance, with most system variables bounded such that practically the entire system remains intact. As a power system is a nonlinear system, its behavior after any disturbance depends on the type and magnitude of the disturbance, its consequences, and the initial operating point. Even though the system does not reach the same steady-state operating equilibrium as that prior to the disturbance, the system is considered stable if the final operating equilibrium after the perturbation is an acceptable steady state, meaning that further intervention through protective or control actions can be avoided.

To introduce this analysis, it is useful to first provide a brief overview of the different operating states of power systems as well as a classification of power-system stability studies.

5.6.3 States of Operation

There are typically considered to be five possible states of operation, as shown in Fig. 5.62.

This classification refers to three sets of equations that describe the dynamic phenomena: one differential and two algebraic (generally nonlinear) equations corresponding to equality constraints, which represent the balance between the generation and the load demand; and inequality constraints, which represent the operating limits.

The normal secure state is a system operating condition that is able to satisfy both the equality and inequality constraints with adequate reserve margins for both transmission and generation taking into account the reasonable stresses to which the system may be sub-

jected. For example, the N-1 security criterion implies that a system in its normal state can withstand a single contingency (i.e., the loss of a line, a transformer, or a generator) and that the new steady state still satisfies all the equality and inequality constraints.

The alert state characterizes a system operating condition that satisfies both the equality and inequality constraints but the security level is considered to be insufficient. This implies that the system is vulnerable; in other words, some of the inequality constraints will be violated in the event of some reasonable contingencies. To bring the system to a normal state, some preventive control actions should be taken.

The emergency state characterizes a system operating condition in which at least one of the inequality constraints is violated but the system is still intact (i.e., all the equality constraints are met). Emergency corrective actions should be initiated to restore the system to the alert state. If these measures are not taken in time or are ineffective, the system will break down and reach the in extremis state in which both equality and inequality constraints are violated. The in extremis state corresponds to a system failure characterized by a loss of system integrity involving uncontrolled islanding and the uncontrolled loss of large blocks of loads.

The restorative state describes a system that is separated into areas that may or may not be energized, and in which restorative actions are carried out to bring the system to either an alert or a normal state.

5.6.4 Classification of Power System Stability

The traditional classification of power system stability is summarized in Fig. 5.63.

A common cause of instability phenomena is an excessive imbalance of active and reactive power in the system, either locally or globally.

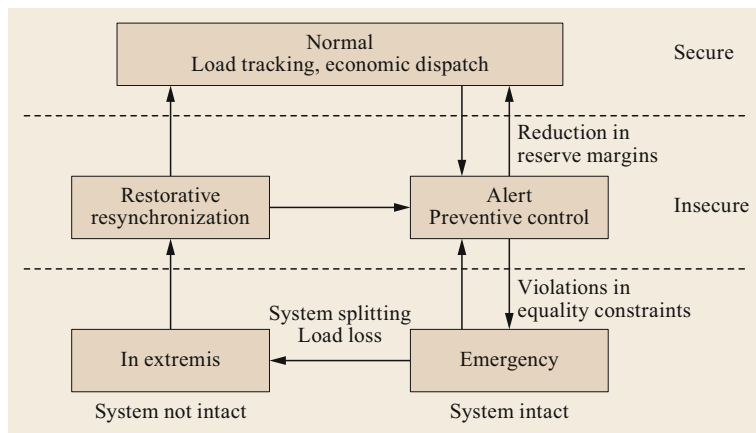


Fig. 5.62 Classification of power system states (adapted from [5.46, 47])

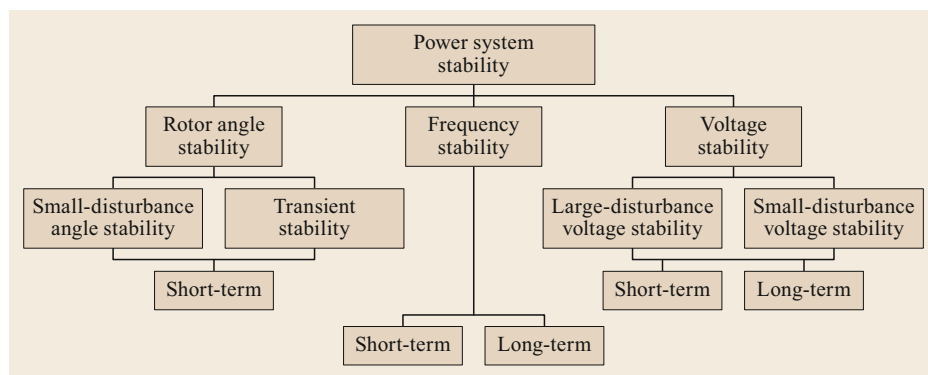


Fig. 5.63
Classification of power system stability (adapted from [5.48])

Rotor Angle Stability

Rotor angle stability refers to the balance of the torques in the rotors of the synchronous generators. This balance is achieved when the mechanical power provided by the prime mover (e.g., the hydro and steam turbines) meets the load fed by the alternator. If there is an imbalance, the rotors of the generators will act as an energy buffer and the kinetic energy stored in them will decrease or increase. Rotor angle stability refers to the ability of a synchronous machine in the power system to maintain synchronism after a disturbance and regain a steady-state condition characterized by a constant speed without long-lasting oscillations. If the disturbance is local and substantial, such as a fault in a line close to a generator, the generator can fall out of step, as it is accelerated during the fault. A protection will promptly trip the generator in order to avoid machine damage. This kind of dynamic phenomenon is called transient instability, and typically develops within a couple of seconds. On the other hand, small-disturbance (or small-signal) stability instead refers to the ability of the power system to maintain synchronism and regain a steady-state condition after disturbances so small that linearization of the system equations is acceptable for the analysis. Transient instability is associated with insufficient synchronizing torque, whilst small-disturbance problems are associated with insufficient damping of oscillations.

Frequency Stability

Frequency stability issues are associated with global power imbalances due to the difference between the total power fed into the system by the prime movers and the power consumed by the loads, including losses. The imbalance is compensated for by the kinetic energy stored in the rotors of the machines, resulting in a frequency deviation. If the imbalance is limited, the frequency is controlled by the governors of the prime movers. If the imbalance is too large, the amplitude of the frequency deviation can prompt interventions from

protections that disconnect loads and generators. The time horizon of frequency stability issues ranges from a few seconds (short-term instability) up to several minutes (long-term instability).

Voltage Stability

Voltage stability refers to the ability of a power system to maintain steady voltages at all buses after a small or large disturbance. Voltage problems are often local and caused by the dynamic responses of loads to disturbance. They are called voltage instabilities, voltage collapses, and load instabilities. Depending on the timescale, voltage stability issues are classified as either short-term (a couple of seconds) or long-term (tens of seconds to minutes). Short-term phenomena are associated with the dynamic responses of fast-acting components (such as induction motors, electronically controlled loads, and HVDC converters) to perturbations. Long-term phenomena are due to the actions of slow-acting equipment, such as step-changing transformers, thermostatically controlled loads, and generator current limiters. As explained above, generators (i.e., synchronous machines) are strongly linked to angular instabilities, and it is sometimes said that they are the driving force for this instability.

5.6.5 P - δ Curves of Synchronous Machines

Before discussing how to study rotor angle stability, we first recall some concepts relating to the operation of a synchronous machine under steady-state and transient conditions.

Selection of the Machine Model

Let us ignore the presence of automatic voltage regulators (AVRs). When the stator current varies for any reason (e.g., a sudden load variation or short circuit), the excitation and damper circuits tend to oppose the consequent variation in the flux. Specifically, some currents start to circulate in these circuits, producing a flux

Table 5.4 Typical parameter values for large generators (adapted from [5.11])

| Parameter | Round rotor | | | Salient pole rotor | |
|-----------|-------------|---------|----------|--------------------|---------|
| | 200 MVA | 600 MVA | 1500 MVA | 150 MVA | 230 MVA |
| X_d | 1.65 | 2.00 | 2.20 | 0.91 | 0.93 |
| X_q | 1.59 | 1.85 | 2.10 | 0.66 | 0.69 |
| X'_d | 0.23 | 0.39 | 0.44 | 0.3 | 0.3 |
| X'_q | 0.38 | 0.52 | 0.64 | – | – |
| X''_d | 0.17 | 0.28 | 0.28 | 0.24 | 0.25 |
| X''_q | 0.17 | 0.32 | 0.32 | 0.27 | 0.27 |
| T'_d | 0.83 | 0.85 | 1.21 | 1.10 | 3.30 |
| T'_q | 0.42 | 0.58 | 0.47 | – | – |
| T''_d | 0.023 | 0.028 | 0.030 | 0.05 | 0.02 |
| T''_q | 0.023 | 0.058 | 0.049 | 0.06 | 0.02 |

that instantaneously opposes the mentioned flux variation. It is possible to distinguish two different states: the subtransient state, which persists until all of the currents in the damper windings have been extinguished, and the subsequent transient state, which ends when the current in the excitation circuit eventually vanishes. The durations of these subtransient and transient states are related to the time constants of the damper and excitation windings, respectively. Accordingly, it is possible to identify the subtransient and transient reactances as they are the reactances of the machine during these two different states. Although the detailed illustration of the synchronous machine model provided by Park is beyond the scope of this chapter, it is worth mentioning that each of these two reactances—subtransient and transient—can be split into two components along the d-axis and the q-axis.

A comparison of typical values of the time constants of alternators (Table 5.4) with the period of the oscillations (0.5–1 s) suggests that the transient model of a synchronous machine should be assumed (the flux is kept constant by the currents induced in the rotor circuits—mainly in the excitation winding—since the currents induced in the damping circuits cease in the subtransient state).

At this point, we feel that it would be helpful to remind the reader of several important points.

In the steady state:

- In a salient pole generator, the large air gap along the q-axis causes the q-axis reactance X_q to be lower than the d-axis reactance X_d ; i.e., $X_q < X_d$
- In a round-rotor generator, $X_q \approx X_d$.

During a transient state:

- In a salient pole generator, once the subtransient state has ended, there are no induced currents along the q-axis. Thus, the flux adopts its rated value, so the transient q-axis reactance $X'_q = X_q$. Also, $X'_q =$

X_q is larger than the transient d-axis reactance X'_d ; i.e., $X_q > X'_d$.

- In a round-rotor generator (where currents can be induced in the rotor's iron as well as in the damping circuits during transients), once the subtransient state has ended, the currents induced in the excitation circuit along the d-axis have an appreciable effect, meaning that $X'_q > X'_d$.

Salient Pole Synchronous Machines: Vector Diagram and P - δ Curves in Steady-State and Transient Conditions

The vector diagrams of a salient pole synchronous machine in steady-state and transient conditions are presented in Table 5.5, which also lists the relevant equations for convenience. These equations can be used to infer the expressions for the P - δ curves. It follows from the vector diagrams and the equations reported in Table 5.5 that the expression for the active power as a function of the rotor electrical angle for a three-phase machine in the steady state is

$$P = 3VI \cos \varphi = 3 \frac{EV}{X_d} \sin \delta + \frac{3}{2} \frac{X_d - X_q}{X_d X_q} V^2 \sin 2\delta, \quad (5.219)$$

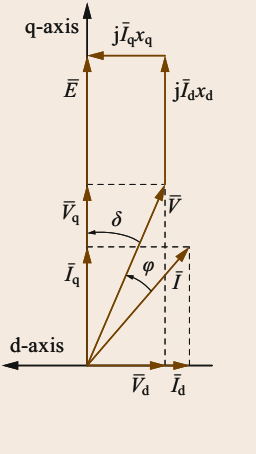
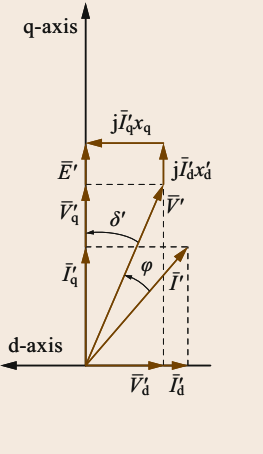
while the expression for a salient rotor machine in a transient state is

$$P' = 3V'I' \cos \varphi' = 3 \frac{E'V'}{X'_d} \sin \delta' + \frac{3}{2} \frac{X'_d - X_q}{X'_d X_q} V'^2 \sin 2\delta'. \quad (5.220)$$

To reinforce these ideas, we now present a quantitative example of a round-rotor synchronous generator that is characterized by the following reactance values:

- $x_d = 1.2$ pu
- $x'_d = 0.25$ pu
- $x'_q = x_q = 0.7$ pu.

Table 5.5 Vector diagrams of a salient pole synchronous machine in steady-state and transient conditions (adapted from [5.11])

| Steady state | | Transient | |
|--|---|---|---|
|  | $x_q < x_d$ $\frac{\bar{V}}{V} + jX_d \bar{I}_d + jX_q \bar{I}_q = \bar{E}$ $\text{Re}(\bar{V}\bar{I}) = V_d I_d + V_q I_q$ $X_q I_q = V_d = V \sin \delta$ $X_d I_d = E - V_q = E - V \cos \delta$ $VI \cos \varphi = V_d I_d + V_q I_q$ $= V \sin \delta \frac{E - V \cos \delta}{X_d} + V \cos \delta \frac{V \sin \delta}{X_q}$ $= \frac{EV}{X_d} \sin \delta + V^2 \left(\frac{1}{X_q} - \frac{1}{X_d} \right) \sin \delta \cos \delta$ $= \frac{EV}{X_d} \sin \delta + \frac{V^2}{2} \frac{X_d - X_q}{X_d X_q} \sin 2\delta$ |  | $x_q > x'_d$ $\frac{\bar{V}'}{V'} + jX'_d \bar{I}'_d + jX'_q \bar{I}'_q = \bar{E}'$ |
| <p>For a three-phase machine, we have</p> $P = 3VI \cos \varphi = 3 \frac{EV}{X_d} \sin \delta + \frac{3}{2} \frac{X_d - X_q}{X_d X_q} V^2 \sin 2\delta$ | | <p>For a three-phase machine, we have</p> $P' = 3V'I' \cos \varphi = 3 \frac{E'V'}{X'_d} \sin \delta' + \frac{3}{2} \frac{X'_d - X'_q}{X'_d X'_q} V'^2 \sin 2\delta'$ | |

Section 5.6

Let us assume that the generator is connected to an infinite power bus with a voltage $v = 1$ pu, and that it is supplying an active power $p = 0.8$ pu and a reactive power $q = 0.2$ pu through an external reactance of $x = 0.2$ pu.

$$p = \frac{ev}{x_d + x} \sin \delta + \frac{(x_d + x) - (x_q + x)}{2(x_d + x)(x_q + x)} v^2 \sin 2\delta$$

$$= 1.2 \sin \delta + 0.2 \sin 2\delta$$

$$p' = \frac{e'v}{x_d + x} \sin \delta + \frac{(x'_d + x) - (x_q + x)}{2(x'_d + x)(x_q + x)} v^2 \sin 2\delta$$

$$= 2.5 \sin \delta - 0.55 \sin 2\delta$$

The two curves are shown in Fig. 5.64. Changing the active and reactive power initially supplied to the infinite power bus from the values $p = 0.8$ pu and $q = 0.2$ pu, respectively, results in the same steady-state P - δ curve as that shown in the figure but a different transient P - δ curve. We shall come back to this observation later.

Round-Rotor Synchronous Machines: Vector Diagram and P - δ Curves in Steady-State and Transient Conditions

The vector diagrams for a round-rotor synchronous machine in steady-state and transient conditions are presented in Table 5.6, along with the relevant equations for convenience. These equations can be used to infer the expressions for the P - δ curves.

It follows from the vector diagrams and the equations reported in Table 5.5 that the expression for the

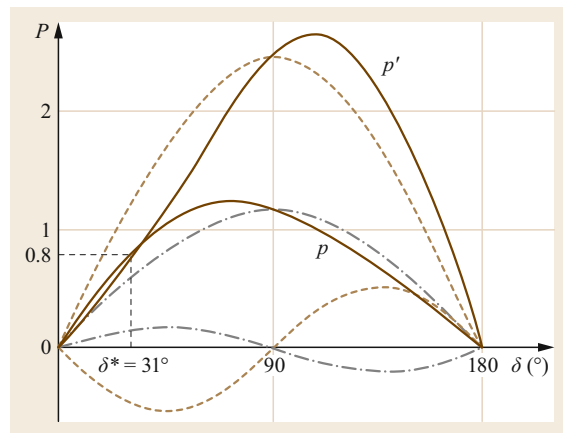


Fig. 5.64 P - δ curves for a salient pole synchronous machine in steady-state and transient conditions (adapted from [5.11])

active power as a function of the rotor electrical angle for a three-phase round-rotor machine in the steady state is

$$P = 3 \frac{EV}{X} \sin \delta, \tag{5.221}$$

while the expression for a round-rotor machine in the transient state is

$$P' = 3 \frac{E'_q V'}{X'_d} \sin \delta - 3 \frac{E'_d V'}{X'_d} \cos \delta + \frac{3}{2} \frac{X'_d - X'_q}{X'_d X'_q} V'^2 \sin 2\delta. \tag{5.222}$$

Table 5.6 Vector diagrams of round-rotor synchronous machines in steady-state and transient conditions (adapted from [5.11])

| Steady state | Transient |
|---|--|
| <p style="text-align: center;">$x_q \approx x_d$ $\frac{x_q}{V} + jX \bar{I} = \bar{E}$</p> | |
| <p>For a three-phase machine, we have $P = 3 \frac{EV}{X} \sin \delta$</p> | <p>For a three-phase machine, we have $P' = 3 \frac{E'_q V'}{X'_d} \sin \delta - 3 \frac{E'_d V'}{X'_d} \cos \delta + \frac{3}{2} \frac{X'_d - X'_q}{X'_d X'_q} V'^2 \sin 2\delta$</p> |

Section 5.6

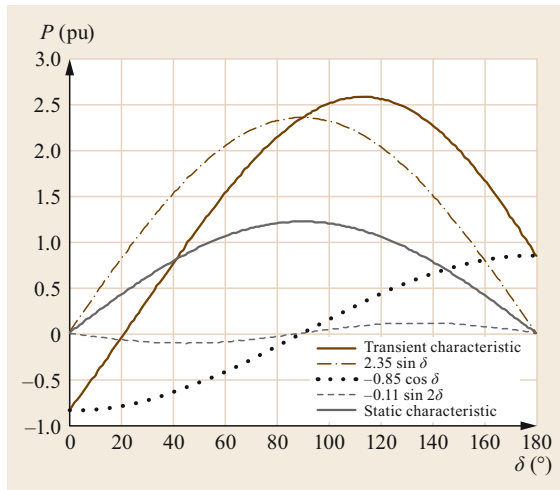


Fig. 5.65 P - δ curves for a round-rotor synchronous machine in steady-state and transient conditions

To demonstrate these ideas, we now present a quantitative example of a round-rotor synchronous generator that is characterized by the following reactance values:

- $x_d = x_q = 1.2$ pu
- $x'_d = 0.25$ pu
- $x'_q = 0.3$ pu.

Also, let us assume that the generator is connected to an infinite power bus with a voltage $v = 1$ pu, and that it supplies an active power $p = 0.8$ pu and a reactive power $q = 0.2$ pu through an external reactance of

$x = 0.2$ pu. The transient and static characteristics, illustrated in Fig. 5.65, are

$$p = \frac{ev}{x_d + x} \sin \delta = 1.2 \sin \delta$$

$$p' = \frac{e'_q v}{x_d + x} \sin \delta - \frac{e'_d v}{x_d + x} \cos \delta + \frac{(x'_d + x) - (x'_q + x)}{2(x'_d + x)(x'_q + x)} v^2 \sin 2\delta$$

$$= 2.35 \sin \delta - 0.85 \cos \delta - 0.11 \sin 2\delta .$$

We can get various curves for this machine depending on the assumptions made. For instance, if we assume that $x'_q = x_q$, the transient characteristics becomes (Fig. 5.66)

$$p' = \frac{e'_q v}{x_d + x} \sin \delta + \frac{(x'_d + x) - (x_q + x)}{2(x'_d + x)(x_q + x)} v^2 \sin 2\delta$$

$$= 2.35 \sin \delta - 0.75 \sin 2\delta .$$

On the other hand, if we assume that $x'_q = x'_d$ (i.e., *isotropy*), the transient characteristics becomes (Fig. 5.67)

$$p' = \frac{e'_q v'}{x'_d} \sin \delta - \frac{e'_d v'}{x'_d} \cos \delta$$

$$e'_d = e' \cos \alpha$$

$$e'_q = e' \sin \alpha$$

$$p' = \frac{e' v'}{x'_d} \sin(\delta - \alpha)$$

$$p' = 2.35 \sin \delta - \cos \delta = 2.6 \sin(\delta - 22.9^\circ) .$$

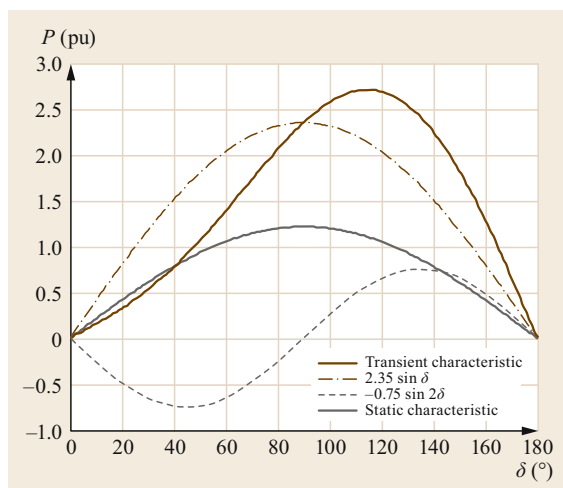


Fig. 5.66 P - δ curves for a round-rotor synchronous machine in steady-state and transient conditions assuming $x'_q = x_q$

For illustrative purposes, Fig. 5.68 presents the three P - δ curves obtained in transient conditions based on the assumptions specified above.

Note that all of the P - δ characteristics presented in this section were obtained using a MATLAB file that can be found in the chapter's supplementary material.

Salient Pole Synchronous Machines: Effect of Varying the Initial Steady-State Operating Conditions on the (P - δ) Curves Obtained in Steady-State and Transient Conditions

Let us consider a generator with the following reactances:

- $x_d = 1.2$ pu
- $x'_d = 0.25$ pu
- $x_q = x'_q = 0.7$ pu.

The generator has a no-load excitation emf $e = 1.7$ pu that is connected to an infinite power bus with a voltage $v = 1$ pu through a reactance $x = 0.2$ pu.

Let us consider three initial conditions:

- $\delta = 20^\circ \rightarrow p = 0.5, q = 0.4$
- $\delta = 40^\circ \rightarrow p = 1.0, q = 0.1$
- $\delta = 60^\circ \rightarrow p = 1.2, q = -0.4$.

In pu, the expressions for active and reactive power are

$$p = \frac{ev}{x_d + x} \sin \delta + \frac{v^2}{2} \frac{x_d - x_q}{x_d + x_d + 2x} \sin 2\delta$$

$$q = \frac{ev}{x_d + x} \cos \delta - v^2 \left(\frac{\sin^2 \delta}{x_q + x} + \frac{\cos^2 \delta}{x_d + x} \right).$$

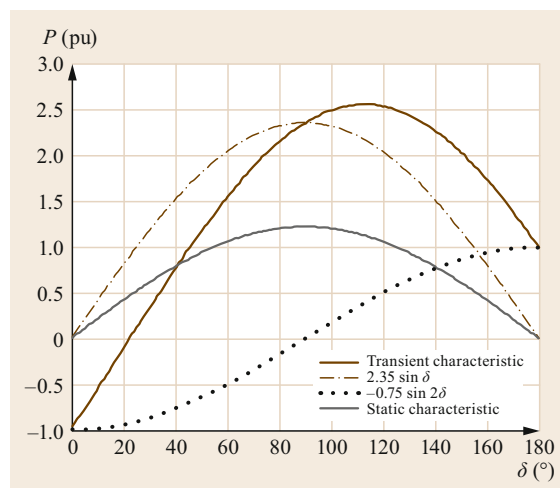


Fig. 5.67 P - δ curves obtained in steady-state and transient conditions for a round-rotor synchronous machine assuming $x'_q = x'_d$ (i.e., isotropy)

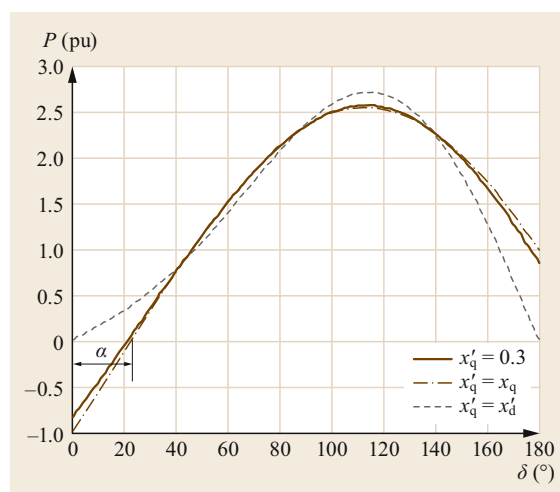


Fig. 5.68 Comparison of the P - δ curves obtained in transient conditions for a round-rotor synchronous machine assuming that $x'_q = 0.3$, $x'_q = x_q$, or $x'_q = x'_d$ (i.e., isotropy)

In the steady state, the magnitude of E remains constant, as do V and all of the reactances. Therefore, applying a different initial active power P , and thus a different δ , does not change the steady-state P - δ curve. Apart from δ , the quantities that differ in the new initial state are the current and its power factor; however, changes to these quantities do not alter the steady-state curve. However, the vector diagram does change if we start from new steady-state operating conditions, as δ , I , and E (which simply rotates) change.

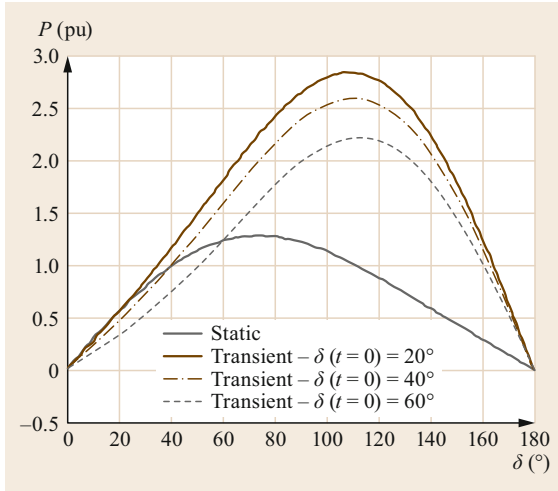


Fig. 5.69 P - δ curves obtained in steady-state and transient conditions for a salient pole synchronous machine with three different initial steady-state operating conditions

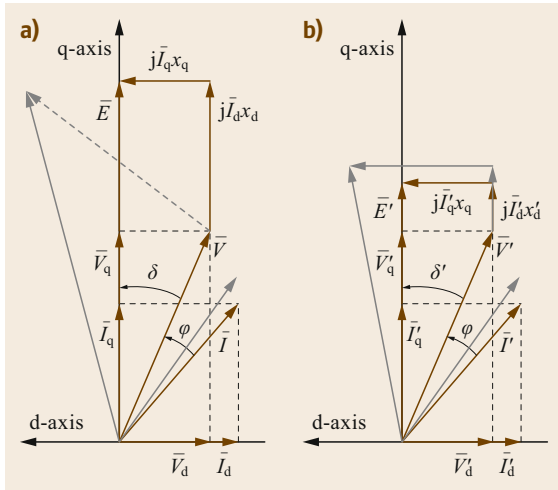


Fig. 5.70 (a) Steady-state and (b) transient vector diagrams for different initial operating conditions, marked in gray (adapted from [5.11])

In the transient state, changing the initial values of the current and the power factor alters the voltage drops at the transient reactances and changes the transient emf, meaning that the P - δ characteristic in the transient state varies depending on the initial operating conditions. Thus, three different initial steady-state operating conditions yield three different transient curves, as shown in Fig. 5.69. The relevant vector diagrams are shown in Fig. 5.70.

Round-Rotor Synchronous Machines: Effect of Varying the Initial Steady-State Operating Conditions on the (P - δ) Curves Obtained in Steady-State and Transient Conditions

Let us consider a generator with the following reactances:

- $x_d = 1.2$ pu
- $x'_d = x'_q = 0.25$ pu.

This generator has a no-load excitation emf $e = 1.7$ pu, which is connected to an infinite power bus with a voltage $v = 1$ through a reactance $x = 0.2$ pu.

Let us consider three initial conditions:

- $\delta = 20^\circ \rightarrow p = 0.5$ pu, $q = 0.4$ pu
- $\delta = 40^\circ \rightarrow p = 1.0$ pu, $q = 0.1$ pu
- $\delta = 60^\circ \rightarrow p = 1.2$ pu, $q = -0.4$ pu.

In pu, the expressions for the active and reactive power are

$$p = \frac{ev}{x_d + x} \sin \delta$$

$$q = \frac{ev}{x_d + x} \cos \delta - \frac{v^2}{x_d + x} .$$

The same considerations that were relevant to the salient pole machine also apply to a round-rotor machine, so again three different initial steady-state operating conditions yield just one steady-state curve but three different transient curves, as shown in Fig. 5.71.

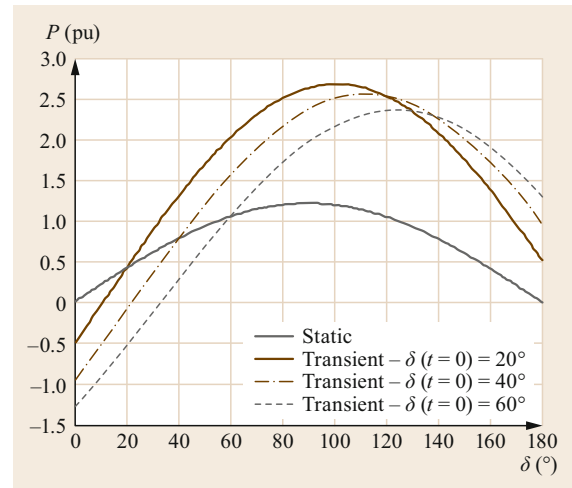


Fig. 5.71 P - δ curves obtained in steady-state and transient conditions for a round-rotor synchronous machine with three different initial steady-state operating conditions

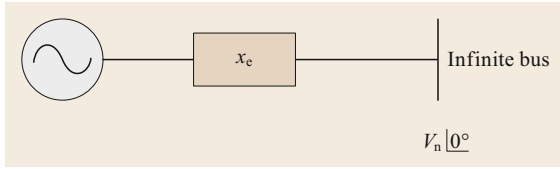


Fig. 5.72 Synchronous machine connected to an infinite power bus

5.6.6 Rotor Angle Stability

Classical Methods

We now review the classical method of analyzing a simple system consisting of a synchronous machine connected to an infinite power bus, as shown in Fig. 5.72.

The following simplifications are made [5.49]:

- The synchronous machine is modeled as a constant emf \vec{E} behind the transient reactance x' , and the angle δ of the emf is assumed to coincide with the difference between the rotor electrical angle and $\omega_0 t$ as illustrated in Fig. 5.73
- The resistances of lines, transformers, and the synchronous machine are ignored
- Voltage and currents are assumed to be symmetrical (i.e., positive sequence)
- The angular velocity is close to nominal
- Static models are used for lines
- The mechanical power P_m (the power from the prime mover) is constant during the transient studied.

Swing Equation

In the following, a subscript m denotes a mechanical quantity while a subscript e denotes an electrical quantity.

The differential equation that describes the rotor dynamics is

$$J \frac{d^2 \theta_m}{dt^2} = T_m - T_e, \quad (5.223)$$

where:

- J = total moment of inertia (kg m²)
- θ_m = mechanical angle of the rotor (rad)
- T_m = mechanical torque from turbine (N m)
- T_e = electrical torque on the rotor (N m).

Multiplying (5.223) by the mechanical angular speed ω_m yields

$$J \omega_m \frac{d^2 \theta_m}{dt^2} = P_m - P_e, \quad (5.224)$$

where:

$$P_m = T_m \omega_m = \text{mechanical power acting on the rotor (W)}$$

$$P_e = T_e \omega_m = \text{electrical power acting on the rotor (W)}.$$

We can express the angular acceleration via the electrical angle instead by inserting $\theta_m = (\theta_e)/p - \theta_{e0}/p$ (where p is the number of pairs of poles on the machine) into (5.224), which gives

$$\frac{1}{p} \omega_m J \frac{d^2 \theta_e}{dt^2} = P_m - P_e. \quad (5.225)$$

It is now convenient to introduce the inertia constant H (in s), defined as

$$H = \frac{\frac{1}{2} J \omega_{m0}^2}{S}, \quad (5.226)$$

where ω_{m0} is the rated mechanical angular speed and S is the MVA rating of the machine.

Using (5.226), and noting that $d^2 \theta_e / dt^2 = d^2 \delta / dt^2$ (where $\delta = \theta_e - \omega_0 t - \theta_{e0}$), (5.225) becomes

$$\frac{2H}{\omega_0} \frac{d^2 \delta}{dt^2} = P_m^{\text{pu}} - P_e^{\text{pu}}, \quad (5.227)$$

where ω_0 indicates the rated electrical angular speed ($\omega_0 = p \omega_{m0}$)², and a superscript pu indicates that the electrical power and mechanical power are expressed in pu with respect to the rating of the synchronous machine. In the case of a synchronous machine connected to an infinite power bus, we can write (omitting the superscript pu for simplicity)

$$P_e = P_e(\delta, \dot{\delta}) = P_s(\delta) + P_d(\dot{\delta}), \quad (5.228)$$

where P_s is the synchronizing power, i.e., making reference to Fig. 5.74,

$$P_s(\delta) = \frac{E' V_n}{x' + x_e} \sin(\delta), \quad (5.229)$$

and P_d is the damping power, with

$$P_d(\dot{\delta}) = D \dot{\delta}. \quad (5.230)$$

P_d is due to the currents in the rotor circuits, and tends to damp out the oscillations.

Taking $x_1 = \delta$ and $x_2 = d\delta/dt$ to be the state variables, (5.227) can be expressed in the state form as

$$\begin{cases} \dot{x}_1 = x_2 \\ \dot{x}_2 = \frac{\omega_0}{2H} (P_m^{\text{pu}} - P_e^{\text{pu}}). \end{cases} \quad (5.231)$$

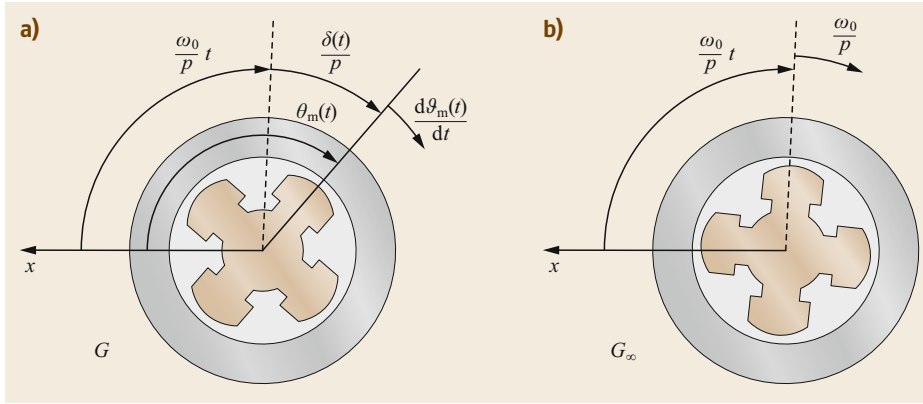


Fig. 5.73a,b Definitions of the quantities used to derive the swing equations. The alternator of interest is shown in (a), while the infinite power machine is depicted in (b)

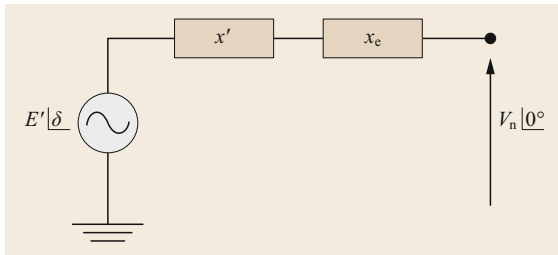


Fig. 5.74 Simple circuit representation of a generator in the transient state

The vector $x = [x_1, x_2]^T$ is the state vector of the system; the equilibrium points (EPs) for the system of equations are given by $\dot{x} = 0$, i.e.,

$$\begin{aligned} x_1 &= \arcsin\left(\frac{P_m}{P_{\max}}\right) \\ x_2 &= 0, \end{aligned} \tag{5.232}$$

where $P_{\max} = E' V_n / (x' + x_e)$.

For the power angle curve shown in Fig. 5.75, there are two values of δ for each value of P_m (when $P_m < P_{\max}$), i.e., two EPs: δ_s and δ_u .

After linearizing (5.231) and introducing a small deviation ($\Delta x_1, \Delta x_2$) from an EP, we can write

$$\begin{bmatrix} \Delta \dot{x}_1 \\ \Delta \dot{x}_2 \end{bmatrix} = \begin{bmatrix} 0 & 1 \\ -\frac{\omega_0}{H} k & -\frac{\omega_0}{H} D \end{bmatrix} \cdot \begin{bmatrix} \Delta x_1 \\ \Delta x_2 \end{bmatrix}, \tag{5.233}$$

where $k = P_{\max} \cos(\delta_e)$ and δ_e is the angle at equilibrium (δ_s or δ_u).

The eigenvalues of the linearized system are given by

$$\lambda = -\frac{1}{2} \frac{\omega_0}{2H} D \pm \sqrt{\frac{\omega_0^2 D^2}{16H^2} - \frac{\omega_0}{2H} k}. \tag{5.234}$$

If k is positive, both eigenvalues have negative real parts. If k is negative, one of the eigenvalues is positive

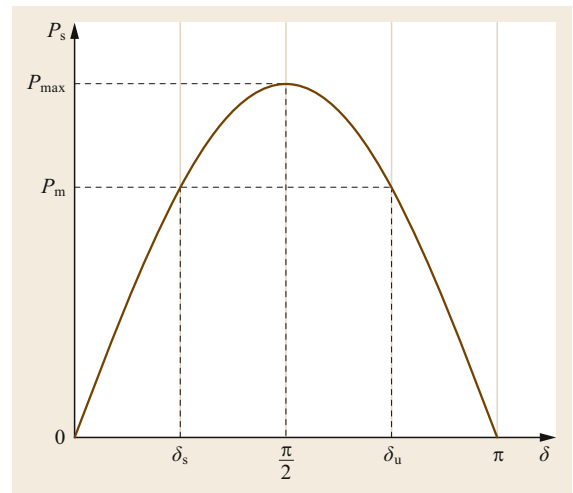


Fig. 5.75 Power angle curve; note that there are two values of δ for each value of P_m

real. Therefore, δ_s is a stable EP and δ_u is an unstable EP. The criterion for stability is algebraic and given by

$$\frac{dP_s}{d\delta} > 0. \tag{5.235}$$

If D is small and $k > 0$, the eigenvalues are complex and are obtained via

$$\lambda = -\sigma \pm j\omega_p, \tag{5.236}$$

where

$$\sigma = \frac{1}{2} \frac{\omega_0}{2H} \times D \quad \text{and} \quad \omega_p = \sqrt{\frac{\omega_0}{2H} \times k - \frac{\omega_0^2 D^2}{16H^2}}.$$

The two EPs (δ_s and δ_u) become closer to each other as P_m increases. The maximum power supplied by the generator is equal to P_{\max} and occurs at $\delta^* = \pi/2$.

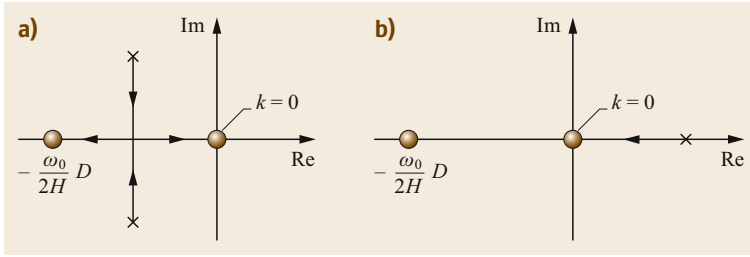


Fig. 5.76a,b Loci of eigenvalues in the s plane (a) at the SEP and (b) at the UEP

The condition for stability can also be stated as

$$\delta_s < \delta^* . \quad (5.237)$$

The loci of eigenvalues in the s plane as P_m is varied are shown in Fig. 5.76.

At the SEP (state equilibrium point), the eigenvalues are initially complex and split into two real values. One of them reaches origin as P_m is increased to P_{\max} (when $k = 0$), while the other eigenvalue approaches $-D\omega_0/(2H)$.

At the UEP (unstable equilibrium point), both eigenvalues are real. As P_m increases, both move towards the origin. At $P_m = P_{\max}$, one of the values is 0 while the other is $-D\omega_0/(2H)$.

There is no equilibrium when $P_m > P_{\max}$.

Equal Area Criterion

Quite often, we are not interested in the exact behavior of the solution to (5.227), only whether the system is stable after a given contingency. By applying the equal area criterion described below, it is possible to investigate the stability of the system in Fig. 5.76 following various disturbances using simple calculations. As our interest is focused on the dynamics during the first swing, the damping can be neglected, i.e., $D = 0$. A necessary but not sufficient condition for stability is that there is a moment in time t_m during this swing when $\dot{\delta}(t_m) = 0$. The corresponding angle is δ_m .

The stability criterion is obtained by manipulating (5.227) and applying the condition $\dot{\delta}(t_m) = 0$. Multiplying (5.227) by $\dot{\delta}$ on both sides yields

$$\dot{\delta} \frac{d^2 \delta}{dt^2} = \frac{\omega_0}{2H} P_a \dot{\delta} , \quad (5.238)$$

which can be written as

$$\delta \frac{1}{2} \frac{d}{dt} \left(\frac{d\delta}{dt} \right)^2 = \frac{d}{dt} \left(\frac{\omega_0}{2H} \int_{\delta_i}^{\delta} P_a d\delta \right) , \quad (5.239)$$

where $P_a = P_m - P_e$.

Equation (5.239) can be integrated to give

$$\frac{d\delta}{dt} = \sqrt{\frac{\omega_0}{H} \int_{\delta_i}^{\delta} P_a d\delta + c} , \quad (5.240)$$

where c is an integration constant with a value of 0 since $\dot{\delta} = 0$ when $\delta = \delta_i$ (δ_i is the pre-disturbance rotor angle).

Thus, a necessary condition for stability is that there is an angle δ_m such that

$$\int_{\delta_i}^{\delta} P_a d\delta = 0 , \quad (5.241)$$

i.e., there is an angle δ_m such that the area below the accelerating power P_a in the δ - P diagram between δ_i and δ_m vanishes. In other words,

$$\int_{\delta_0}^{\delta^*} P_a d\delta = \int_{\delta_0}^{\delta^*} (P_m - P_e) d\delta = 0 . \quad (5.242)$$

A graphical interpretation of this formula is shown in Fig. 5.77. This is the *equal area criterion*. The two areas represent the *fictitious* kinetic energies absorbed/released and then released/absorbed by the rotor.

Heffron–Phillips Model of a Generator Connected to an Infinite Power Bus

The Heffron–Phillips model is a linear model that takes into account the actions of the voltage control and the exciter [5.50]. This model justifies and illustrates the use of power system stabilizers (PSS).

The rotor angle dynamics in pu can be written as

$$\frac{d\delta}{dt} = \omega_0 (\omega_{pu} - 1) \quad (5.243)$$

$$2H \frac{d\omega_{pu}}{dt} = T_m - T_s - D\omega_{pu} , \quad (5.244)$$

where $\omega_{pu} = \omega/\omega_0$, D is the damping coefficient, and T_m and T_s are the mechanical and the synchronizing

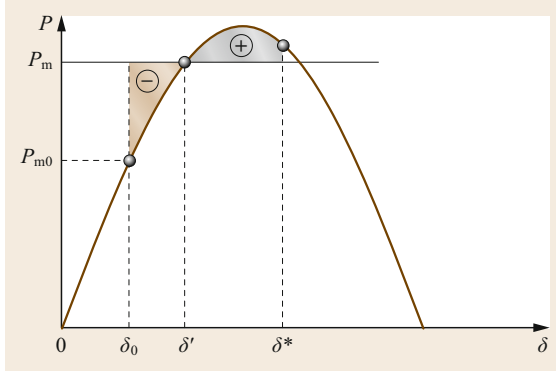


Fig. 5.77 Graphical interpretation of the equal area criterion

torques, respectively. Assuming that $\omega_{pu} \approx 1$ pu, we can write

$$T_s = \frac{|E'| |V_\infty|}{x' + x_e} \sin \delta, \quad (5.245)$$

where E' is the transient internal voltage, V_∞ is the voltage at the infinite power bus (the bus of the network to which many generators are connected), x' is the transient reactance of the alternator, and x_e is the reactance of the link between the alternator and the infinite power bus. For small variations, the linearized approximation of (5.245) is

$$\Delta T_s = k_1 \Delta \delta + k_2 \Delta |E'|, \quad (5.246)$$

where

$$k_1 = \left(\frac{\partial T_s}{\partial \delta} \right)_0 = \frac{|E'_0| |V_\infty|}{x' + x_e} \cos \delta_0 \quad (5.247)$$

$$k_2 = \left(\frac{\partial T_s}{\partial |E'|} \right)_0 = \frac{|V_\infty|}{x' + x_e} \sin \delta_0. \quad (5.248)$$

In order to account for the variation of $|E'|$ with respect to both ΔE_f (which is proportional to the variation of the excitation voltage) and to $\Delta \delta$, the equation relevant to the flux decay of the excitation winding is included as

$$v_f = r_f i_f + \frac{d\lambda_f}{dt}, \quad (5.249)$$

where v_f is the excitation voltage, i_f is the excitation current, and λ_f is the flux linkage. Equation (5.249) can be written at the stator side as

$$|E_f| = |E| + T'_0 \frac{d|E'|}{dt}. \quad (5.250)$$

Here, $T'_0 = L_f / r_f$, where r_f is the resistance and L_f is the self-inductance of the excitation winding.

As a first approximation, we can write

$$\frac{|E| - |V_\infty| \cos \delta}{|E'| - |V_\infty| \cos \delta} \approx \frac{\tilde{x}}{\tilde{x}'}, \quad (5.251)$$

where $\tilde{x}' = x' + x_e$ and $\tilde{x} = x_s + x_e$ (x_s is the synchronous reactance).

From (5.251),

$$|E| = \frac{1}{k_3} |E'| + \left(1 - \frac{1}{k_3} \right) |V_\infty| \cos \delta, \quad (5.252)$$

where

$$k_3 = \frac{\tilde{x}'}{\tilde{x}}. \quad (5.253)$$

Inserting (5.252) into (5.250) gives

$$k_3 T'_0 \frac{d|E'|}{dt} + |E'| = k_3 |E_f| + (1 - k_3) |V_\infty| \cos \delta. \quad (5.254)$$

Introducing the Laplace transform for small variations leads to

$$(sk_3 T'_0 + 1) \Delta |E'| = k_3 \Delta |E_f| - k_4 k_3 \Delta \delta, \quad (5.255)$$

where

$$k_4 = \left(\frac{1}{k_3} - 1 \right) |V_\infty| \sin \delta. \quad (5.256)$$

The relevant block diagram is shown in Fig. 5.78.

As shown in Fig. 5.78, the feedback loop arises because of the link between $\Delta |E'|$ and $\Delta \delta$. When the exciter and voltage regulator are included, $\Delta |E_f|$ depends on the output voltage at the generator terminals $|V_t|$ through the excitation system.

When the excitation voltage is constant ($\Delta |E_f| = 0$), the field flux variations $\Delta |E'|$ are only caused by the feedback of $\Delta \delta$ through the coefficient k_4 . This represents the demagnetizing effect of the armature reaction.

The change in air-gap torque due to the field flux variations caused by rotor angle changes (indicated as $\Delta T'_s$ in the block diagram) is given by

$$\left. \frac{\Delta T'_s}{\Delta \delta} \right|_{\Delta |E_f|=0} = \frac{k_2 k_3 k_4}{1 + sk_3 T'_0}, \quad (5.257)$$

where the constants k_2 , k_3 , and k_4 are usually positive. The contributions of $\Delta |E'|$ to the synchronizing torque $\Delta T'_s$ and the damping torque ΔT_d depend on the oscillating frequency as follows:

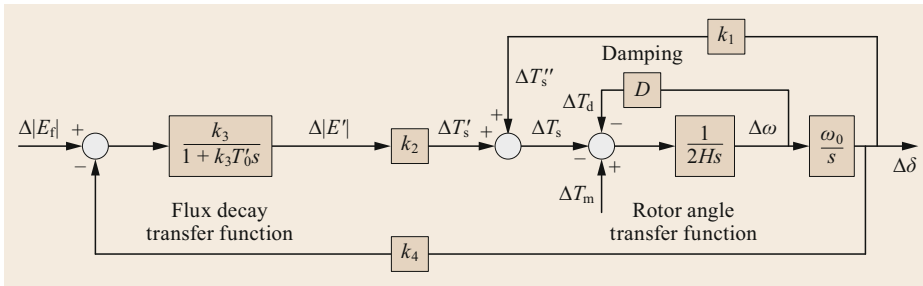


Fig. 5.78 Block diagram of an alternator with damping and flux decay accounted for

- (1) In the steady state and at very low oscillating frequencies (i.e., $s = j\omega \rightarrow 0$),

$$\Delta T'_s = -k_2 k_3 k_4 \Delta \delta. \tag{5.258}$$

The variation in the field flux due to $\Delta \delta$ feedback introduces a negative synchronizing torque component. The system becomes monotonically unstable when this exceeds $k_1 \Delta \delta$ (i.e., T'_s). The steady-state stability limit is reached when

$$k_2 k_3 k_4 = k_1. \tag{5.259}$$

- (2) At oscillating frequencies $\gg 1/(k_3 T'_0)$,

$$\Delta T'_s = \frac{-k_2 k_3 k_4 \Delta \delta}{j\omega k_3 T'_0}. \tag{5.260}$$

Equation (5.260) can be written as

$$\Delta T'_s = j \frac{k_2 k_4 \Delta \delta}{\omega T'_0}. \tag{5.261}$$

Thus, the component of the air-gap torque due to $\Delta |E'|$ leads $\Delta \delta$ by 90° , or is in phase with $\Delta \omega$. Hence, $\Delta |E'|$ results in a positive damping component that is added to ΔT_d .

- (3) At a typical machine oscillating frequency of about 1 Hz, $\Delta |E'|$ results in a positive damping torque component and a negative synchronizing torque component. The net effect is to slightly reduce the synchronizing torque component and increase the damping torque component.

k_4 is generally positive, although there are a few cases in which it may be negative, such as for a hydraulic generator without damper windings that is operating with a light load and is connected by a line with a relatively high resistance to reactance ratio to a larger system.

A simple model of the voltage control system and exciter is shown in Fig. 5.79.

For small variations, we can write

$$\Delta |V_t| = k_s \Delta \delta + k_6 \Delta |E'|, \tag{5.262}$$

where $k_s = |\partial |V_t| / \partial \delta|_0$ and $k_6 = |\partial |V_t| / \partial |E'|_0$.

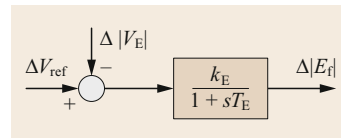


Fig. 5.79 Simple model of the voltage control system and exciter

k_6 is positive whereas k_5 can be positive or negative (it is negative under heavy loading conditions and with high external impedance).

The block scheme of Fig. 5.80 is obtained by including the block scheme of Fig. 5.79 in that of Fig. 5.78.

The stability criterion is given by

$$k_5 k_E + k_4 > 0, \tag{5.263}$$

so when $k_5 < 0$, (5.263) limits the value of k_E . In order to maintain a high value of k_E in the steady state, a PSS is adopted.

A simple PSS scheme is shown in Fig. 5.81.

Multi-Machine Stability Studies

The equal area criterion cannot be used directly in systems with three or more machines. When a multi-machine system operates under electromechanical transient conditions, machine oscillations occur in the transmission system connecting the machines. In this case, we introduce the following assumptions to formulate the so-called classical model:

1. The mechanical power input of each machine remains constant throughout the swing computation
2. The damping power is negligible
3. Each machine can be represented by a constant transient reactance in series with a constant transient internal voltage
4. The mechanical rotor angle of each machine coincides with δ , the electrical phase angle of the internal voltage
5. All loads can be considered shunt impedances to ground, with values that are governed by the prevailing conditions immediately prior to the transient condition.

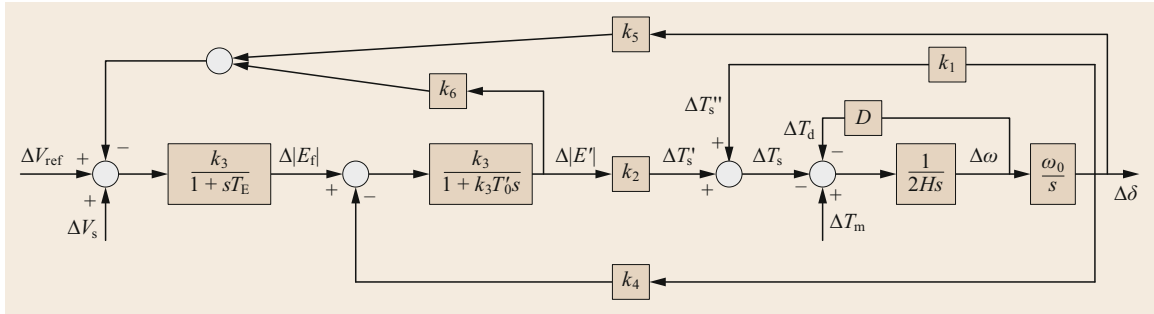


Fig. 5.80 Block diagram of an alternator with the damping, flux decay, voltage control system, and exciter considered

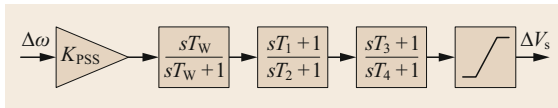


Fig. 5.81 Simple PSS scheme, where K_{PSS} is the gain, T_w is the washout time constant, and the other time constants (T_1 , T_2 , T_3 , and T_4) are those of the two stage lead-lag block for phase compensation

The system conditions before the fault and the network configuration both during and after the fault must be known in any transient stability study. Consequently, in the multi-machine case, two preliminary steps are performed:

- The steady-state pre-fault conditions for the system are calculated using a power flow code
- The pre-fault network representation is determined and then modified to account for the fault and post-fault conditions.

We know the active power, reactive power, and voltage values at each generator terminal and load bus for the preliminary steps. The transient internal voltage of each generator is then calculated using

$$\vec{E}' = \vec{V}_t + jx'\vec{I}, \tag{5.264}$$

where \vec{V}_t is the corresponding terminal voltage and \vec{I} is the output current. Each load is converted into a constant admittance to ground and its bus using

$$Y_L = \frac{P_L - jQ_L}{V_L^2}, \tag{5.265}$$

where $P_L + jQ_L$ is the load and \vec{V}_L is the magnitude of the corresponding bus voltage.

The bus admittance matrix used for the pre-fault power flow calculation is now augmented to include the transient reactance of each generator and the shunt admittance of each load, as illustrated in Fig. 5.82.

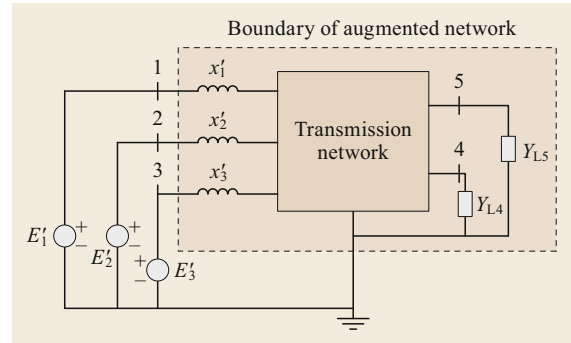


Fig. 5.82 Model of augmented network nodal analysis

The injected currents are zero at all buses except for the internal buses of the generators. In the second preliminary step, the bus admittance matrix is modified to correspond to the faulted and post-fault conditions. Since only the internal buses of the generator have injections, all other buses can be eliminated by Kron reduction. The power injected into the network from each generator is calculated using the corresponding power angle equation. For example, in Fig. 5.82, the power supplied by generator 1 is given by

$$P_{1l} = E_1'^2 G_{11} + E_1' E_2' Y_{12} \cos(\delta_{12} - \vartheta_{12}) + E_1' E_3' Y_{13} \cos(\delta_{13} - \vartheta_{13}), \tag{5.266}$$

where $\delta_{12} = \delta_1 - \delta_2$, $\bar{Y}_{12} = Y_{12} e^{j\vartheta_{12}}$, and $\bar{Y}_{13} = Y_{13} e^{j\vartheta_{13}}$.

Similar equations can be written for P_{l2} and P_{l3} using the Y_{ij} elements of the 3×3 bus admittance matrix.

The P_{li} expressions are used in the swing equations

$$\frac{2H_i}{\omega_0} \frac{\partial^2 \delta_i}{\partial t^2} = P_{mi} - P_{ei} \quad i = 1, 2, 3, \tag{5.267}$$

which represent the motion of each rotor during and after the fault. The solution depends on the location and the duration of the fault and the Y_{bus} that results from the removal of the faulted line.

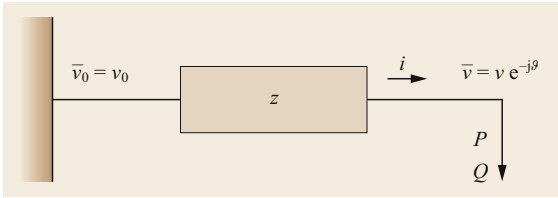


Fig. 5.83 Scheme of a load connected to an infinite bus through a line

5.6.7 Voltage Stability

Just as the single machine to infinite bus system is used to describe some basic properties of angular stability, some fundamental aspects of voltage stability can be described by referring to the simple system shown in Fig. 5.83, where a load with active power P and reactive power Q is supplied through a line with longitudinal impedance z (shunt capacitance is neglected) from a bus with constant voltage v_0 (infinite bus).

In steady-state and balanced conditions, this simple system is expressed by

$$\bar{i} = \frac{\bar{v}_0 - \bar{v}}{\bar{z}} \quad (5.268)$$

$$P - jQ = \bar{v}^* \bar{i}, \quad (5.269)$$

where \bar{v}^* indicates the conjugate of the voltage phasor.

Replacing i in (5.269) with (5.268) yields the equation

$$P - jQ = \frac{v^* v_0 - v^2}{z}, \quad (5.270)$$

which can be rearranged by introducing the line resistance r , the reactance x , and the angle θ (the difference between the angles of v_0 and v),

$$(r + jx)(P - jQ) + v^2 = vv_0(\cos \vartheta + j \sin \vartheta). \quad (5.271)$$

Equating the real and imaginary parts leads to

$$\begin{aligned} rP + xQ + v^2 &= vv_0 \cos \vartheta \\ xP - rQ &= vv_0 \sin \vartheta. \end{aligned} \quad (5.272)$$

The angle θ can be eliminated by squaring both sides and adding the two equations, to give

$$v^4 + (r^2 + x^2)(P^2 + Q^2) + 2(rP + xQ)v^2 = v^2 v_0^2. \quad (5.273)$$

Dividing by $|v|^2$ results in the typical equation used in the Distflow method [5.51] to calculate the steady-state operating conditions in a radial distribution network,

$$v^2 = v_0^2 - (r^2 + x^2)i^2 - 2(rP + xQ). \quad (5.274)$$

By neglecting the effects of voltage variations on both P and Q , (5.273) can be written as a quadratic equation in the variable $u = v^2$,

$$u^2 - [v_0^2 - 2(rP + xQ)u + (r^2 + x^2)(P^2 + Q^2)] = 0. \quad (5.275)$$

Equation (5.275) only has feasible solutions (i.e., solutions that are real numbers) if the discriminant is larger than or equal to 0, i.e.,

$$v_0^4 - 4(rP + xQ)v_0^2 - 4(xP - rQ)^2 \geq 0, \quad (5.276)$$

which can also be used as a stability index.

If r can be ignored, (5.275) can be rewritten as

$$\hat{u}^2 + (2\hat{Q} - 1)\hat{u} + \hat{P}^2 + \hat{Q}^2 = 0, \quad (5.277)$$

where $\hat{u} = u/v_0^2$, $\hat{P} = xP/v_0^2$, and $\hat{Q} = xQ/v_0^2$.

The solutions to (5.277) are

$$\hat{u} = \frac{1}{2} - \hat{Q} \pm \sqrt{\left(\frac{1}{2} - \hat{Q}\right)^2 - \hat{P}^2 - \hat{Q}^2}, \quad (5.278)$$

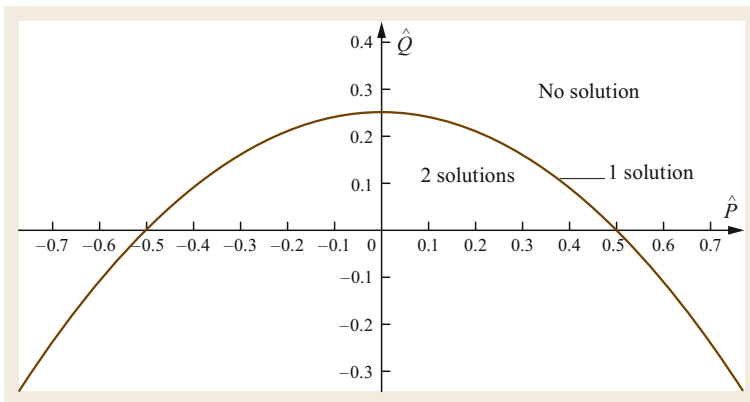


Fig. 5.84 Feasibility condition when the resistance is ignored

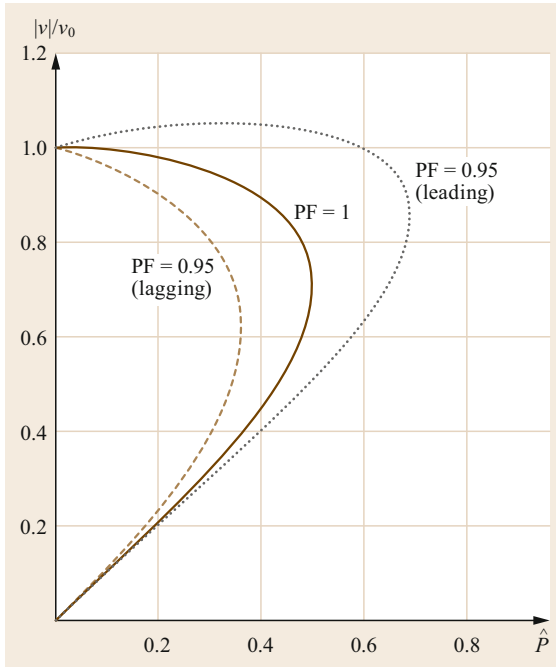


Fig. 5.85 Nose curves for different values of the power factor PF

with the feasibility condition

$$\hat{P}^2 + \hat{Q} \leq \frac{1}{4}. \quad (5.279)$$

The feasibility condition is depicted in Fig. 5.84. Below the curve there are two real solutions; on the curve there is a single solution; and above the curve there are no real solutions.

In the case of a constant power factor (i.e., $\hat{Q} = \hat{P} \tan \varphi$ with $\tan \varphi$ constant), the feasibility condition (5.279) becomes

$$\hat{P}^2 + \hat{P} \tan \varphi - \frac{1}{4} \leq 0. \quad (5.280)$$

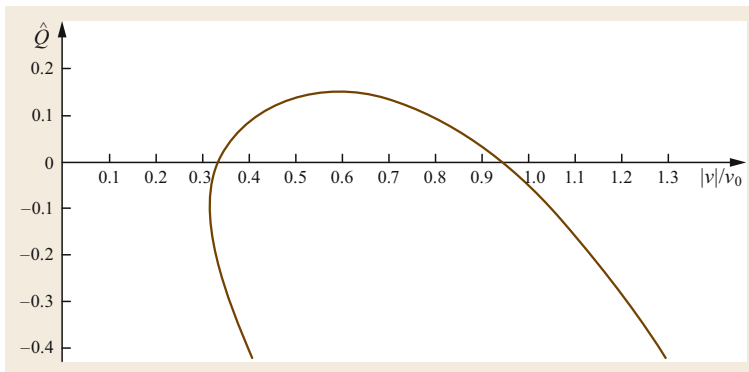


Fig. 5.86 QV curve for $\hat{P} = 0.1$

When $\hat{P} \geq 0$ (load consumption), the critical conditions are $\hat{P}_{\max} = \cos \varphi / [2(1 + \sin \varphi)]$, $\hat{Q}_{\max} = \sin \varphi / [2(1 + \sin \varphi)]$, and $\hat{u}_{\text{cr}} = 1 / [2(1 + \sin \varphi)]$.

For constant power factor values, the curves presented in Fig. 5.85 are obtained. These show the variation of v/v_0 as a function of $\hat{P} \geq 0$ based on (5.278). Such curves are often called nose curves or power voltage (PV) curves. Just as for the case considered in Fig. 5.84, three cases can be distinguished regarding the number of possible operating points: (a) there are two solutions when \hat{P} is less than the tip of the nose; (b) there is one solution at the tip of the nose; and (c) there are no solutions for larger values of \hat{P} .

In case (a), the upper solution corresponds to high voltage and low current while the lower one corresponds to low voltage and high current. The upper solution is obviously of particular interest since it reduces the power loss.

The power factor has a significant influence on the nose curve (as shown in Fig. 5.85), and therefore on the voltage stability limit. \hat{P}_{\max} decreases as the reactive power drawn by the load increases.

If \hat{P} is assumed to be constant, applying (5.277) yields the QV curve, which shows the amount of reactive power that must be provided to the network with a given load to obtain a predefined voltage level. Figure 5.86 shows this curve for $\hat{P} = 0.1$. The voltage sensitivity factor dv/dQ can be used as a stability criterion. Since we usually expect the voltage to increase when the adsorption of reactive power from the bus decreases, stability is obtained when dv/dQ is negative. This condition is met for voltages higher than 0.6 pu in Fig. 5.86.

In three dimensions, (5.277) defines an infinite paraboloid, as illustrated by Fig. 5.87.

The relationship between the load power and voltage variations depends on the timescale considered. At short timescales of a few seconds, the physical processes associated with the load device determine the characteristics, whereas various control actions must be considered at longer timescales.

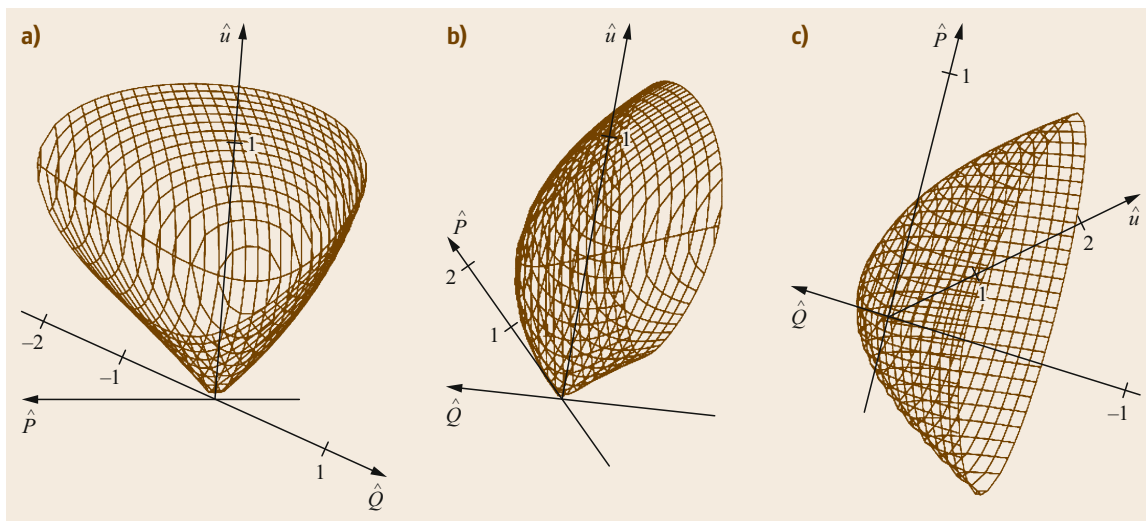


Fig. 5.87a–c Surfaces illustrating the relationship between voltage, active power, and reactive power; (a) and (b) show lateral views whereas (c) depicts the top view

One generic model often used for short timescales is the exponential

$$P_L = P_{L0} \left(\frac{V}{V_0} \right)^{k_p}, \quad (5.281)$$

where P_{L0} is the active power absorbed when the voltage is equal to the rated value V_0 . A similar expression, albeit usually with a different exponent value, can be used for the reactive power.

At longer timescales, the control actions that are applied to keep the load power constant are typically those of the thermostatically controlled load and those of the variable tap changers of distribution transformers.

Figure 5.88 shows the load characteristic (with $k_p = 1.75$) plotted together with two different nose curves. The solid one is the unity power factor curve of Fig. 5.85; the dotted nose curve refers to the case in which the reactance doubles due to a fault.

Load control is achieved by increasing the load admittance in order to increase the load power. Indeed, one of the definitions of voltage stability is that an increase in load admittance results in an increase in load power.

At point A in Fig. 5.88, an increase in load admittance shifts the load curve to the right and then increases the load power. Thus, the system is voltage stable according to the definition above. If a disturbance occurs, the equivalent network impedance increases dramatically and the nose curve shifts to the dotted one. The new operating point will be point B. The load controller will try to restore the load power to the previous value

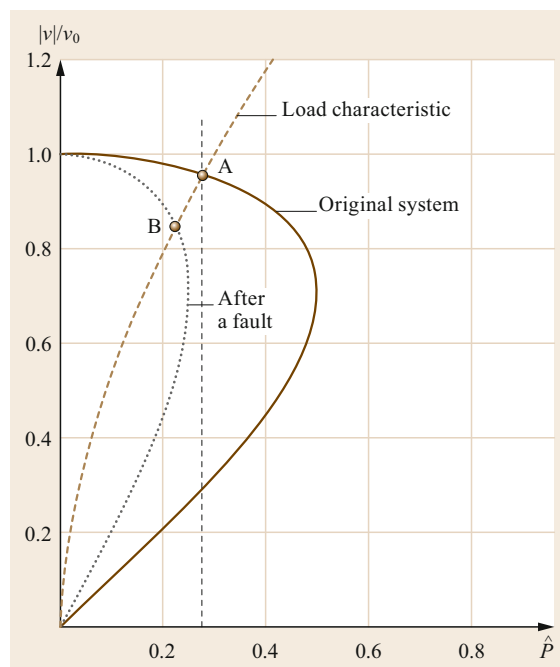


Fig. 5.88 The load characteristic crosses the nose curve at point A before and at point B after a network fault that doubles the equivalent reactance

represented by crossing point A. The controller will increase the load admittance, decreasing the voltage and shifting the operating point to the tip of the nose. The power cannot be restored to the original value since the tip of the nose curve is to the left of the vertical curve.

With the operating point at the tip of the nose, increasing the load admittance further causes a decrease in power because the voltage drop is larger than the in-

crease in current. This situation is clearly unstable and the system will collapse. Note that this description does not consider the actions of undervoltage protections.

5.7 Power System Control

In this section, we largely focus on frequency control. We will refer to the basic scheme shown in Fig. 5.89, which comprises a generating unit equipped with a turbine-alternator group connected to the grid. However, this scheme is becoming less common in real power systems due to the increasing utilization of renewable energy from solar (mainly photovoltaics) and wind technologies, as these types of generators are usually connected to the network and make use of inverters.

Frequency control is performed due to power quality considerations and requirements (some loads and components of power plants such as induction motors, steam, gas, and hydro turbines may be significantly affected by frequency deviations of a few Hz) and to maintain the global equilibrium in the network between the power produced by the power stations and the power consumed by the loads. The disconnection of a generating unit, a line trip, or an increased load decrease the frequency, while the disconnection of a load or a sudden increase in the power produced increases the frequency. Within this context, each mismatch is initially compensated for mainly by the kinetic energy stored in the rotors of the synchronous generators and induction motors. However, this kinetic energy is limited, so frequency deviations need to be promptly compensated through appropriate frequency control actions.

In the scheme shown in Fig. 5.89, a load increase (decrease) corresponds to a decrease (increase) in the alternator angular velocity that needs to be compensated for through appropriate action of the speed governor (Reg), which opens (closes) the turbine valve. The speed governor control system may require some other input signals (b) in addition to the angular velocity.

The frequency regulation and the available reserve of a system are designed such that the frequency does not shift outside predefined limits even when the largest

disturbances that can be reasonably expected occur (e.g., the largest generator in the system trips).

5.7.1 Generation Reserve

As the energy stored in the rotating masses is fairly small, a power reserve must always be available to ensure that the balance between the power provided by the turbines and the power requested by the electrical system is maintained. In this respect, during the system planning stage, it is useful to distinguish between *normal operation* and a *disturbance* as reasons for utilizing the reserve. Power imbalances due to incorrect load forecasts and random load variations are both compensated for using the normal operation reserve. On the other hand, typical disturbances are plant outages or line trips.

The reserves are categorized according to the time needed to activate them:

- The *spinning reserve* is provided by the margins between the current power output and the maximum and minimum limits of a generating unit. This reserve can be activated in a few seconds, and is used during primary frequency control.
- The *supplementary reserve* is employed to restore the spinning reserve when it has been used in the event of a large perturbation, and it is often activated by automatic generation control (AGC) after tens of seconds. Thus, it is significantly slower to activate than primary frequency control; indeed, it is designed not to interact with it. This phase is known as secondary frequency control.
- The *back-up reserve* is a slow reserve that can be activated within a couple of hours to restore a faster reserve when it has been used. This phase is known as tertiary frequency control.

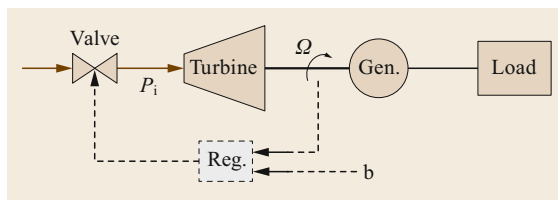


Fig. 5.89 Basic scheme of a speed governor

Figure 5.90 illustrates the concepts of primary, secondary, and tertiary frequency control using an example of a large perturbation in the network of continental Europe. The entire system is involved during primary control; secondary control action is expected to be limited to the affected area only; whilst the rescheduling associated with tertiary control is applied to just a few power stations.

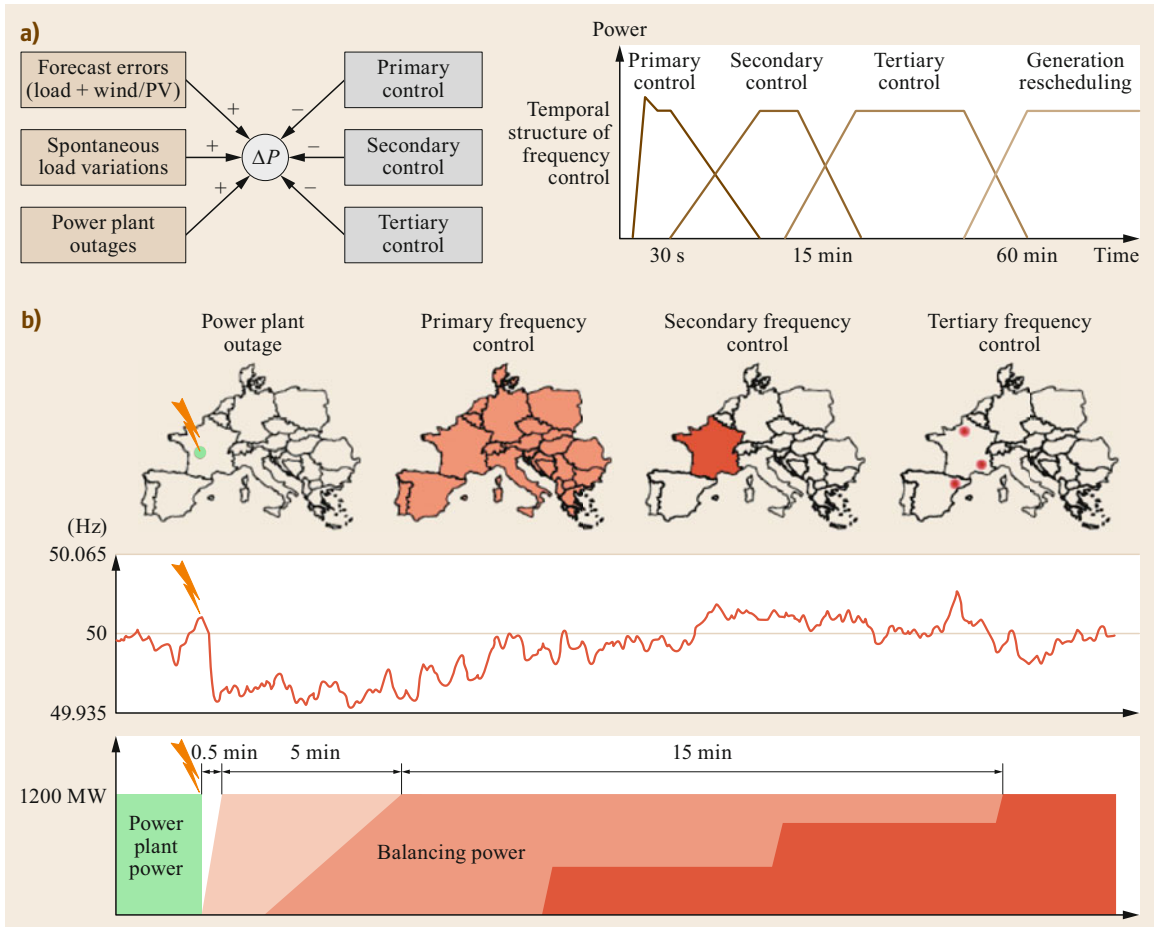


Fig. 5.90a,b Primary, secondary, and tertiary frequency control: (a) general scheme and (b) example showing the activation of each control phase after a large perturbation in the European network [5.52]

5.7.2 Dynamics of the Generators

After a disturbance in a large power system, the frequency varies across the system. For typical disturbances, however, the frequencies of the different machines can be regarded as being close to an average *system frequency* defined by a *center of inertia* (COI). A model that is valid for reasonable frequency deviations is described below.

We start with the swing equation (torque version) in pu,

$$\dot{\omega}_i = \frac{1}{2H_i}(T_{mi} - T_{ei}) \tag{5.282}$$

The initial condition for (5.282) is the pre-disturbance frequency, which is assumed equal to the rated frequency $\omega_i(t_0) = \omega_0$. The angular frequency deviation

$\Delta\omega_i$ is given by

$$\Delta\omega_i = \omega_i - \omega_0, \tag{5.283}$$

which, in SI units, yields

$$\frac{2H_i S_{ni}}{\omega_0} \Delta\dot{\omega}_i = \frac{\omega_0}{\omega_i} (P_{mi} - P_{ei}), \tag{5.284}$$

where, for each unit i , S_n is the rated power, H is the constant of inertia, and P_m and P_e are the mechanical and electrical power, respectively. If we assume that it is a highly meshed system, all generating units can be assumed to be connected to the same bus. The COI frequency can be defined as

$$\omega = \frac{\sum_i H_i S_{ni} \omega_i}{\sum_i H_i S_{ni}} \tag{5.285}$$

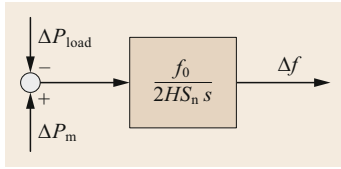


Fig. 5.91 Block diagram representing the inertia of the system

All generating units can be considered to be aggregated into a single unit

$$\Delta \dot{\omega} = \frac{\omega_0^2}{2HS_n} (P_m - P_e), \quad (5.286)$$

where:

$S_n = \sum_i S_{ni}$ is the total rating, i.e., the sum of the power ratings of the generators

$H = \sum_i H_i S_{ni} / \sum_i S_{ni}$ is the total constant of inertia

$P_m = \sum_i P_{mi}$ is the total mechanical power

$P_e = \sum_i P_{ei}$ is the total electrical power.

By assuming that $\omega = \omega_0$ on the right-hand side, a linear approximation of (5.286),

$$\Delta \dot{\omega} = \frac{\omega_0}{2HS_n} (P_m - P_e), \quad (5.287)$$

can be obtained. Equation (5.284) can also be expressed in terms of frequency as

$$\Delta \dot{f} = \frac{f_0}{2HS_n} (P_m - P_e). \quad (5.288)$$

After a disturbance, we can write

$$\Delta \dot{f} = \frac{f_0}{2HS_n} (\Delta P_m - \Delta P_{load}), \quad (5.289)$$

where ΔP_m and ΔP_{load} denote the variations in the total mechanical and electrical power outputs (taking into account the variations in the system power losses) with respect to the respective steady-state values before the perturbation.

Equation (5.289) can be represented by the block diagram shown in Fig. 5.91, where s is the Laplace variable.

5.7.3 Frequency Dependence of the Load

The aggregated system load is clearly frequency dependent. This has a stabilizing effect on the system frequency f . In addition to a component that depends on f , large rotating motors provide a contribution that depends on the time derivative \dot{f} (known as the rate of change of the frequency, ROCOF) due to the change in

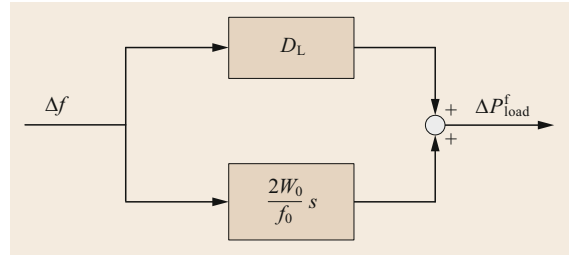


Fig. 5.92 Model used for the frequency-dependent behavior of the aggregated load

the kinetic energy stored in the rotating masses of the motor. Both of these frequency dependences are incorporated into the load model

$$\Delta P_{load}^f = D_L \Delta f + g(\Delta \dot{f}). \quad (5.290)$$

The function $g(\Delta \dot{f})$ can be derived by observing that the kinetic energy of rotating masses can be expressed by

$$W(f) = \frac{1}{2} J (2\pi f)^2 \quad (5.291)$$

and that ΔW can be approximated by

$$\Delta W = \frac{2W_0}{f_0} \Delta f, \quad (5.292)$$

where $W_0 = J/2(2\pi f_0)^2$. Hence,

$$g(\Delta \dot{f}) = \frac{2W_0}{f_0} \Delta \dot{f}. \quad (5.293)$$

The values of W_0 and D_L are highly dependent on the composition of the load and can vary over time. Typical values of the constant D_L are such that the load variation is between 0 and 2% of the frequency variation.

A model of the loads is provided in Fig. 5.92.

5.7.4 Dynamic Response of an Uncontrolled Power System

The model generated by combining the models used for the system inertia and the load is shown in Fig. 5.93.

Figure 5.94 shows the typical stable response of the frequency over time following an increasing or decreasing disturbance ΔP_L .

The stabilizing effect of the frequency dependence of the load is generally too small to maintain the frequency within reasonable bounds.

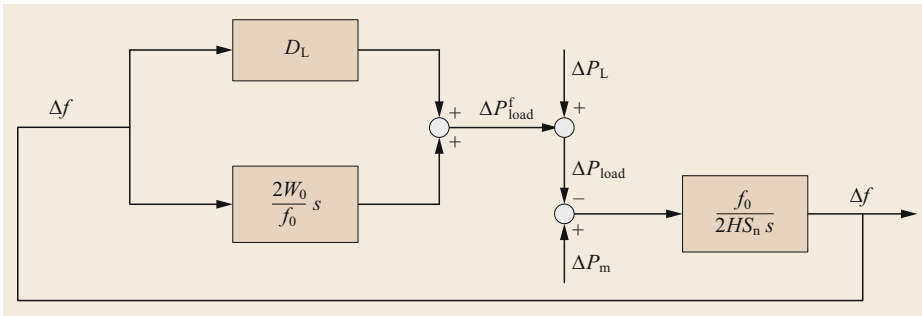


Fig. 5.93 Model of an uncontrolled system

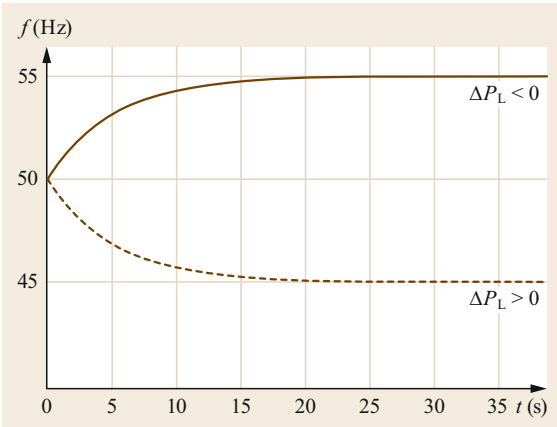


Fig. 5.94 Typical behavior of the frequency in the system shown in Fig. 5.93 after a perturbation

frequency control, the goal is to quickly return the frequency to acceptable values. However, even after primary control has acted, some of the frequency error will remain. Moreover, all of the generators must contribute to primary control, irrespective of the location of the disturbance.

In secondary frequency control (also called AGC or load frequency control), the power set points of the generators are adjusted in order to compensate for the frequency error remaining after the primary control has acted. Moreover, for large systems consisting of several control areas, the secondary control returns the power flows in the tie lines between the areas to the scheduled value.

Underfrequency load shedding is a form of system protection that acts on timescales of less than a second. As this scheme is only applicable when there is a loss of load across entire regions, it must only be activated when necessary to save the system from a blackout.

5.7.5 Control Structure for Frequency Control

The automatic control system consists of two main parts: primary control and secondary control, as shown in Fig. 5.95. Primary control refers to control actions that are performed locally (at the power plant) based on the set points for frequency and power. In primary

Dynamic Characteristics of Primary Control

The action of the governor for the generic unit *i* can be described by

$$(f_0 - f) \frac{1}{R_i} + (P_{m0,i}^{\text{set}} - P_{m,i}^{\text{set}}) = 0, \quad (5.294)$$

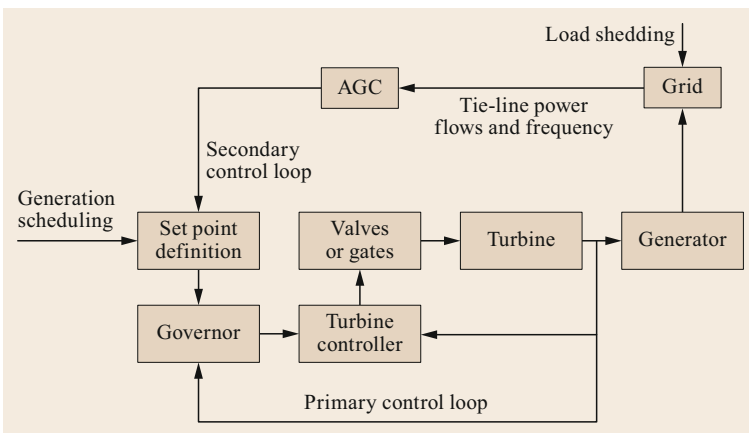


Fig. 5.95 Structure of the frequency control system

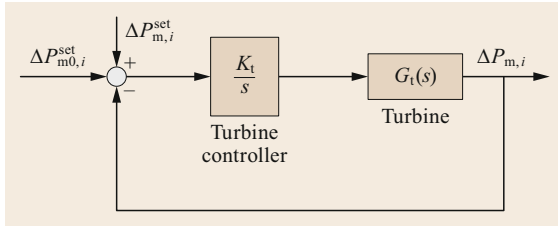


Fig. 5.96 Scheme of the turbine control loop

where R_i is the speed droop (in Hz/MW), which typically ranges from 4% to 8%.

Assuming an integral turbine power controller, we obtain the scheme depicted in Fig. 5.96.

If the dynamics of the turbine are neglected, we get

$$\Delta P_{m,i}(s) = \frac{1}{1 + T_i s} [\Delta P_{m0,i}^{set}(s) + \Delta P_{m,i}^{set}(s)], \quad (5.295)$$

where the time constant $T_i = 1/K_i$ is small compared to the frequency dynamics of the system.

By defining

$$\frac{1}{R} = \sum_i \frac{1}{R_i}, \quad (5.296)$$

we get

$$\Delta P_{m,i}^{set} = -\frac{1}{R} \Delta f, \quad (5.297)$$

where $\Delta P_m^{set} = \sum_i \Delta P_{m,i}^{set}$ and Δf is the frequency variation of the COI.

The models for the turbine control and the governor can be inserted into the model derived in the previous section, as shown in Fig. 5.97.

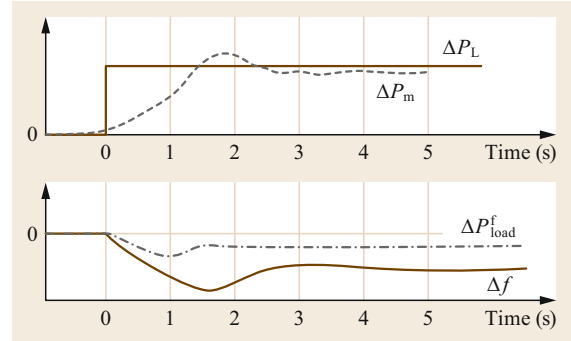


Fig. 5.98 Typical response of the system with primary control

We now analyze the effect of a disturbance in the system above. Both a loss of generation and a loss of load can be simulated by imposing a positive or negative step input on the variable ΔP_L . For obvious reasons, a change in the set value of the system frequency f_0 is not considered here.

From the block diagram shown in Fig. 5.100, the transfer function between ΔP_L and Δf ($\Delta P_m^{set} = 0$) is

$$\Delta f(s) = -\frac{1 + sT_t}{\left[\frac{1}{R} + D_L(1 + sT_t) + \left(\frac{2W_0}{S_n} + 2H \right) \frac{S_n}{f_0} s(1 + sT_t) \right]} \Delta P_L(s). \quad (5.298)$$

The step response for $\Delta P_L(s) = \Delta P_L/s$ is illustrated in Fig. 5.98.

The frequency deviation in the steady state is

$$\Delta f_\infty = \lim_{s \rightarrow 0} (s \Delta f_s) = -\frac{\Delta P_L}{\frac{1}{R} + D_L}. \quad (5.299)$$

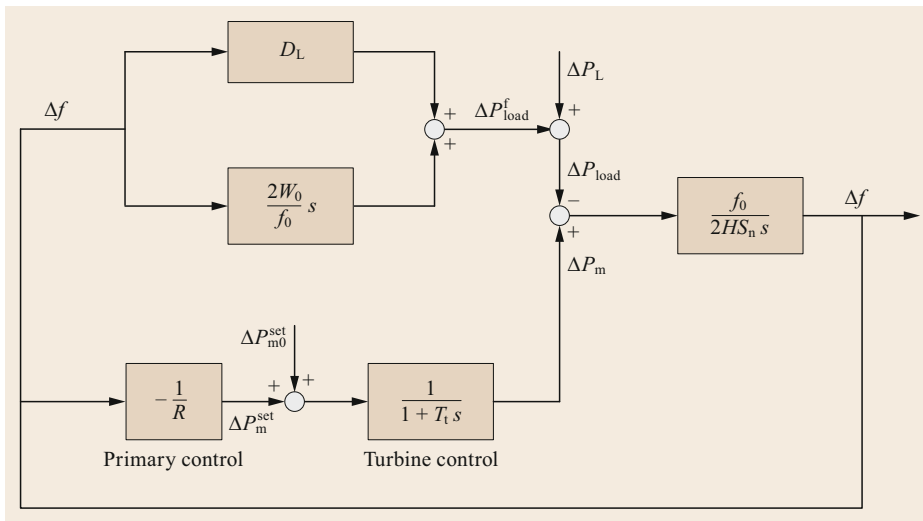


Fig. 5.97 Model of the system with primary control

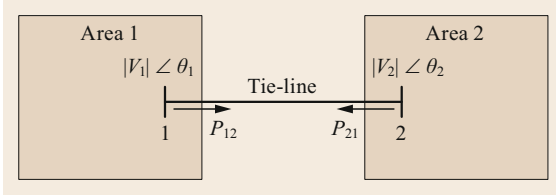


Fig. 5.99 Scheme for a two-area system

In real systems, the turbine controller time constant T_t is much smaller than the time constant of the frequency dynamics T_M presented in Fig. 5.94, so

$$T_M = \frac{2W_0}{S_n} + 2H. \quad (5.300)$$

Transfer function (5.298) can be approximated as

$$\Delta f(s) = -\frac{1}{1 + \frac{S_n}{f_0} T_M \frac{1}{R + D_L} s} \frac{\Delta P_{L,1}(s)}{\frac{1}{R} + D_L}. \quad (5.301)$$

The equivalent time constant for a step response is

$$T_{eq} = T_M \frac{S_n}{f_0} \frac{1}{\frac{1}{R} + D_L}. \quad (5.302)$$

Dynamic Model of a Two-Area System

In practice, a large interconnected power system is always divided into various control blocks or areas. For a simplified analysis, a system with two areas can be represented by two single bus systems with a tie-line between them, as shown in Fig. 5.99.

If we assume that $|V_1|$ and $|V_2|$ are constant and ignore the power loss in the tie-line, the power exchange P_{12} over the tie-line is

$$P_{12} = \frac{|V_1||V_2|}{x} \sin(\theta_1 - \theta_2), \quad (5.303)$$

where x is the equivalent reactance of the tie line and θ_1 and θ_2 are the voltage angles.

For small deviations, we obtain

$$\begin{aligned} \Delta P_{12} &= \left. \frac{\partial P_{12}}{\partial \theta_1} \right|_0 \Delta \theta_1 + \left. \frac{\partial P_{12}}{\partial \theta_2} \right|_0 \Delta \theta_2 \\ &= \frac{|V_1||V_2|}{x} \cos(\theta_1^0 - \theta_2^0) (\Delta \theta_1 - \Delta \theta_2) \end{aligned} \quad (5.304)$$

or

$$\Delta P_{12} = P_T (\Delta \theta_1 - \Delta \theta_2) \quad (5.305)$$

with

$$P_T = \frac{|V_1||V_2|}{x} \cos(\theta_1^0 - \theta_2^0). \quad (5.306)$$

Using this model, the block diagram of the power system can be extended as shown in Fig. 5.100.

We now study the behavior after a load change in area 1, where area 1 is considered to be much smaller than area 2, which can be regarded as an infinite bus. As $\Delta f_2 = 0$, $\Delta \theta_2 = 0$, so

$$\Delta P_{12} = 2\pi P_T \int \Delta f_1 dt. \quad (5.307)$$

Without any generator setpoint changes (i.e., $\Delta P_{m0,1}^{\text{set}} = 0$), the transfer functions for a change of $\Delta P_{L,1}(s)$ are

$$\Delta f_1(s) = -\frac{s}{\left[2\pi P_T + \left(D_{L1} \frac{1}{R_1(1+sT_{t1})} \right) s + \left(\frac{T_{M1} S_{n1}}{f_0} \right) s^2 \right]} \Delta P_{L,1}(s) \quad (5.308)$$

$$\Delta T_{12} = \frac{2\pi P_T}{s} \Delta f_1(s) \quad (5.309)$$

$$\Delta T_{12}(s) = -\frac{2\pi P_T}{\left[2\pi P_T + \left(D_{L1} \frac{1}{R_1(1+sT_{t1})} \right) s + \left(\frac{T_{M1} S_{n1}}{f_0} \right) s^2 \right]} \Delta P_{L,2}(s). \quad (5.310)$$

The step response for $\Delta P_{L,1}(s) = \Delta P_{L,1}/s$ is shown in Fig. 5.101.

The steady-state frequency deviation is

$$\Delta f_\infty = \lim_{s \rightarrow 0} s \Delta f_1(s) = 0, \quad (5.311)$$

and the steady-state deviation of the tie-line power is

$$\Delta P_{12\infty} = \lim_{s \rightarrow 0} s \Delta P_{12}(s) = \Delta P_{L,1}. \quad (5.312)$$

The infinite bus brings the frequency deviation Δf_1 back to 0. This is achieved by increasing P_{21} such that the load variation $\Delta P_{L,1}$ is fully compensated for.

While this is beneficial for the system frequency in area 1, unscheduled and persistent energy exchange has arisen between the two areas.

Automatic Generation Control

Following the application of primary frequency control after a disturbance, a static frequency error will generally persist unless additional control actions are taken.

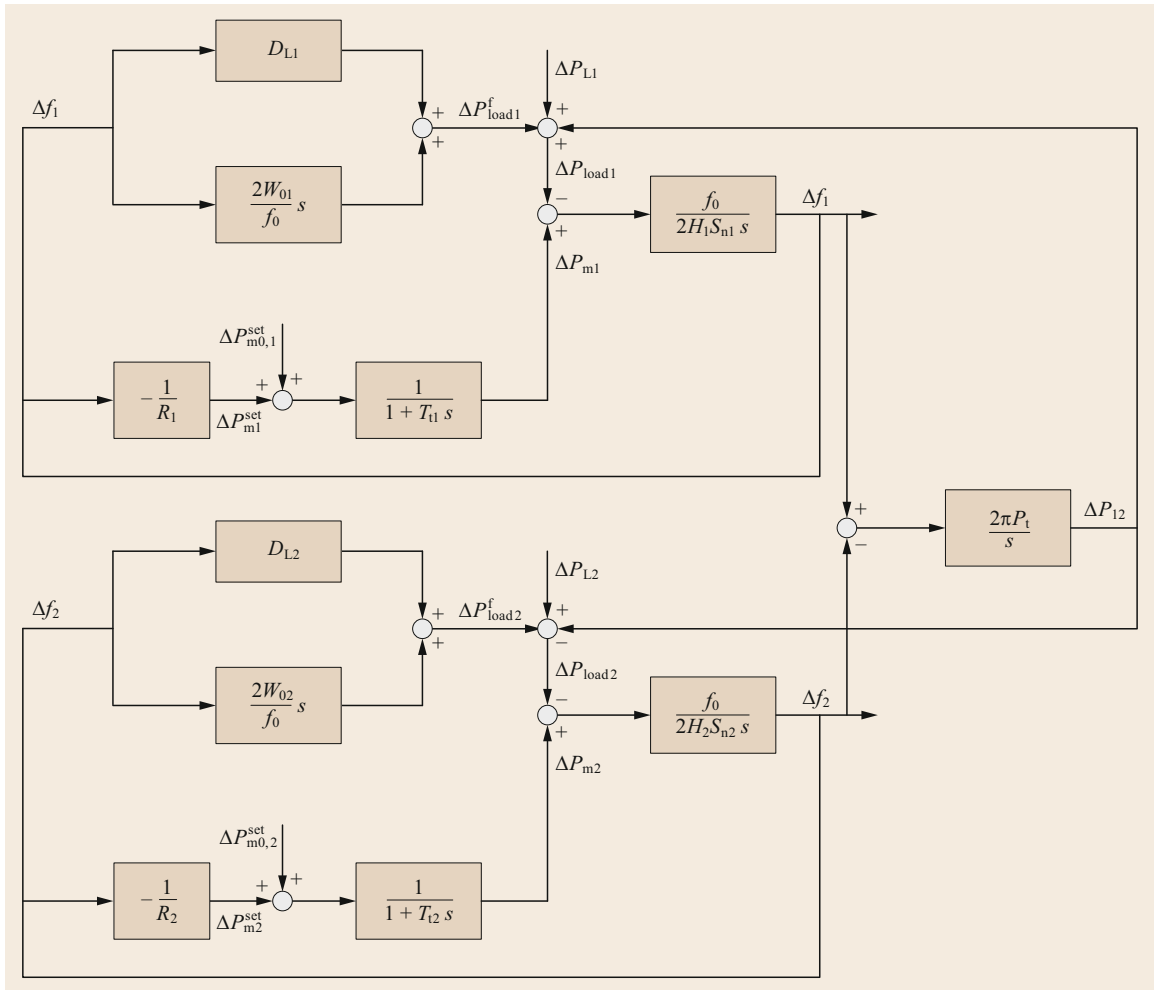


Fig. 5.100 Dynamic model of a two-area system

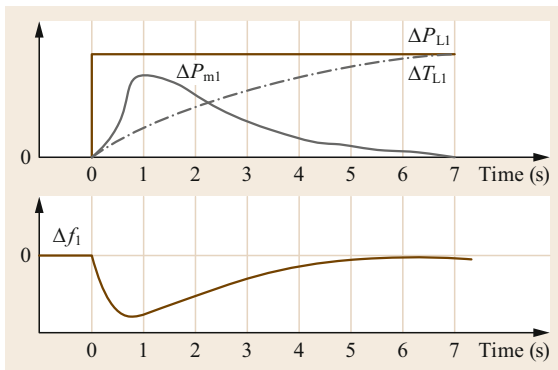


Fig. 5.101 Step response of the two-area system model

Furthermore, primary frequency control may change the scheduled interchanges between different areas in an interconnected system. The restoration of both the

frequency and the power interchanges to their pre-disturbance values is accomplished through the AGC.

In an N -area system, there are N AGC _{i} controllers, one for each area i . Each implements a proportional-integral (PI) controller, i.e.,

$$\Delta P_{AGC_i} = - \left(C_{P_i} + \frac{1}{s T_{N_i}} \right) \Delta e_i, \quad (5.313)$$

with C_{P_i} typically ranging between 0.1 and 1 and T_{N_i} between 30 and 200 s, implying that AGC reacts much more slowly than primary frequency control.

The error Δe_i is termed the area control error (ACE) for area i , and

$$ACE_i = \sum_{j \in \Omega_i} (P_{ij} - P_{ij}^0) + B_i (f_i - f_0), \quad (5.314)$$

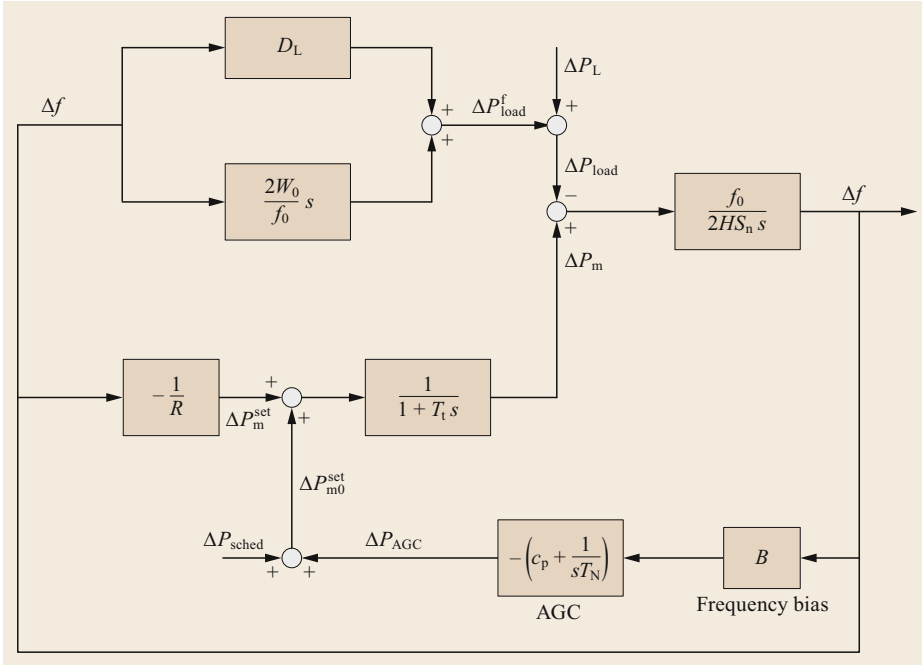


Fig. 5.102 Model of a single-area system with AGC

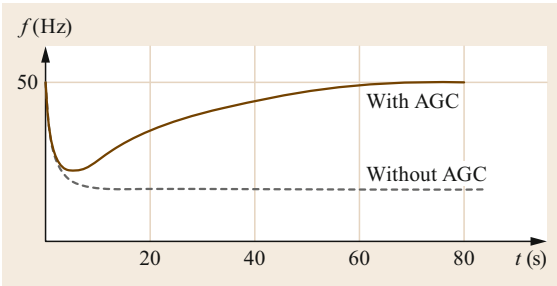


Fig. 5.103 Step response of a single-area system with AGC

where P_{ij} is the power transfer from area i to area j and P_{ij}^0 is the corresponding scheduled value. Defining

$$\Delta P_i = \sum_{j \in \Omega_i} (P_{ij} - P_{ij}^0), \tag{5.315}$$

where the summation includes all of the areas j directly connected to area i , ACE_i can be written as

$$ACE_i = \Delta P_i + B_i(f_i - f_0). \tag{5.316}$$

The constant B_i is called the frequency bias factor (MW/Hz). It is assumed that the frequency references are the same in all areas. The goal is to bring all ACE_i values to 0.

The variables are thus ΔP_i and f , i.e., there are $N + 1$ variables in total, which are uniquely defined by N

linear equations ($ACE_i = 0$) and

$$\sum_i \Delta P_i = 0. \tag{5.317}$$

Selection of Frequency Bias Factors

Let us consider a two-area system. The load is increased by ΔP_L in area 2. If the power in the tie-line is to be kept constant, the generation in area 2 must be increased by ΔP_L after the AGC has reacted. Before the AGC has reacted, we have a frequency deviation of Δf in both areas, which means that for area 1,

$$\Delta f = -R_1 \Delta P_{12}, \tag{5.318}$$

and for area 2,

$$\Delta f = -R_2(\Delta P_L - \Delta P_{12}), \tag{5.319}$$

and $\Delta P_{12} = \Delta P_{21}$. The two ACEs can now be written as

$$\begin{aligned} ACE_1 &= \Delta P_{12} + B_1 \Delta f = \Delta P_{12} + B_1(-R_1 \Delta T_{12}) \\ &= \Delta P_{12}(1 - B_1 R_1) \end{aligned} \tag{5.320}$$

and

$$\begin{aligned} ACE_2 &= \Delta P_{21} + B_2 \Delta f \\ &= \Delta P_{21} + B_2[-R_2(\Delta P_L - \Delta P_{12})] \\ &= \Delta P_{12}(1 - B_2 R_2) - B_2 R_2 \Delta P_L \end{aligned} \tag{5.321}$$

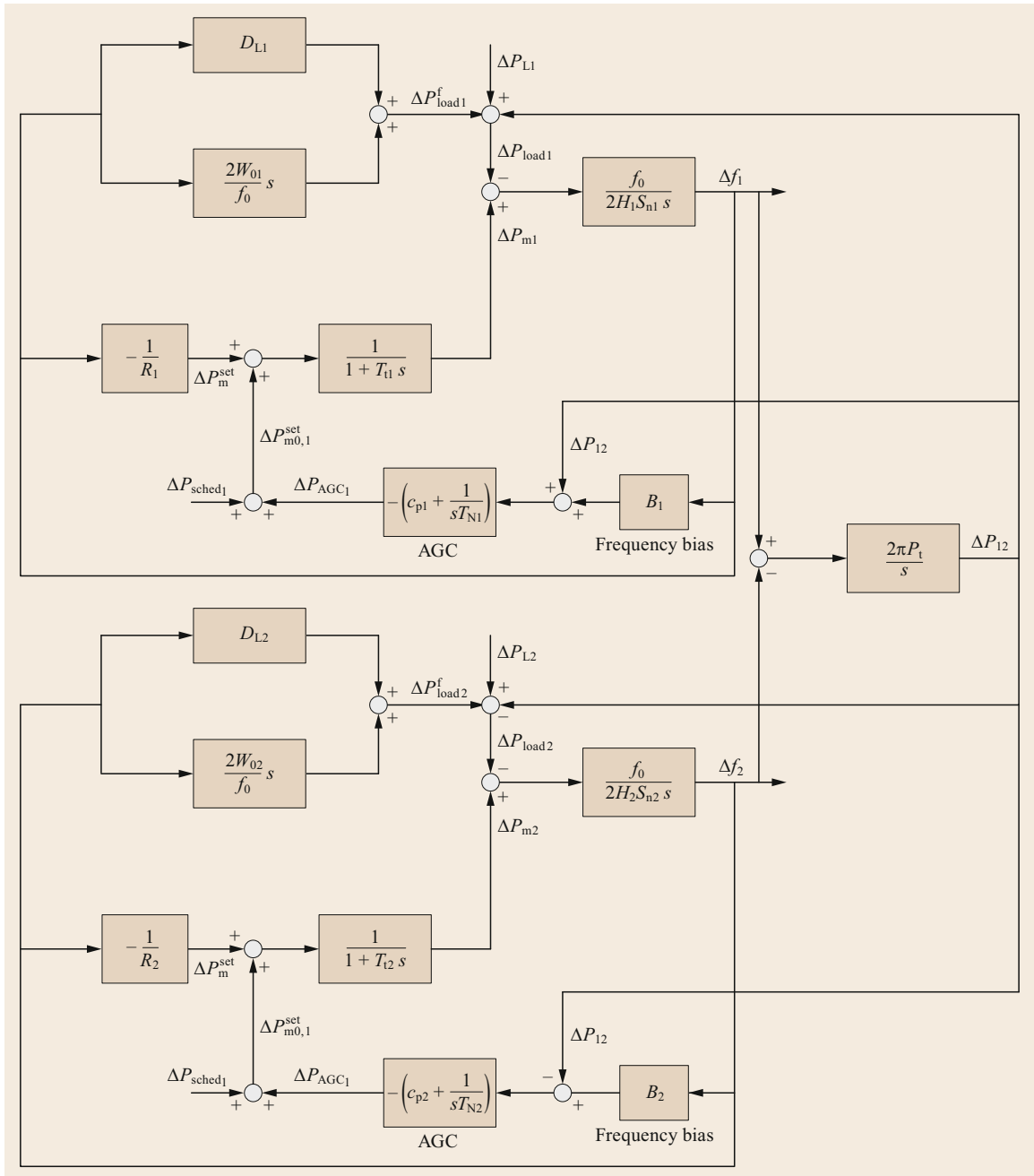


Fig. 5.104 Model of a two-area system with AGC

In this case, it is desirable that the AGC controller for area 1 should not react. If we set $B_1 = 1/R_1$, we can see from (5.320) that $ACE_1 = 0$. If $B_2 = 1/R_2$ is chosen, the ACE in area 2 becomes

$$ACE_2 = -\Delta P_L. \tag{5.322}$$

This means that only controller 2 reacts to a load perturbation ΔP_L in the same area.

In the multi-area case, this corresponds to selecting $B_i = 1/R_i$ for all areas, which is known as noninteractive control. However, for the controller described by (5.313), all positive values of B_i will guarantee that all

Fig. 5.105 Step response of a two-area system model with AGC ▶

the ACE_i tend to 0. The application of noninteractive control results in reduced control effort and costs.

Dynamic Characteristics of AGC

We now include the AGC control in both the single-area and two-area models.

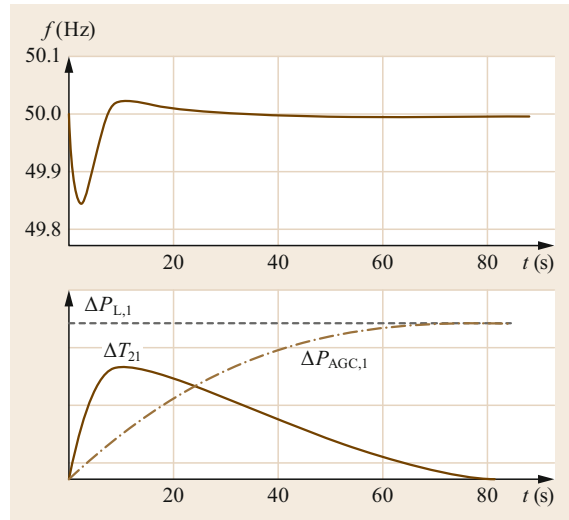
Single-Area System

AGC only acts to restore the nominal system frequency, as illustrated in Fig. 5.102, where P_{sched} indicates the scheduled value of the power output of the generators. Figure 5.103 shows how the system frequency response is brought back to the rated value after a load increase.

Two-Area System

A model of a two-area system with AGC is shown in Fig. 5.104.

If area 1 is assumed to be much smaller than area 2, the step response of the system for a load increase



of $\Delta P_{L,1}$ is shown in Fig. 5.105. Due to the action of AGC, the perturbation in area 1 is fully compensated for by the generators in the same area (area 1) after the transients have decayed.

5.8 Propagation of Electromagnetic Transients Along Transmission Lines

In *steady-state* operating conditions, the wavelength of the sinusoidal currents and voltages is large compared with the physical dimensions of the network. Therefore, for steady-state analysis, a *lumped* element representation of transmission lines is generally adequate. However, for transient analysis, this is no longer the case, and the travel time of the electromagnetic waves must be taken into account.

For example, in the case of insulation coordination analysis against overvoltages (particularly those due to lightning), we need to account for the fact that voltages and currents induced by lightning strikes have non-negligible frequency contents above 1 MHz. If the travel time of the electromagnetic field within the boundaries of the region of interest cannot be neglected with respect to the period over which electromagnetic quantities vary, then the lumped element model must be replaced in order to accurately represent electromagnetic field propagation along the line. Although the electric field cannot be expressed as the gradient of a scalar potential in our analysis of the electromagnetic field along lossless transmission lines, we can assume a transverse electromagnetic mode (TEM) of propagation (i.e., no component of the electric field or the magnetic field in the direction of propagation), so the rotor of the electric field is null in each plane orthog-

onal to the direction of propagation. This means that the integrals of the electric field in these planes can be expressed as potential differences. For lossy lines, and assuming a quasi-transverse electromagnetic mode of propagation, we can still apply the useful concepts of phase-to-ground and line-to-line voltages. In the quasi-TEM approximation, it is assumed that the electric and magnetic field components along the line are non-null but small enough to make the rotor of the electric field practically null in the plane orthogonal to the line.

Research into electromagnetic transients along transmission lines and relevant phenomena has developed impressively since the introduction of the Electromagnetic Transients Program [5.8] developed by *Herman Dommel* in the 1970s, and there have been various textbooks devoted to this subject [5.27, 28, 53, 54]. In this section, we limit our discussion to a brief summary of the basic concepts.

5.8.1 Traveling Waves in a Lossless Line

In order to introduce the equations describing the response of a transmission line to a transient, we consider a single line conductor that has ground return and is at a constant height above the ground (Fig. 5.106). The developments that follow are somewhat inspired

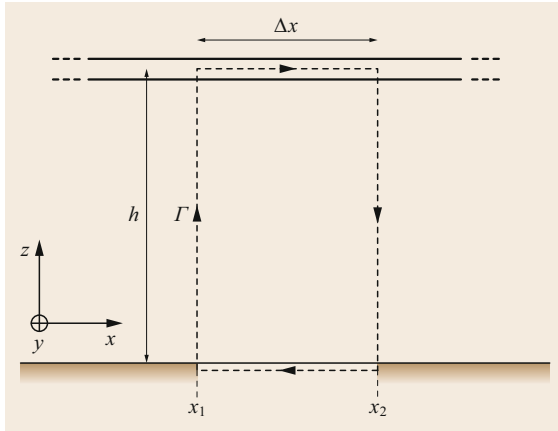


Fig. 5.106 A single line-conductor section and the path of integration of the electric field that passes through the line

by [5.55], except that we consider a voltage source at one of the line terminations rather than an overhead line excited by an external electromagnetic field. The following approach can also be applied to a line consisting of two straight conductors that are parallel to each other.

Let us assume a triplet of Cartesian orthogonal axes x , y , and z , where the x -axis is parallel to the axis of the line conductor that lies in the x - z plane. The line height is $z = h$. The current in the line conductor is assumed to be positive if it is directed along the positive x -axis. Let us consider a closed path Γ that passes through the line and the ground (which lies in the x - y plane), with vertical sections perpendicular to the ground. Let the path Γ be oriented according to the y -axis and the right-hand rule. The integral of the electric field along Γ is given by

$$\oint_{\Gamma} \bar{E} d\bar{l} = \int_0^h E_z(x_1, 0, z, t) dz + \int_{x_1}^{x_2} E_x(x, 0, h, t) dx - \int_0^h E_z(x_2, 0, z, t) dz - \int_{x_1}^{x_2} E_x(x, 0, 0, t) dx \quad (5.323)$$

If the conductors are ideal (i.e., both the line and the ground have infinite conductivity), the electric field components along x are null, so

$$\oint_{\Gamma} \bar{E} d\bar{l} = \int_0^h E_z(x_1, 0, z, t) dz - \int_0^h E_z(x_2, 0, z, t) dz \quad (5.324)$$

Assuming TEM propagation, the integrals of the electric field in the y - z plane can be expressed as differences in scalar potentials. Therefore, assuming that the potential is zero at the ground, the integral of E along Γ can

be written as

$$\oint_{\Gamma} \bar{E} d\bar{l} = u(x_2, t) - u(x_1, t) \quad (5.325)$$

The law of electromagnetic induction

$$\oint_{\Gamma} \bar{E} d\bar{l} = -\frac{\partial}{\partial t} \int_{S_{\Gamma}} \bar{B} d\bar{S} \quad (5.326)$$

where B is the magnetic flux density and S_{Γ} is any surface with Γ as a contour, gives

$$u(x_2, t) - u(x_1, t) = -\frac{\partial}{\partial t} \int_{x_1}^{x_2} \int_0^h B_y(x, 0, z, t) dx dz \quad (5.327)$$

By taking $x_2 = x_1 + \Delta x$, where Δx is small, we can write

$$\int_{x_1}^{x_2} \int_0^h B_y(x, 0, z, t) dx dz = \int_0^h B_y(x_1, 0, z, t) dz \Delta x \quad (5.328)$$

where

$$\int_0^h B_y(x_1, 0, z, t) dz = L' i(x_1, t) \quad (5.329)$$

in which L' is the line inductance pu length.

We can then write

$$u(x_1 + \Delta x, t) - u(x_1, t) = -\frac{\partial}{\partial t} [L' i(x_1, t) \Delta x] \quad (5.330)$$

Dividing by Δx and assuming that the line is nondeformable, we get

$$\frac{u(x_1 + \Delta x, t) - u(x_1, t)}{\Delta x} = -L' \frac{\partial i(x_1, t)}{\partial t} \quad (5.331)$$

By taking the limit as Δx approaches zero, we obtain the first telegrapher's equation,

$$\frac{\partial u(x_1, t)}{\partial x} = -L' \frac{\partial i(x_1, t)}{\partial t} \quad (5.332)$$

Let us now consider a cylindrical surface surrounding the Δx section of the line conductor (Fig. 5.107). We denote the base surfaces orthogonal to the plane y - z at x_1 and x_2 as S_1 and S_2 , respectively, and label the lateral surface as S_l .

The flux of the current density through the cylindrical surface has three components, i.e.,

$$\oint \bar{J} d\bar{S} = -\int_{S_1} J_x dS + \int_{S_l} \bar{J} d\bar{S} + \int_{S_2} J_x dS \quad (5.333)$$

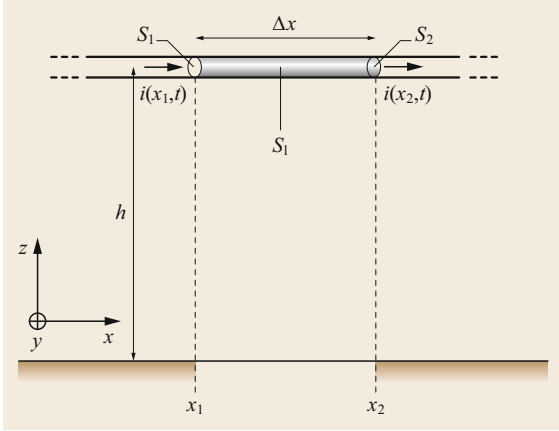


Fig. 5.107 A single line-conductor section and the surface of integration of the current density

If the insulating medium surrounding the conductor is ideal (i.e., it has null conductivity), the radial component of the current density is null, so

$$\oint \bar{J} d\bar{S} = - \int_{S_1} J_x dS + \int_{S_2} J_x dS. \quad (5.334)$$

The fluxes of the current density through S_1 and S_2 are the line currents at x_1 and x_2 ; therefore,

$$\oint \bar{J} d\bar{S} = i(x_2, t) - i(x_1, t). \quad (5.335)$$

The law of charge conservation

$$\oint_S \bar{J} d\bar{S} = - \frac{\partial}{\partial t} \int_{\tau_S} \rho d\tau, \quad (5.336)$$

where ρ is the charge density and τ_S is the volume with S as a boundary, gives

$$i(x_2, t) - i(x_1, t) = - \frac{\partial}{\partial t} [C' u(x_1, t) \Delta x], \quad (5.337)$$

where C' is the line capacitance pu length. By taking $x_2 = x_1 + \Delta x$, where Δx is small, we can write

$$\frac{i(x_1 + \Delta x, t) - i(x_1, t)}{\Delta x} = -C' \frac{\partial u(x_1, t)}{\partial t}. \quad (5.338)$$

Taking the limit as Δx approaches zero, we obtain the second telegrapher's equation

$$\frac{\partial i(x_1, t)}{\partial x} = -C' \frac{\partial u(x_1, t)}{\partial t}. \quad (5.339)$$

Rewriting the two telegrapher's equations with reference to a generic abscissa x yields

$$\frac{\partial u(x, t)}{\partial x} + L' \frac{\partial i(x, t)}{\partial t} = 0 \quad (5.340)$$

$$\frac{\partial i(x, t)}{\partial x} + C' \frac{\partial u(x, t)}{\partial t} = 0. \quad (5.341)$$

By differentiating the first wave equation with respect to x and the second with respect to t and using substitution, we obtain

$$\frac{\partial^2 u(x, t)}{\partial x^2} = L' C' \frac{\partial^2 i(x, t)}{\partial t^2}. \quad (5.342)$$

Differentiating the first wave equation with respect to t and the second with respect to x and using substitution, we get an analogous equation for the current,

$$\frac{\partial^2 i(x, t)}{\partial x^2} = L' C' \frac{\partial^2 u(x, t)}{\partial t^2}. \quad (5.343)$$

Both of these equations have the form of the 1-D (one-dimensional) wave equation

$$\frac{\partial^2 f(x, t)}{\partial x^2} = \frac{1}{v^2} \frac{\partial^2 f(x, t)}{\partial t^2}, \quad (5.344)$$

where v is the speed of the wave in the direction of propagation.

Therefore, the telegrapher's equations describe the propagation of the voltage and the current along a transmission line. It is worth noting that the propagation speed, given by

$$v = \frac{1}{\sqrt{L' C'}}, \quad (5.345)$$

for a lossless line is practically equal to the speed of light. In fact, for a single line conductor of radius R and height h above the perfectly conducting ground,

$$L' = \frac{\mu_0}{2\pi} \ln \left(\frac{2h}{R} \right) \quad (5.346)$$

$$C' \approx \frac{2\pi\epsilon_0}{\ln(2h/R)}. \quad (5.347)$$

Inserting this into (5.345) gives

$$v = \frac{1}{\sqrt{\mu_0 \epsilon_0}}. \quad (5.348)$$

According to D'Alembert, the solution to the 1-D wave equation is

$$f(x, t) = f_1(x - vt) + f_2(x + vt), \quad (5.349)$$

where f_1 is a forward-traveling wave (i.e., a wave traveling in the positive x direction) while f_2 is a backward-traveling wave (i.e., a wave traveling in the negative x direction).

It is easy to verify that (5.349) is a solution of (5.344) by observing that

$$\begin{aligned}\frac{\partial f_1(x-vt)}{\partial t} &= -v \frac{\partial f_1(x-vt)}{\partial x} \\ \frac{\partial f_2(x+vt)}{\partial t} &= v \frac{\partial f_2(x+vt)}{\partial x}.\end{aligned}\quad (5.350)$$

We then find that the solution of the wave equation for the voltage takes the form

$$u(x, t) = u_1(x - vt) + u_2(x + vt), \quad (5.351)$$

and that there is an analogous equation for the current,

$$i(x, t) = i_1(x - vt) + i_2(x + vt). \quad (5.352)$$

These two solutions are not independent; in fact, the relationship between forward and backward voltage and current waves can be shown (via substitution and differentiation) to be

$$\begin{aligned}i_1(x) &= \frac{u_1(x)}{Z_0} \\ i_2(x) &= -\frac{u_2(x)}{Z_0},\end{aligned}\quad (5.353)$$

where Z_0 is the surge impedance of the line, given by

$$Z_0 = \sqrt{\frac{L'}{C'}}. \quad (5.354)$$

Substituting (5.346) and (5.347) into (5.354) yields

$$Z_0 = 60 \ln \left(\frac{2h}{R} \right) \quad (5.355)$$

for a single lossless line conductor.

It is worth noting that $u_1(\xi)$ with $\xi = x - vt$ represents a forward-traveling wave, because ξ assumes the same value at x_0 and time t_0 as it does at $x_0 + v\Delta t$ and time $t_0 + \Delta t$, and that an observer traveling forward at speed v would see the same voltage value.

A forward-traveling voltage wave is shown schematically in Fig. 5.108.

The same approach can be adopted for backward-traveling waves.

Note that it is changes in charge density that travel at the propagation speed v , not the charges themselves.

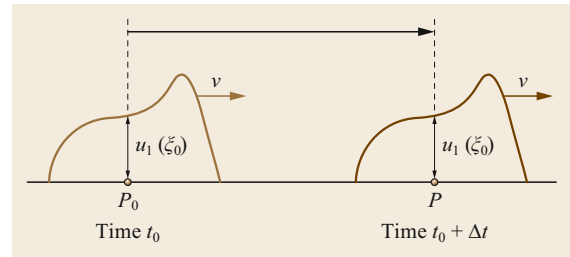


Fig. 5.108 Schematic of a forward-traveling voltage wave (adapted from [5.36])

In the absence of an external electromagnetic field coupled with the transmission lines, the traveling voltage and current waves depend on the boundary conditions at the line terminations (i.e., energizations, surge impedance discontinuities, loads, etc.).

Figure 5.109 presents four simple cases involving traveling waves: forward-traveling waves at the top and backward-traveling waves at the bottom with different polarities. According to (5.353), forward-traveling voltage and current waves have the same polarity, while backward-traveling voltage and current waves have opposite polarities.

5.8.2 Reflection and Transmission Coefficients

We now consider a discontinuity in the surge impedance of the line. Such a discontinuity may occur where there is a change in geometric size or a junction of a cable line with an overhead line that has bare conductors, or where there is a busbar with several lines connected, or where lumped devices are connected (e.g., a load or a transformer or a surge-protection device). When the traveling waves reach such a discontinuity, reflection and transmission (or refraction) processes occur due to the principle of energy conservation, and new voltage and current waves start to travel away from that point.

If the point of discontinuity M connects two lines L_1 and L_2 with different surge impedances Z_1 and Z_2 , a pair of incident voltage and current waves v_i and i_i from L_1 give rise to a pair of transmitted waves v_t and i_t that travel forward along L_2 as well as a pair of reflected waves v_r and i_r that travel backward along L_1 .

The voltage and the current at the point of discontinuity must obey the equations (see also Fig. 5.110)

$$u_i + u_r = u_t \quad (5.356)$$

$$i_i + i_r = i_t. \quad (5.357)$$

If we define the transmission coefficient τ_v as the ratio of v_t to v_i and the reflection coefficient ρ_v as the

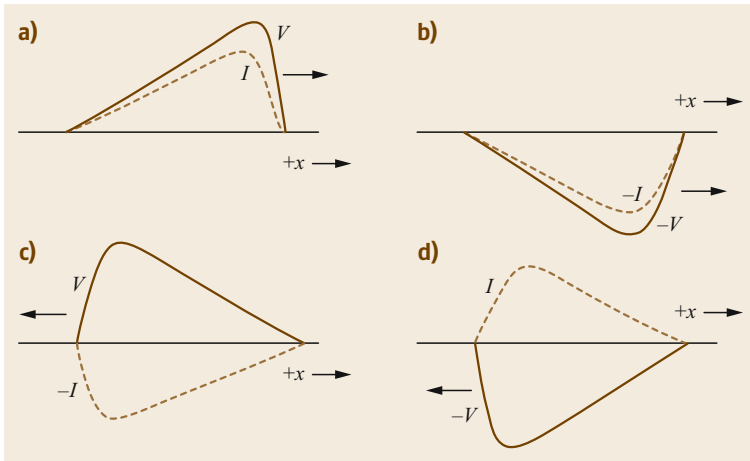


Fig. 5.109a-d Schematic of four combinations of forward- and backward-traveling voltage and current waves: (a) positive forward-traveling waves, (b) negative forward-traveling waves, (c) negative backward-traveling current wave, (d) positive backward-traveling current wave (adapted from [5.28])

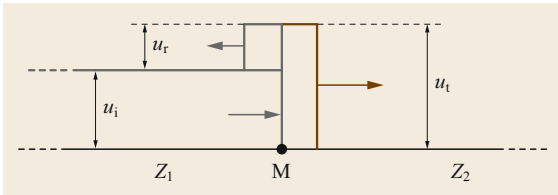


Fig. 5.110 Voltage waves reflected and transmitted at a point of discontinuity in the surge impedance (adapted from [5.36])

ratio of v_r to v_i , (5.356) yields

$$1 + \rho_v = \tau_v \tag{5.358}$$

Analogously, we can define the transmission coefficient τ_i as the ratio of i_t to i_i and the reflection coefficient ρ_i as the ratio of i_r to i_i .

Inserting (5.353) into (5.357) gives

$$\frac{u_i}{Z_1} - \frac{u_r}{Z_1} = \frac{u_t}{Z_2} \tag{5.359}$$

By adding and subtracting each member of (5.356) and (5.359), we obtain

$$u_t = \frac{2Z_2}{Z_1 + Z_2} u_i \tag{5.360}$$

$$u_r = \frac{Z_2 - Z_1}{Z_2 + Z_1} u_i \tag{5.361}$$

Therefore, the transmission coefficient τ_v is

$$\tau_v = \frac{2Z_2}{Z_1 + Z_2} \tag{5.362}$$

while the reflection coefficient ρ_v is

$$\rho_v = \frac{Z_2 - Z_1}{Z_1 + Z_2} \tag{5.363}$$

Analogously, the transmission coefficient τ_i is

$$\tau_i = \frac{2Z_1}{Z_1 + Z_2} \tag{5.364}$$

and the reflection coefficient ρ_i is

$$\rho_i = \frac{Z_1 - Z_2}{Z_2 + Z_1} \tag{5.365}$$

Line terminations are line discontinuities that give rise to surge wave reflections. For an ideal lossless line that is terminated on a resistive lumped device, these reflections can easily be explained using reflection and transmission coefficients, as they are constant and scalar in this case. The reflections at a short-circuited end and at an open end can be considered a particular case of resistive termination, as illustrated below.

The surge response at a generic line termination can be calculated via Thévenin's theorem so long as reflections at the far termination of a line of finite length do not influence phenomena at the termination of interest within the considered observation time.

The system corresponding to (5.356), (5.357), and (5.353), i.e.,

$$\begin{cases} u_i + u_r = u_t \\ i_i + i_r = i_t \\ u_t = Z_2 i_t \\ u_r = -Z_1 i_r \end{cases} \tag{5.366}$$

yields

$$2v_i - Z_1 i_t = u_t \tag{5.367}$$

which is the equation of a Thévenin equivalent circuit with a no-load voltage of $2v_i$ and an equivalent impedance of Z_1 .

Analogously, system (5.366) can also be solved for the incident current,

$$2i_i - \frac{u_t}{Z_1} = i_t. \tag{5.368}$$

This corresponds to a Norton equivalent circuit with a short-circuit current of $2i_i$ and an equivalent conductance of $1/Z_1$.

Reflections at an Open Termination

An incident voltage wave undergoes complete reflection at an open termination. Superposition of the incident wave on a reflected wave of the same amplitude and polarity produces voltage doubling at the line termination. On the other hand, the incident current wave is canceled out by a reflected wave of equal and opposite amplitude, thereby resulting in a null current overall at the open end. The amplitudes and polarities of the reflected voltage and current waves can be deduced by considering the boundary conditions and the energy balance at the line termination. Voltage doubling can be viewed as a consequence of the increase in electric energy associated with the cancellation of the current at the line termination, as well as the associated magnetic energy. The same results can be deduced by noting that an open end can be considered a termination on a device with a very large equivalent resistance. The surge impedance seen by the surge waves is therefore very large. By taking the limits of (5.361) and (5.365) as Z_2 approaches infinity, we obtain $\rho_v = 1$ and $\rho_i = -1$. Ultimately, we have $v_t = 2v_i$, $v_r = v_i$, $i_t = 0$, and $i_r = -i_i$ at an open end. The effect of incident and reflected wave superposition at an open line end in the case of stepwise incident voltage and current waves is presented schematically in Fig. 5.111.

For a surge waveform of limited duration, superposition of the incident and reflected voltage waves only occurs close to the open end, and the ultimate effect of the reflection is a voltage with a mirrored waveform that propagates in the opposite direction. The case of a tri-

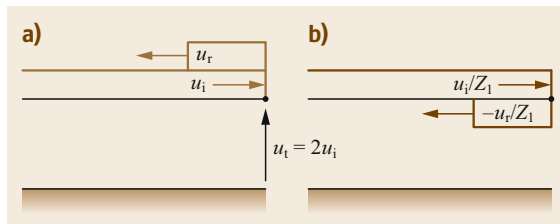


Fig. 5.111a,b Incident and reflected voltage waves (a) and current waves (b) at the open end of a transmission line (adapted from [5.36])

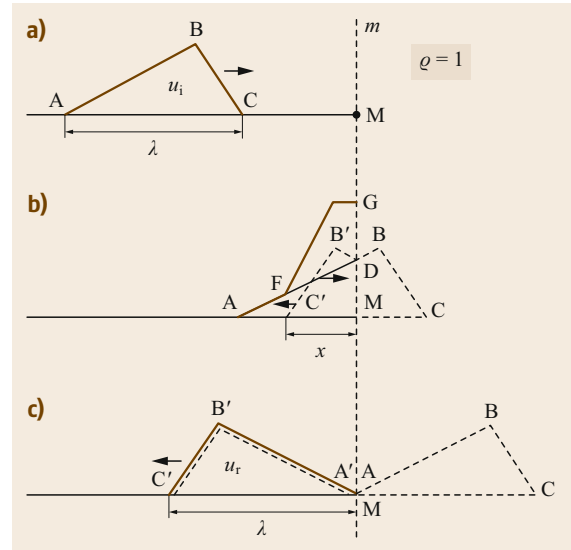


Fig. 5.112a-c A triangular voltage (a) before, (b) during, and (c) after reflection at the open end of a line (adapted from [5.36])

angular wave is presented in Fig. 5.112, which shows the diagram of the incident wave (ABC, propagating to the right) in Fig. 5.112a, the superposition of the diagram of the incident wave (ADM) on the wave $C'B'DM$ (the mirror image of the wave $CBDM$ with respect to the straight line m), which gives rise to wave AFG in Fig. 5.112b, and the mirrored wave $C'B'A'$ propagating to the left in Fig. 5.112c.

Reflections at a Short-Circuited End

Another extreme case is a short-circuited end. An identical approach to that used for an open end can be applied for a short-circuited end, but with the behavior of the voltage and current waves swapped. An incident voltage wave undergoes complete but negative reflection, resulting in a null voltage overall at the short-circuited end, while the current amplitude doubles. The amplitudes and polarities of the reflected voltage and current waves can be deduced by considering the boundary conditions and the energy balance at the line termination, as well as by noting that a short-circuited end can be considered a termination on a device with very low resistance. Thus, by taking the limits of (5.361) and (5.365) as Z_2 approaches zero, we obtain $\rho_v = -1$ and $\rho_i = 1$. Ultimately, we have $v_t = 0$, $v_r = -v_i$, $i_t = 2i_i$, and $i_r = 0$ at the short-circuited end. The effect of superposing the incident and reflected waves at a short-circuited line end in the case of stepwise incident voltage and current waves is presented schematically in Fig. 5.113.

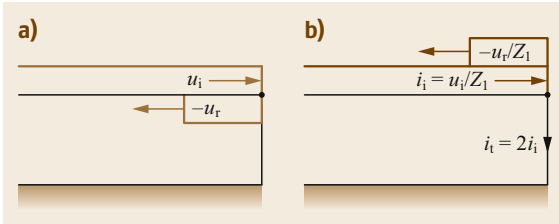


Fig. 5.113a,b Incident and reflected voltage waves (a) and current waves (b) at the short-circuited end of a transmission line (adapted from [5.36])

Reflections at an Inductive Termination

Reflection at an inductive termination is similar to that at an open circuit immediately after the arrival of the incident wave, but ultimately resembles reflection at a short circuit. The voltages (in pu with respect to the amplitude of the voltage source) at three points along a 60 km line with a step voltage source at $x = 0$ and a 25 mH inductance at $x = 60$ km are depicted in Fig. 5.114. Figure 5.115 reports the voltage profiles along the line at three different times. The results presented in this and subsequent sections are obtained using a finite-difference time-domain solution of the telegrapher’s equations, and using Bergeron’s lines to solve the boundary conditions.

The waveform of the inductive terminal voltage can be justified by substituting the Laplace transform of the inductor constitutive equation

$$u_t(s) = Ls i_t(s) \tag{5.369}$$

into the Laplace transformation of (5.367), with

$$u(s) = \frac{E}{s} . \tag{5.370}$$

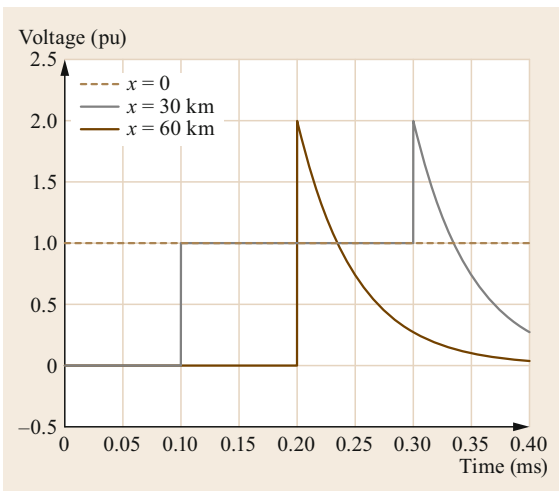


Fig. 5.114 Voltage waveforms along a 60 km line in the case of an inductive termination

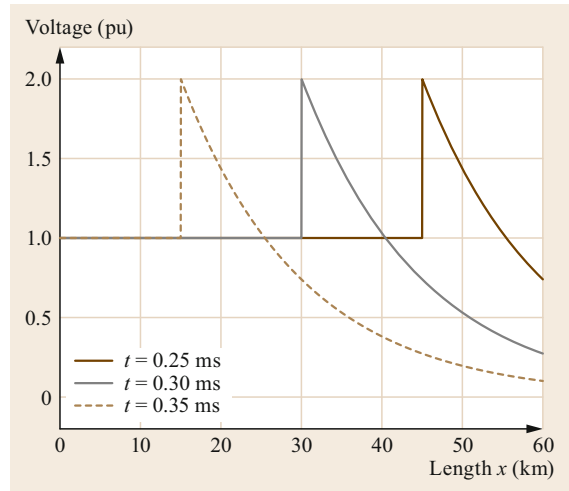


Fig. 5.115 Voltage profiles along a 60 km line at different times in the case of an inductive termination

This leads to

$$u_t(s) = E \frac{2T}{1 + Ts} \tag{5.371}$$

$$i_t(s) = \frac{E}{Z_1} \frac{2}{s(1 + Ts)} \tag{5.372}$$

where

$$T = \frac{L}{Z_1} , \tag{5.373}$$

which correspond to

$$u_t(t) = 2Ee^{-\frac{t}{T}} \tag{5.374}$$

$$i_t(t) = \frac{2E}{Z_1} (1 - e^{-\frac{t}{T}}) . \tag{5.375}$$

Reflections at a Capacitive Termination

Reflection at a capacitive termination is similar to that at a short circuit immediately after the arrival of the incident wave, but ultimately resembles reflection at an open circuit. The voltages (in pu with respect to the amplitude of the voltage source) at three points along a 60 km line with a step voltage source at $x = 0$ and a 100 nF capacitance at $x = 60$ km are presented in Fig. 5.116. Figure 5.117 shows the voltage profiles along the line at three different times.

The waveform of the capacitive terminal voltage can be justified by substituting the Laplace transform of the capacitor constitutive equation

$$u_t(s) = \frac{1}{Cs} i_t(s) \tag{5.376}$$

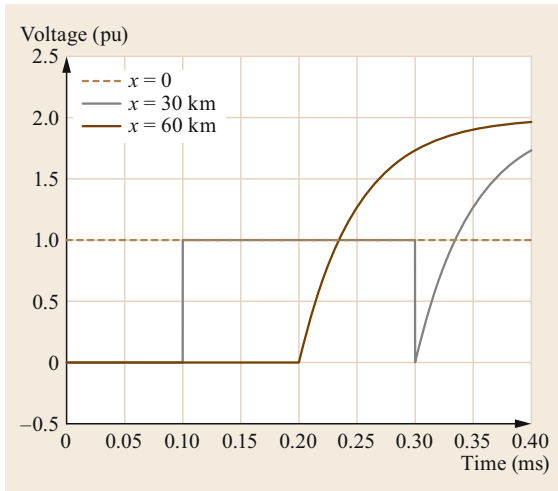


Fig. 5.116 Voltage profiles along a 60 km line at different times in the case of a capacitive termination

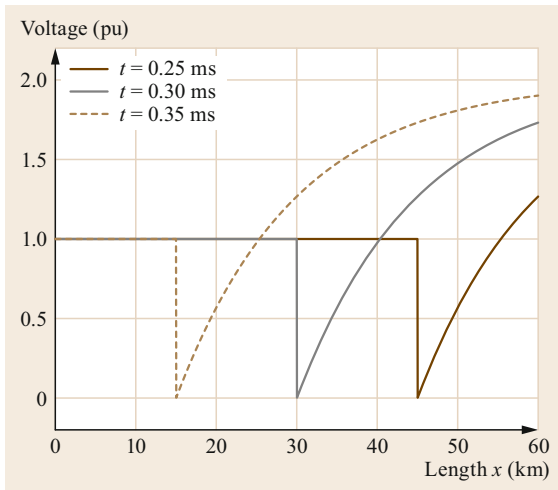


Fig. 5.117 Voltage waveforms along a 60 km line in the case of a capacitive termination

into the Laplace transformation of (5.367) and using (5.370), thus obtaining

$$u_t(s) = E \frac{2}{s(1 + Ts)} \tag{5.377}$$

$$i_t(s) = E \frac{2C}{1 + Ts} \tag{5.378}$$

where

$$T = CZ_1 \tag{5.379}$$

Finally, antitransforming these equations yields

$$u_t(t) = 2E \left(1 - e^{-\frac{t}{T}} \right) \tag{5.380}$$

$$i_t(t) = \frac{2E}{T} e^{-\frac{t}{T}} \tag{5.381}$$

5.8.3 Multiple Reflections in a Line of Finite Length

In a line of finite length, the voltage and the current at a point along the line are obtained by superposing the waves traveling in both directions—the incident wave and the waves that have been reflected at the line ends. If one of the terminations is connected to an ideal voltage source, the voltage at that terminal will always be equal to the voltage impressed by the generator, meaning that any reflected wave that moves backward from the opposite end will be canceled out by the new reflection at the generator. In other words, the reflection coefficient at the generator side is equal to -1 . In this section, we consider multiple reflections along the line in the extreme cases of open and short-circuited ends, as well as two cases of multiple reflection along a line with a resistive termination.

Open End

Figure 5.118 presents the case of a single conductor line of finite length d with one termination (A) connected to a DC voltage source and the other termination (M) kept open. The voltage reflection coefficients are 1 at A and -1 at M. Therefore, the voltage is doubled at the open end and restored to the impressed voltage value E at the source. Due to the backward voltage wave reflected by the open end, the voltage along the line is $2E$ so long as the doubling effect is canceled out by the

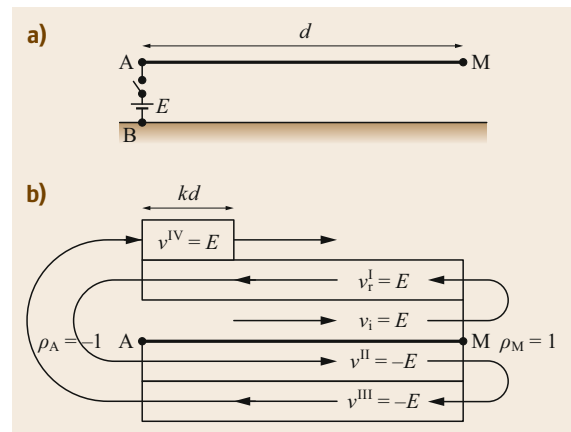


Fig. 5.118 (a) The schematic depicts a single line conductor of finite length d with a DC voltage source at the left end (A) and an open right end (M), while the schematic in (b) shows the effect of multiple reflections on the voltage at the point a distance kd along the line from the powered end (adapted from [5.36])

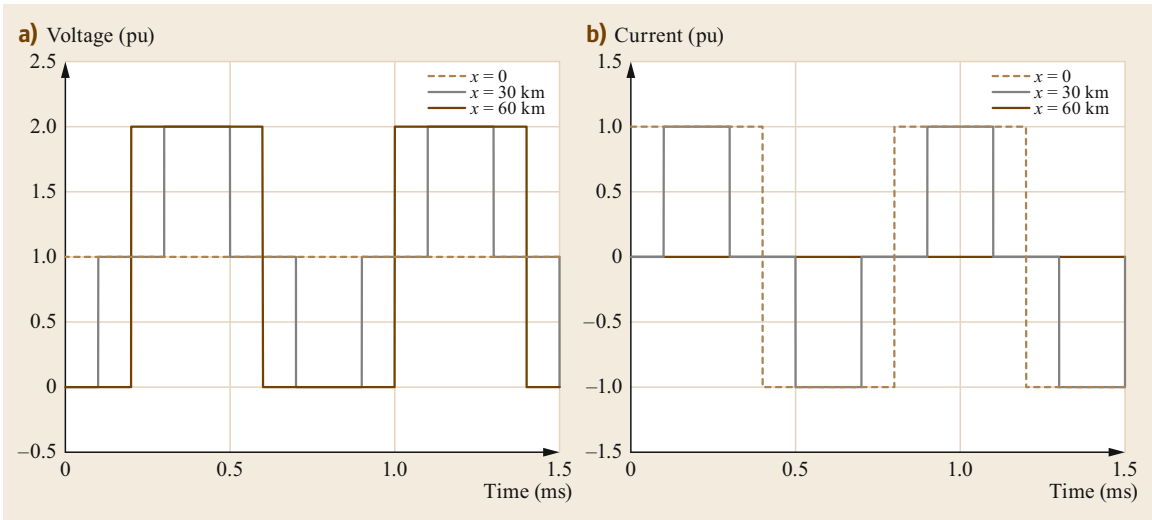


Fig. 5.119 (a) Voltages and (b) currents at different points along a 60 km line with a step voltage source at $x = 0$ and an open end at $x = 60$ km. Voltage/current values are in pu with respect to the incident voltage/current wave amplitude

forward voltage wave from the source, as illustrated in Fig. 5.119 for the terminal ends and the middle point of a 60 km line. The figure also shows the currents at the same points along the line; the waveform can be justified by observing that the current reflection coefficients are -1 at the open end and 1 at the receiving end. The voltage and current waveforms along the line present oscillatory components that persist due to the assumed absence of dissipative elements along the line and at the line ends.

Short-Circuited End

Figure 5.120 presents the case of a single line conductor of finite length d with one termination (A) connected to a DC voltage source and the other termination (M) short-circuited. The voltage reflection coefficients are -1 at both ends. Therefore, the voltage is canceled at

the short-circuited end and restored to the impressed voltage value E at the source. The voltage along the line is E so long as it is not canceled out by the backward voltage wave reflected at the short-circuited end, as illustrated in Fig. 5.121 for the terminal ends and the middle point of a 60 km line. The figure also shows the current at the same points; the waveform can be justified by observing that the current reflection coefficient is 1 at both ends.

Resistive End

Figure 5.122 presents the case of a single line conductor with one termination (A) connected to a DC voltage source and the other termination (M) feeding a resistance R . The diagram showing the reflected voltage waves refers to the case where R is equal to $3Z$ (Z is the surge impedance of the line), which—according

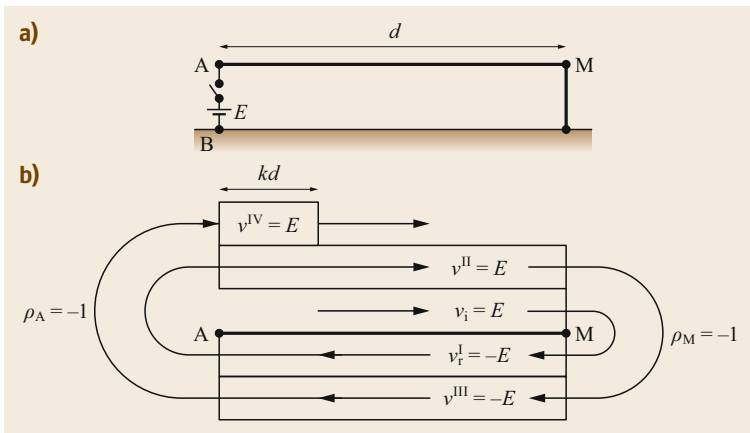


Fig. 5.120 (a) The schematic depicts a single line conductor of finite length d with a DC voltage source at the left end (A) and a short-circuited right end (M), while the schematic in (b) shows the effect of multiple reflections on the voltage at a point a distance kd along the line from the powered end (adapted from [5.36])

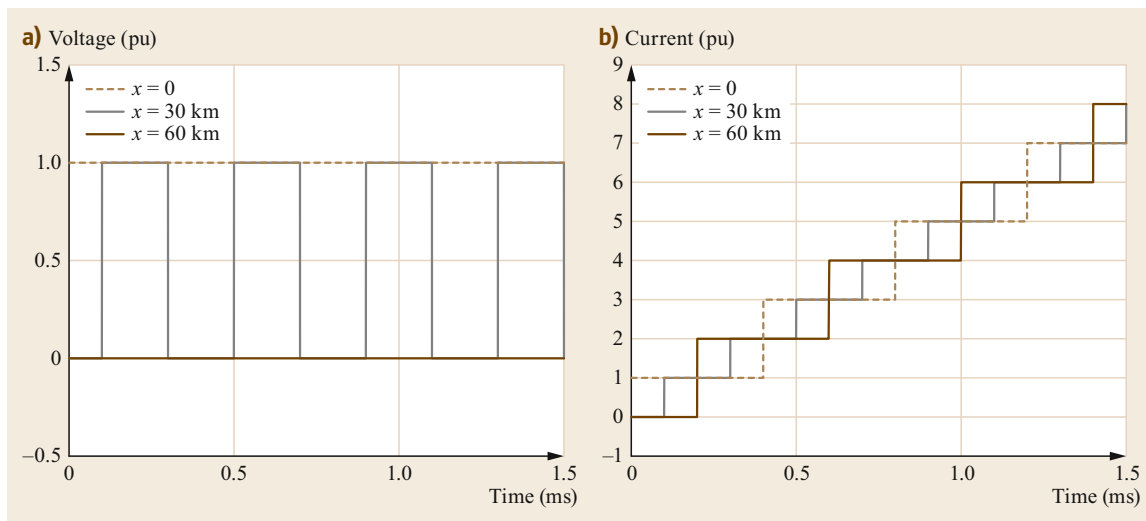


Fig. 5.121 (a) Voltages and (b) currents at different points along a 60 km line with a step voltage source at $x = 0$ and a short-circuited end at $x = 60$ km. Voltage/current values are in pu with respect to the incident voltage/current wave amplitude

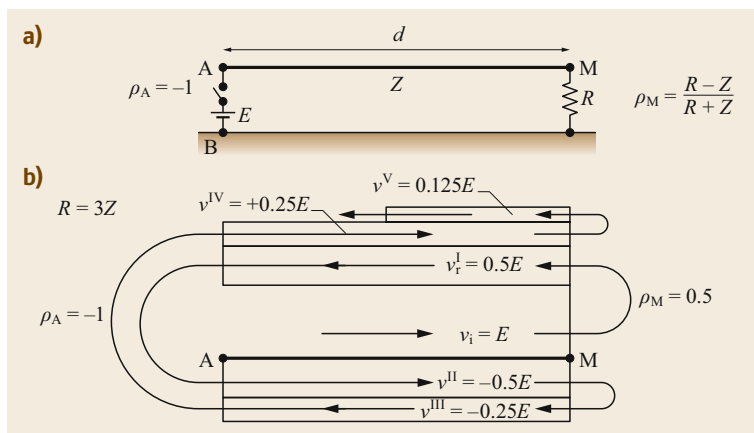


Fig. 5.122 (a) The schematic depicts a single line conductor of finite length d with a DC voltage source at the left end (A) and a resistance R (which is three times larger than the surge impedance of the line, Z) at the right end (M), while the schematic in (b) shows the effect of multiple reflections of the voltage at a point along the line (adapted from [5.36])

to (5.363)—gives a voltage reflection coefficient of 0.5 at M. The voltage coefficient is -1 at A, just as in the previous cases. The backward-traveling voltage waves increase the voltages along the line, whereas the forward-traveling ones reflected by the source reduce them. The voltages along the line, and in particular the voltage at M (see Fig. 5.123), show an oscillatory trend with an overshoot with respect to the steady-state value. It is worth noting that the oscillations are not persistent as they are damped by the energy dissipation in R .

Figure 5.124 presents a case study that is similar to the previous one but with R equal to one-third of the surge impedance of the line Z , which gives—according to (5.363)—a voltage reflection coefficient of -0.5 at M. In this case, the backward-traveling voltage

waves reduce the voltages along the line, whereas the forward-traveling ones reflected by the source increase them (due to the voltage reflection coefficient of -1 at A). The voltages along the line, and in particular the voltage at M (see Fig. 5.125), show an increasing aperiodic trend towards the steady-state value.

Sinusoidal Source

We now consider the case of a transmission line energized by an ideal 50 Hz sinusoidal voltage source. The voltages in the figures presented in this section are expressed in pu with respect to the amplitude of the voltage source, while the currents are given with respect to the amplitude of the incident current wave (i.e., the ratio of the voltage source amplitude to the surge impedance of the line).

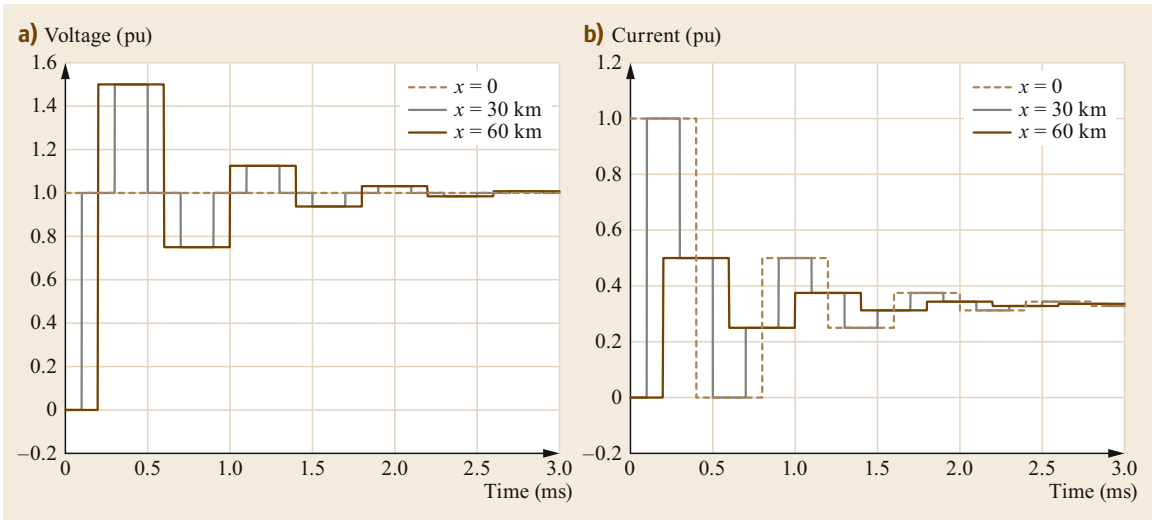


Fig. 5.123 (a) Voltages and (b) currents at different points along a 60 km line with a step voltage source at $x = 0$ and a resistance that is three times the surge impedance at $x = 60$ km. Voltage/current values are in pu with respect to the incident voltage/current wave amplitude

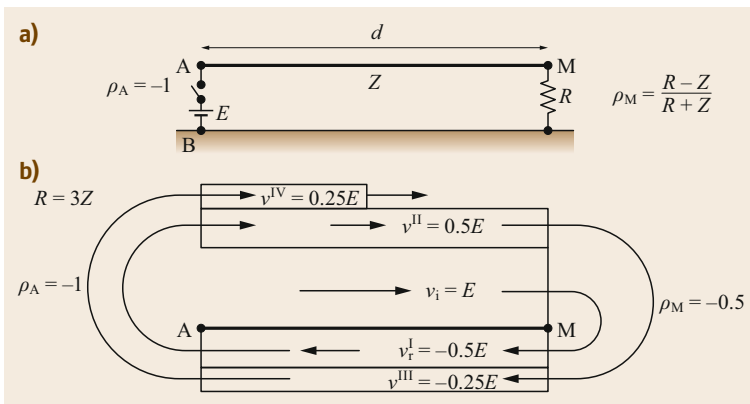


Fig. 5.124 (a) The schematic depicts a single line conductor of finite length d with a DC voltage source at the left end (A) and a resistance R that is one-third the surge impedance of the line (Z) at the right end (M), while the schematic in (b) shows the effect of multiple reflections of the voltage at a point along the line (adapted from [5.36])

Figures 5.126 and 5.127 present the voltage profiles along a 6000 km transmission line 1 ms before and 1 ms after the incident voltage wave reaches the non-energized termination. Different resistive terminations are considered; in particular, the receiving end is assumed to be connected to a resistance R that is equal to the surge impedance Z_0 , three times Z_0 , or one-third of Z_0 . The voltage profiles before the arrival of the wave at the receiving end are the same, but they differ after the wave has been reflected. It is worth noting that the incident voltage amplitude varies sinusoidally along the line length with a period of 6000 km, which is the wavelength of a signal at 50 Hz traveling at the speed of light.

Figures 5.128 and 5.129 show the same comparison as Fig. 5.127, but they present the results obtained for

lines 600 and 60 km long, respectively. Note that the incident voltage wave amplitude still varies sinusoidally in these two figures, but that the variation is less prominent.

Figure 5.130 compares the above three cases with different line lengths in terms of the voltage and current waveforms obtained at the two ends of the line. The resistive termination is assumed to have a resistance equal to the surge impedance of the line. Under these conditions, neither voltage nor current reflection takes place, and the line is often said to be *matched*. The voltage and current waves (in pu) coincide. When the line length is equal to the wavelength, the voltage waveforms at the line ends coincide, except for the delay with which the receiving end is energized. For shorter lines, a displacement between the waveforms can be observed.

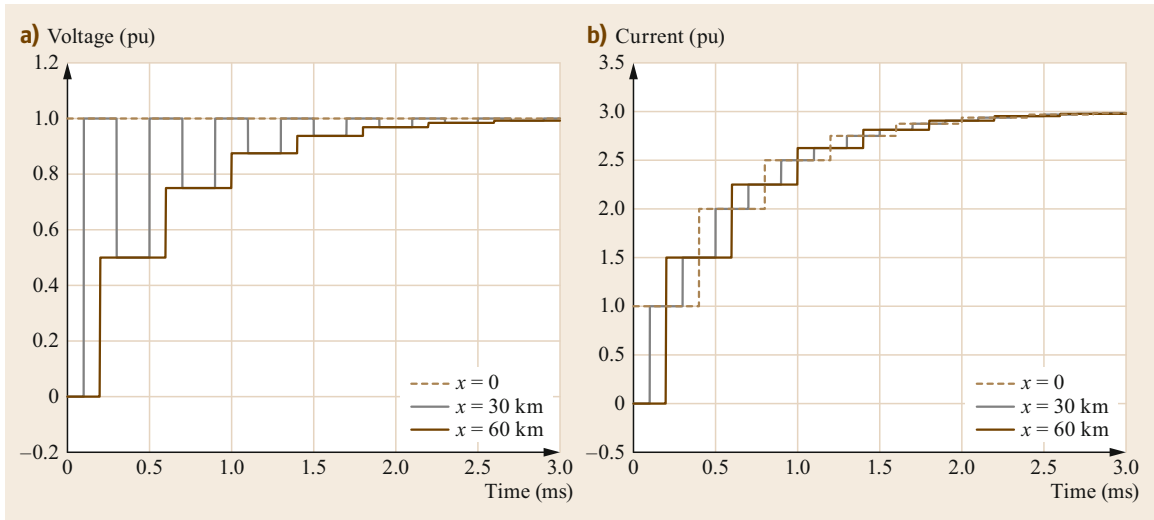


Fig. 5.125 (a) Voltages and (b) currents at different points along a 60 km line with a step voltage source at $x = 0$ and a resistance that is one-third of the surge impedance at $x = 60$ km. Voltage/current values are in pu with respect to the incident voltage/current wave amplitude

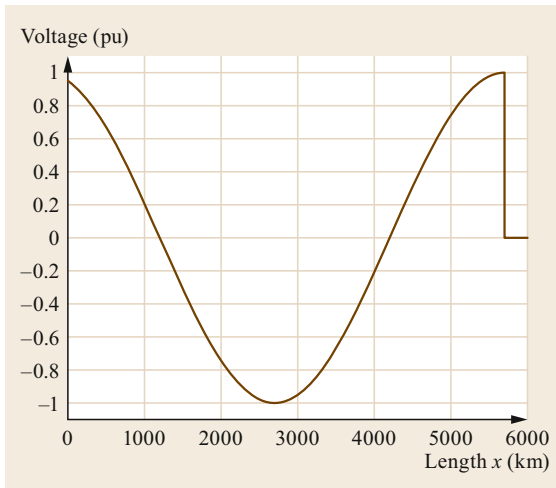


Fig. 5.126 Voltage profile along a 6000 km line 19 ms after energization by a 50 Hz sinusoidal voltage source connected at $x = 0$. Voltage values are given in pu with respect to the source voltage amplitude

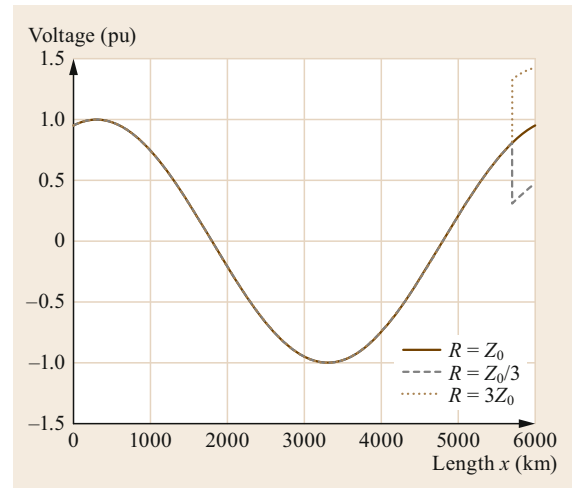


Fig. 5.127 Voltage profile along a 6000 km line 21 ms after energization by a 50 Hz sinusoidal voltage source connected at $x = 0$. The other termination at $x = 6000$ km is resistive; cases where this resistance R is equal to, larger than, or lower than the surge impedance Z_0 of the line are considered. Voltage values are given in pu with respect to the source voltage amplitude

A comparison between the voltage waveforms obtained at the receiving end when different resistive terminations are present is provided in Fig. 5.131. It can be observed that the speed of the transition between the transient and the steady-state responses of the line increases as the line shortens and the termination resistance increases.

Comparisons between the current waveforms obtained at the sending and receiving line terminations when different resistive terminations are present are re-

ported in Figs. 5.132 and 5.133, respectively. In contrast to the voltage waveform, which only changes at the receiving end depending on the resistance of the resistive termination, it should be noted that the current at the sending end can vary too. In particular, for line lengths of 600 and 60 km, the current waveform is modified by the backward-reflected current waves.

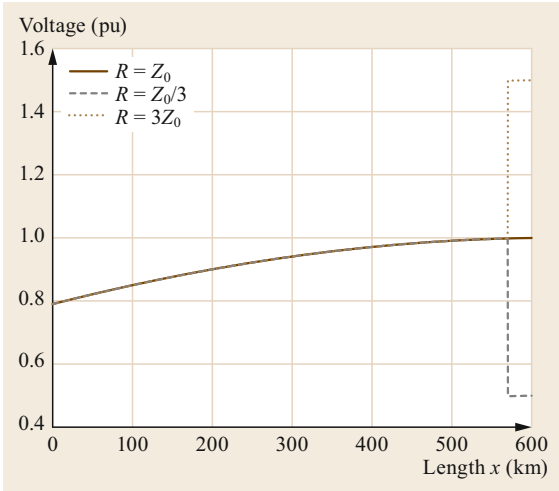


Fig. 5.128 Voltage profile along a 600 km line 2.1 ms after energization by a 50 Hz sinusoidal voltage source connected at $x = 0$. The other termination at $x = 600$ km is resistive; cases where this resistance R is equal to, larger than, or lower than the surge impedance Z_0 of the line are considered. Voltage values are given in pu with respect to the source voltage amplitude

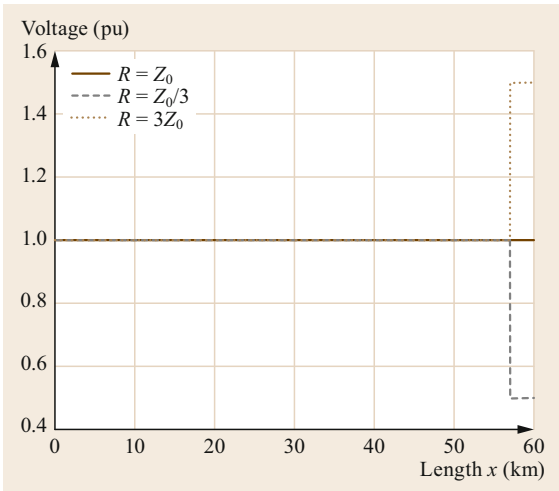


Fig. 5.129 Voltage profile along a 60 km line 0.21 ms after energization by a 50 Hz sinusoidal voltage source connected at $x = 0$. The other termination at $x = 60$ km is resistive; cases where this resistance R is equal to, larger than, or lower than the surge impedance Z_0 of the line are considered. Voltage values are given in pu with respect to the source voltage amplitude

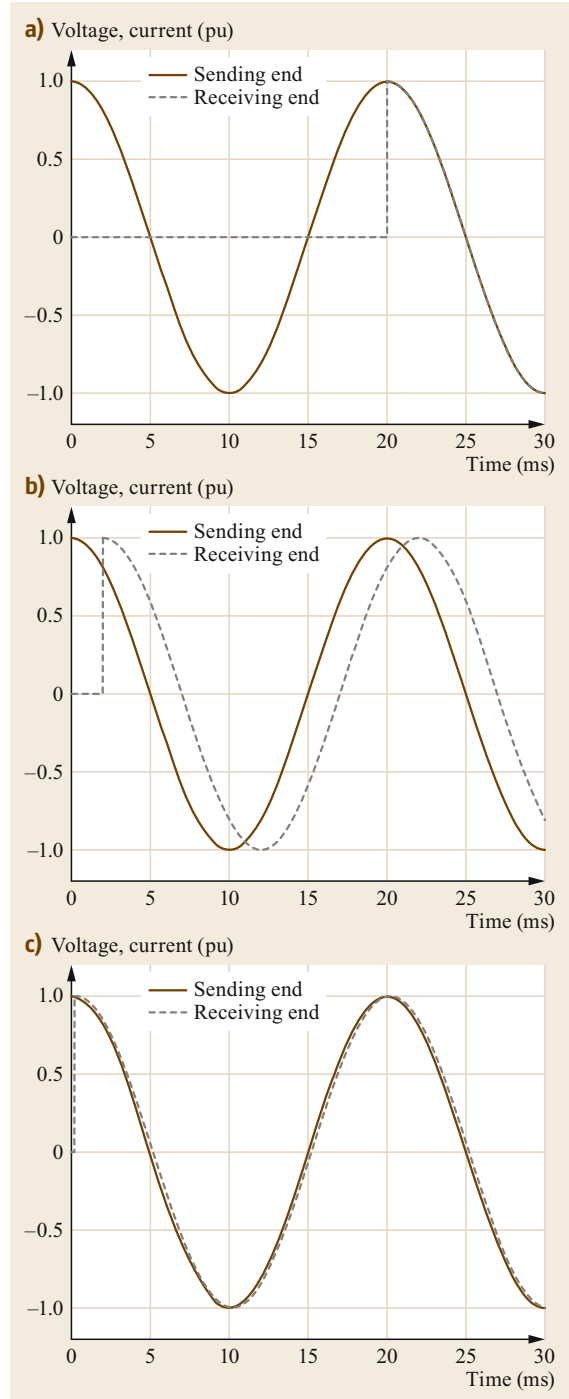


Fig. 5.130a–c Voltage and current waveforms at the sending and receiving ends of a transmission line, where the sending end is connected to a 50 Hz sinusoidal voltage source and the receiving end is connected to a resistance R that is equal to the surge impedance Z_0 of the line. Values are given in pu with respect to the source voltage amplitude E and E/Z_0 . Line lengths: (a) 6000 km, (b) 600 km, (c) 60 km

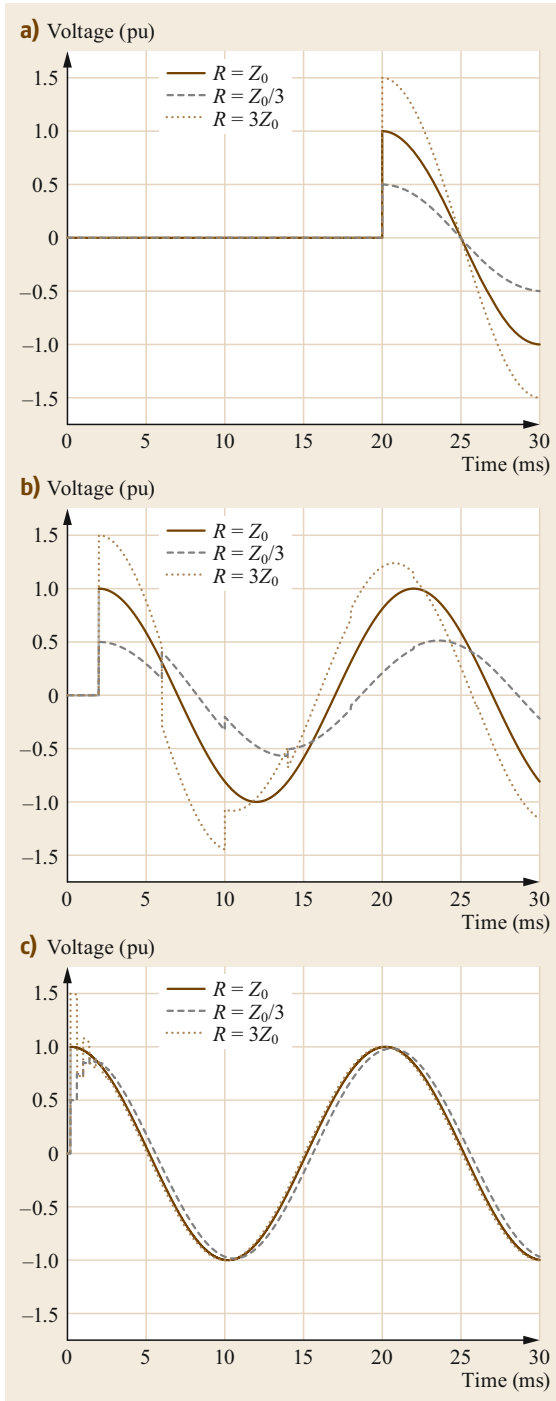


Fig. 5.131a–c Voltage waveforms at the receiving end of a transmission line, where the sending end is connected to a 50 Hz sinusoidal voltage source and the receiving end is connected to a resistance R that is equal to, larger than, or lower than the surge impedance Z_0 of the line. Values are given in pu with respect to the source voltage amplitude. Line lengths: (a) 6000 km, (b) 600 km, and (c) 60 km

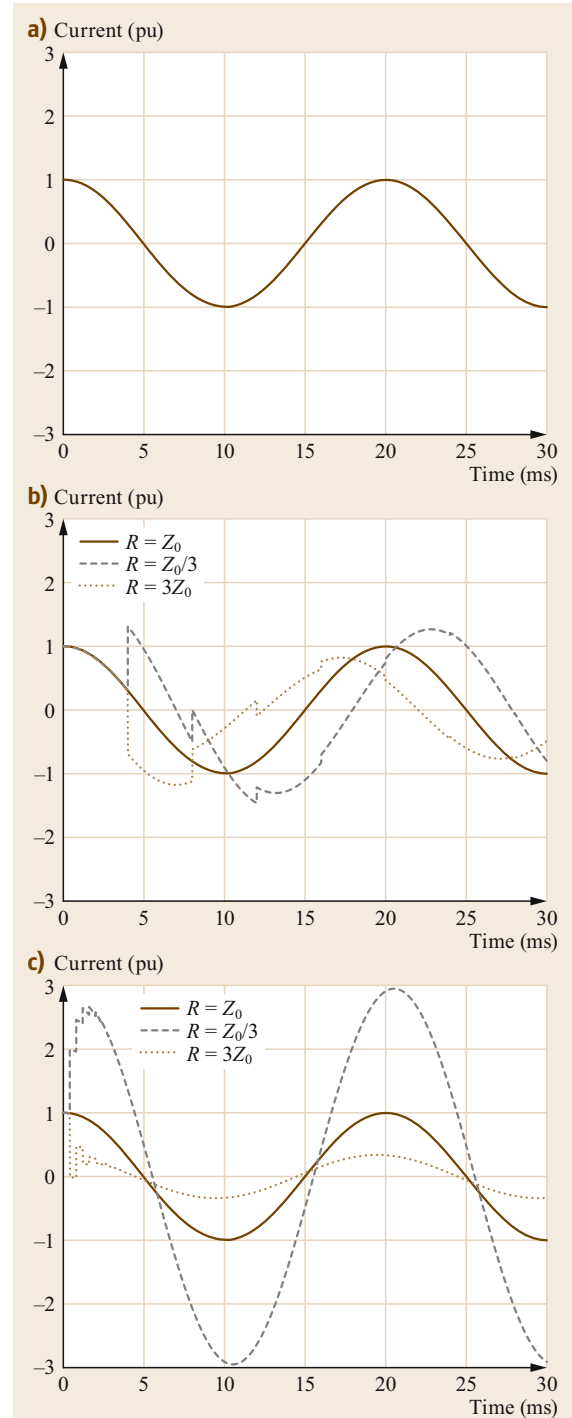


Fig. 5.132a–c Current waveforms at the sending end of a transmission line, where the sending end is connected to a 50 Hz sinusoidal voltage source and the receiving end is connected to a resistance R that is equal to, larger than, or lower than the surge impedance Z_0 of the line. Values are in pu with respect to the amplitude of the incident current wave. Line length: (a) 6000 km, (b) 600 km, and (c) 60 km

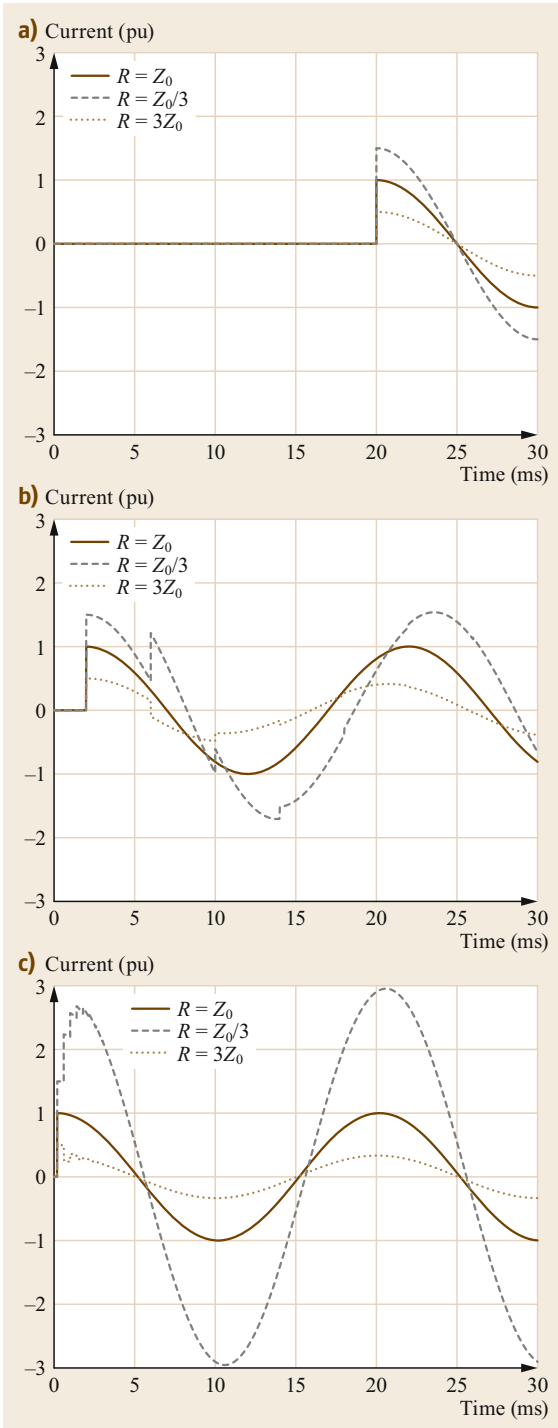


Fig. 5.133a–c Current waveforms at the receiving end of a transmission line, where the sending end is connected to a 50 Hz sinusoidal voltage source and the receiving end is connected to a resistance R that is equal to, larger than, or lower than the surge impedance Z_0 of the line. Values are in pu with respect to the amplitude of the incident current wave. Line length: (a) 6000 km, (b) 600 km, and (c) 60 km

5.9 Electric Power Systems of the Future: Smart Grids

Electric power systems are continually evolving. Drivers of this evolution over the last few decades include the liberalization and development of competitive electricity markets, the increasingly widespread use of HVDC links to improve transmission capabilities and enhance interconnection, the growth in renewable energy sources (RESs), and the integration of distributed generation (DG). In the future, the expected large-scale adoption of electric vehicles and electric transportation technologies will lead to further power system development. Such development may include the implementation of a global power grid [5.56].

5.9.1 Evolution of Power Systems Towards Increased Deployment of Renewable Energy Resources

In this section, we focus on DG. There are many reasons for using DG in power systems, but the two main motivations are the introduction of the open electricity market and environmental requirements [5.57].

In Italy, the amount of power generated by RESs has increased considerably since the mid-2000s. Figure 5.134 shows how the power produced by each type of electric power plant has evolved in Italy since 1963. This graph is largely representative of those of many other countries in Europe too. From 2004 to 2013, the share of the total power generated in Italy that is contributed by RES plants increased from 26% to 39%, and this share reached 45% in 2017 (Fig. 5.135).

Since many RES technologies (photovoltaic units and several types of wind turbines in particular) are used in conjunction with power electronic convert-

ers [5.58, 59], the characteristics and fast dynamics of these devices tend to modify the behavior of the power system, especially during large perturbances.

The trends expected for Italy over the next decade are also expected to occur for Europe in general. Figure 5.136 shows the European targets for 2030 in relation to the transition to a zero-carbon economy, as well as the ambitions for 2050. This framework was adopted by the European Council in October 2014, and the targets for renewables and energy efficiency were revised in 2018.

The key targets for 2030 are:

- Cuts of at least 40% in greenhouse gas emissions with respect to 1990 levels
- A renewable energy share of at least 32%
- An improvement in energy efficiency of at least 32.5%.

The compositions of power systems in the future will also be influenced by the actions of transmission system operators (TSOs). Both Terna and ENTSO-E (the Italian TSO and the European network of TSOs, respectively) have set out possible future scenarios for the evolution of power systems up to 2040 [5.52, 61]. ENTSO-E forecasts that by 2040, between 65% and 81% of the electricity demand in the European Union (EU) will be met by renewable energy sources. Ensuring that this scenario is feasible and guaranteeing the economic sustainability and reliability of the electricity supply will require the implementation of technical solutions for storage system development and the strengthening of interconnections between states. Such measures should make it possible to exploit up to

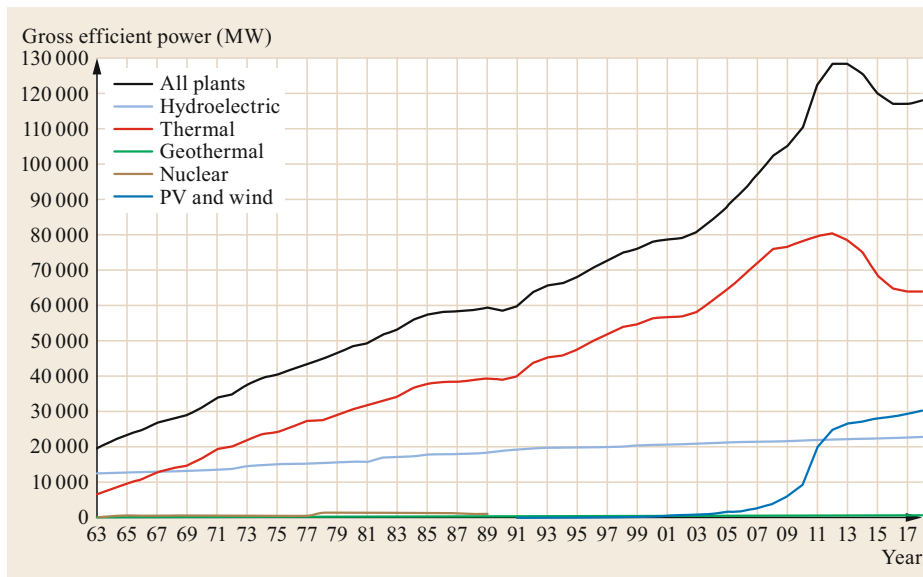


Fig. 5.134

Evolution of the contributions of various types of electric power plants to the total power produced in Italy since 1963 (from www.terna.it)

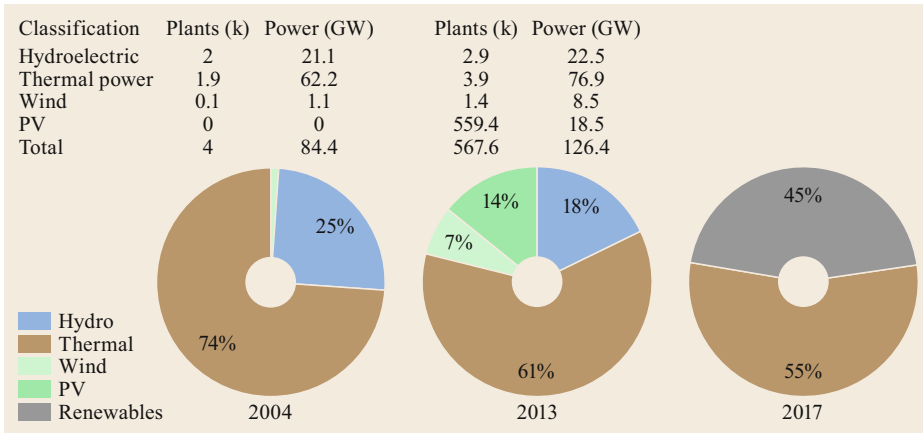


Fig. 5.135 Italian power generation mix in 2004, 2013, and 2017. The pie charts and tables for 2004 and 2013 provide data on the power generation mix in Italy, including the types of power plants that contribute power, the number of plants of each type, the power contributed by each type, and the percentage contribution of each type to the total power generated in Italy. The pie chart for 2017 only presents the percentage contributions of renewables and thermal plants to the total power (from www.terna.it)

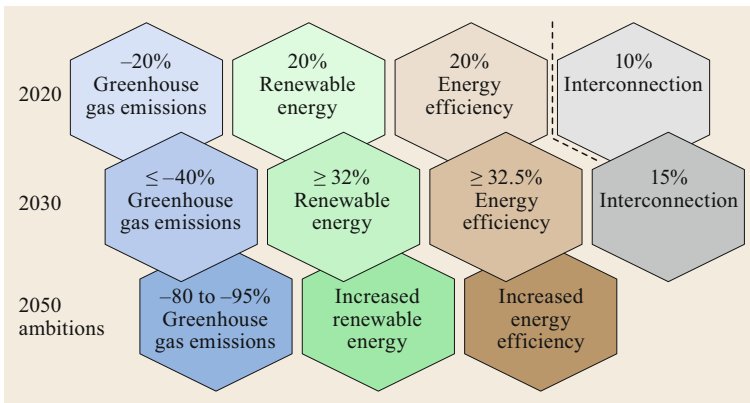


Fig. 5.136 European targets for 2030 in relation to the transition to a zero-carbon economy (adapted from [5.60])

150 TWh of energy produced from nonprogrammable sources that would otherwise remain unused. In this regard, the EU has announced a thousand billion euro investment plan that aims to convert all conventional generation units to renewables ones by 2050 [5.62]. Unity across borders will be crucial to achieving clean energy production [5.63]. The European electric grid is the largest synchronous grid in the world, and the level of interconnectivity among European countries is expected to grow significantly over the next few decades in order to improve cross-border energy exchange.

The intermittent nature of the output from renewable energy sources (e.g., wind and solar) necessitates sufficient backup generation to meet the demand for electricity [5.64]. This is even more important if wind and solar generate 100% of the required energy on average. The need for backup generation can, however, be reduced through the utilization of storage systems and/or grid extensions. Interconnections can improve grid stability

and reduce energy prices, so huge investments aimed at strengthening transmission line capabilities in order to create a European supergrid are expected. The EU has set an interconnection target of at least 10% by 2020 in order to encourage EU countries to link their installed electricity production capacities [5.63]. This means that each nation should have sufficient transmission lines to allow at least 10% of the electricity produced by its power plants to be transported across its borders to neighboring countries at any time. The level of interconnection is also expected to rise to 15% by 2030 [5.65].

5.9.2 Power System Structure: Why We Need Smart(er) Grids

We discussed the structure of a power system in Sect. 5.1. Historically, generators were connected directly at the transmission level, and power flows were unidirectional from the transmission level towards the

loads connected at lower voltage levels. However, power systems have changed in structure over the last few decades to allow the deployment of a large number of RESs. The increasing penetration of RESs and DG into power systems has totally changed the power flows in these systems, as many generating units are now connected directly at the subtransmission and distribution levels, meaning that distribution grids have been transformed from passive to active networks.

The impact of renewable generation on electric power systems presents a challenge to transmission and distribution systems operators [5.66], and has resulted in a need for *smarter* grids for the reasons listed below.

High Variability in the Amount of Power Produced by RESs

This characteristic of RESs requires:

- Smarter management of the grid
- Extensive information and communications technology (ICT) deployment (e.g., metering, cosimulation tools, . . .)
- Deployment of storage systems.

Penetration of RESs

The increasingly widespread adoption of RESs poses problems:

- Generators are often used in conjunction with power electronic converters, which degrades system stability due to a lack of inertia
- Power quality issues arise.

Integration of Electric Vehicles

The expected increase in electric vehicle utilization implies that:

- Network transformers must be upgraded in terms of size and capability
- The possibility of supporting the network with vehicle-to-grid (V2G) applications should be explored.

Inverted Power Flows

The inverted power flows that result from the inclusion of RESs in power systems are problematic because:

- The lines were not designed for bidirectional flows
- Voltage profiles along the distribution feeders are altered
- Protection failures may occur.

5.9.3 The Definition of a Smart Grid

The reasons mentioned above have led to the introduction of the concept of a *smart grid*. There are various definitions of a smart grid; we report a few of them below:

1. *European Technology Platform on SmartGrids*: “A SmartGrid is an electricity network that can intelligently integrate the actions of all users connected to it—generators, consumers and those that do both—in order to efficiently deliver sustainable, economic and secure electricity supplies.”
2. *US Department of Energy*: “A smart grid uses digital technology to improve reliability, security, and efficiency (both economic and energy) of the electric system from large generation, through the delivery systems to electricity consumers and a growing number of distributed-generation and storage resources.”
3. *Department of Energy and Climate Change, UK*: “A smart grid uses sensing, embedded processing and digital communications to enable the electricity grid to be observable (able to be measured and visualized), controllable (able to be manipulated and optimized), automated (able to adapt and self-heal), fully integrated (fully interoperable with existing systems and with the capacity to incorporate a diverse set of energy sources).”
4. *Electric Power Research Institute, USA*. This institute is developing the IntelliGridSM initiative, which is laying the technical foundations for smart grids. According to the Electric Power Research Institute, a smart grid is a “power system made up of numerous automated transmission and distribution systems, all operating in a coordinated, efficient and reliable manner;” “a power system that handles emergency conditions with *self-healing* actions and is responsive to energy-market and utility business-enterprise needs;” and “a power system that serves millions of customers and has an intelligent communications infrastructure enabling the timely, secure and adaptable information flow needed to provide reliable and economic power to the evolving digital economy.”
5. *Eurelectric*: “A smart grid is an electricity network that can intelligently integrate the behavior and actions of all users connected to it—generators, consumers and those that do both—in order to efficiently ensure sustainable, economic and secure electricity supply. As such, a smart grid, involving a combination of software and hardware allowing more efficient power routing and enabling consumers to manage their demand, is an important part of the solution for the future.”

5.9.4 Growth in the Utilization of ICT in Power Systems

The increasing use of ICT is an important characteristic of the development of power systems, as illustrated in Fig. 5.137. In transmission and distribution networks, the adoption of DG, together with electricity market procedures and the expected sudden growth in elec-

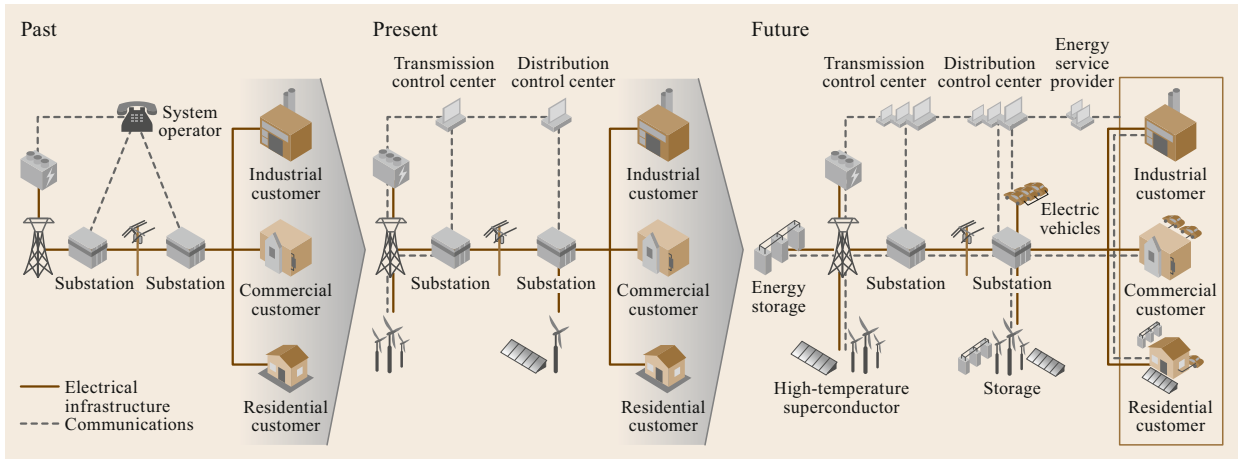


Fig. 5.137 Evolution of the utilization of ICT in power systems (from IEA, International Energy Agency)

tric vehicle deployment, is leading or will lead to more complex interactions among system components. Thus, in the future, it will be necessary to apply the most advanced ICT solutions to power system operation to ensure that reliability and performance targets are met. Enhancing MV and LV distribution network observability using both direct (smart metering) and indirect (state estimation [5.67], pseudomeasures [5.68], and load and production forecasts) methods can lay the groundwork for the development of new services and value-added functionalities [5.69].

The development of new tools that can be used to model the dynamic behavior of power systems and communications networks should facilitate the increased application of new ICT-based monitoring, control, and protection approaches in electric power grids [5.70, 71]. The expected key requirements of a ITC–power system cosimulation platform are easy configuration, good operating system compatibility, an ability to interconnect with external third-party programs/systems, a hardware-in-the-loop (HIL) capability, time synchronization, the ability to adjust the level of detail of the model (in both power and communications modeling), the interoperability needed to import models, and scalability.

5.9.5 Microgrids

The implementation of active distribution network technologies is leading to the formulation of new system concepts. The microgrid paradigm is perhaps the most promising novel network type [5.64]. A microgrid consists of a group of interconnected distributed energy resources such as microturbines, fuel cells, and photovoltaic arrays together with storage devices (i.e., flywheels, energy capacitors, and batteries) and controllable loads. Such systems offer considerable scope

for control and autonomous operation. They are interconnected to the distribution network but have the ability to voluntarily perform connection and disconnection maneuvers, meaning that they can smoothly and reliably switch between grid-connected and island modes (Fig. 5.138).

5.9.6 Energy Communities

Mechanisms enabling energy transactions between neighbors are becoming feasible in several countries. These mechanisms provide an incentive to install DG units (especially those based on RESs), which will encourage power generation that exceeds the local load, thus allowing the power demands of users connected nearby to the same distribution network to be exploited. As an example, on December 2018, the European Union approved the first part of a comprehensive legislative package entitled *Clean Energy for All Europeans* (CEP) [5.74]. This EU directive establishes appropriate legal frameworks for energy communities. A local energy community (LEC) can be defined as a set of end-users with local generation and storage units that cooperate to achieve common goals, in particular the minimum energy procurement costs and the efficient use of renewable resources [5.75].

Figure 5.139 illustrates the concepts of self-consumption, collective self-consumption, and the LEC [5.73]. Collective self-consumption, which builds on the well-established idea of self-consumption, involves cooperation between renewable energy self-consumers located in the same building or apartment block. In the figure, the LEC consists of a set of residential or small industrial sites, each acting as a prosumer, and it generally includes generation and battery energy storage units as well as loads. The LEC operates on an internal LV distribution network connected to the

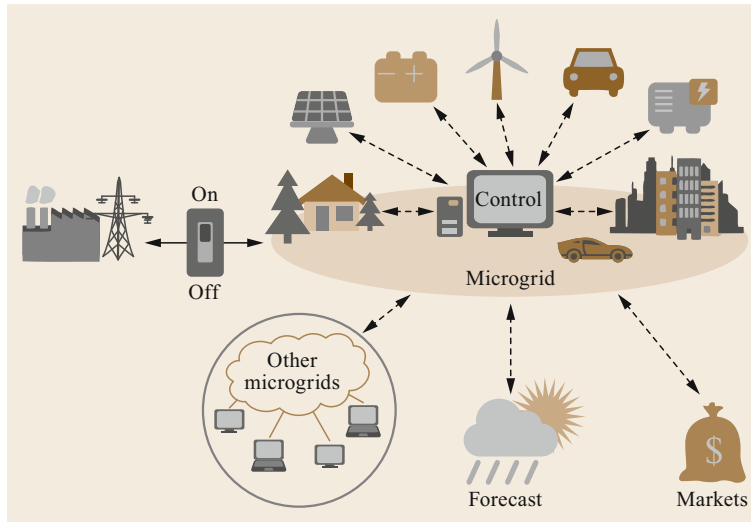


Fig. 5.138 Schematic of a microgrid (adapted from [5.72])

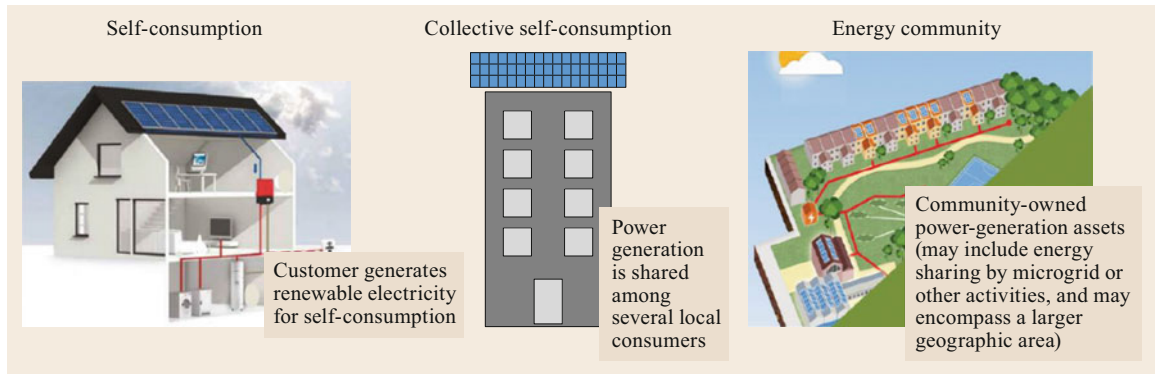


Fig. 5.139 From self-consumption to LEC (adapted from [5.73])

external utility grid, and the prosumers use the available energy resources cooperatively. Specific scheduling procedures are generally needed to fully exploit the available resources and the flexibility of the system (see, for example, [5.76] and references therein). Technologies such as demand response appear to be more easily applicable in LECs than by the utility. Local en-

ergy communities may also incorporate aggregators for electric vehicles [5.77].

Additional Information and Exercises

Additional information and supplementary exercises relating to this chapter can be found at https://go.sn.pub/SHb_PowerSystems_Nucci_PowerSystemsAnalysis.

References

- 5.1 E.W. Kimbark: *Synchronous Machines*, Power System Stability, Vol. 3 (Wiley, New York 1956)
- 5.2 D. Zanobetti, M. Pezzi: *Lezioni di impianti elettrici* (Clueb, Bologna 1981)
- 5.3 F. Iliceto: *Impianti elettrici* (Pàtron, Bologna 1984)
- 5.4 R. Marin, M. Valtorta: *Trasmissione e interconnessione* (CEDAM, Padova 1973)
- 5.5 P. Kundur: *Power System Stability and Control* (McGraw-Hill, New York 1994)
- 5.6 J. Grainger, W. Stevenson: *Power System Analysis* (McGraw-Hill, New York 1994)
- 5.7 J.P. Barret, P. Bornard, B. Meyer: *Power System Simulation* (Springer, Berlin, Heidelberg 1996)
- 5.8 H.W. Dommel: *EMTP Theory Book*, 2nd edn. ((Microtran Power System Analysis Corporation, Vancouver 1996)
- 5.9 F. Saccomanno: *Electric Power Systems Analysis and Control* (Wiley, New York 2003)
- 5.10 R. Marconato: *Steady State Behavior Controls, Short Circuits and Protection Systems*, Vols. 1 and 2 (CEI, Milano 2004)
- 5.11 J. Machowski, J.W. Bialek, J.R. Bumby: *Power System Dynamics: Stability and Control* (Wiley, New York 2008)
- 5.12 H. Saadat: *Power System Analysis*, 3rd edn. (McGraw-Hill, New York 2010)

- 5.13 A.J. Wood, B.F. Wollenberg, G.B. Sheblé: *Power Generation, Operation, and Control*, 3rd edn. (Wiley, Hoboken 2013)
- 5.14 J.D. Glover, M.S. Sarma, T.J. Overbye: *Power System Analysis and Design* (Cengage Learning, London 2012)
- 5.15 A. Gómez Expósito, A.J. Conejo, C. Cañizares: *Electric Energy Systems: Analysis and Operation*, 2nd edn. (CRC, Boca Raton 2018)
- 5.16 B.J. Cory, N. Jenkins, J. Ekanayake, G. Strbac, B.M. Weedy: *Electric Power Systems* (Wiley, Hoboken 2013)
- 5.17 F. Milano: *Power System Modelling and Scripting* (Springer, Heidelberg, Berlin 2013)
- 5.18 N. Mohan: *Electric Power Systems: A First Course* (Wiley, Hoboken 2012)
- 5.19 L.L. Grigsby: *The Electric Power Engineering Handbook* (CRC, Boca Raton 2012)
- 5.20 D.P. Kothari, I.J. Nagrath: *Modern Power System Analysis* (Tata McGraw-Hill, New Delhi 2011)
- 5.21 M.D. Ilic, J. Zaborszky: *Dynamics and Control of Large Electric Power Systems* (Wiley, New York 2000)
- 5.22 A.K. Singh, B.C. Pal: *Dynamic Estimation and Control of Power Systems* (Elsevier, Amsterdam 2018)
- 5.23 P.M. Anderson: *Power System Protection* (McGraw-Hill, New York 1999)
- 5.24 V. Vittal, J.D. McCalley, P.M. Anderson, A.A. Fouad: *Power System Control and Stability*, 3rd edn. (Wiley-IEEE, Hoboken 2020)
- 5.25 P.W. Sauer, M.A. Pai, J.H. Chow: *Power System Dynamics and Stability: With Synchrophasor Measurement and Power System Toolbox*, 2nd edn. (Wiley-IEEE, Hoboken 2018)
- 5.26 M. Eremia, M. Shahidehpour: *Handbook of Electrical Power System Dynamics: Modeling, Stability, and Control* (Wiley, Hoboken 2013)
- 5.27 A. Ametani, N. Nagaoka, Y. Baba, T. Ohno, K. Yamabuki: *Power System Transients: Theory and Applications*, 2nd edn. (CRC, Boca Raton 2016)
- 5.28 A. Greenwood: *Electrical Transients in Power Systems*, 2nd edn. (Wiley, New Delhi 1991)
- 5.29 M. Ceraolo, D. Poli: *Fundamentals of Electric Power Engineering: From Electromagnetics to Power Systems* (Wiley, Hoboken 2014)
- 5.30 J.C. Das: *Power System Analysis: Short-Circuit Load Flow and Harmonics*, 2nd edn. (CRC, Boca Raton 2012)
- 5.31 M.L. Crow: *Computational Methods for Electric Power Systems*, 3rd edn. (CRC, Boca Raton 2015)
- 5.32 A.A. Sallam, O.P. Malik: *Power System Stability: Modelling, Analysis and Control* (IET, London 2015)
- 5.33 C. Sulzberger: Pearl Street in miniature: Models of the electric generating station, *IEEE Power Energy Mag.* **11**(2), 76–85 (2013)
- 5.34 The Edison Electric Lighting Station, *Sci. Am.* **47**(9), 127–130 (1882)
- 5.35 L. de Andrade, T.P. de Leao: A brief history of direct current in electrical power systems. In: *Third IEEE Hist. Electro-Technol. Conf. (HISTELCON)* (2012) pp. 1–6
- 5.36 A. Paolucci: *Lezioni di trasmissione dell'energia elettrica* (Cleup, Padova 1990)
- 5.37 J.B. Ward, H.W. Hale: Digital computer solution of power-flow problems, *Trans. Am. Inst. Electr. Eng.* **75**(3), 398–404 (1956)
- 5.38 J.E. Van Ness: Iteration methods for digital load flow studies, *Trans. Am. Inst. Electr. Eng.* **78**(3), 583–586 (1959)
- 5.39 H.W. Hale, R.W. Goodrich: Digital computation of power flow – Some new aspects, *Trans. Am. Inst. Electr. Eng.* **78**(3), 919–923 (1959)
- 5.40 J. Carpentier: Optimal power flows, *Int. J. Electr. Power Energy Syst.* **1**(1), 3–15 (1979)
- 5.41 B. Stott: Decoupled Newton load flow, *IEEE Trans. Power Appar. Syst.* **91**(5), 1955–1959 (1972)
- 5.42 B. Stott, O. Alsac: Fast decoupled load flow, *IEEE Trans. Power Appar. Syst.* **93**(3), 859–869 (1974)
- 5.43 R. Marconato: *Steady State Behavior Controls, Short Circuits and Protection Systems*, *Electric Power Systems*, Vol. 2 (CEI, Milano 2004)
- 5.44 V. Cataliotti: *Impianti Elettrici*, Vol. 1 (Flaccovio, Palermo 2008)
- 5.45 J. Mahseredjian, S. Denetiere, L. Dubé, B. Khodabakhchian, L. Gérin-Lajoie: On a new approach for the simulation of transients in power systems, *Electr. Power Syst. Res.* **77**(11), 1514–1520 (2007)
- 5.46 L.H. Fink, K. Carlsen: Operating under stress and strain, *IEEE Spectrum* **15**(3), 48–53 (1978)
- 5.47 T.E.D. Liacco: Systems security: The computer's role, *IEEE Spectrum* **15**(6), 43–50 (1978)
- 5.48 P. Kundur, J. Paserba, V. Ajjarapu, G. Andersson, A. Bose, C. Canizares, N. Hatziaargyriou, D. Hill, A. Stankovic, C. Taylor, T. Van Cutsem, V. Vittal, IEEE/CIGRE Joint Task Force on Stability Terms and Definitions: Definition and classification of power system stability, *IEEE Trans. Power Syst.* **19**(3), 1387–1401 (2004)
- 5.49 G. Andersson: *Power System Analysis* (ITET ETH, Zurich 2012), Lecture 227–0526–00
- 5.50 D. Mondal, A. Chakrabarti, A. Sengupta: *Power System Small Signal Stability Analysis and Control* (Academic Press, New York 2020)
- 5.51 M.E. Baran, F.F. Wu: Network reconfiguration in distribution systems for loss reduction and load balancing, *IEEE Trans. Power Deliv.* **9**(4), 101–102 (1989)
- 5.52 L. Schmitt: *Connecting Europe: Electricity*, ENTSO-E Reports (ENTSO-E AISBL, Brussels 2018)
- 5.53 N.R. Watson, J. Arrillaga: *Power Systems Electromagnetic Transients Simulation* (IET, London 2003)
- 5.54 J.A. Martínez-Velasco: *Transient Analysis of Power Systems: A Practical Approach* (Wiley, New York 2020)
- 5.55 C.A. Nucci, F. Rachidi, M. Rubinstein: Derivation of telegrapher's equations and field-to transmission line interaction. In: *Electromagnetic Field Interaction with Transmission Lines* (WIT Press, Boston 2008)
- 5.56 P. Deane, M. Brinkerink: Connecting the continents – A global power grid, *IEEE Power Energy Mag.* **18**(2), 121–127 (2020)
- 5.57 M. Bollen, H. Fainan: *Integration of Distributed Generation in the Power System*, IEEE Press Series on Power Engineering (Wiley-Blackwell, New York 2011)
- 5.58 V. Perelmutter: *Renewable Energy Systems: Simulation with Simulink and SimPowerSystems* (CRC, Boca Raton 2016)
- 5.59 F. Blaabjerg, D.M. Ionel: *Renewable Energy Devices and Systems with Simulations in MATLAB and ANSYS* (CRC, Boca Raton 2017)

- 5.60 A. Ali, W. Li, R. Hussain, X. He, B.W. Williams, A.H. Memon: Overview of current microgrid policies, incentives and barriers in the European Union, United States and China, *Sustainability* **9**(7), 1146 (2017)
- 5.61 Terna: *Documento di descrizione degli scenari* (Terna, Rome 2018)
- 5.62 European Commission: *Financing the Green Transition: The European Green Deal Investment Plan and Just Transition Mechanism* (EC, Brussels 2020)
- 5.63 Commission Expert Group: *Electricity Interconnections with Neighbouring Countries. Second Report of the Commission Expert Group on Electricity Interconnection Targets* (EC, Brussels 2019)
- 5.64 D. Connolly, H. Lund, B.V. Mathiesen: Smart Energy Europe: The technical and economic impact of one potential 100% renewable energy scenario for the European Union, *Renew. Sustain. Energy Rev.* **60**, 1634–1653 (2016)
- 5.65 European Commission: *Communication on Strengthening Europe's Energy Networks* (EC, Brussels 2017)
- 5.66 M. Bollen: *The Smart Grid: Adapting the Power System to New Challenges*, Synt. Lect. Power Electron. (Morgan, London 2011) p. 2013
- 5.67 A. Abur, A.G. Expósito: *Power System State Estimation* (CRC, Boca Raton 2004)
- 5.68 S. Sarri, L. Zanni, M. Popovic, J.Y. Le Boudec, M. Paolone: Performance assessment of linear state estimators using synchrophasor measurements, *IEEE Trans. Instrum. Meas.* **65**(3), 535–548 (2016)
- 5.69 F. Conte, S. Massucco, M. Saviozzi, F. Silvestro: A stochastic optimization method for planning and real-time control of integrated PV-storage systems: Design and experimental validation, *IEEE Trans. Sustain. Energy* **30**(29)(LV), 1–10 (2017)
- 5.70 R. Bottura, A. Borghetti: Simulation of the volt/var control in distribution feeders by means of a networked multiagent system, *IEEE Trans. Ind. Inform.* **10**(4), 2340–2353 (2014)
- 5.71 A. Borghetti, R. Bottura, M. Barbiroli, C.A. Nucci: Synchrophasors-based distributed secondary voltage/VAR control via cellular network, *IEEE Trans. Smart Grid* **8**(1), 262–274 (2017)
- 5.72 M. Stadler, A. Naslé: Planning and implementation of bankable microgrids, *Electr. J.* **32**(5), 24–29 (2019)
- 5.73 Council of European Energy Regulators: *Regulatory Aspects of Self-Consumption and Energy Communities* (CEER, Brussels 2019)
- 5.74 European Commission: Clean energy for all Europeans, *Euroheat Power* **14**(2), 3–4 (2019)
- 5.75 Council of European Energy Regulators: Renewable Self-Consumers and Energy Communities. CEER White Paper Series, paper # VIII (CEER, Brussels 2017)
- 5.76 S. Lilla, C. Orozco, A. Borghetti, F. Napolitano, F. Tossani: Day-ahead scheduling of a local energy community: An alternating direction method of multipliers approach, *IEEE Trans. Power Syst.* **35**(2), 1132–1142 (2020)
- 5.77 E.L. Karfopoulos, K.A. Panourgias, N.D. Hatziargyriou: Distributed coordination of electric vehicles providing V2G regulation services, *IEEE Trans. Power Syst.* **31**(4), 2834–2846 (2016)

Carlo Alberto Nucci

Department of Electrical, Electronic and Information Engineering
University of Bologna
Bologna, Italy
carloalberto.nucci@unibo.it



Carlo Alberto Nucci graduated in Electrical Engineering in 1982 from the University of Bologna, where he is Professor of Electrical Power Systems since 2000. He has received fellowships from IEEE and CIGRÉ, an HC degree from University Politecnica di Bucharest, the CIGRE TC award, and the ICLP SC Golde Award. He is Editor-in-Chief of the journal *Electric Power Systems Research* and a Member of the Academy of Science of the Institute of Bologna.

Alberto Borghetti

Department of Electrical, Electronic and Information Engineering
University of Bologna
Bologna, Italy
alberto.borghetti@unibo.it



Alberto Borghetti (IEEE M'97–SM'03–F'15) graduated in electrical engineering from the University of Bologna in 1992, and is now Professor of Electrical Power Systems at the same institution. He received ICLP SC and CIGRÉ TC awards in 2016 and 2018, respectively. He is currently serving as an Editor on the journal *IEEE Transactions on Power Systems* and as Editor-in-Chief of the journal *Electrical Engineering*.

Fabio Napolitano



Department of Electrical, Electronic and Information Engineering
University of Bologna
Bologna, Italy
fabio.napolitano@unibo.it

Fabio Napolitano received his MS and PhD (Hons.) in electrical engineering from the University of Bologna in 2003 and 2009, respectively. He subsequently became an Assistant Professor (in 2010) and an Associate Professor (in 2020). His research interests include power system transients—particularly those due to indirect lightning strikes—and lightning protection systems.

Fabio Tossani



Department of Electrical, Electronic and Information Engineering
University of Bologna
Bologna, Italy
fabio.tossani@unibo.it

Fabio Tossani received his BS (Hons.), MS (Hons.), and PhD in electrical engineering from the University of Bologna in 2010, 2012, and 2016, respectively. He is currently a junior Assistant Professor in the Power Systems Laboratory of the Department of Electrical, Electronic and Information Engineering “Guglielmo Marconi,” University of Bologna.